Winter 12-15-2021

Influence of Aging and Cerebrovascular Disease on Neuroimaging Measures of Alzheimer Disease

Lauren Nicole Koenig
Washington University in St. Louis

WASHINGTON UNIVERSITY IN ST. LOUIS

Division of Biology and Biomedical Sciences
Neurosciences

Dissertation Examination Committee:
Tammie L.S. Benzinger, Chair
Joshua S. Shimony, Co-Chair
Manu Goyal
Tamara Hershey
Jin-Moo Lee

Influence of Aging and Cerebrovascular Disease in the Diagnosis of Alzheimer Disease

by

Lauren N. Koenig

A dissertation presented to
The Graduate School
of Washington University in
partial fulfillment of the
requirements for the degree
of Doctor of Philosophy

December 2021
St. Louis, Missouri

Table of Contents

List of Figures vi
List of Tables viii
List of Abbreviations x
Acknowledgments xii
Abstract xiv
Chapter 1: Introduction 1
1.1 Alzheimer Disease Continuum 1
1.2 Atrophy in Aging and Preclinical AD 8
1.3 Atrophy in Clinical Diagnosis of AD 11
1.4 Interplay of AD, Stroke, and Race 14
1.5 White Matter Hyperintensities in AD 16
Chapter 2: Regional Age-Related Atrophy After Screening for Preclinical Alzheimer Disease (Koenig et al., 2022) 20
2.1 Introduction 20
2.2 Methods 22
2.2.1 Participants 22
2.2.2 Clinical Assessment 23
2.2.3 MR Imaging 24
2.2.4 PET Imaging 24
2.2.5 T1w/T2w Myelin Maps 25
2.2.6 Statistics 26
2.3 Results 29
2.3.1 Demographics 29
2.3.2 Regional Variation in Strength of Age-Related Atrophy 31
2.3.3 Regional Variation in Non-Linear Patterns of Age-Related Atrophy 31
2.3.4 Relationship of T1w/T2w Myelin Content and Slope of Age-Related Atrophy 35
2.3.5 Atrophy in Preclinical AD vs. Normal Aging 35

2.4 Discussion 38
2.5 Acknowledgements 40
2.6 Supplemental 45
Chapter 3: Improving Volumetric Models for Symptomatic Alzheimer Disease (Koenig et al., 2020) 57
3.1 Introduction 58
3.2 Methods 60
3.2.1 Participants 60
3.2.2 Imaging 64
3.2.3 Normal Aging Curves 65
3.2.4 Region Selection for AD Classification 67
3.2.5 Development of Classification Models 67
3.3 Results 68
3.3.1 Participants 68
3.3.2 Normal Aging Curves 68
3.3.3 Region Selection for AD Classification 68
3.3.4 Classification Models: Impact of Adjusting for Age-Related Atrophy 69
3.3.5 Classification Models: Impact of Age as a Predictor 72
3.3.6 Classification Models: Selecting a Model 72
3.3.7 Classification Models: Specific Diagnoses in the Clinical Cohort 75
3.3.8 Classification Models: MMSE and CDR in the Clinical Cohort 79
3.3.9 SARA as a Possible Clinical Tool 82
3.4 Discussion 84
3.5 Acknowledgements 87
3.6 Supplemental 89
Chapter 4: Interaction of Stroke, Race, and Amyloid (Koenig et al., 2021) 105
4.1 Introduction 106
4.2 Methods 108

4.2.1 Participants 108
4.2.2 Demographics 109
4.2.3 Imaging Measures 110
4.2.4 Clinical and Cognitive Measures 111
4.2.5 Statistical Analysis 111
4.3 Results 113
4.3.1 Participants 113
4.3.2 Demographics 113
4.3.3 Amyloid PET Outcome Measures 117
4.3.4 Quantitative MRI Outcome Measures 117
4.3.5 Radiologic MRI Outcome Measures 117
4.3.6 Cognitive Outcome Measures 118
4.3.7 Model Covariates 124
4.3.8 Models Using Infarct Definition of Stroke 124
4.3.9 CDR At One Year Follow-Up 124
4.4 Discussion 125
4.5 Acknowledgements 127
4.6 Supplemental 128
Chapter 5: White Matter Hyperintensities in Preclinical Alzheimer Disease 139
5.1 Introduction 140
5.2 Methods 141
5.2.1 Participants 141
5.2.2 Clinical Assessment and Demographics 143
5.2.3 MR Imaging 144
5.2.3 PET Imaging 147
5.2.3 Statistics 148
5.2.4 Machine Learning 148
5.3 Results 150
5.3.1 Demographic and Clinical Measures 150

5.3.2 WMH Summary Measures 151
5.3.3 WMH Machine Learning – Optimization 156
5.3.4 WMH Machine Learning – Description of Optimal Models 157
5.4 Discussion 163
5.5 Supplemental 166
Chapter 6: Conclusions 177
6.1 Overall Summary 177
6.2 Comments on Chapter 2: Regional Age-Related Atrophy After Screening for Preclinical Alzheimer Disease 178
6.3 Comments on Chapter 3: Improving Volumetric Models for Symptomatic Alzheimer Disease 182
6.4 Comments on Chapter 4: Interaction of Stroke, Race, and Amyloid 186
6.5 Comments on Chapter 5: White Matter Hyperintensities in Alzheimer Disease 188
6.6 Overall Conclusions 190
References 192

List of Figures

Figure 1.1: Revised AD Cascade Model (Jack et al., 2013) 4

Figure 1.2: AD Cascade in DIAN (Bateman et al., 2012) 4

Figure 1.3: A/T/N Framework (Jack et al., 2018) 7

Figure 1.4: Impact of Preclinical AD on Functional Connectivity Measures (Brier et al., 2014b) 9

Figure 1.5: Receiver Operating Characteristic Analyses for Distinguishing Alzheimer Disease (AD) Dementia and Mild Cognitive Impairment (MCI) Due to AD From Non-AD Neurodegenerative Disorders (Ossenkoppele et al., 2018a) 12

Figure 1.6: Group Difference vs Classification Ability (Arbabshirani et al., 2017) 19

Figure 2.1: Example Regions in the Normal Aging Cohort 28

Figure 2.2: Regional Maps of Age-Related Atrophy 35

Figure 2.3: T1w/T2w Myelin Map in Healthy Younger Adults 38

Figure 2.4: Example Regions for Normal Aging Cohort vs. Preclinical AD Cohort 39

Figure 3.1: Examples of Region-Specific Atrophy Observed in Normal Aging 72

Figure 3.2: Distribution of Predicted Probabilities and Accuracy Statistics for the SARA Model 79

Figure 3.3: Distribution of Predicted Probabilities for the SARA Model for Specific Diagnoses in the Clinical Cohort 83

Figure 3.4: MMSE Aligns, but is Not Equivalent, to Predicted Probability in SARA 86

Figure 3.5: Possible Use of SARA in a Clinical Setting 89

Supplemental Figure S3.1: Histogram of Ages in the Normal Aging Cohort 103

Supplemental Figure S3.2: Frequency of Region Selection for AD Classification 109

Supplemental Figure S3.3: CDR Aligns, but is Not Equivalent, to Predicted Probability in SARA 113

Figure 4.1: Continuous Outcome Measures 129

Figure 4.2: Categorical Outcome Measures 131

Supplemental Figure S4.1: Continuous Demographic Measures 139

Supplemental Figure S4.2: Longitudinal MMSE Models by Stroke and Race 141

Figure 5.1: Predefined Regions of White Matter Hyperintensities Clusters (Phuah et al., 2019) 158

Figure 5.2: White Matter Hyperintensity Volumes by Diagnosis 167

Figure 5.3: Voxel Frequency Maps of White Matter Hyperintensities 172

Figure 5.4: Voxel-level Variable Importance in the Random Forest Model with All Voxels 176

Supplemental Figure S5.1: WMH by Diagnosis in the Training Cohort 182

Supplemental Figure S5.2: WMH by Diagnosis in the Test Cohort 184

List of Tables

Table 2.1: Demographics 31

Table 3.1: Demographics 69

Table 3.2: AUCs for All Classification Models in Test and Clinical Cohorts 76

Table 3.3: Comparisons of Classification Models' AUCs 77

Supplemental Table S3.2: Inclusion Criteria for All Cohorts 100

Supplemental Table S3.3: Specific Diagnostic Groups in the Clinical Cohort – Definitions and Group Size 101

Supplemental Table S3.4: Imaging Acquisition Details 104

Supplemental Table S3.5: Detailed Description of Centiloid Conversion 106

Supplemental Table S3.6: Age-Related Atrophy Adjustment Reduces Volumetric Correlation with Age 108

Supplemental Table S3.7: Coefficients for All Classification Models 110

Supplemental Table S3.8: Select Models' AUCs for the Specific Diagnoses in the Clinical Cohort 111

Table 4.1: Demographics 125

Table 4.2: Group Differences by Race and Stroke Status 132

Supplemental Table S4.1: Demographics When Stroke is Defined by Radiologic Presence of Infarct 142

Supplemental Table S4.2: Group Differences by Race and Stroke Status When Stroke is Defined by Radiologic Presence of Infarct 144

Supplemental Table S4.3: Baseline Data of Acute Stroke Participants with and without Follow-Up 146

Supplemental Table S4.4: Baseline Data of Acute Stroke Participants By CDR at 1 Year Follow-Up 148

Table 5.1: Demographics and WMH Summary Measures 166

Table 5.2: Model Preprocessing Optimization 174

Supplemental Table S5.1: Demographics and WMH Summary Measures in the Training Cohort 180

Supplemental Table S5.2: Demographics and WMH Summary Measures in the Test Cohort 181

Supplemental Table S5.3: WMH Linear Models with Amyloid, *APOE4*, and MMSE 186

Supplemental Table S5.4: Accuracy Metrics for All Model with the 2x Case Weights 188

List of Abbreviations

AA: African American

AD: Alzheimer disease

Adj: Adjusted for age-related atrophy

ADNI: Alzheimer's Disease Neuroimaging Initiative

ADRC: Alzheimer Disease Research Center

ANOVA: Analysis of variance

APOE4: Apolipoprotein E ε4

ARIA: Amyloid-related imaging abnormalities

AUC: Receiver operating characteristic's area under the curve

BMI: Body mass index

CAA: Cerebral amyloid angiopathy

CDR™: Clinical Dementia Rating™

CI: Confidence interval

CN: Cognitively normal

CSF: Cerebrospinal fluid

CV: Cortical volume

DIAN: Dominantly Inherited Alzheimer Network

FDG: [^{18}F]-fluorodeoxyglucose

FLAIR: Fluid attenuated inversion recovery

HbA1c: Hemoglobin A1c

HCV: Hippocampal volume

HIPAA: Health Insurance Portability and Accountability Act

MCI: Mild cognitive impairment

MDC: Memory Diagnostic Center

MMSE: Mini Mental State Exam

MNI152: Montreal Neurosciences Institute 152 atlas

MPRAGE: Magnetization-prepared, rapid gradient-echo

MRI: Magnetic resonance imaging

N/A: Not applicable

NHW: Non-Hispanic White

NIA: National Institute on Aging

NIH: National Institutes of Health

NIHSS: National Institutes of Health Stroke Scale

OASIS: Open Access Series of Neuroimaging Studies

PCAD: Preclinical Alzheimer disease

PET: Positron emission tomography

PIB: [^{11}C]-Pittsburgh Compound B

ROI: Region of interest

SARA: Select Atrophied Regions in Alzheimer disease

SD: Standard deviation

SE: Standard error

SUVR RSF: Standard uptake value ratio (regional spread function applied)

SV: Subcortical volume measure

T: Cortical thickness measure

TOAST: Trial of Org 10172 in Acute Stroke Treatment

WMH: White matter hyperintensities

Acknowledgments

I, of course, need to start off by acknowledging my mentors, Drs. Tammie Benzinger and Joshua Shimony. Tammie was my primary mentor and provided so much support to help me grow as a scientist. She was always there to help provide direction and insight, while also allowing me the freedom to pursue what I found interesting. Her incredible breadth of knowledge meant I always came out of our meetings having learned something new. Josh as my co-mentor was also essential to my success. He was always willing to offer feedback on my newest draft, or just sit down and chat. He helped me troubleshoot and understand what I was seeing in my results. Most importantly though, was the emotional support I received from both Tammie and Josh. While my time at Washington University was amazing, I also struggled a lot as I tried to complete my PhD. Without the understanding and support from Tammie and Josh, I would not have made it to this point. They were able to convince me to keep going and finish my PhD, and their support did not waver when I decided my career plans included leaving academia.

I would also like to thank the rest of the Benzinger lab. While the Benzinger lab is much larger than the average lab, each person is absolutely essential. None of my studies would have been possible without the coordinators and processing team working together to get us the data we need for these studies. I also need to add a special thanks to Dr. Brian Gordon, who provided lots of help, insight, and knowledge of the Alzheimer field and Knight ADRC studies. All of the data in my dissertation comes from human studies, which is different from most dissertations in the Division of Biological and Biomedical Sciences. As such, an extra big thank you goes out to the participants in the various research studies that provided me with the data used in these analyses. I used data from over 2000 volunteers from the Knight Alzheimer Disease Research

Center (ADRC), the Dominantly Inherited Alzheimer's Network (DIAN), the Alzheimer's Disease Neuroimaging Initiative (ADNI), the Open Access Series of Neuroimaging Studies (OASIS), and patients from the Memory Diagnostic Center at Washington University in St. Louis, the Barnes-Jewish Hospital Stroke Registry, and from St. John's Mercy Medical Center Stroke Service.

Finally, I would like to thank my friends and family, those who supported me through this difficult journey. While my mentors helped me keep going despite the challenges, my friends at Washington University were the ones that showed me I was not the only one having difficulties. It is much easier to face difficulties together, whether they are from the Covid-19 pandemic or the general troubles of graduate school, than to struggle alone. While my family was less familiar with the PhD process, they were always supportive and proud of me, believing in me even when I did not.

Lauren N. Koenig

Washington University in St. Louis

December 2021

ABSTRACT OF THE DISSERTATION

Influence of Aging and Cerebrovascular Disease on Neuroimaging Measures of Alzheimer Disease

for Arts & Sciences Graduate Students

by

Lauren Nicole Koenig

Doctor of Philosophy in Biology and Biomedical Sciences

Neurosciences

Washington University in St. Louis, 2021

Professor Tammie L.S. Benzinger, Chair

Professor Joshua S. Shimony, Co-Chair

The overall goal of this dissertation is to gain a better understanding of how Alzheimer disease relates to normal aging and cerebrovascular disease to impact neuroimaging measures in a clinically meaningful way. Both aging and cerebrovascular disease are known to influence measures of Alzheimer disease, making it difficult to separate what changes are attributable specifically to Alzheimer disease. We hypothesize that a better understanding of these relationships will allow future studies to appropriately take these factors into account. In Chapters 2 and 3 we attempt to separate out the influences of normal aging and Alzheimer disease on measures of atrophy. In Chapter 2 we show that non-linear, region-specific patterns of atrophy occur with aging, but we are not able to detect additional atrophy occurring in preclinical Alzheimer disease. Thus, preclinical Alzheimer disease is likely not confounding aging research so long as careful cognitive screening of the participants is done. In Chapter 3 we show that controlling for the age-related atrophy we describe in Chapter 2 does not improve volumetric

prediction of symptomatic Alzheimer disease, likely because age-related atrophy contributes to symptoms. Despite this, volumetric predictions were still useful in detecting symptomatic Alzheimer disease in research cohorts and in patient populations. In Chapters 4 and 5 we change focus to vascular dementia, examining if cerebrovascular disease develops independently or synergistically with Alzheimer disease. In Chapter 4 we find that preclinical Alzheimer disease is not more prevalent, and thus is not a risk factor, in stroke nor in post-stroke dementia. Finally, in Chapter 5 we find that patterns of white matter hyperintensities, as a reflection of small vessel disease, have greater volumes in symptomatic Alzheimer disease relative to normal aging and preclinical Alzheimer disease. However, white matter hyperintensities could not distinguish normal aging from preclinical Alzheimer disease, leaving it unclear if white matter hyperintensities develop as a later part of Alzheimer disease or simply co-occur and have an additive effect on cognition.

Chapter 1: Introduction

1.1 Alzheimer Disease Continuum

It was around a century ago that Alzheimer disease (AD) was first discussed as a distinct form of dementia. Alois Alzheimer used recent developments in histological techniques to visualize the pathologies in the brain of the recently deceased Auguste Deter. The buildup of amyloid and tau he described are still used today to define and characterize AD. Other post mortem studies were done to follow up on Alzheimer's work, such as Robert Katzman's work in 1976 that clarified that the early-onset (presenile) dementia that Alzheimer specifically saw had the same histopathological characteristics as the more common senile AD (Bondi et al., 2017), However, much of the early research on AD instead focused on studying the symptomatic presentation of the disease. This type of research improved our understanding of the cognitive impacts of AD and allowed diagnostic criteria for AD dementia to be revised and standardized. Even after these improvements, clinical diagnosis of AD remains challenging; symptom presentation in AD can vary widely and overlaps with other disorders. Current diagnostic criteria allow at best a clinical diagnosis of AD dementia to match histopathologic diagnosis in 80% of cases (Beach et al., 2012).

This problem is compounded in the prodromal stages of AD. Studies had found that people with apolipoprotein E ε4 (*APOE4*) alleles were not only at an increased risk for developing AD (Katzman and Kawas, 1994; Strittmatter et al., 1993), but also showed greater cognitive decline in those who did not meet clinical diagnostic criteria for dementia (Bondi et al., 1999, 1995; Reed et al., 1994). While some researchers had previously argued the importance of studying the early stages of AD, the fact that *APOE4* impacted cognition in people before they

were at the level considered ‘dementia’ emphasized this point. This prodromal stage of AD was termed mild cognitive impairment (MCI). MCI was originally used as a distinct diagnosis of mild dementia; it was not specific to AD as it did not specify etiology. As more research was done on MCI in the 2000s, it was demonstrated that amnestic MCI indicates prodromal AD in most cases and so is part of AD (Petersen and Morris, 2005).

Even as MCI became the hot topic in AD research, others argued we should be looking even earlier in the disease course. In contrast to prodromal AD where there is some impairment but not enough to qualify as dementia, preclinical AD refers to the period where an individual does not express cognitive symptoms but does show molecular changes in the brain. Preclinical AD is indicated by the buildup of amyloid, and was originally reported in neuropathology studies (Morris et al., 1996). As biomarkers continued to be refined and developed, we became able to detect preclinical AD in living people. Amyloid can now be detected with positron emission tomography (PET) imaging or cerebrospinal fluid (CSF) analysis. Other biomarkers have been developed that complement these. Similar to amyloid, tau proteins can now also be measured with PET imaging or CSF analysis. [18F]-fluorodeoxyglucose (FDG) PET can measure metabolic changes, while magnetic resonance imaging (MRI) can measure tissue atrophy, changes in neural response, and vascular pathology.

Unlike the prior post mortem studies, these biomarkers can be used at any time in the disease course, not just at time of death. These biomarkers made longitudinal studies of pathology possible, and also led to a large increase in the amount of cross-sectional data available. This increase in data substantially increased the support for the amyloid cascade hypothesis of AD (Hardy and Higgins, 1992). The amyloid cascade hypothesis lays out a series

of pathologic changes in AD, proposing that brain amyloidosis leads to tau tangles, which in turn leads to neurodegeneration, which then finally causes cognitive impairment (Jack et al., 2010). This model has been updated over the years and expanded with new biomarkers (Figure 1.1) (Jack et al., 2013). While the original cascade model was a hypothesis based on disparate data, longitudinal studies from the Dominantly Inherited Alzheimer Network (DIAN) have shown data in autosomal dominant AD supporting this serial change in biomarkers (Figure 1.2) (Bateman et al., 2012; McDade et al., 2018).

Figure 1.1: Revised AD Cascade Model (Jack et al., 2013)

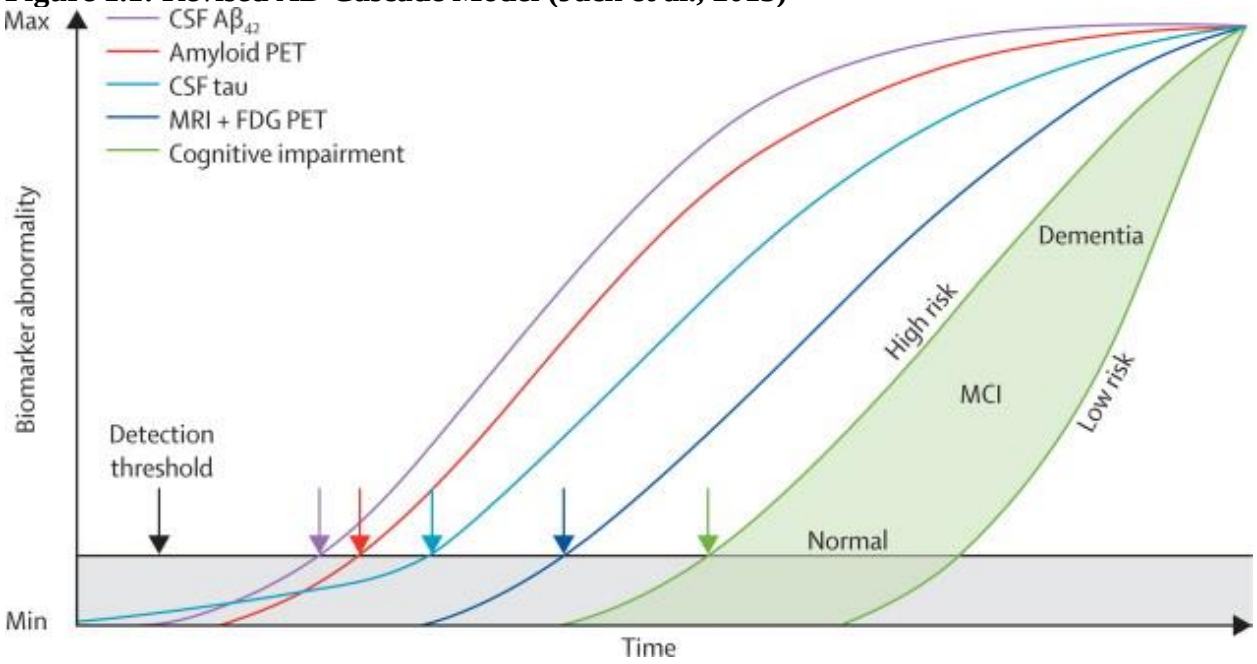

Figure 1.2: AD Cascade in DIAN (Bateman et al., 2012)

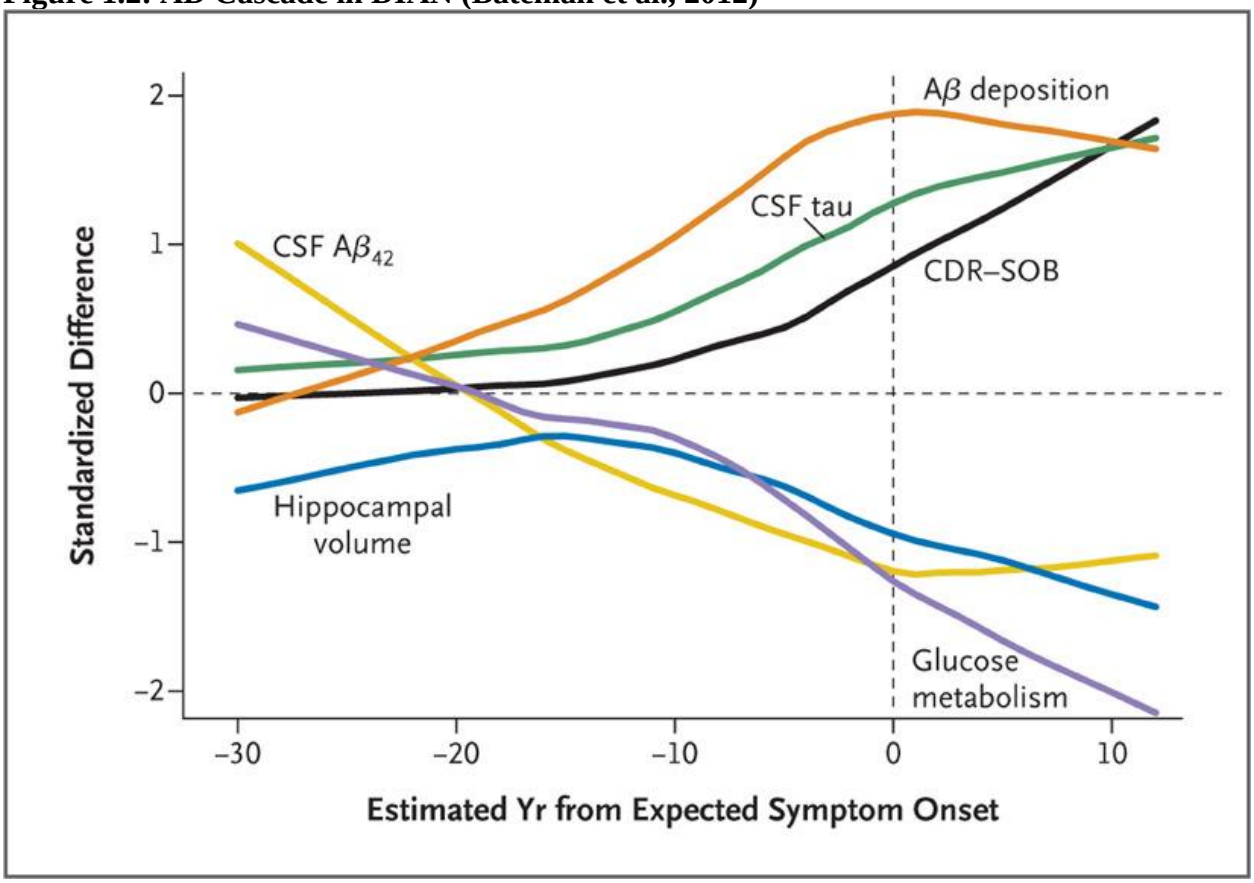

In 2011, the National Institute on Aging (NIA) codified the preclinical stage of AD, included biomarker data as part of the diagnostic criteria (McKhann et al., 2011). This was a fairly new step as the first outline of biomarkers to diagnose AD was seen just a few years earlier (Dubois et al., 2007). By incorporating biomarkers and not just relying on symptom presentation, a shift began towards a more biological definition of AD. This was outlined most clearly in 2018 through the now widespread A/T/N framework (Jack et al., 2018). While this framework was specifically described as a research definition of AD and not a clinical definition, it used amyloid and tau pathology to clearly define what should be considered part of AD (Figure 1.3).

This new A/T/N framework did not go against the biomarker cascade hypothesis, but shifts it into language describing the 'AD continuum' and emphasizes how multimodal biomarkers should be used to best diagnose AD. By describing AD as a 'continuum' it also reinforced that the cutoffs we use to define the various stages of AD are artificial. This is less problematic in some biomarkers that increase quickly at a certain point in the disease, but makes defining amyloid positivity difficult as it gradually rises over a decade. It is important to note that amyloid is used to determine who is on the AD continuum, but is not necessarily credited as the primary cause of the disease. It is seen as an early marker but not necessarily causal to the changes that follow.

While imperfect, the AD continuum framework allows us to use amyloid biomarkers to separate those with and without Alzheimer pathology. Throughout the work in this dissertation, amyloid is used in this way to define those who are in the Alzheimer continuum, with cognitive impairment further splitting those with amyloid into those who are in the preclinical AD stage and those who are in the symptomatic AD stage. This is done with the acknowledgement that

both of these groups are heterogeneous, and that cross-sectional data does not indicate which preclinical AD participants will become symptomatic in the near future.

Figure 1.3: A/T/N Framework (Jack et al., 2018)

<table>
<tr><th>AT(N) profiles</th><th colspan="2">Biomarker category</th></tr>
<tr><td>A-T-(N)-</td><td colspan="2">Normal AD biomarkers</td></tr>
<tr><td>A+T-(N)-</td><td>Alzheimer's pathologic change</td><td rowspan="4">Alzheimer's continuum</td></tr>
<tr><td>A+T+(N)-</td><td>Alzheimer's disease</td></tr>
<tr><td>A+T+(N)+</td><td>Alzheimer's disease</td></tr>
<tr><td>A+T-(N)+</td><td>Alzheimer's and concomitant suspected non Alzheimer's pathologic change</td></tr>
<tr><td>A-T+(N)-</td><td colspan="2">Non-AD pathologic change</td></tr>
<tr><td>A-T-(N)+</td><td colspan="2">Non-AD pathologic change</td></tr>
<tr><td>A-T+(N)+</td><td colspan="2">Non-AD pathologic change</td></tr>
</table>

1.2 Atrophy in Aging and Preclinical AD

The developments described in the previous section have led to broad impacts not just in Alzheimer research, but in the field of aging. Due to the newness of our understanding of preclinical AD and the limited tools available to detect it, many prior studies of aging did not take preclinical AD into account. While preclinical AD does not have as extensive an impact on the brain as later stages of AD, it can have an inordinate impact on normal aging studies. This is due to the high prevalence of preclinical AD in elderly populations; we now know that over a third of adults develop preclinical AD by age 70 (Jack et al., 2018, 2014). The confounding effects of preclinical AD on normal brain aging have previously been shown in resting-state functional MRI and neuropsychological measures: increasing standard deviations and clouding the difference between symptomatic AD and cognitively normal controls (Brier et al., 2014b; Hassenstab et al., 2016; Jack et al., 2014). Figure 1.4 shows how functional connectivity, a measure derived from resting state functional MRI, can appear to have age-related changes when the changes are actually driven by the preclinical AD participants (red line) as opposed to the amyloid negative participants (black line).

Figure 1.4: Impact of Preclinical AD on Functional Connectivity Measures (Brier et al., 2014b)

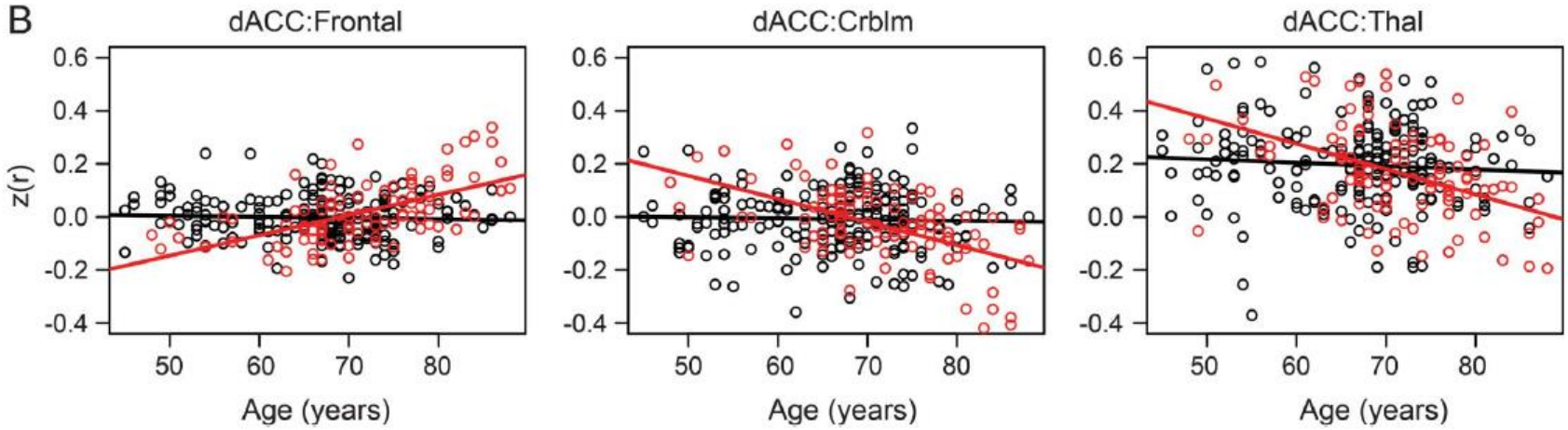

Extensive prior work has shown atrophy associated with normal aging, along with regional variability and inter-individual differences in trajectories (Irwin et al., 2018; Lockhart and DeCarli, 2014; Raz et al., 2010, 2005). However, there is limited understanding of the impact of undetected Alzheimer pathology on studies of age-related atrophy. These studies have used either measures of amyloid pathology or longitudinal tracking to ensure no cognitive impairment develops (Armstrong et al., 2019b; Fjell et al., 2014a, 2014b, 2013a; Knopman et al., 2013). However, sample sizes were small in these studies and studies could not screen for preclinical AD using both measures of amyloid and longitudinal tracking simultaneously. As such, it has not yet been established how age-related atrophy behaves in a cohort not confounded by preclinical AD, limiting our understanding of how aging impacts the brain. It is important we understand how these measures of cerebral atrophy relate to aging due to the strong association of atrophy with cognitive decline, even in the context of no known neurodegenerative disease (Armstrong et al., 2020; Fletcher et al., 2018b).

In Chapter 2, we use cognitively normal controls from AD studies to screen for preclinical AD. Using this screened cohort, we describe the spatial pattern of age-related atrophy without preclinical AD's confounding effect, furthering our understanding of aging. In addition to examining the amount of atrophy, we also examine the pattern across the lifespan in order to take into account the non-linearity in atrophy that some previous studies have reported (Irwin et al., 2018; Lockhart and DeCarli, 2014). We will also assess the need to control for other factors that may confound measures of atrophy such as sex (Armstrong et al., 2019b; Chételat et al., 2010; Jack et al., 2015; Lockhart and DeCarli, 2014; Wang et al., 2019) and *APOE4* status (Armstrong et al., 2019a; Erten-Lyons et al., 2013; Irwin et al., 2018; Kelly et al., 2018; Mishra et al., 2018; Raz et al., 2010; Smith et al., 2012). Finally, we directly assess how our normal

aging cohort differs from preclinical AD, determining to what extent prior volumetric studies of aging are confounded by this undetected preclinical AD.

1.3 Atrophy in Clinical Diagnosis of AD

While atrophy differences between normal aging and preclinical AD has not been established, atrophy in symptomatic AD has been well characterized. Despite the extensive research in this area, the use of quantitative biomarkers of atrophy in clinical practice is still limited. Typical AD-specific biomarkers rely on in vivo detection and quantification of amyloid-β and tau, AD's hallmark proteins. This molecular analysis requires CSF analyses or PET imaging, which are limited by expense and inaccessibility. Additionally, PET imaging has risks associated with radioactivity, while lumbar punctures include risks of back pain, post-dural puncture headache, and bleeding (Duits et al., 2016). In comparison MRI is non-invasive, well tolerated by patients, and is already included as standard of care in the United States for diagnostic evaluation of patients with new cognitive complaints (Knopman et al., 2001). However, the numerous benefits of MRI are offset by the fact that current volumetric MRI measures do not reach the same level of specificity as amyloid and tau biomarkers. Current MRI biomarkers approach the accuracy of PET and CSF biomarkers in separating AD from unimpaired individuals (Frisoni et al., 2010; Morris et al., 2016), but cannot maintain this accuracy in cohorts comprising patients with various causes of dementia (Wollman and Prohovnik, 2003) in the same way amyloid biomarkers can (Figure 1.5) (Ossenkoppele et al., 2018b).

Figure 1.5: Receiver Operating Characteristic Analyses for Distinguishing Alzheimer Disease (AD) Dementia and Mild Cognitive Impairment (MCI) Due to AD From Non-AD Neurodegenerative Disorders (Ossenkoppele et al., 2018a)

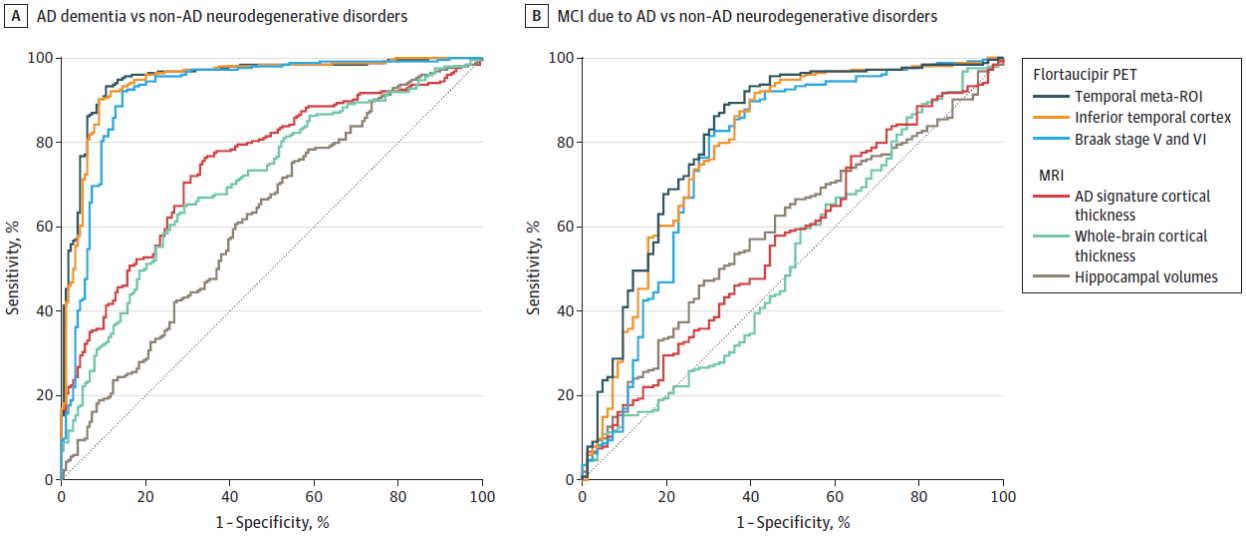

Biomarkers are useful in clinical practice, helping to narrow the differential diagnosis and refine the treatment of dementia patients (Rabinovici et al., 2019). In AD clinical trials, biomarkers can improve accuracy, utility, and cost effectiveness of screening, and can assess response to investigational therapies (Jack et al., 2018; Sevigny et al., 2016; Sperling et al., 2014). The value of AD biomarkers is expected to further increase as AD-modifying therapies are realized, such as the recent approval of Aducanumab by the United States Food and Drug Administration, which will create a need and rationale for population level screening and an influx of patients requiring timely diagnosis and treatment (Dunn et al., 2021; Liu et al., 2017). If MRI-based biomarkers could be improved, it would be of immense clinical benefit as it would fulfill the need for an accessible, AD-specific biomarker that can be applied in broad clinical populations.

It is likely that MRI-based biomarkers are confounded by age-related brain atrophy or other undetected co-pathologies attributed to aging such as vascular disease (Fotenos et al., 2005). Controlling for these confounds may be one method to improve MRI-based biomarkers of AD. In Chapter 3 we investigate if controlling for the age-related atrophy we describe in Chapter 2 can be used to improve a volumetric classification model of symptomatic AD. Previous studies on volumetric classification of AD have indicated the hippocampus, temporal lobes, amygdala, parahippocampal gyrus, middle temporal gyrus, entorhinal cortex and insula as the most important gray matter regions for the classification of AD (Mateos-Pérez et al., 2018a). However, we use an unbiased, data-driven approach to determine which regions are most important to classifying AD so that our model is optimized for our intended use. Many previous studies have used machine learning for similar imaging-based AD diagnostic problems, but simpler regression models have matched them in accuracy (Mateos-Pérez et al., 2018a). As such,

we focus on validating a simple to understand and freely available algorithm that is easier for doctors and patients to trust and to implement. We then compare models that have and have not been adjusted for age-related atrophy in both a research cohort and a cohort of patients from a local dementia clinic with a variety of diagnoses. By using these differing cohorts, we will get a better idea of how the algorithm performs in different environments.

1.4 Interplay of AD, Stroke, and Race

Chapters 2 and 3 focus on the interplay of AD and normal aging, but other factors are also able to confound our understanding of AD. Outside of AD, the most common pathology seen in the aging brain is cerebrovascular disease. Part of what we described as age-related atrophy in previous chapters may in fact be caused by undetected cerebrovascular disease. It is still unclear to what extent pathologies in AD and in vascular dementia (dementia resulting from cerebrovascular disease) are interacting, but the prevalence of combined AD and vascular dementia is greater than it should be if AD and cerebrovascular disease are fully independent (Armstrong, 2019). It is possible that mild AD and vascular dementia are independent but their additive pathologies make it more likely for the patient to be diagnosed. Alternatively, they could be interacting more directly, such as if vascular disease accelerates the development of AD. This second theory is a variation on the two-hit vascular hypothesis of AD, which posits that an initial cerebrovascular ‘hit’ leads to a second amyloid ‘hit’ which then causes AD dementia (Nelson et al., 2016; Sweeney et al., 2015; Zlokovic, 2011).

One type of vascular dementia where this debate plays out is post-stroke dementia. Many older adults who have had a stroke develop dementia within a year of their stroke, with a hazard ratio for patients with prevalent strokes of 1.69 (Heiss et al., 2016). Diagnosis of this post-stroke dementia is correlative, based on the temporal relation to stroke, with many possible

etiologies (Skrobot et al., 2018). One of those many possible etiologies is AD. It has been hypothesized that post-stroke dementia is caused by a stroke accelerating the development of AD in those who already had preclinical AD.

In Chapter 4 we determine the interplay of stroke and pre-existing preclinical AD using amyloid biomarkers in a cohort of acute stroke patients. Due to our community-based sampling of stroke patients, our cohort is diverse enough to also investigate racial disparities in stroke. It is important to examine racial differences in this cohort as both AD and stroke have known racial disparities, but their interaction is unclear. Past abuses have led to an understandable hesitance for minorities to participate in research, making it difficult to rectify our lack of understanding in these areas (Hooper et al., 2019). The studies that have begun to address racial disparities have found a higher incidence of AD and of stroke in the Black population relative to the non-Hispanic White (NHW) population.

Black individuals are not only twice as likely to have a stroke (Benjamin et al., 2017), but are more likely to die from their stroke (Yang et al., 2017). These racial differences have primarily been explained by differences in stroke risk factors such as higher rates of hypertension and diabetes, and lower socio-economic status and education. Similar disparities are seen in AD, with most studies showing higher rates of dementia, and specifically higher rates of pathology-confirmed AD, in Black individuals (Neill R. Graff-Radford et al., 2016; Green, 2002; Mayeda et al., 2016, p. 201; Tang et al., 2001). These differences have also been explained by higher rates of risk factors, especially *APOE4* as the most prevalent genetic risk factor for AD (Neill R. Graff-Radford et al., 2016). Papers reporting no racial differences in AD are often those that have controlled for baseline racial differences in education, cognitive scores, and *APOE4* (Brickman et al., 2008; Fillenbaum et al., 1998; Annette L. Fitzpatrick et al., 2004; John C.

Morris et al., 2019; Riudavets et al., 2006a). In Chapter 4 we will investigate the relationship between preclinical AD and post-stroke dementia, as well as how any racial differences impact this relationship.

1.5 White Matter Hyperintensities in AD

Other types of vascular pathology, such as the white matter hyperintensities (WMH) seen in small vessel disease can also lead to vascular dementia (Bos et al., 2018; Wardlaw et al., 2019). However, WMHs are common in old age even without accompanying symptoms (Alber et al., 2019), and have a complicated relationship to cognitive symptoms (van den Berg et al., 2018; Vargas-González and Hachinski, 2019). Similar to the two-hit hypothesis described in section 1.4, it is unclear if WMHs are an aspect of AD or if they simply co-occur and have an additive effect on the brain (Koncz and Sachdev, 2018). With this second possibility, WMHs below the level of vascular dementia may still impact the expression of AD – worsening the impairment from what would have been experienced in the absence of cerebrovascular disease.

With the addition of vascular pathology, preclinical AD or very mild AD may have symptoms exacerbated enough to be considered symptomatic AD. This would explain the association of WMHs with other types of dementia, including AD (Bos et al., 2018; Joki et al., 2018). This is supported by studies showing that WMHs do not impact cognitive progression in AD (Eldholm et al., 2018), but do associate with conversion from normal cognition to MCI (Bangen et al., 2018a). A 2017 review suggests amyloid and WMHs are independent yet additive (Roseborough et al., 2017), but a more recent paper showed amyloid PET correlated with a periventricular pattern of WMHs in non-demented older adults, and that part of this relationship is due to cerebral amyloid angiopathy (CAA) (Graff-Radford et al., 2019).

There is even greater evidence of a direct interaction in dominantly inherited AD, where WMH volumes have been shown to begin increasing approximately 6 years before expected symptom onset (Joseph-Mathurin et al., 2021; Lee et al., 2016). This suggests that WMHs arise as a part of dominantly inherited AD and not through a comorbid disease. This type of longitudinal study has not been replicated in sporadic AD, and it is still unclear if WMHs are different in the preclinical stage. If WMHs are developing even in the preclinical stage of AD, this would support the idea that the greater volume of WMHs in AD is directly caused by AD even in sporadic cases of AD. It would disprove the theory that the higher prevalence of WMHs in symptomatic AD is fully explained by the fact that co-occurring pathologies are more likely to be diagnosed.

In Chapter 5, we will use machine learning to examine if WMHs in preclinical AD participants are distinct from cognitively normal controls in amount or pattern. As part of this study, we will use machine learning. Machine learning has been used extensively in the field of radiology and allows more complex patterns and relationships to be examined (Mateos-Pérez et al., 2018a). As shown in Figure 1.6, classification algorithms can detect group differences, especially in heterogeneous groups, that are missed by traditional statistics. By combining statistics with machine learning we will have the greatest chance of uncovering a relationship if it does exist. To otherwise increase the likelihood of us detecting this relationship, we will examine patterns of WMHs within pre-determined white matter regions that previous work has associated with amyloid (Phuah et al., 2019). By looking at these specific regions in the brain, we will have fewer ‘noise’ voxels that could obscure group differences. We will also be able to better assess if specific patterns of WMHs differ in AD, as opposed to simply the overall WMH volume. Prior studies have suggested spatial patterns of WMHs are important, especially on the

difference between periventricular and subcortical WMHs, but there is not yet a consensus (Alber et al., 2019).

If we are able to separate preclinical AD from controls, it would suggest that the pathological processes of AD are directly causing the increase in WMHs, advancing our scientific understanding of these two disease processes. Conversely, if the difference in WMHs is only seen at the level of symptomatic AD, it may be that the two pathologies are simply co-occurring and their combined impact on the brain is leading to dementia. In the chapters that follow, we will explore measures of atrophy and cerebrovascular disease in both preclinical and symptomatic AD. We will determine the specific spatial patterns these different pathologies show in these different contexts, and search for evidence supporting or rejecting the independence of vascular pathology and AD.

Figure 1.6: Statistical Group Differences vs. Classification Ability (Arbabshirani et al., 2017)

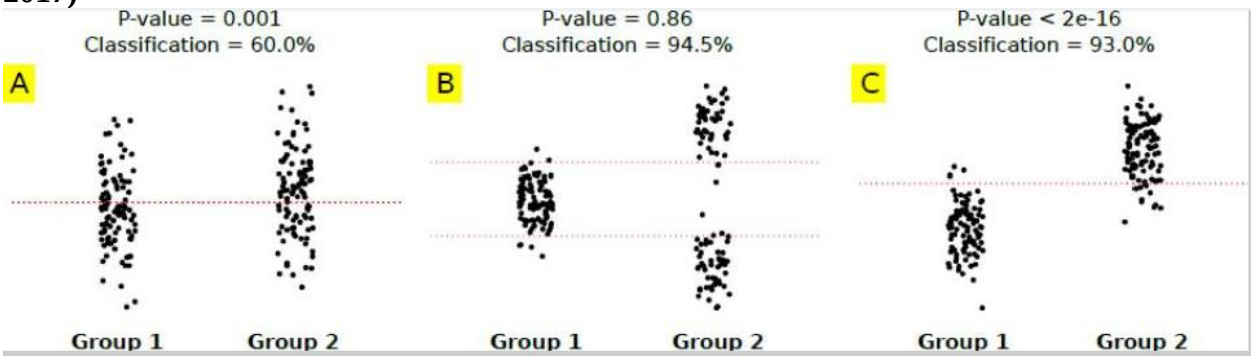

Chapter 2: Regional Age-Related Atrophy After Screening for Preclinical Alzheimer Disease (Koenig et al., 2022)

Brain atrophy occurs in aging even in the absence of dementia, but it is unclear to what extent this is due to undetected preclinical Alzheimer disease. Here we examine a cross-sectional cohort (ages 18-88) free from confounding influence of preclinical Alzheimer disease, as determined by amyloid PET scans and three years of clinical evaluation post-imaging. We determine the regional strength of age-related atrophy using linear modeling of brain volumes and cortical thicknesses with age. Age-related atrophy was seen in nearly all regions, with greatest effects in the temporal lobe and subcortical regions. When modeling age with the estimated derivative of smoothed aging curves, we found that the temporal lobe declined linearly with age, subcortical regions declined faster at later ages, and frontal regions declined slower at later ages than during midlife. This age-derivative pattern was distinct from the linear measure of age-related atrophy and significantly associated with a measure of myelin. Atrophy did not detectably differ from a preclinical Alzheimer disease cohort when age ranges were matched.

2.1 Introduction

Older adults constitute an increasingly large fraction of our society, making research on brain aging important for public health. Cerebral atrophy associated with aging is in particular a concern due to its association with cognitive decline, independent of known neurodegenerative diseases (Armstrong et al., 2020; Fletcher et al., 2018b). Previous studies have shown regional variability and non-linear changes in this atrophy occurring with age. In general, these studies show the strongest atrophy in frontal and temporal regions, and a pattern of accelerated atrophy in temporal regions (Irwin et al., 2018; Lockhart and DeCarli, 2014). It has been hypothesized

that these non-linear regional patterns may in part be due to mid-life increases in cerebral myelination causing the appearance of reduced gray matter density (Irwin et al., 2018). However, myelin may also be acting as a proxy for other regional properties of the brain such as intracortical circuit complexity and aerobic glycolysis levels (Glasser et al., 2014).

Measures of age-related atrophy are complicated by abundant confounding factors inherent within studies of aging. One major factor is cardiovascular disease, with atrophy correlating with WMHs (Coutu et al., 2017; Habes et al., 2021), high blood pressure (Armstrong et al., 2019a; Lockhart and DeCarli, 2014), and diabetes (Hamed, 2017; Suzuki et al., 2019). Some studies indicate sex or gender differences in age-related atrophy, with greater atrophy in men for select regions (Armstrong et al., 2019b; Chételat et al., 2010; Jack et al., 2015; Lockhart and DeCarli, 2014; Wang et al., 2019). Additionally, apolipoprotein E ε4 (*APOE4*) – the greatest genetic risk factor for sporadic Alzheimer disease (AD) – has also been associated with greater rates of atrophy even in the unimpaired (Armstrong et al., 2019a; Erten-Lyons et al., 2013; Irwin et al., 2018; Kelly et al., 2018; Mishra et al., 2018; Raz et al., 2010; Smith et al., 2012). A previous study has shown that this effect of *APOE4* is linked to increasing amyloid levels, indicative of preclinical AD (Mishra et al., 2018).

Preclinical AD is characterized by the absence of cognitive symptoms and the presence of parenchymal deposits of amyloid-β peptide, one of the hallmarks of AD. Despite its association with atrophy (Becker et al., 2011; Chételat et al., 2012; Dickerson et al., 2009; Fagan et al., 2009; Fjell et al., 2010; Fletcher et al., 2018a, 2016; Oh et al., 2014; Pettigrew et al., 2017; Schott et al., 2010; Storandt et al., 2009; Xie et al., 2020), preclinical AD can only be detected on an individual basis using measures of amyloid. As such, it often goes undetected in studies of aging populations and may be contaminating results. For example, screening out participants

with preclinical AD has been shown to reduce variability and age-related decline in neuropsychological tests (Hassenstab et al., 2016) and resting-state functional connectivity measures (Brier et al., 2014b). However, it is unclear if this confound extends to measures of atrophy.

Prior studies have assessed the impact of undetected Alzheimer pathology (Armstrong et al., 2019b; Fjell et al., 2014a, 2014b, 2013a; Knopman et al., 2013), using either measures of amyloid pathology or longitudinal tracking to ensure no cognitive impairment develops. However, sample sizes were small in these studies and screening used longitudinal tracking or amyloid measures separately. In this study we use cognitively normal participants from longitudinal AD studies, allowing us to screen a large cohort for preclinical AD using both amyloid positron emission tomography (PET) and longitudinal tracking of cognition in the same individuals. Using this screened cohort, we measure age-related volumetric changes across the brain that occur independent of preclinical AD.

2.2 Methods

2.2.1 Participants

The n = 383 participants in the Normal Aging cohort came from two open-source databases: Open Access Series of Imaging Studies (OASIS) (LaMontagne et al., 2019) and the Dominantly Inherited Alzheimer Network (DIAN). The n = 115 participants in the Preclinical AD cohort were all from OASIS. All procedures in this retrospective study were Health Insurance Portability and Accountability Act (HIPAA) compliant and approved by the Washington University Institutional Review Board; informed consent was gained for all participants.

Both the Normal Aging and the Preclinical AD cohorts only included participants who were evaluated as 'cognitively normal' or 'no dementia' in their clinical assessment and who had a global Clinical Dementia Rating™ (CDR™) (Morris, 1993) of 0 within 1 year of magnetic resonance imaging (MRI). The Normal Aging cohort, which has been previously described (Koenig et al., 2020), only included participants who remained CDR = 0 for a minimum of 3 years after MRI. Participants over age 45 were only included if they additionally had a negative amyloid PET scan (defined in section 2.2.4) within 1 year of their MRI. The longitudinal CDR and negative amyloid PET scan limited the possibility that the participants in the Normal Aging cohort were in the preclinical stage of AD. The Preclinical AD cohort differed from the Normal Aging cohort in that it required a positive amyloid PET scan and did not require longitudinal CDR assessment.

While the Normal Aging cohort included participants from DIAN, a study on autosomal dominant AD caused by rare mutations, only non-mutation carriers (control group) were included. DIAN was used due to its similarity to studies in the OASIS database and because DIAN has amyloid PET data available in the 45-60 age range. When compared to OASIS participants in the overlapping age range (age 42-59), there were no differences in volumetric data after multiple comparisons (see section 2.2.6 and Supplemental Table S2.1). Both OASIS and DIAN include self-reported race and gender. We use the term gender and not sex to match the terminology of the questionnaire used, but participants were offered only 'Male' and 'Female' as options and sex was not assessed separately.

2.2.2 Clinical Assessment

Experienced clinicians, blinded to amyloid status, evaluated each participant for the possibility of a clinical diagnosis of dementia, and only those considered to be cognitively

normal were included in this study. Their assessment, outlined previously (Morris et al., 2006), integrated results from a semi-structured interview conducted with the participant and a knowledgeable collateral source, a thorough neurological examination, and bedside measures of cognitive function (including Mini Mental State Exam (MMSE) (Folstein et al., 1975) among others).

2.2.3 MR Imaging

The MR imaging parameters for OASIS are approximate due to the variety of studies included. Scanner strength was primarily 3T (n = 19 were 1.5T) within OASIS, while DIAN was 3T. OASIS T1-weighted magnetization-prepared, rapid gradient-echo (MPRAGE) images primarily had 2 set of parameters. The first used TR = 2.3 s, TE = 3.16 ms, TI = 1 s, a flip angle of 8 degrees, and a spatial resolution of $1 \times 1 \times 1$ mm^3. The second used TR = 2.3 s, TE = 2.95 ms, TI = 0.9 s, a flip angle of 9 degrees, and a spatial resolution of $1 \times 1 \times 1$ mm^3 or $1 \times 1 \times 1.2$ mm^3. DIAN T1 scans had TR = 2.3 s, TE = 2.95 ms, TI = 0.9 s, a flip angle of 9 degrees, and a spatial resolution of $1 \times 1 \times 1.2$ mm^3.

Volumetric T1-weighted images underwent regional tissue segmentation with FreeSurfer (version 5.0 or 5.1 for 1.5T scans and version 5.3 for 3T scans) (Fischl, 2012). Regional volumes (cortical and subcortical) were adjusted for head size with a regression approach using intracranial volume (Buckner et al., 2004). Left and right hemispheric data were combined by summing volumes and averaging cortical thicknesses.

2.2.4 PET Imaging

[^{11}C]-Pittsburgh compound B (PIB) was used as the amyloid tracer in DIAN participants, with a dosage of ~15 mCi, and data collected 40-70 minutes post-injection. Within OASIS, 287 participants were imaging using PIB, with a dosage of ~13 mCi and data collected 30-60 minutes

post-injection. The remaining 75 participants were imaged using Florbetapir ([^{18}F]-AV45), with a dosage of ~10 mCi and data collected 50-70 minutes post-injection.

PET images were processed with an in-house pipeline (Su, 2021) using FreeSurfer-derived regions and a cerebellar cortex reference region. Signal spillover was addressed with partial volume correction, specifically with a regional spread function (geometric transfer matrix) technique based on the scanner point spread function and the relative distance between regions (Su et al., 2015, 2013). The mean cortical standard uptake value ratio with regional spread function applied (SUVR RSF) was defined as the average SUVR RSF from the precuneus, prefrontal cortex, gyrus rectus, and lateral temporal regions (Su et al., 2019).

A negative amyloid PET scan was defined as having a mean cortical SUVR RSF < 1.42 (Centiloid < 16.4) for PIB PET or SUVR RSF < 1.19 (Centiloid < 20.6) for Florbetapir PET. The Centiloid conversion process, used to more easily compare the two amyloid tracers, is documented in detail in the initial Centiloid paper (Klunk et al., 2015), with specific equations in follow-up papers (Su et al., 2019, 2018). Harmonization procedures such as this are imperfect, and so to remain as accurate as possible we used cutoffs determined individually for each tracer and then converted into Centiloid, as opposed to a unified Centiloid cutoff.

2.2.5 T1w/T2w Myelin Maps

This study uses a spatial map of the ratio of T1w/T2w image intensities in a cohort of 1071 healthy young adults (ages 22-37, mean 29) from the Human Connectome Project (Glasser and Van Essen, 2011; Glasser et al., 2014, 2016b). The original map was averaged within each region of the Desikan-Killiany atlas used by FreeSurfer to allow comparison. Prior work has shown that this ratio correlates with cerebral cortical myelin content due to differences in lipids, free and myelin-bound water, and iron content (Glasser and Van Essen, 2011).

2.2.6 Statistics

We first examined if gender, MMSE, *APOE4*, race, and education influenced linear models of each regional volume (after normalization for intracranial volume) and each cortical thickness in the Normal Aging cohort. A separate linear model was run for every factor and regional volume/thickness pairing, with a Bonferroni-Holm corrected $p < 0.05$ considered significant. Bonferroni-Holm, which progressively adapts the significance threshold, was done separately for each of the five factors, and across the 101 examined brain regions. Race in this study was self-reported and binarized to whether or not a person is non-Hispanic White (NHW) due to the strong skew towards NHW participants. As few significant correlations were observed for any of these factors, we did not include these as covariates in the remaining analyses.

We next modeled each regional volume and thickness by age. We used the resulting standardized coefficients (β-weights) to compare the strength and directionality of age-related atrophy across regions. We then addressed non-linear changes that occur with age using the estimated derivative of normal aging curves. Normal aging curves were determined by smoothing the Normal Aging cohort's data for each FreeSurfer region with a locally weighted scatter-plot smoother regression, resulting in a non-linear estimate of age-related atrophy. By correlating age with the estimated derivative at each age, we estimate the pattern of age-related atrophy across the lifespan. We display examples of these normal aging curves and their estimated derivatives in Figure 1. As these are cross-sectional data, the estimated derivative is the change in the region's smoothed average by age, not an individual participant's trajectory over time. As with the previous analysis, we again corrected each set of *p*-values for multiple comparisons across the 101 regions using Bonferroni-Holm.

The 34 β-values for each of the four resulting cortical maps (from linear models of cortical volumes or thicknesses; as predicted by age or the age-derivative) were correlated with the myelin map described above. As this is a spatial correlation, Spearman's rank correlation was used. To maintain consistency, these *p*-values were also corrected for multiple comparisons across the 4 pairings using Bonferroni-Holm.

Finally, we used linear models to assess the impact of amyloid on regional volumes and thicknesses. The Preclinical AD cohort (amyloid positive) and the participants above age 60 in the Normal Aging cohort (amyloid negative) were combined, and a linear model was run for each region using age, amyloid positivity, and their interaction. This process was also repeated by replacing the dichotomous amyloid positivity with a continuous measure of amyloid (Centiloid). Each set of *p*-values was corrected for multiple comparisons across the 101 regions using Bonferroni-Holm.

Figure 2.1: Example Regions in the Normal Aging Cohort

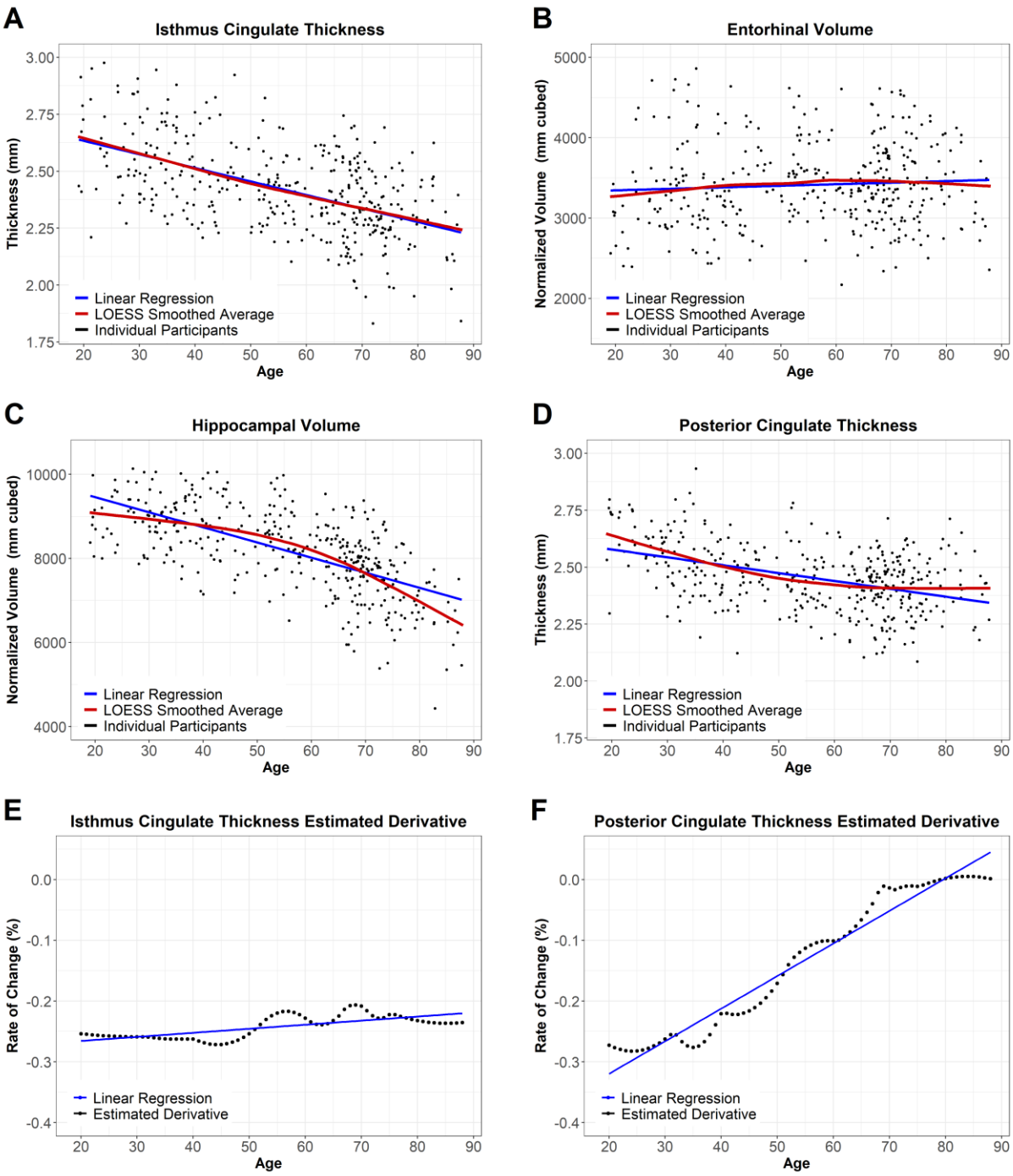

Figure 2.1 displays example normal aging curves and estimated derivative graphs. Figure 2.1a-d displays in blue the linear model whose β-weight is graphed in Figure 2.2a. In red is the loess regression, used to calculate the estimated derivative graphed in Figure 2.1e and 2.1f (for Figure 2.1a and 2.1d, respectively). The blue line in Figure 2.1e and 2.1f represents the linear model whose β-weight is graphed in Figure 2.2b.

2.3 Results

2.3.1 Demographics

Demographics for both cohorts and the subset of the Normal Aging cohort above age 60 are listed in Table 2.1. As expected, the Normal Aging cohort had a lower frequency of *APOE4* alleles and lower amyloid levels than the Preclinical AD cohort. No regions in the Normal Aging cohort showed significant associations with *APOE4* status, MMSE, or years of education, and few regions showed significant associations with gender or race after correction for multiple comparisons (Supplemental Table S2.1). As such, the later analyses did not adjust for these factors.

Significant differences by gender were observed in intracranial volume ($\beta = 0.601$, corrected $p < 0.001$), fusiform volume ($\beta = 0.200$, corrected $p = 0.008$), frontal pole volume ($\beta = 0.182$, corrected $p = 0.03$), lateral occipital volume ($\beta = 0.178$, $p = 0.04$), amygdala volume ($\beta = 0.230$, corrected $p < 0.001$), and lateral ventricle volume ($\beta = -0.197$, $p = 0.01$). Significant differences by race were in cuneus volume ($\beta = 0.186$, $p = 0.03$), inferior temporal volume ($\beta = 0.182$, $p = 0.04$), lateral occipital volume ($\beta = 0.198$, $p = 0.01$), middle temporal volume ($\beta = 0.220$, $p = 0.001$), and optic chiasm volume ($\beta = -0.195$, $p = 0.01$). In these models, a positive β weight indicates larger volumes/thicknesses in men or NHWs, respectively.

Table 2.1: Demographics

	Normal Aging Cohort	Normal Aging Cohort (Age > 60)	Preclinical AD Cohort
n	383	192	115
n by Data Source			
DIAN	134	0	0
OASIS	249	192	115
Age (median)	18-88 (60)	60-88 (70)	61-89 (74)
Gender (% M)	35.8	33.9	47.8
MMSE (median)	24-30 (30)*	26-30 (30)	23-30 (29)
APOE4 (% with an ε4 allele)	24.8	22.4	55.6
Race (% non-Hispanic White)	89.8*	89.1	90.4
Education (years) (median)	9-22 (16)	10-20 (16)	8-20 (16)
Amyloid** (median)	-9.34-19.0 (-0.880)*	-9.34-19.0 (-0.453)	16.4-141 (63.4)

* indicates missing data: 2 MMSEs, 6 Races, and 124 Amyloid (all from those under age 45) from the Normal Aging cohort

** Mean Cortical SUVR RSF in Centiloids

APOE4: Apolipoprotein E ε4; DIAN: Dominantly Inherited Alzheimer Network; MMSE: Mini Mental State Exam; OASIS: Open Access Series of Neuroimaging Studies; SUVR RSF: Standard uptake value ratio (regional spread function applied)

2.3.2 Regional Variation in Strength of Age-Related Atrophy

Almost all regions showed a significant association between atrophy and age in the Normal Aging cohort (Supplemental Table S2.2). The only non-significant regional measures were caudal anterior cingulate thickness, entorhinal volume, temporal pole volume, corpus callosum posterior volume, intracranial volume, total subcortical gray matter volume, and fifth ventricle (cavum septum pallucidum) volume. While volumetric measures of the remaining regions were significantly associated with age, the strength of that relationship varied. The strongest age effects were seen in the temporal lobe and subcortical regions (Figure 2.2a). Of the regions and composites not pictured in Figure 2.2a, summary measures such as total cortex volume and total gray matter volume also showed some of the strongest age effects (Supplemental Table S2.2).

2.3.3 Regional Variation in Non-Linear Patterns of Age-Related Atrophy

The previous section, 2.3.3, used standardized β-weights from linear models to compare the strength of the relationship between age and regional volumetrics. Select regions declined in a linear fashion. Many regions showed non-linear patterns, with atrophy appearing to accelerate or decelerate at older ages. We assessed the non-linear pattern of each region by smoothing our data to create normal aging curves and then estimating the derivative of that curve at each age. Figure 2.2.1 displays examples of these normal aging curves and the corresponding estimated derivatives, and the normal aging curves for all examined regions can be viewed interactively at https://lnkoenig.shinyapps.io/NormalAgingVolumetrics_ShinyApp/.

Almost all regions' age-derivative showed a significant association with age (Supplemental Table S2.2). The regions showing non-significant correlations of age were banks of the superior temporal sulcus thickness, fusiform thickness, and pars opercularis volume. Non-

significance in this case indicates no relationship, i.e., rate of atrophy did not change across the age range suggesting either linear decline or no atrophy with age. The strength of the association between age and the age-derivative, again represented using β-weights, is displayed spatially in Figure 2.2b and appears distinct from the age-association pattern in Figure 2.2a. Of those regions that showed the most age-related atrophy, the temporal cortex showed an overall linear decline with age, while atrophy in subcortical regions appears to accelerate with age. In contrast, frontal regions appear to show higher rates of atrophy at midlife as opposed to late life. Of the regions not pictured in Figure 2.2b, the corpus callosum stood out as a region stable at younger ages that atrophies rapidly in old age.

Figure 2.2: Regional Maps of Age-Related Atrophy

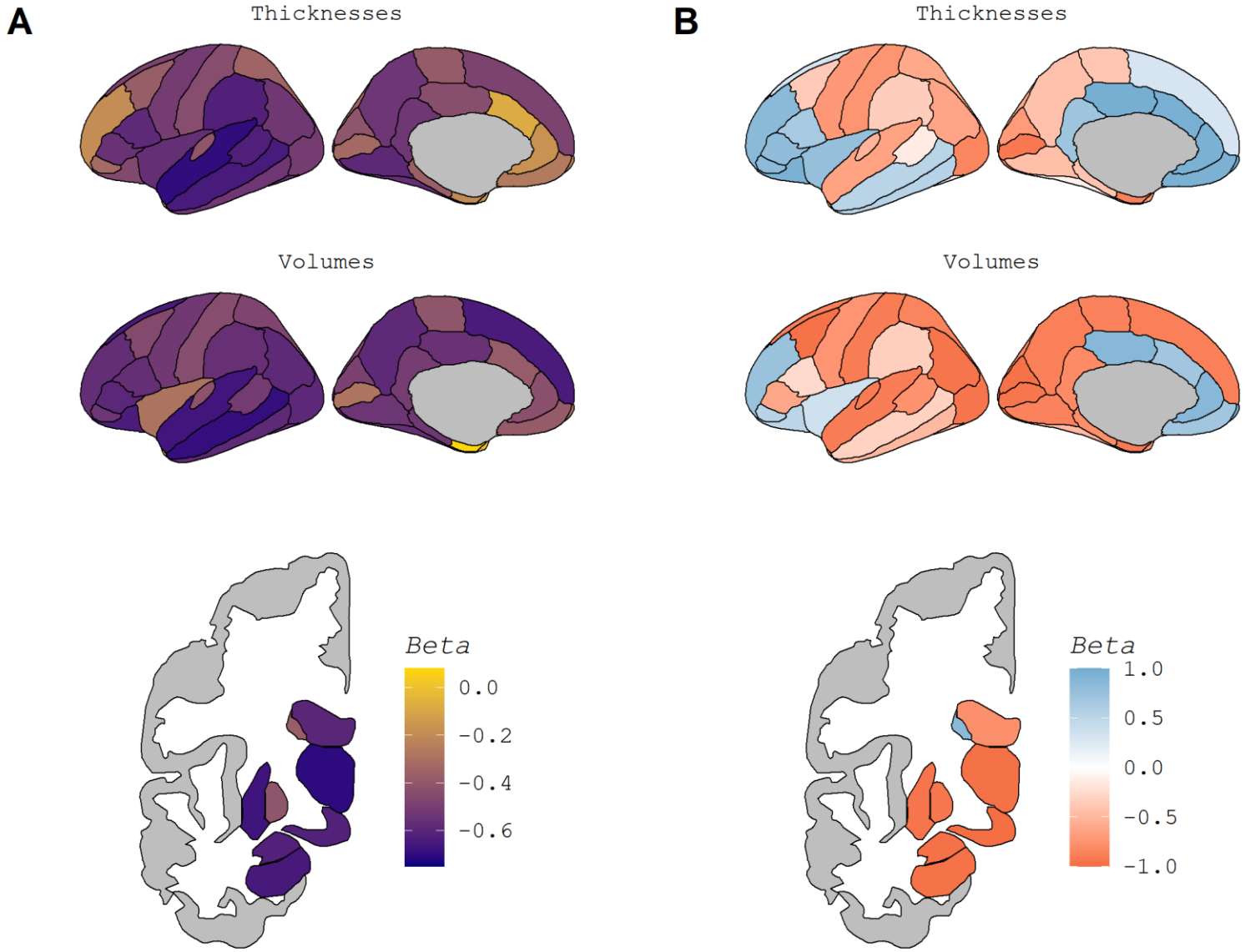

Figure 2.2 displays regional maps of the standardized β-weights from the linear models used to assess age-related atrophy. Figure 2.2a displays the overall age-effect, taken from a direct comparison of participants' ages and regional volume/thickness (blue line in Figure 2.1a-d). A darker purple indicates more atrophy with age, while yellow indicates a lack of atrophy. Figure 2.2b displays the pattern of atrophy with age, taken from the association of the age-derivative with age (blue line in Figure 2.1e-f). Blue in Figure 2.2b indicates regions whose rate of atrophy becomes less severe as age increases, while red indicates regions whose atrophy accelerates at later ages. To maintain the color schemes, the lateral ventricles are displayed with a reversed sign.

2.3.4 Relationship of T1w/T2w Myelin Content and Slope of Age-Related Atrophy

To quantify if the spatial patterns we observed in Figure 2 related to myelin levels, we correlated each set of 34 cortical β-weights in Figure 2 to an average T1w/T2w myelin map. This myelin map was generated on a separate cohort of healthy young adults (ages 22-37, mean 29) and was and is displayed in Figure 3. The regional pattern of the strength of age-related atrophy was not significantly associated with the regional map of myelin (rho = -0.060, corrected p = 0.74 for cortical volumes; rho = -0.348, corrected p = 0.09 for cortical thicknesses). However, the regional pattern of the estimated derivative βs was significantly associated with the regional map of myelin (rho = -0.640, corrected $p < 0.001$ for cortical volumes; rho = -0.546, corrected p = 0.003 for cortical thicknesses). The directionality of the correlation is such that regions with higher myelin content are more likely to follow the pattern shown in Figure 1C, with atrophy that accelerates in late life. Conversely, lower myelin regions were more likely to show the pattern in Figure 1D: atrophy greatest in midlife that tapered at older ages. While this result emphasizes the distinctness of the two patterns, the moderate correlation suggests other factors are also at play.

2.3.5 Atrophy in Preclinical AD vs. Normal Aging

The impact of amyloid was assessed using those over age 60 in the Normal Aging cohort (amyloid negative) and the Preclinical AD cohort (amyloid positive). Linear models used age, amyloid, and age × amyloid to predict regional volumes/thicknesses. No significant effects of amyloid or age × amyloid were found after accounting for age and correcting for multiple comparisons (Supplemental Table S2.3, with examples in Figure 2.4).

Figure 2.3: T1w/T2w Myelin Map in Healthy Younger Adults

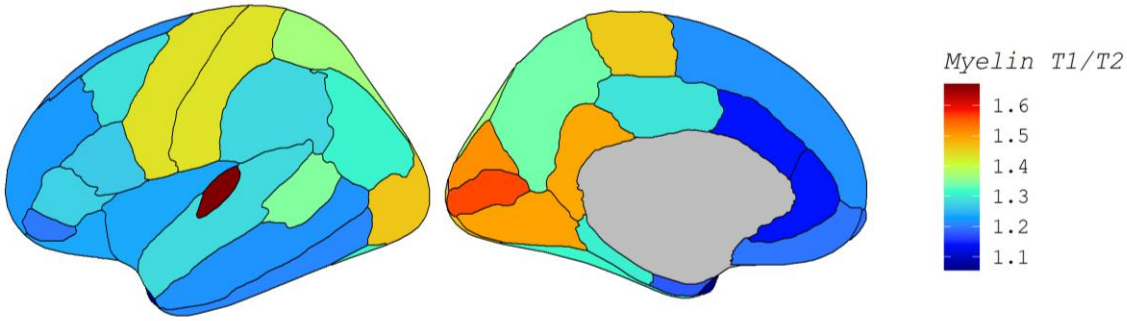

Figure 2.3 displays the cerebral cortical myelin map that was correlated with each of the four regional maps in Figure 2.2. Myelin content was measured by the ratio of T1w/T2w image intensities in a separate cohort of healthy adults.

Figure 2.4: Example Regions for Normal Aging Cohort vs. Preclinical AD Cohort

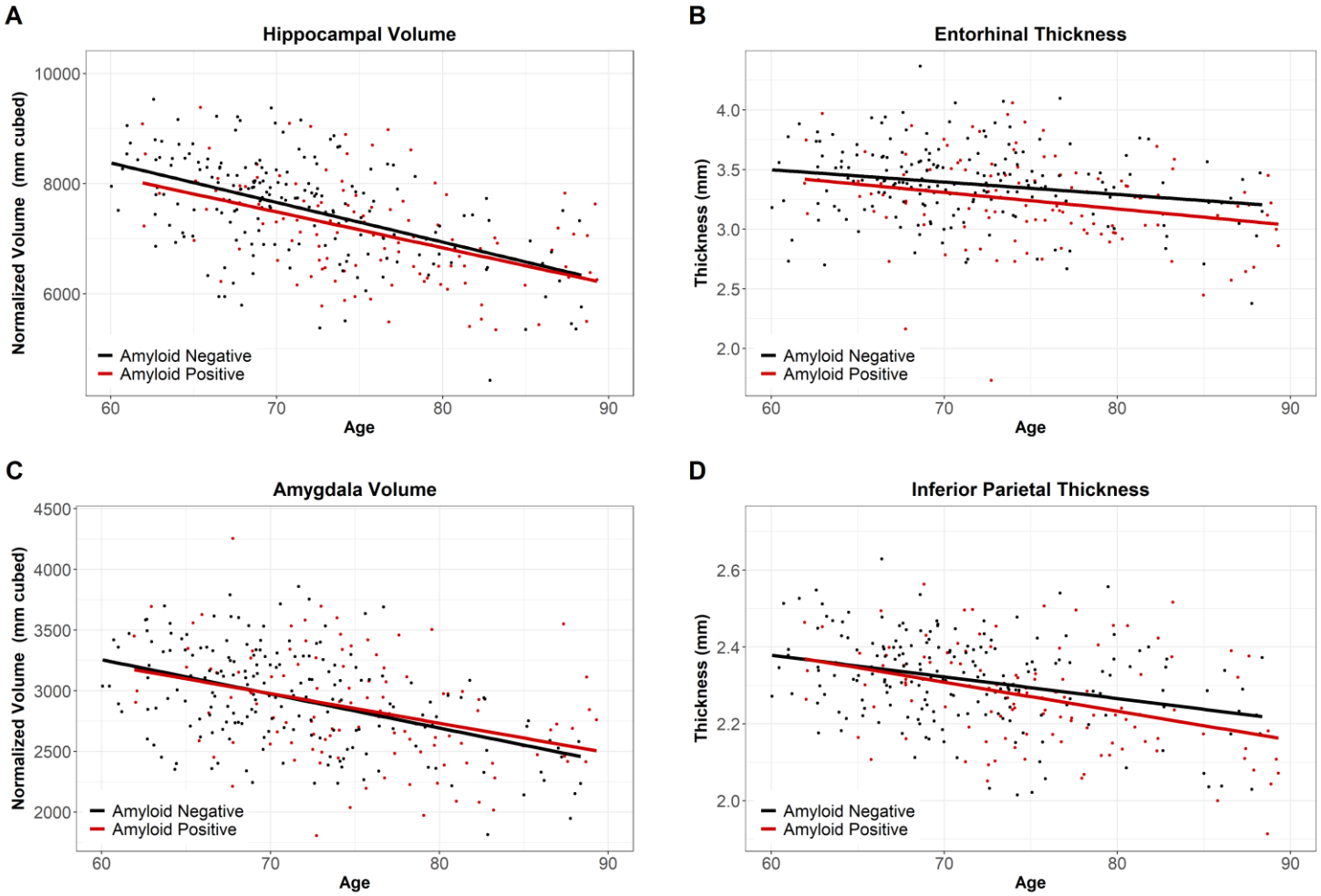

Figure 2.4 displays the overlap of the Normal Aging cohort (Amyloid Negative, black) and the Preclinical AD cohort (Amyloid Positive, red), indicating our non-significant findings for amyloid and age × amyloid.

AD: Alzheimer disease

2.4 Discussion

In this paper we report regional variation in age-related atrophy, with different spatial patterns for the effect size of age-related atrophy and in the non-linear pattern observed across the lifespan. Temporal regions showed the greatest association with age, while frontal and cingulate areas showed a deceleration of atrophy with age (i.e., higher atrophy in mid-life than late-life). This reduced rate of atrophy in late life contrasted to most regions which showed an acceleration of atrophy in late life. This pattern of non-linearity was spatially related to myelin levels determined by T1w/T2w intensity ratio. As this ratio was determined in a separate cohort of healthy adults, this suggests that the observed pattern is the end result of a fundamental organizational property of the brain. The lack of correlation between myelin and the direct association with age further supports that the two observed patterns are unique. The direction of the myelin and age-derivative correlation suggests that regions that characteristically have higher myelin content in midlife are more vulnerable to accelerated atrophy in later life. While causality is not clear, this could in part be due to the greater vulnerability of myelinating cells to oxidative stress (Nasrabady et al., 2018). No differences were detected between our Normal Aging cohort and our Preclinical AD cohort, though a larger sample may reveal subtle differences.

Limitations of this study include its cross-sectional design, the lack of diversity in our participants, and our inability to control for vascular influences on structural brain measures in these analyses. Group averages in aging volumetrics have been shown to be commensurate across cross-sectional and longitudinal designs (Fjell et al., 2013b; Fotenos et al., 2005). However, by looking only at a single time-point per participant, we were unable to assess possible subtypes of patterns of aging in individuals. Our Normal Aging cohort, collated from several studies of aging and AD, is predominantly highly educated and non-Hispanic White. A

more representative cohort may show greater age-related atrophy due to the association of social inequities with chronic health conditions and other social determinants of health. As such, our study may be closer to a measure of 'healthy aging' than the 'normal aging' an average individual in our society experiences.

While our cohort may not be representative of the broader population, it does reduce the probability that some unmeasured factors are confounding our measures of aging. Vascular disease is one such unmeasured factor that is common within the population represented in this study and likely impacts our results. Differences in blood pressure, even in non-hypertensive individuals, have correlated with volumetric differences (Lockhart and DeCarli, 2014). Additionally, regional volumetrics may be influenced by other non-AD neurodegenerative pathologic processes that are less common and more difficult to detect (e.g., argyrophilic grain disease, primary aging-related tauopathy, hippocampal sclerosis of aging, limbic-predominant aging-related TDP-43 encephalopathy neuropathologic change, aging related tau astrogliopathy, frontotemporal lobar degeneration, Lewy body disease). For our detected pathology, amyloid, we are limited in that we did not follow our preclinical AD participants longitudinally. We would expect some but not all of these participants to develop AD in the near future, and these two subgroups would likely have different rates and patterns of atrophy. One final limitation is that the FreeSurfer regions used in this study were relatively coarse regions defined based on gyral and sulcal landmarks that contain significant structural and functional heterogeneity. This limits the neurobiological interpretability of regional effects as compared to cortical areas based on multiple modalities (Glasser et al., 2016a) or more homogeneous functional regions (Gordon et al., 2016).

Despite these limitations, our results indicate that age-related atrophy is a regionally heterogeneous process, with severity of atrophy and lifespan pattern of atrophy varying independently across regions. We also showed that age-related atrophy is not significantly associated with amyloid positivity in the absence of cognitive symptoms. This suggests that volumetric studies in older adults do not need to include amyloid PET scans to screen for preclinical AD or track their participants longitudinally for dementia if they instead use the same rigorous dementia screening that we used at baseline (integrating a comprehensive history with a trusted collateral source and neurological examination). Similar studies done previously had smaller sample sizes and were unable to screen by both longitudinal cognition and amyloid levels. That we were able to do so gives additional weight to our negative findings. Future studies should further investigate the association we saw between myelin and the lifespan pattern of atrophy, as well as the potential influence of non-AD neurodegenerative pathologies.

2.5 Acknowledgements

Data collection and sharing for this project was supported by The Dominantly Inherited Alzheimer's Network (DIAN, U19AG032438) funded by the National Institute on Aging (NIA), the German Center for Neurodegenerative Diseases (DZNE), Raul Carrea Institute for Neurological Research (FLENI), Partial support by the Research and Development Grants for Dementia from Japan Agency for Medical Research and Development, AMED, and the Korea Health Technology R&D Project through the Korea Health Industry Development Institute (KHIDI).This manuscript has been reviewed by DIAN Study investigators for scientific content and consistency of data interpretation with previous DIAN Study publications. We acknowledge the altruism of the participants and their families and contributions of the DIAN research and support staff at each of the participating sites for their contributions to this study.

Data were provided in part by OASIS-3: Principal Investigators: T. Benzinger, D. Marcus, J. Morris; National Institutes of Health (NIH) P50AG00561, P30NS09857781, P01AG026276, P01AG003991, R01AG043434, UL1TR000448, R01EB009352. Florbetapir [^{18}F] doses were provided by Avid Radiopharmaceuticals, a wholly owned subsidiary of Eli Lilly.

This work was supported by the Knight Alzheimer Research Imaging (KARI) Program, Knight Alzheimer Disease Research Center (ADRC), ADRC Center Grant (NIH/NIA P50AG005681), the Charles and Joanne Knight Alzheimer Disease Research Center Support Fund, the Barnes-Jewish Hospital Foundation (BJHF) Adult Children's Study (ACS) NIH/NIA P01AG026276, support for image acquisition – CCIR/ICTS Human Imaging Unit (NIH/NCATS UL1TR000448), and support for imaging informatics – CNDA/XNAT through the Neuroimaging Informatics and Analysis Center (1P30NS098577) and R01 EB009352. These funding sources had no involvement in study design; in the collection, analysis and interpretation of data; in the writing of the report; or in the decision to submit the article for publication.

Lauren Koenig reports funding from NIH grants P01AG026276, P01AG003991, and R01AG054567.

Randall Bateman, Professor of Neurology at Washington University's School of Medicine (WUSM) receives lab research funding from the National Institutes of Health, Alzheimer's Association, BrightFocus Foundation, Rainwater Foundation Tau Consortium, Association for Frontotemporal Degeneration, the Cure Alzheimer's Fund, Centene Corporation, Tau SILK Consortium (AbbVie, Biogen, and Eli Lilly and Company), the Barnes-Jewish Hospital Foundation, NfL Consortium (AbbVie, Biogen, Roche) and an anonymous organization.

Randall Bateman has received honoraria as a speaker/consultant/advisory board member from Amgen, AC Immune, Eisai, F. Hoffman-LaRoche, and Janssen; and reimbursement of travel expenses from AC Immune, F. Hoffman-La Roche and Janssen.

Unrelated to this article, Randall Bateman serves as principal investigator of the DIAN-TU, which is supported by the Alzheimer's Association, GHR Foundation, an anonymous organization and the DIAN-TU Pharma Consortium (Active: Eli Lilly and Company/Avid Radiopharmaceuticals, F. Hoffman-La Roche/Genentech, Biogen, Eisai, Janssen, and United Neuroscience. Previous: Abbvie, Amgen, AstraZeneca, Forum, Mithridion, Novartis, Pfizer, Sanofi). The DIAN-TU-001 Clinical Trial is supported by Pharmaceutical Partners Eli Lilly and Company, F. Hoffman-La Roche and Janssen, the Alzheimer's Association, NIH U01AG042791, NIH U01AG42791-S1 (FNIH and Accelerating Medicines Partnership), NIH R01AG046179, NIH R56AG053267, NIH R01AG053267, NIH U01AG059798, NIH R01AG068319, Avid Radiopharmaceuticals, GHR Foundation, and an anonymous organization. In-kind support has been received from CogState and Bracket.

Washington University, Randall Bateman, and David Holtzman have equity ownership interest in C2N Diagnostics and receive royalty income based on technology (stable isotope labeling kinetics and blood plasma assay) licensed by Washington University to C2N Diagnostics. Randall Bateman receives income from C2N Diagnostics for serving on the scientific advisory board. Washington University, with Randall Bateman as co-inventor, has submitted the US nonprovisional patent application ‘Methods for Measuring the Metabolism of CNS Derived Biomolecules in Vivo’ and provisional patent application ‘Plasma Based Methods for Detecting CNS Amyloid Deposition’.

Dr. Holtzman reports grants, personal fees and other from C2N Diagnostics, personal fees from Genentech, personal fees from Denali, personal fees from Cajal Neuroscience, personal fees from Takeda, and personal fees from Merck outside the submitted work. In addition, Dr. Holtzman has a patent Antibodies to tau licensed, and a patent Antibody to Abeta licensed.

Dr. Yakushev reports personal fees from Blue Earth Diagnostics, ABX-CRO, grants from Alzheimer Research Initiative Germany, Federal Ministry of Education and Research Germany, German Research Foundation, and personal fees from Piramal outside the submitted work.

Dr. Day reports grants from NIH/NIA, during the conduct of the study; personal fees from Parabon Nanolabs, Inc., personal fees from DynaMed (EBSCO Health), outside the submitted work; and is the clinical director for the Anti-NMDA Receptor Encephalitis Foundation (uncompensated), has provided record review and expert medical testimony on legal cases pertaining to management of Wernicke encephalopathy, and holds stocks (> $10,000) in ANI Pharmaceuticals (a generic pharmaceutical company).

Dr. Jack serves on an independent data monitoring board for Roche, has served as a speaker for Eisai, and consulted for Biogen, but he receives no personal compensation from any commercial entity. He receives research support from NIH and the Alexander Family Alzheimer's Disease Research Professorship of the Mayo Clinic.

Dr. Mummery reports personal fees from Biogen, personal fees from Roche, and personal fees from Washington University outside the submitted work.

Dr. Morris reports grants from NIH P01 AG03991, grants from NIH P30 AG066444, grants from NIH P01 AG026276, and grants from NIH U19 AG032438 during the conduct of the study.

Dr. Benzinger participated in clinical trials sponsored by Eli Lilly, Roche, and Biogen. Avid Radiopharmaceuticals (a wholly owned subsidiary of Eli Lilly provided doses of [^{18}F]-florbetapir, partial funding for [^{18}F]-florbetapir scanning, precursor for [^{18}F]-flortaucipir and technology transfer for manufacturing of [^{18}F]-flortaucipir).

2.6 Supplemental

Supplemental Table S2.1: Relationship of Demographics to Volumes and Thicknesses

FreeSurfer Region	Data Source *p*-value	Gender *p*-value	*APOE4* *p*-value	MMSE *p*-value	Race *p*-value	Education *p*-value	Region Type
Banks Superior Temporal Sulcus Thickness	1	1	1	1	1	1	T
Caudal Anterior Cingulate Thickness	1	0.20	1	1	1	1	T
Caudal Middle Frontal Thickness	1	1	1	1	1	1	T
Cuneus Thickness	1	1	1	1	0.43	1	T
Entorhinal Thickness	1	1	0.65	1	1	1	T
Frontal Pole Thickness	1	1	1	1	1	1	T
Fusiform Thickness	1	1	1	1	1	1	T
Inferior Parietal Thickness	1	1	1	1	1	1	T
Inferior Temporal Thickness	1	1	1	1	1	1	T
Insula Thickness	1	1	1	1	1	1	T
Isthmus Cingulate Thickness	0.42	1	1	1	1	1	T
Lateral Occipital Thickness	1	1	1	1	0.88	1	T
Lateral Orbitofrontal Thickness	1	1	1	1	1	1	T
Lingual Thickness	1	1	1	1	1	1	T
Medial Orbitofrontal Thickness	1	1	1	1	1	1	T
Middle Temporal Thickness	1	1	1	1	1	1	T
Paracentral Thickness	1	1	1	1	1	1	T
Parahippocampal Thickness	1	1	1	0.53	1	1	T
Pars Opercularis Thickness	1	1	1	1	1	1	T
Pars Orbitalis Thickness	1	0.23	1	1	1	1	T
Pars Triangularis Thickness	1	1	1	1	1	1	T
Pericalcarine Thickness	1	1	1	1	1	1	T
Postcentral Thickness	1	1	1	1	0.31	1	T
Posterior Cingulate Thickness	1	1	1	1	1	1	T
Precentral Thickness	1	1	1	1	1	1	T

FreeSurfer Region	Data Source *p*-value	Gender *p*-value	*APOE4* *p*-value	MMSE *p*-value	Race *p*-value	Education *p*-value	Region Type
Precuneus Thickness	1	1	1	1	1	1	T
Rostral Anterior Cingulate Thickness	1	1	1	1	1	1	T
Rostral Middle Frontal Thickness	1	1	1	1	1	1	T
Superior Frontal Thickness	1	1	1	1	1	1	T
Superior Parietal Thickness	1	1	1	1	1	1	T
Superior Temporal Thickness	0.50	1	1	1	1	1	T
Supramarginal Thickness	1	1	1	1	1	1	T
Temporal Pole Thickness	1	1	1	1	0.28	1	T
Transverse Temporal Thickness	1	1	1	0.30	1	1	T
Banks Superior Temporal Sulcus Volume	1	1	1	1	0.14	1	CV
Caudal Anterior Cingulate Volume	1	1	1	1	1	1	CV
Caudal Middle Frontal Volume	1	1	1	1	1	1	CV
Cuneus Volume	1	1	1	1	**0.03**	1	CV
Entorhinal Volume	1	1	1	0.16	1	1	CV
Frontal Pole Volume	1	**0.03**	1	1	1	1	CV
Fusiform Volume	1	**0.008**	1	1	1	1	CV
Inferior Parietal Volume	1	0.67	1	1	1	1	CV
Inferior Temporal Volume	1	0.33	1	1	**0.04**	1	CV
Insula Volume	1	1	1	1	1	1	CV
Isthmus Cingulate Volume	1	1	1	1	1	1	CV
Lateral Occipital Volume	1	**0.04**	1	1	**0.01**	1	CV
Lateral Orbitofrontal Volume	1	1	1	1	0.51	1	CV
Lingual Volume	1	0.28	1	1	1	1	CV
Medial Orbitofrontal Volume	1	0.21	1	1	1	1	CV
Middle Temporal Volume	1	1	1	1	**0.002**	1	CV
Paracentral Volume	1	1	1	1	1	1	CV
Parahippocampal Volume	1	1	1	1	1	1	CV
Pars Opercularis Volume	1	1	1	1	1	1	CV

FreeSurfer Region	Data Source *p*-value	Gender *p*-value	*APOE4* *p*-value	MMSE *p*-value	Race *p*-value	Education *p*-value	Region Type
Pars Orbitalis Volume	1	1	1	1	1	1	CV
Pars Triangularis Volume	1	1	1	1	1	1	CV
Pericalcarine Volume	1	1	1	1	1	1	CV
Postcentral Volume	1	1	1	1	1	1	CV
Posterior Cingulate Volume	1	1	1	1	1	1	CV
Precentral Volume	1	1	1	1	1	1	CV
Precuneus Volume	1	1	1	1	0.06	1	CV
Rostral Anterior Cingulate Volume	1	1	1	1	1	1	CV
Rostral Middle Frontal Volume	1	1	1	1	1	1	CV
Superior Frontal Volume	1	1	1	1	1	1	CV
Superior Parietal Volume	1	1	1	1	0.19	1	CV
Superior Temporal Volume	1	1	1	1	1	1	CV
Supramarginal Volume	0.11	1	1	1	0.14	1	CV
Temporal Pole Volume	1	0.95	1	1	1	1	CV
Transverse Temporal Volume	1	1	1	1	1	1	CV
Amygdala Volume	0.08	< **0.001**	1	1	1	1	SV
Caudate Volume	1	1	1	1	1	1	SV
Hippocampus Volume	1	0.48	1	1	1	1	SV
Lateral Ventricle Volume	1	**0.01**	1	1	1	1	SV
Pallidum Volume	1	1	1	1	1	1	SV
Putamen Volume	1	1	1	1	1	1	SV
Thalamus Proper Volume*	1	0.57	1	1	1	1	SV
Ventral DC Volume*	1	0.54	1	1	1	1	SV
Accumbens Area Volume*	0.77	0.07	1	1	1	1	Other
Brain Stem Volume	1	0.33	1	1	1	1	Other
Corpus Callosum Anterior Volume	1	1	1	1	1	1	Other
Corpus Callosum Central Volume	1	1	1	1	1	1	Other
Corpus Callosum Mid Anterior Volume	1	1	1	1	1	1	Other

FreeSurfer Region	Data Source *p*-value	Gender *p*-value	*APOE4* *p*-value	MMSE *p*-value	Race *p*-value	Education *p*-value	Region Type
Corpus Callosum Mid Posterior Volume	1	1	1	1	1	1	Other
Corpus Callosum Posterior Volume	1	1	1	0.23	1	1	Other
Cerebellum Cortex Volume	1	1	1	1	0.06	1	Other
Cerebellum White Matter Volume	1	1	1	1	1	1	Other
Choroid Plexus Volume*	1	1	1	1	1	1	Other
Cortex Volume	1	0.61	1	1	0.19	1	Other
Cortical White Matter Volume	1	1	1	1	1	1	Other
Cerebrospinal fluid (CSF) Volume	1	1	1	1	1	1	Other
Inferior Lateral Ventricle Volume	1	0.58	1	1	1	1	Other
Intracranial Volume	1	< **0.001**	1	1	0.12	1	Other
Non-White Matter Hypointensities Volume*	1	1	1	1	1	1	Other
Optic Chiasm Volume*	1	1	1	1	**0.01**	1	Other
Subcortical Gray Matter Volume	1	1	1	1	1	1	Other
Supratentorial Volume	1	1	1	1	0.37	1	Other
Total Gray Matter Volume	1	0.59	1	1	0.08	1	Other
Vessel Volume*	1	1	1	1	1	1	Other
White Matter Hypointensities Volume*	1	1	1	1	1	1	Other
3rd Ventricle Volume	1	1	1	1	1	1	Other
4th Ventricle Volume	0.08	1	1	1	1	1	Other
5th Ventricle Volume	1	1	1	1	1	1	Other

P-values are post-correction for multiple comparisons, and are from individual simple linear regression models. The 'Data Source' results included only the n = 27 DIAN participants and n = 55 OASIS participants that overlapped in age (age 42-59).

*The indicated regions are known to have low measurement accuracy with FreeSurfer and so should be interpreted with caution.

APOE4: Apolipoprotein E ε4; CV: Cortical volume; DIAN: Dominantly Inherited Alzheimer Network; MMSE: Mini Mental State Exam; OASIS: Open Access Series of Neuroimaging Studies; T: Cortical thickness measure

Supplemental Table S2.2: Relationship of Age to Volumes and Thicknesses

FreeSurfer Region	Age β	Age *p*-value	Estimated Derivative β	Estimated Derivative *p*-value	Region Type
Banks Superior Temporal Sulcus Thickness	-0.629	< **0.001**	-0.141	0.50	T
Caudal Anterior Cingulate Thickness	-0.081	**0.57**	0.974	< **0.001**	T
Caudal Middle Frontal Thickness	-0.372	< **0.001**	-0.368	**0.02**	T
Cuneus Thickness	-0.409	< **0.001**	-0.697	< **0.001**	T
Entorhinal Thickness	-0.200	**0.001**	-0.874	< **0.001**	T
Frontal Pole Thickness	-0.225	< **0.001**	0.947	< **0.001**	T
Fusiform Thickness	-0.564	< **0.001**	-0.094	0.50	T
Inferior Parietal Thickness	-0.527	< **0.001**	-0.63	< **0.001**	T
Inferior Temporal Thickness	-0.531	< **0.001**	0.532	< **0.001**	T
Insula Thickness	-0.564	< **0.001**	0.769	< **0.001**	T
Isthmus Cingulate Thickness	-0.529	< **0.001**	0.713	< **0.001**	T
Lateral Occipital Thickness	-0.508	< **0.001**	-0.838	< **0.001**	T
Lateral Orbitofrontal Thickness	-0.459	< **0.001**	0.95	< **0.001**	T
Lingual Thickness	-0.589	< **0.001**	-0.443	**0.002**	T
Medial Orbitofrontal Thickness	-0.264	< **0.001**	0.947	< **0.001**	T
Middle Temporal Thickness	-0.648	< **0.001**	0.525	< **0.001**	T
Paracentral Thickness	-0.384	< **0.001**	-0.389	**0.009**	T
Parahippocampal Thickness	-0.364	< **0.001**	-0.407	**0.006**	T
Pars Opercularis Thickness	-0.581	< **0.001**	0.652	< **0.001**	T
Pars Orbitalis Thickness	-0.324	< **0.001**	0.841	< **0.001**	T
Pars Triangularis Thickness	-0.55	< **0.001**	0.799	< **0.001**	T
Pericalcarine Thickness	-0.329	< **0.001**	-0.921	< **0.001**	T
Postcentral Thickness	-0.442	< **0.001**	-0.736	< **0.001**	T
Posterior Cingulate Thickness	-0.437	< **0.001**	0.978	< **0.001**	T
Precentral Thickness	-0.509	< **0.001**	-0.715	< **0.001**	T

FreeSurfer Region	Age β	Age *p*-value	Estimated Derivative β	Estimated Derivative *p*-value	Region Type
Precuneus Thickness	-0.535	< **0.001**	-0.431	**0.003**	T
Rostral Anterior Cingulate Thickness	-0.168	**0.009**	0.953	< **0.001**	T
Rostral Middle Frontal Thickness	-0.192	**0.002**	0.848	< **0.001**	T
Superior Frontal Thickness	-0.480	< **0.001**	0.307	0.05	T
Superior Parietal Thickness	-0.344	< **0.001**	-0.602	< **0.001**	T
Superior Temporal Thickness	-0.700	< **0.001**	-0.643	< **0.001**	T
Supramarginal Thickness	-0.622	< **0.001**	-0.346	**0.02**	T
Temporal Pole Thickness	-0.184	**0.003**	-0.689	< **0.001**	T
Transverse Temporal Thickness	-0.411	< **0.001**	-0.529	< **0.001**	T
Banks Superior Temporal Sulcus Volume	-0.512	< **0.001**	-0.754	< **0.001**	CV
Caudal Anterior Cingulate Volume	-0.382	< **0.001**	0.687	< **0.001**	CV
Caudal Middle Frontal Volume	-0.454	< **0.001**	-0.964	< **0.001**	CV
Cuneus Volume	-0.487	< **0.001**	-0.966	< **0.001**	CV
Entorhinal Volume	0.074	0.60	-0.911	< **0.001**	CV
Frontal Pole Volume	-0.293	< **0.001**	0.972	< **0.001**	CV
Fusiform Volume	-0.557	< **0.001**	-0.482	< **0.001**	CV
Inferior Parietal Volume	-0.585	< **0.001**	-0.947	< **0.001**	CV
Inferior Temporal Volume	-0.586	< **0.001**	-0.489	< **0.001**	CV
Insula Volume	-0.291	< **0.001**	0.356	**0.02**	CV
Isthmus Cingulate Volume	-0.507	< **0.001**	-0.805	< **0.001**	CV
Lateral Occipital Volume	-0.590	< **0.001**	-0.949	< **0.001**	CV
Lateral Orbitofrontal Volume	-0.640	< **0.001**	0.502	< **0.001**	CV
Lingual Volume	-0.539	< **0.001**	-0.861	< **0.001**	CV
Medial Orbitofrontal Volume	-0.385	< **0.001**	0.689	< **0.001**	CV
Middle Temporal Volume	-0.693	< **0.001**	-0.311	0.05	CV
Paracentral Volume	-0.408	< **0.001**	-0.862	< **0.001**	CV
Parahippocampal Volume	-0.525	< **0.001**	-0.778	< **0.001**	CV

FreeSurfer Region	Age β	Age *p*-value	Estimated Derivative β	Estimated Derivative *p*-value	Region Type
Pars Opercularis Volume	-0.562	< **0.001**	-0.266	0.08	CV
Pars Orbitalis Volume	-0.536	< **0.001**	0.530	< **0.001**	CV
Pars Triangularis Volume	-0.595	< **0.001**	-0.615	< **0.001**	CV
Pericalcarine Volume	-0.280	< **0.001**	-0.941	< **0.001**	CV
Postcentral Volume	-0.442	< **0.001**	-0.905	< **0.001**	CV
Posterior Cingulate Volume	-0.549	< **0.001**	0.868	< **0.001**	CV
Precentral Volume	-0.522	< **0.001**	-0.741	< **0.001**	CV
Precuneus Volume	-0.584	< **0.001**	-0.878	< **0.001**	CV
Rostral Anterior Cingulate Volume	-0.431	< **0.001**	0.870	< **0.001**	CV
Rostral Middle Frontal Volume	-0.565	< **0.001**	0.743	< **0.001**	CV
Superior Frontal Volume	-0.643	< **0.001**	-0.876	< **0.001**	CV
Superior Parietal Volume	-0.471	< **0.001**	-0.852	< **0.001**	CV
Superior Temporal Volume	-0.666	< **0.001**	-0.894	< **0.001**	CV
Supramarginal Volume	-0.557	< **0.001**	-0.335	**0.03**	CV
Temporal Pole Volume	0.004	1	-0.733	< **0.001**	CV
Transverse Temporal Volume	-0.416	< **0.001**	-0.913	< **0.001**	CV
Amygdala Volume	-0.618	< **0.001**	-0.972	< **0.001**	SV
Caudate Volume	-0.371	< **0.001**	0.847	< **0.001**	SV
Hippocampus Volume	-0.652	< **0.001**	-0.965	< **0.001**	SV
Lateral Ventricle Volume	0.601	< **0.001**	0.769	< **0.001**	SV
Pallidum Volume	-0.409	< **0.001**	-0.936	< **0.001**	SV
Putamen Volume	-0.670	< **0.001**	-0.949	< **0.001**	SV
Thalamus Proper Volume*	-0.706	< **0.001**	-0.974	< **0.001**	SV
Ventral DC Volume*	-0.621	< **0.001**	-0.987	< **0.001**	SV
Accumbens Area Volume*	-0.690	< **0.001**	-0.964	< **0.001**	Other
Brain Stem Volume	-0.292	< **0.001**	-0.971	< **0.001**	Other
Corpus Callosum Anterior Volume	-0.358	< **0.001**	-0.976	< **0.001**	Other

FreeSurfer Region	Age β	Age *p*-value	Estimated Derivative β	Estimated Derivative *p*-value	Region Type
Corpus Callosum Central Volume	-0.416	< **0.001**	-0.970	< **0.001**	Other
Corpus Callosum Mid Anterior Volume	-0.429	< **0.001**	-0.965	< **0.001**	Other
Corpus Callosum Mid Posterior Volume	-0.439	< **0.001**	-0.967	< **0.001**	Other
Corpus Callosum Posterior Volume	-0.070	0.60	-0.967	< **0.001**	Other
Cerebellum Cortex Volume	-0.568	< **0.001**	-0.731	< **0.001**	Other
Cerebellum White Matter Volume	-0.445	< **0.001**	-0.973	< **0.001**	Other
Choroid Plexus Volume*	0.378	< **0.001**	0.861	< **0.001**	Other
Cortex Volume	-0.752	< **0.001**	-0.751	< **0.001**	Other
Cortical White Matter Volume	-0.475	< **0.001**	-0.972	< **0.001**	Other
Cerebrospinal fluid (CSF) Volume	0.357	< **0.001**	0.971	< **0.001**	Other
Inferior Lateral Ventricle Volume	0.502	< **0.001**	0.754	< **0.001**	Other
Intracranial Volume	-0.019	1	0.895	< **0.001**	Other
Non-White Matter Hypointensities Volume*	0.442	< **0.001**	0.766	< **0.001**	Other
Optic Chiasm Volume*	0.294	< **0.001**	-0.936	< **0.001**	Other
Subcortical Gray Matter Volume	-0.105	0.28	-0.625	< **0.001**	Other
Supratentorial Volume	-0.692	< **0.001**	-0.973	< **0.001**	Other
Total Gray Matter Volume	-0.789	< **0.001**	-0.861	< **0.001**	Other
Vessel Volume*	0.191	**0.002**	-0.975	< **0.001**	Other
White Matter Hypointensities Volume*	0.439	< **0.001**	0.811	< **0.001**	Other
3rd Ventricle Volume	0.637	< **0.001**	0.842	< **0.001**	Other
4th Ventricle Volume	0.153	**0.02**	0.872	< **0.001**	Other
5th Ventricle Volume	0.104	0.28	0.869	< **0.001**	Other

P-values are post-correction for multiple comparisons, and are from individual simple linear regression models.

*The indicated regions are known to have low measurement accuracy with FreeSurfer and so should be interpreted with caution.

CV: Cortical volume; T: Cortical thickness measure

Supplemental Table S2.3: Impact of Preclinical AD Results

FreeSurfer Region	Age *p*-value	Amyloid Status *p*-value	Age × Amyloid Status *p*-value	Region Type
Banks Superior Temporal Sulcus Thickness	< **0.001**	1	1	T
Caudal Anterior Cingulate Thickness	0.23	1	1	T
Caudal Middle Frontal Thickness	**0.01**	1	1	T
Cuneus Thickness	0.23	1	1	T
Entorhinal Thickness	0.15	1	1	T
Frontal Pole Thickness	1	1	1	T
Fusiform Thickness	< **0.001**	1	1	T
Inferior Parietal Thickness	< **0.001**	1	1	T
Inferior Temporal Thickness	0.05	1	1	T
Insula Thickness	0.67	1	1	T
Isthmus Cingulate Thickness	0.25	1	1	T
Lateral Occipital Thickness	< **0.001**	1	1	T
Lateral Orbitofrontal Thickness	1	1	1	T
Lingual Thickness	< **0.001**	1	1	T
Medial Orbitofrontal Thickness	1	1	1	T
Middle Temporal Thickness	< **0.001**	1	1	T
Paracentral Thickness	0.07	1	1	T
Parahippocampal Thickness	**0.02**	1	1	T
Pars Opercularis Thickness	**0.03**	1	1	T
Pars Orbitalis Thickness	1	1	1	T
Pars Triangularis Thickness	0.25	1	1	T
Pericalcarine Thickness	0.18	1	1	T
Postcentral Thickness	< **0.001**	1	1	T
Posterior Cingulate Thickness	1	1	1	T
Precentral Thickness	**0.002**	1	1	T
Precuneus Thickness	< **0.001**	1	1	T

FreeSurfer Region	Age *p*-value	Amyloid Status *p*-value	Age × Amyloid Status *p*-value	Region Type
Rostral Anterior Cingulate Thickness	1	1	1	T
Rostral Middle Frontal Thickness	1	1	1	T
Superior Frontal Thickness	**0.006**	1	1	T
Superior Parietal Thickness	**0.005**	1	1	T
Superior Temporal Thickness	**< 0.001**	1	1	T
Supramarginal Thickness	**< 0.001**	1	1	T
Temporal Pole Thickness	1	1	1	T
Transverse Temporal Thickness	**< 0.001**	1	1	T
Banks Superior Temporal Sulcus Volume	**0.02**	1	1	CV
Caudal Anterior Cingulate Volume	1	1	1	CV
Caudal Middle Frontal Volume	**0.03**	1	1	CV
Cuneus Volume	**< 0.001**	1	1	CV
Entorhinal Volume	1	1	1	CV
Frontal Pole Volume	1	1	1	CV
Fusiform Volume	**< 0.001**	1	1	CV
Inferior Parietal Volume	**< 0.001**	1	1	CV
Inferior Temporal Volume	**< 0.001**	1	1	CV
Insula Volume	1	1	1	CV
Isthmus Cingulate Volume	**< 0.001**	1	1	CV
Lateral Occipital Volume	**< 0.001**	1	1	CV
Lateral Orbitofrontal Volume	**0.02**	1	1	CV
Lingual Volume	**< 0.001**	1	1	CV
Medial Orbitofrontal Volume	1	1	1	CV
Middle Temporal Volume	**< 0.001**	1	1	CV
Paracentral Volume	0.23	1	1	CV
Parahippocampal Volume	**< 0.001**	1	1	CV
Pars Opercularis Volume	0.02	1	1	CV
Pars Orbitalis Volume	0.05	1	1	CV

FreeSurfer Region	Age *p*-value	Amyloid Status *p*-value	Age × Amyloid Status *p*-value	Region Type
Pars Triangularis Volume	< **0.001**	1	1	CV
Pericalcarine Volume	**0.03**	1	1	CV
Postcentral Volume	< **0.001**	1	1	CV
Posterior Cingulate Volume	0.07	1	1	CV
Precentral Volume	< **0.001**	1	1	CV
Precuneus Volume	< **0.001**	1	1	CV
Rostral Anterior Cingulate Volume	1	1	1	CV
Rostral Middle Frontal Volume	0.16	1	1	CV
Superior Frontal Volume	< **0.001**	1	1	CV
Superior Parietal Volume	< **0.001**	1	1	CV
Superior Temporal Volume	< **0.001**	1	1	CV
Supramarginal Volume	**0.004**	1	1	CV
Temporal Pole Volume	1	1	1	CV
Transverse Temporal Volume	**0.001**	1	1	CV
Amygdala Volume	< **0.001**	1	1	SV
Caudate Volume	1	1	1	SV
Hippocampus Volume	< **0.001**	1	1	SV
Lateral Ventricle Volume	< **0.001**	1	1	SV
Pallidum Volume	**0.004**	1	1	SV
Putamen Volume	< **0.001**	1	1	SV
Thalamus Proper Volume*	< **0.001**	1	1	SV
Ventral DC Volume*	< **0.001**	1	1	SV
Accumbens Area Volume*	< **0.001**	1	1	Other
Brain Stem Volume	< **0.001**	1	1	Other
Corpus Callosum Anterior Volume	< **0.001**	1	1	Other
Corpus Callosum Central Volume	< **0.001**	1	1	Other
Corpus Callosum Mid Anterior Volume	< **0.001**	1	1	Other
Corpus Callosum Mid Posterior Volume	< **0.001**	1	1	Other

FreeSurfer Region	Age *p*-value	Amyloid Status *p*-value	Age × Amyloid Status *p*-value	Region Type
Corpus Callosum Posterior Volume	0.05	1	1	Other
Cerebellum Cortex Volume	0.07	1	1	Other
Cerebellum White Matter Volume	**< 0.001**	1	1	Other
Choroid Plexus Volume*	**0.04**	1	1	Other
Cortex Volume	**< 0.001**	1	1	Other
Cortical White Matter Volume	**< 0.001**	1	1	Other
Cerebrospinal fluid (CSF) Volume	**0.003**	1	1	Other
Inferior Lateral Ventricle Volume	**< 0.001**	1	1	Other
Intracranial Volume	1	1	1	Other
Non-White Matter Hypointensities Volume*	**< 0.001**	1	1	Other
Optic Chiasm Volume*	1	1	1	Other
Subcortical Gray Matter Volume	1	1	1	Other
Supratentorial Volume	**< 0.001**	1	1	Other
Total Gray Matter Volume	**< 0.001**	1	1	Other
Vessel Volume*	1	1	1	Other
White Matter Hypointensities Volume*	**< 0.001**	1	1	Other
3rd Ventricle Volume*	**< 0.001**	1	1	Other
4th Ventricle Volume*	1	1	1	Other
5th Ventricle Volume*	1	1	1	Other

P-values are post-correction for multiple comparisons, and are from multiple linear regression models.

*The indicated regions are known to have low measurement accuracy with FreeSurfer and so should be interpreted with caution.

AD: Alzheimer disease; CV: Cortical volume; T: Cortical thickness measure

Chapter 3: Improving Volumetric Models for Symptomatic Alzheimer Disease (Koenig et al., 2020)

Volumetric biomarkers for Alzheimer disease are attractive due to their wide availability and ease of administration, but have traditionally shown lower diagnostic accuracy than measures of neuropathological contributors to Alzheimer disease. Our purpose was to optimize the diagnostic specificity of structural MRIs for Alzheimer disease using quantitative, data-driven techniques. This retrospective study assembled several non-overlapping cohorts (total n = 1287) with publicly available data and clinical patients from Barnes-Jewish Hospital (data gathered 1990-2018). The Normal Aging cohort (n = 383) contained amyloid biomarker negative, cognitively normal participants, and provided a basis for determining age-related atrophy in other cohorts. The Training (n = 216) and Test (n = 109) cohorts contained participants with symptomatic Alzheimer disease and cognitively normal controls. Classification models were developed in the Training cohort and compared in the Test cohort using the receiver operating characteristics' areas under the curve. Additional model comparisons were done in the Clinical cohort (n = 579), which contained patients who were diagnosed with dementia due to various etiologies in a tertiary care outpatient memory clinic. While the Normal Aging cohort showed regional age-related atrophy, classification models were not improved by including age as a predictor or by using volumetrics adjusted for age-related atrophy. The optimal model used multiple regions (hippocampal volume, inferior lateral ventricle volume, amygdala volume, entorhinal thickness, and inferior parietal thickness) and was able to separate Alzheimer disease and cognitively normal controls in the Test cohort with an area under the curve of 0.961. In the Clinical cohort, this model separated Alzheimer disease from non-Alzheimer disease diagnoses

with an area under the curve of 0.820, an incrementally greater separation of the cohort than by hippocampal volume alone (area under the curve of 0.801, $p = 0.06$). Greatest separation was seen for Alzheimer disease vs. frontotemporal dementia and for Alzheimer disease vs. non-neurodegenerative diagnoses. Volumetric biomarkers distinguished individuals with symptomatic Alzheimer disease from cognitively normal controls and other dementia types but were not improved by controlling for normal aging.

3.1 Introduction

Typical Alzheimer disease (AD)-specific biomarkers rely on in vivo detection and quantification of amyloid-β and tau, AD's hallmark proteins. These biomarkers are increasingly used to narrow the differential diagnosis and refine the treatment of symptomatic patients in clinical practice (Rabinovici et al., 2019) based upon their appropriate use criteria (Johnson et al., 2013; Shaw et al., 2018). Despite this increased use, histological confirmation (the diagnostic reference standard) currently confirms an AD diagnosis for only 83% of AD patients at autopsy (Beach et al., 2012). In clinical trials, biomarkers can improve accuracy, utility, and cost effectiveness of screening, and can assess response to investigational therapies (Jack et al., 2018; Sevigny et al., 2016; Sperling et al., 2014). Their value is expected to further increase as AD-modifying therapies are realized, creating a need and rationale for population-level screening and an influx of patients requiring timely diagnosis and treatment (Liu et al., 2017).

Established AD biomarkers require cerebrospinal fluid (CSF) analyses or positron emission tomography (PET) imaging, which are limited by expense and inaccessibility. In addition, PET imaging exposes patients to radioactivity and lumbar punctures may cause back pain, headache, and bleeding (Duits et al., 2016). These issues highlight the need for accessible, AD-specific biomarkers that can be applied to broad clinical populations. The solution may lie in

brain magnetic resonance imaging (MRI), which is already standard of care in the United States for diagnostic evaluation of patients with new cognitive complaints (Knopman et al., 2001).

Current MRI biomarkers match the high accuracy of PET and CSF markers in separating AD from unimpaired individuals (Frisoni et al., 2010; Morris et al., 2016). However, MRI biomarkers cannot maintain the high accuracy of amyloid biomarkers in cohorts of patients with various causes of dementia (Ossenkoppele et al., 2018b; Wollman and Prohovnik, 2003). One thing likely impairing MRI-based biomarkers is the confounding influence of age-related brain atrophy or other undetected co-pathologies attributed to aging (Fotenos et al., 2005). For example, the confounding influence of preclinical AD in cohorts of cognitively normal (CN) older adults for other neuroimaging and cognitive measures has been shown previously (Brier et al., 2014a; Hassenstab et al., 2016; Jack et al., 2014).

Taking this into account, we sought to optimize the diagnostic specificity of structural MRIs for AD using quantitative, data-driven techniques. Specifically, we considered whether individually adjusting volumetric measures for age-related atrophy would improve volumetric-based AD biomarkers. We compared unadjusted AD classification models to those using normal aging curves generated from cognitively normal participants free from biomarker evidence of AD. These models were validated in a research cohort with biomarker-confirmed AD and cognitively normal individuals and in a large clinical cohort containing patients with various neurodegenerative dementing diseases (including AD) who underwent MRI as part of their diagnostic evaluation for the cause of dementia.

3.2 Methods

3.2.1 Participants

The 1287 participants in the Normal Aging (n = 383), Training (n = 216), Test (n = 109), and Clinical (n = 579) cohorts were composed from research studies or clinical patient records (collected 1990-2018). All procedures in this retrospective study were Health Insurance Portability and Accountability Act (HIPAA) compliant and approved by the Washington University Institutional Review Board. Informed consent was waived for the Clinical cohort and gained for all others. Those not in the Clinical cohort were from open-source datasets and have been reported in various previous publications; the analyses of this paper and the inclusion of the participants in the Clinical cohort are unique. All participants are described in Table 3.1, and Supplemental Table S3.1 gives these demographics separated by data source and diagnosis. All participants met the inclusion criteria described in Supplemental Table S3.2, which at minimum included a clinical assessment.

The Normal Aging cohort was restricted to cognitively normal participants who had a global Clinical Dementia Rating™ (CDR™) (Morris, 1993) of 0 stable across longitudinal follow-up, and were free of substantial AD pathology as determined by a negative amyloid PET scan (defined in section 3.2.2 Imaging). See Supplemental Table S3.2 for full inclusion criteria and Supplemental Figure S3.1 for distribution of ages. These participants were sourced from Open Access Series of Imaging Studies 3 (OASIS) and the Dominantly Inherited Alzheimer Network (DIAN). OASIS is an open-source dataset that is a retrospective compilation of data for > 1000 participants. OASIS data was collected across several ongoing projects through the Knight Alzheimer Disease Research Center (ADRC) over the course of 30 years and includes cognitively normal controls and AD patients at various stages of impairment (LaMontagne et al.,

2019). DIAN is a similar open-source dataset that includes a greater number of younger controls due to its focus on dominantly inherited AD.

The Training and Test cohorts contained cognitively normal and amyloid negative controls as well as cognitively impaired (CDR > 0) participants with a clinical diagnosis of AD and a PET scan indicating cerebral amyloidosis (full inclusion criteria in Supplemental Table S3.2). Participants were sourced from OASIS and the Alzheimer's Disease Neuroimaging Initiative (ADNI). ADNI is another open-source dataset that includes several hundred healthy controls and AD patients at various stages of impairment from multiple sites across the United States. Two-thirds of the cognitively normal and symptomatic AD participants from these sources (not overlapping with the controls in the Normal Aging cohort) were randomly assigned to the Training cohort with the remaining one-third becoming the Test cohort. Random assignment was done separately for the cognitively normal and AD participants to maintain equal distributions of AD diagnoses.

The Clinical cohort drew from patients seen at the Washington University Memory Diagnostic Center (MDC) outpatient clinic in Saint Louis, MO. Patients were split into symptomatic AD diagnoses and various non-AD diagnoses (including cognitively normal). See Supplemental Table S3.2 for full inclusion criteria. Patients listed separately as 'Uncertain' (153/579) did not have an etiologic cause of dementia indicated; without this, they could not be used to test the classification models. The AD and non-AD groups were also split into groups of more specific diagnoses (Supplemental Table S3.3).

All participants underwent a clinical assessment conducted by experienced clinicians including a semi-structured interview with the participant and a knowledgeable collateral source

as well as a thorough neurological examination (see Supplemental Table S3.2 for full inclusion criteria). A clinical diagnosis of dementia was considered at the conclusion of each assessment, integrating results from the clinical assessment and bedside measures of cognitive function (Day et al., 2017). Dementia severity was classified using the participant's CDR in accordance with established scoring rules (Morris, 1993). Etiologic diagnoses of dementia conformed to diagnostic criteria in use in clinical and research practices for AD (McKhann et al., 2011), dementia with Lewy bodies (McKeith et al., 2017), frontotemporal dementia (Rascovsky et al., 2011), and vascular cognitive impairment (Skrobot et al., 2018). See Supplemental Table S3.3 for a breakdown of specific diagnoses in the Clinical cohort. Clinical diagnosis was made blinded to amyloid status in the OASIS participants, but not in the ADNI participants.

All CDRs and Mini Mental State Exams (MMSEs) (Folstein et al., 1975) used in this study occurred within a year of MRI, and those sourced from DIAN and ADNI all had a time difference of 0 days. Participants sourced from OASIS had an average time difference of 99 days and the Clinical cohort had an average time difference of 118 days.

Table 3.1: Demographics

	Normal Aging Cohort	Training Cohort	Test Cohort	Clinical Cohort – Defined Diagnosis	Clinical Cohort – Uncertain Diagnosis
N	383	216	109	426	153
n by Data Source					
DIAN	134	0	0	0	0
OASIS	249	136	77	0	0
ADNI	0	80	32	0	0
MDC	0	0	0	426	153
Diagnosis (% with symptomatic AD)	0	43.5	43.1	61.5	N/A
Age (median)	18-88 (60)	57-88 (75)	57-86 (74)	46-88 (73)	55-87 (73)
Sex (% Men)	35.8	49.1	52.3	48.1	49.0
CDR [0,0.5,1,2,3]	383,0,0,0,0	122,43,44,5,2	62,17,26,4,0	50,235,97,26,0*	8,122,10,3,0*
MMSE (median)	24-30 (30)*	7-30 (28)	9-30 (28)	1-30 (20)*	1-30 (21)*
APOE4 (% with an ε4 allele)	27.9	51.6*	39.4	N/A	N/A
Amyloid Mean Cortical SUVR RSF – Centiloid (median)	-9.34-19.0 (-0.880)*	-8.40-154 (14.0)	-14.0-142 (11.4)	N/A	N/A
Race (% non-Hispanic White)	91.2*	90.3	79.8	86.9	84.3
Education (years) (median)	9-22 (16)*	7-24 (16)	8-22 (16)	Median Completed College*	Median Completed College*

Table 3.1 presents the demographic information for all cohorts. The Clinical cohort has been separated into those given either an AD or non-AD diagnosis vs. those whose diagnosis was uncertain (and thus were not used to measure model accuracy).

A '*' indicates missing data: 2 MMSEs, 124 Amyloids (all under age 45), and 6 Races from the Normal Aging cohort; 1 *APOE4* from the Training cohort; 4 MMSEs, 18 CDRs, and 40 Educations from the Clinical cohort – Defined Diagnosis; 1 MMSE, 10 CDRs, and 11 Educations from the Clinical cohort – Uncertain Diagnosis

AD: Alzheimer disease; ADNI: Alzheimer's Disease Neuroimaging Initiative; *APOE4*: Apolipoprotein E ε4; CDR: Clinical Dementia Rating; DIAN: Dominantly Inherited Alzheimer Network; MDC: Memory Diagnostic Center; MMSE: Mini Mental State Exam; OASIS: Open Access Series of Neuroimaging Studies; SUVR RSF: Standard uptake value ratio (regional spread function applied)

3.2.2 Imaging

All volumetric T1-weighted images underwent regional tissue segmentation with FreeSurfer 5.3 (freesurfer.net) using the Desikan-Killiany atlas (Desikan et al., 2006). Regional volumes (cortical and subcortical) underwent intracranial volume adjustment using a regression approach (Buckner et al., 2004), which fits a line to each region and the intracranial volume calculated by FreeSurfer. While studies typically fit this line to their entire cohort, we used the Normal Aging cohort alone to mimic the conditions that would be used if the tool were to be implemented into clinical practice, enabling reproducibility at the single-subject level. Volumes after intracranial volume correction were summed across hemispheres and cortical thicknesses (not corrected for intracranial volume per standard practice) were averaged across hemispheres. For more specific imaging details see Supplemental Table S3.4.

Amyloid PET imaging used Florbetapir ([^{18}F]-AV45) or [^{11}C]-Pittsburgh compound B (PIB) and was processed with an in-house pipeline (Su, 2021) using FreeSurfer-derived regions with a cerebellar cortex reference region. Partial volume correction in order to address signal spillover was done with a regional spread function (geometric transfer matrix) technique based on the scanner point spread function (determined at each imaging site) and the relative distance between regions (Su et al., 2015, 2013). We defined a negative amyloid PET scan as having a mean cortical standard uptake value ratio with regional spread function applied (SUVR RSF) < 1.42 (Centiloid < 16.4) for PIB PET or SUVR RSF < 1.19 (Centiloid < 20.6) for Florbetapir-PET. The mean cortical SUVR RSF was defined as the average SUVR RSF from the precuneus, prefrontal cortex, gyrus rectus, and lateral temporal regions (Su et al., 2019). We used cutoffs determined individually for each tracer, as opposed to a unified Centiloid cutoff, since these individually established cutoffs are likely more accurate due to the imperfect nature of

harmonization procedures such as Centiloid conversion (see Supplemental Table S3.5 for Centiloid conversion details). Further imaging details varied by cohort (Supplemental Table S3.4).

3.2.3 Normal Aging Curves

To describe age-related atrophy, normal aging curves were generated for each FreeSurfer region using the Normal Aging cohort data. For each cortical thickness and intracranial-corrected volume at each age, the mean for each cortical thickness and intracranial-corrected volume was calculated using a locally weighted scatter-plot smoother regression and a smoothed sliding window of two years for standard deviation. The Training, Test, and Clinical cohorts were then adjusted for age-related atrophy by transforming the volumes and cortical thicknesses into z-scores using these age-specific means and standard deviations (Figure 3.1). The hemisphere-combined volumes and thicknesses, with volumes adjusted for intracranial volume, are referred to as ‘unadjusted for age-related atrophy’. The unadjusted dataset that has undergone the z-score adjusted described above is referred to as ‘adjusted for age-related atrophy’. This adjustment for age-related atrophy greatly reduced the correlation of volumetric data with age (examples in Supplemental Table S3.6).

Figure 3.1: Examples of Region-Specific Atrophy Observed in Normal Aging

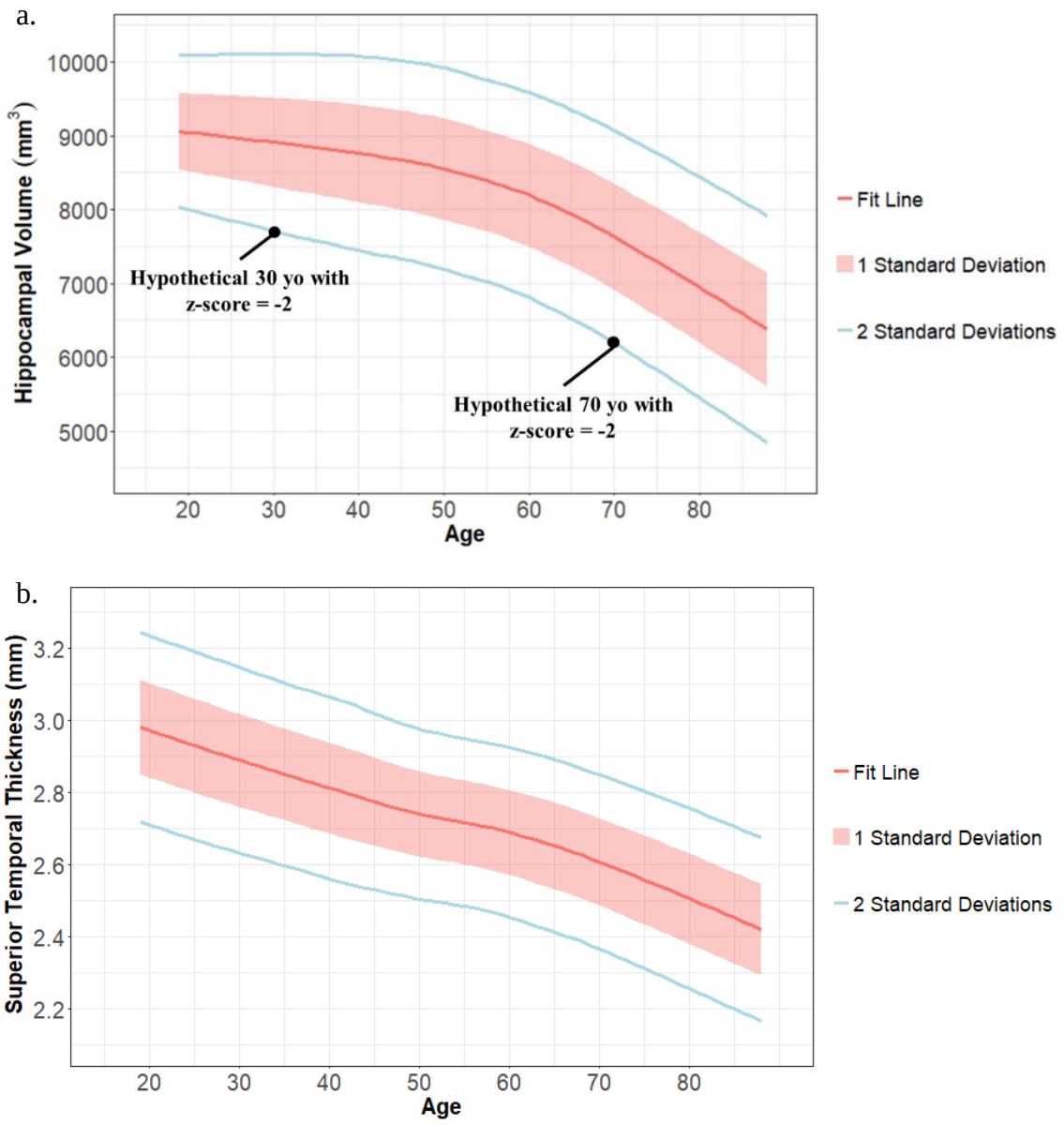

Figure 3.1 shows Hippocampal Volume (3.1a) and Superior Temporal Thickness (3.1b) as representatives of the normal aging curves used to adjust other participants' volumes and cortical thicknesses for age-related atrophy. The red line displays the estimated average volumes. The red ribbon and blue line display the first and second standard deviations from that average, which is calculated locally. Figure 3.1a additionally displays two black dots representing how two hypothetical participants at different ages could have different volumes but the same z-score after adjustment for age-related atrophy. Standard deviation is fairly consistent across the adult lifespan for both regions, but the averages suggest increasingly rapid atrophy at later ages for Hippocampal Volume vs. a steady decline for Superior Temporal Thickness.

3.2.4 Region Selection for AD Classification

Volumetric measures that optimally predicted symptomatic AD relative to cognitively normal controls were selected using the Training cohort. For 1000 iterations, a random 50% sample of the Training cohort was fit to a least absolute shrinkage and selection operator logistic regression. All regional volumes and cortical thicknesses, as measured by FreeSurfer, participant age, sex, and scanner strength (1.5 or 3T), were included as predictors (see Supplemental Figure S3.2 for entire list). This regression minimizes the sum of squared errors and has a bound on the sum of the absolute values of the coefficients, which sets many coefficients to zero. The variables not set to zero within each iteration were recorded, determining the frequency each variable was selected. This process was done using data adjusted with the normal aging curves and separately using unadjusted data (volumes still corrected by intracranial volume). The final region set included regions selected in over half the iterations for both sets of data.

3.2.5 Development of Classification Models

All classification models in this study used a logistic regression model (R package 'stats' (Bolar, 2019)) fit to the Training cohort to predict an AD diagnosis. The Age model included only chronological age as a predictor. The Hippocampal Volume (HCV) model used only hippocampal volume. The Select Atrophied Regions in Alzheimer disease (SARA) model used the regions selected in the region selection process described in section 3.2.4. The HCV_{adj} and $SARA_{adj}$ models differ from HCV and SARA in that they use data that has undergone the z-score adjustment to remove age-related atrophy, as described in section 3.2.3, while the HCV and SARA models use the unadjusted data (volumes still corrected by intracranial volume). The models HCV+Age, SARA+Age, HCV_{adj}+Age, and $SARA_{adj}$+Age added chronological age as an additional predictor. In this way, the HCV_{adj}+Age and $SARA_{adj}$+Age models used age as a risk

factor for AD, and separately to determine age-specific means and standard deviations when normalizing age-related changes in brain volumes and cortical thicknesses.

Models' receiver operating characteristics' area under the curve (AUCs) were compared using the Delong method (DeLong et al., 1988) with significance set to $p < 0.003$ (Bonferroni-corrected $p < 0.05$), and confidence intervals (CI) computed using 2000 stratified bootstrap replicates. Accuracy statistics, when reported, used thresholds determined by the maximal Youden's J statistic within the Training cohort (Youden, 1950).

3.3 Results

3.3.1 Participants

Table 3.1 details the demographics for each cohort, while Supplemental Table S3.1 breaks down demographics by data source and AD/non-AD diagnosis.

3.3.2 Normal Aging Curves

Figure 3.1 displays the age-related atrophy observed in the Normal Aging cohort, which is free of biomarker evidence of AD. Graphs of other regions can be accessed at https://github.com/benzinger-icl/SARA.

3.3.3 Region Selection for AD Classification

The hippocampal volume, inferior lateral ventricle volume, amygdala volume, entorhinal cortical thickness, and inferior parietal cortical thickness were selected in over half of the iterations in both the adjusted and unadjusted data and were thus used in all multi-region (SARA) models. Unadjusted coefficients for all models are in Table S3.7. Age and nucleus accumbens were additionally selected when using data adjusted for age-related atrophy, while inferior parietal volume and banks of the superior temporal sulcus volume were selected only

when using unadjusted data. Frequency of selection for all regions can be found in Supplemental Figure S3.2.

3.3.4 Classification Models: Impact of Adjusting for Age-Related Atrophy

AUCs for each model within the Test and Clinical cohorts are shown in Table 3.2; *p*-values for all comparisons are in Table 3.3. In the Test cohort, no significant differences were found between models using adjusted and unadjusted data. In the Clinical cohort, HCV+Age vs. HCV_{adj}+Age, and SARA+Age vs. $SARA_{adj}$+Age similarly showed no statistical difference in their AUCs, but HCV and SARA had higher AUCs than their counterparts HCV_{adj} (0.801 vs. 0.743, $p < 0.001$) and $SARA_{adj}$ (0.820 vs. 0.764, $p < 0.001$). Thus, our adjustment for age-related atrophy did not improve classification ability within our cohorts and instead lowered classification ability in models that did not include age. Without reason to pursue the more complex processing required to adjust for age-related atrophy, further analyses were limited to unadjusted models.

Table 3.2: AUCs for All Classification Models in Test and Clinical Cohorts

Model:	Test Cohort AUCs (95% CI)	Clinical Cohort AUCs (95% CI)
Age	0.675 *(0.572-0.778)*	0.742 *(0.694-0.790)*
HCV	0.944 *(0.902-0.987)*	0.801 *(0.756-0.846)*
SARA	0.961 *(0.925-0.997)*	0.820 *(0.776-0.864)*
HCV + Age	0.950 *(0.909-0.991)*	0.792 *(0.747-0.838)*
SARA + Age	0.962 *(0.924-0.999)*	0.799 *(0.753-0.845)*
HCV_{adj}	0.948 *(0.905-0.992)*	0.743 *(0.693-0.792)*
$SARA_{adj}$	0.952 *(0.911-0.993)*	0.764 *(0.714-0.813)*
HCV_{adj} + Age	0.949 *(0.908-0.991)*	0.793 *(0.748-0.840)*
$SARA_{adj}$ + Age	0.961 *(0.925-0.997)*	0.799 *(0.752-0.845)*

Table 3.2 displays each model's AUC (for AD vs. non-AD diagnoses) in the Test cohort and Clinical cohort along with its associated 95% CI. The AUC of a receiver operating characteristic plot (not displayed) gives a measure of model performance that does not depend on a specific cut-off or threshold. The various SARA models include hippocampal volume, inferior lateral ventricle volume, entorhinal thickness, amygdala volume, and inferior parietal thickness. X + Age indicates model X with age added as a covariate; X_{adj} indicates Model X using volumes and cortical thicknesses that have been adjusted for age-related atrophy.

AD: Alzheimer disease; Adj: Adjusted for age-related atrophy; AUC: Receiver operating characteristic's area under the curve; CI: Confidence interval; HCV: Hippocampal volume; SARA: Select Atrophied Regions in Alzheimer disease

Table 3.3: Comparisons of Classification Models' AUCs

	Test Cohort *p*-value	Clinical Cohort *p*-value
Impact of Adjusting for Age-Related Atrophy		
HCV vs. HCV_{adj}	0.77	< **0.001**
SARA vs. $SARA_{adj}$	0.32	< **0.001**
HCV+Age vs. HCV_{adj}+Age	0.45	0.48
SARA+Age vs. $SARA_{adj}$+Age	0.87	0.88
Impact of Age as a Predictor		
HCV vs. HCV+Age	0.20	**0.001**
SARA vs. SARA+Age	0.87	< **0.001**
HCV vs. Age	< **0.001**	0.02
SARA vs. Age	< **0.001**	**0.002**
Single vs. Multi Region Model		
HCV vs. SARA	0.18	0.06

Table 3.3 states the *p*-values for the Delong tests comparing AUCs in order to select the optimal classification model. Significant differences (after accounting for multiple comparisons) are bolded. The SARA models include hippocampal volume, inferior lateral ventricle volume, entorhinal thickness, amygdala volume, and inferior parietal thickness. X + Age indicates model X with age added as a covariate; X_{adj} indicates Model X using volumes and cortical thicknesses that have been adjusted for age-related atrophy.

Adj: Adjusted for age-related atrophy; AUC: Receiver operating characteristic's area under the curve; HCV: Hippocampal volume; SARA: Select Atrophied Regions in Alzheimer disease

3.3.5 Classification Models: Impact of Age as a Predictor

In the Test cohort, HCV and SARA models showed no statistical differences from their counterparts HCV+Age and SARA+Age (Table 3.3), but did outperform the Age model (0.944 vs. 0.675, $p < 0.001$; and 0.961 vs. 0.675, $p < 0.001$). In the Clinical cohort, HCV and SARA had higher AUCs than their counterparts HCV+Age and SARA+Age (0.801 vs. 0.792, $p = 0.001$ and 0.820 vs. 0.799, $p < 0.001$), but only SARA maintained a significantly higher AUC than the Age model (0.820 vs. 0.742, $p = 0.002$).

3.3.6 Classification Models: Selecting a Model

The AUCs of HCV and SARA were not significantly different from each other within the Test or Clinical cohorts (Table 3.3), but SARA's AUC was numerically higher than HCV's AUC in both cohorts (Table 3.2). SARA was selected as the optimal model for this reason in addition to being the only model significantly better than age alone in the Clinical cohort. Figure 3.2 provides more detail on the probabilities of AD predicted by SARA for the participants in the Test and Clinical cohorts, as well as accuracy measures such as sensitivity and specificity. The x-axes represent the possible output from the SARA model, where a 1.00 indicates a predicted 100% probability of a symptomatic AD diagnosis. The y-axes indicate the probability density function, which is a smoothed histogram normalized to an area of 1 and allows comparison of different sized groups. An example of how to read Figure 3.2a is to take the area under the curve of the cognitively normal line from x = 0 to 0.25. This is approximately 0.62, indicating that 62% of the cognitively normal controls in the Test cohort had a probability between 0-25%.

Figure 3.2: Distribution of Predicted Probabilities and Accuracy Statistics for the SARA Model

a. Test Cohort

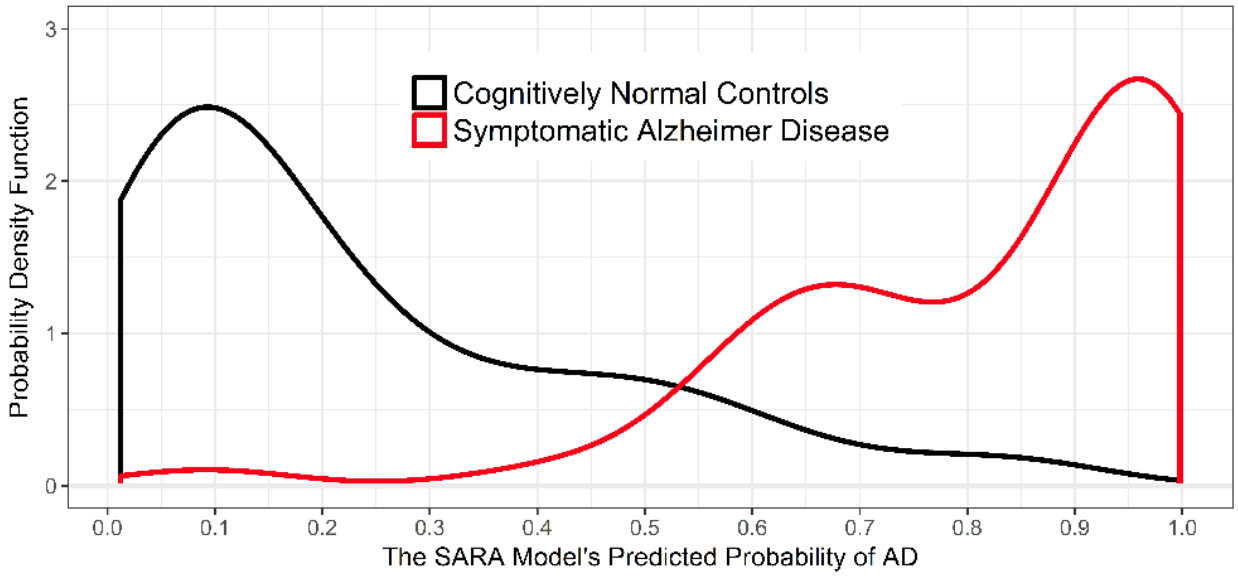

b. Clinical Cohort

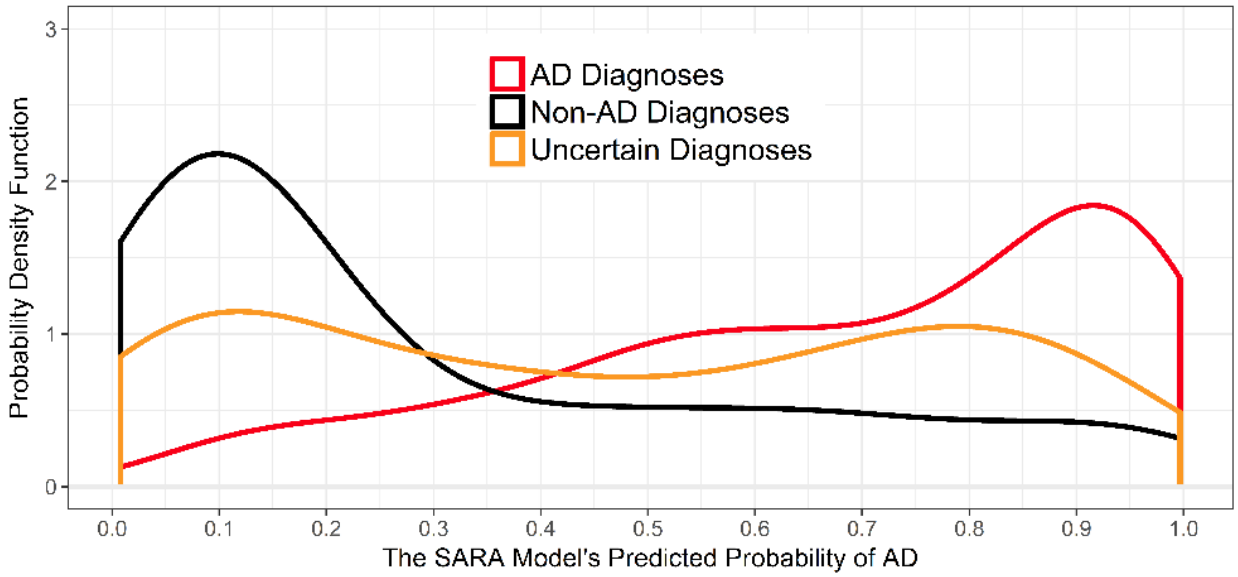

c.	Test Cohort	Clinical Cohort
Accuracy *(95 % CI)*	85.3 *(78.9-91.7);* 93/109	77.9 *(73.9-81.7);* 332/426
Sensitivity *(95 % CI)*	97.9 *(93.6-100);* 46/47	83.6 *(79.0-87.8);* 219/262
Specificity *(95 % CI)*	75.8 *(64.5-85.5);* 47/62	68.9 *(62.2-75.6);* 113/164
Positive Predictive Value *(95 % CI)*	75.4 *(67.7-83.9);* 46/61	81.1 *(77.6-84.7);* 219/270
Negative Predictive Value *(95 % CI)*	97.9 *(93.6-100);* 47/48	72.4 *(66.7-78.3);* 113/156

Figure 3.2a and 3.2b display the distribution of the SARA model's output for the Test cohort and Clinical cohort, respectively. Both 3.2a and 3.2b show good separation between the AD and non-AD groups. 3.2b has slightly less separation and additionally displays the Uncertain Diagnoses

group – those that were unable to be classified into the AD or non-AD groups. 3.2c displays more traditional diagnostic test measures for SARA using a cutoff of 0.381 (derived using the maximal Youden's J statistic in the Training cohort) along with the 95% CI.

AD: Alzheimer disease; CI: Confidence interval; SARA: Select Atrophied Regions in Alzheimer disease

3.3.7 Classification Models: Specific Diagnoses in the Clinical Cohort

While models were compared using their ability to separate AD from non-AD diagnoses, the heterogeneity of the Clinical cohort allowed us to examine more specific clinical diagnoses (groups defined in Supplemental Table S3.3). For non-AD diagnoses, these included other dementia types and non-dementia diagnoses that explained the cognitive complaints of the patient. For AD diagnoses, this included sub-groups of AD to test how the model behaved in atypical AD patients. Figure 3.3 displays the unique probability density functions for each of the more specific etiologic diagnoses in the Clinical cohort, with the AD and non-AD diagnoses groups included for comparison. The AUCs for each sub-group are in Supplemental Table S3.8, but small group sizes prevented robust statistical analyses. Thus, the following is qualitative rather than an assessment of *p*-values.

Figure 3.3a, with more detail in Supplemental Table S3.8, demonstrates that AD sub-groups have a high classification accuracy with only slightly lower predicted probabilities in the early-onset AD (age < 65) and AD variant (such as Posterior Cortical Atrophy) groups as compared to typical (amnestic, late onset) AD. Figure 3.3b indicates SARA was good at distinguishing AD from the non-neurodegenerative diagnoses, including mood and sleep disorders; in total AD vs. non-neurodegenerative diagnoses had an AUC of 0.877 (95% confidence interval (CI): 0.833-0.922). Figure 3.3c shows SARA was less able to separate AD from other neurodegenerative diagnoses and had a combined AUC of 0.719 (95% CI: 0.640-0.799). Only frontotemporal dementia participants (subtypes combined due to small n) approached the same level of separation from AD as the non-neurodegenerative diagnoses.

The impact of using the multi-region SARA over the simple HCV model also varied by diagnosis (Supplemental Table S3.8). SARA had only a marginally larger AUC than HCV for

separating Typical AD from non-AD diagnoses (0.827 vs. 0.819), but substantial improvements were seen for separating AD variants from non-AD diagnoses (0.795 vs. 0.697).

Figure 3.3: Distribution of Predicted Probabilities for the SARA Model for Specific Diagnoses in the Clinical Cohort

a. Alzheimer Disease Diagnoses

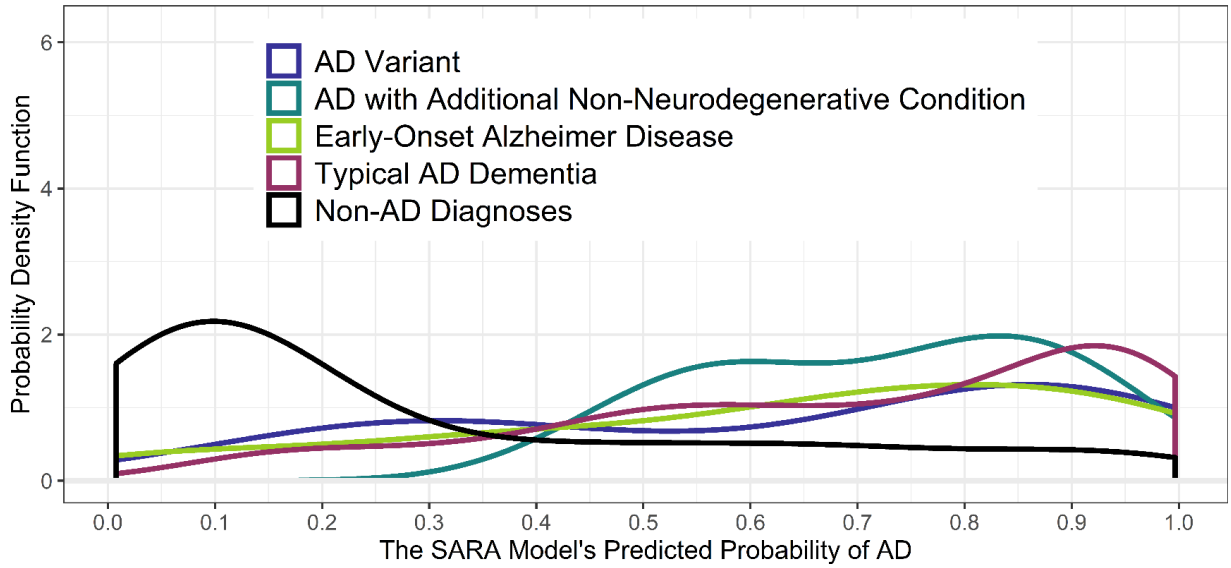

b. Non-Neurodegenerative Non-AD Diagnoses

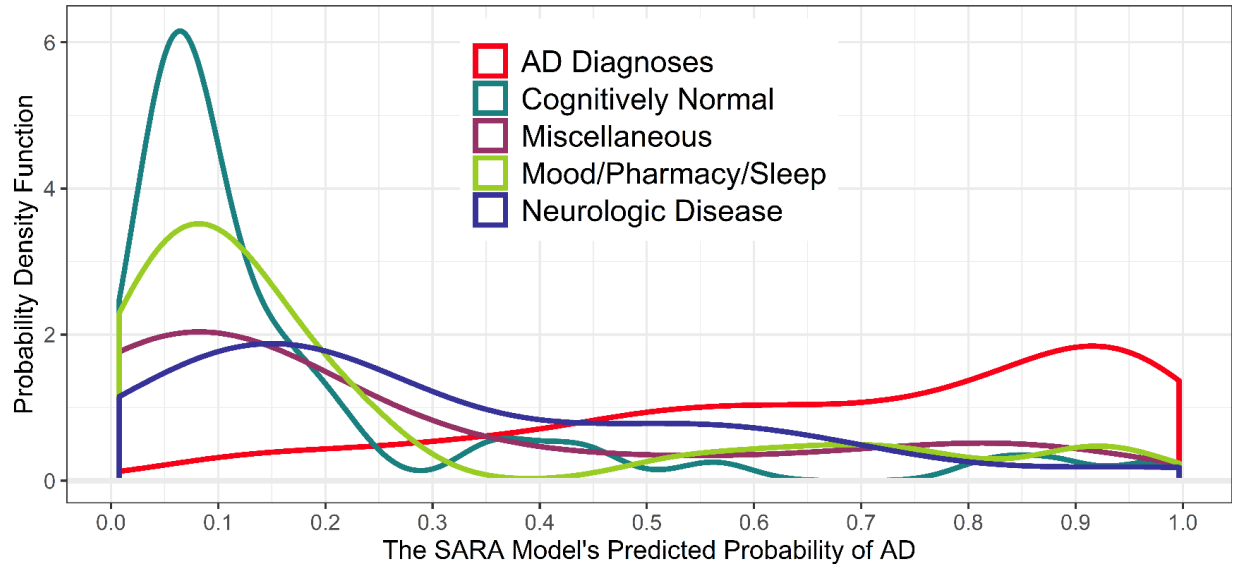

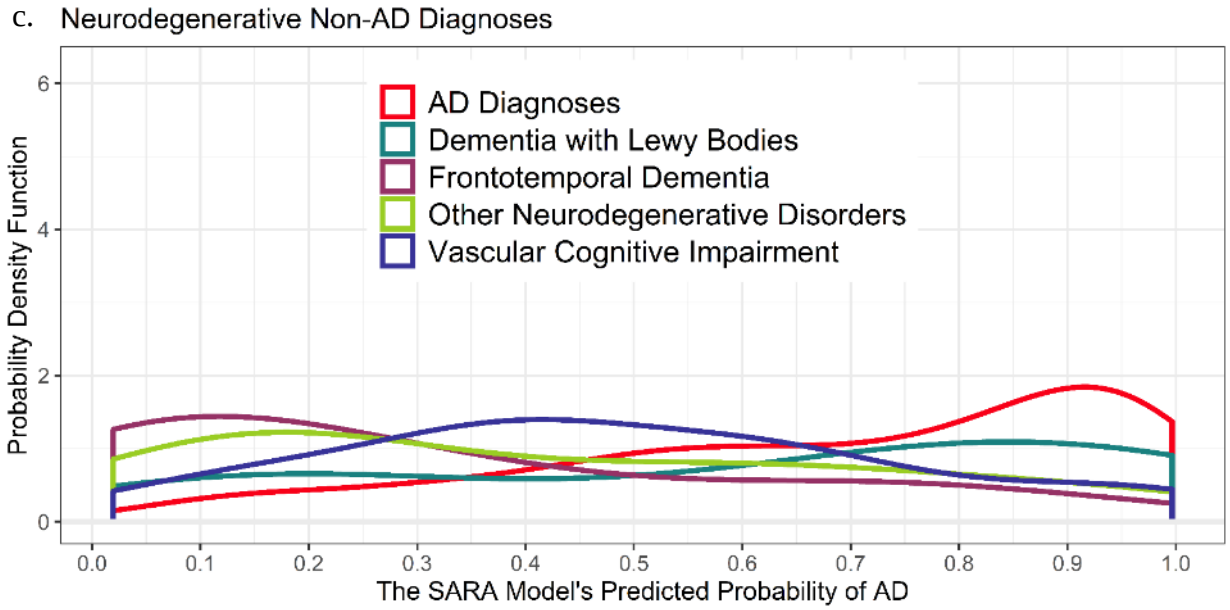

Figure 3.3 displays the distribution of the SARA model's output in the Clinical cohort using more specific diagnoses than the AD and non-AD binary from Figure 3.1b. Figure 3.3a displays the specific AD diagnoses along with the combined non-AD Diagnoses line taken from Figure 3.2b. Figure 3.3b displays the specific non-AD diagnoses that are non-neurodegenerative in nature and overlays the combined AD Diagnoses line. 3.3c displays the specific non-AD diagnoses that are neurodegenerative in nature and overlays the combined AD Diagnoses line. Note the change in y-axes scale from Figure 3.2 due to the tight distribution of cognitively normal patients in 3.3b.

AD: Alzheimer disease; SARA: Select Atrophied Regions in Alzheimer disease

3.3.8 Classification Models: MMSE and CDR in the Clinical Cohort

Figure 3.4a shows the probability density plot of the Clinical cohort separated by participants' MMSE, while Supplemental Figure S3.3a separates by CDR. MMSEs and CDRs were collected within one year of the MRI (average time difference of 118 days). The strong relationship between level of impairment and SARA's predicted probability of symptomatic AD reflects an alignment between an individual's level of impairment and atrophy in the regions used in SARA (atrophy indicated by a model output closer to one). Despite this strong relationship, SARA maintained a fairly high AUC (0.773) within the group of participants with MMSEs 26-29 (n = 154, Figure 3.4b). This indicates the SARA model had good classification ability beyond predicting level of impairment. This was similarly true for participants with a global CDR of 0.5, which had an AUC of 0.782 (n = 235, Supplemental Figure S3.3b). This pattern persisted even when considering only those whose MMSE and CDR occurred within 30 days of their MRI, with AUCs of 0.806 (n = 63) and 0.771 (n = 101), respectively.

Figure 3. 4: MMSE Aligns, but is Not Equivalent, to Predicted Probability in SARA

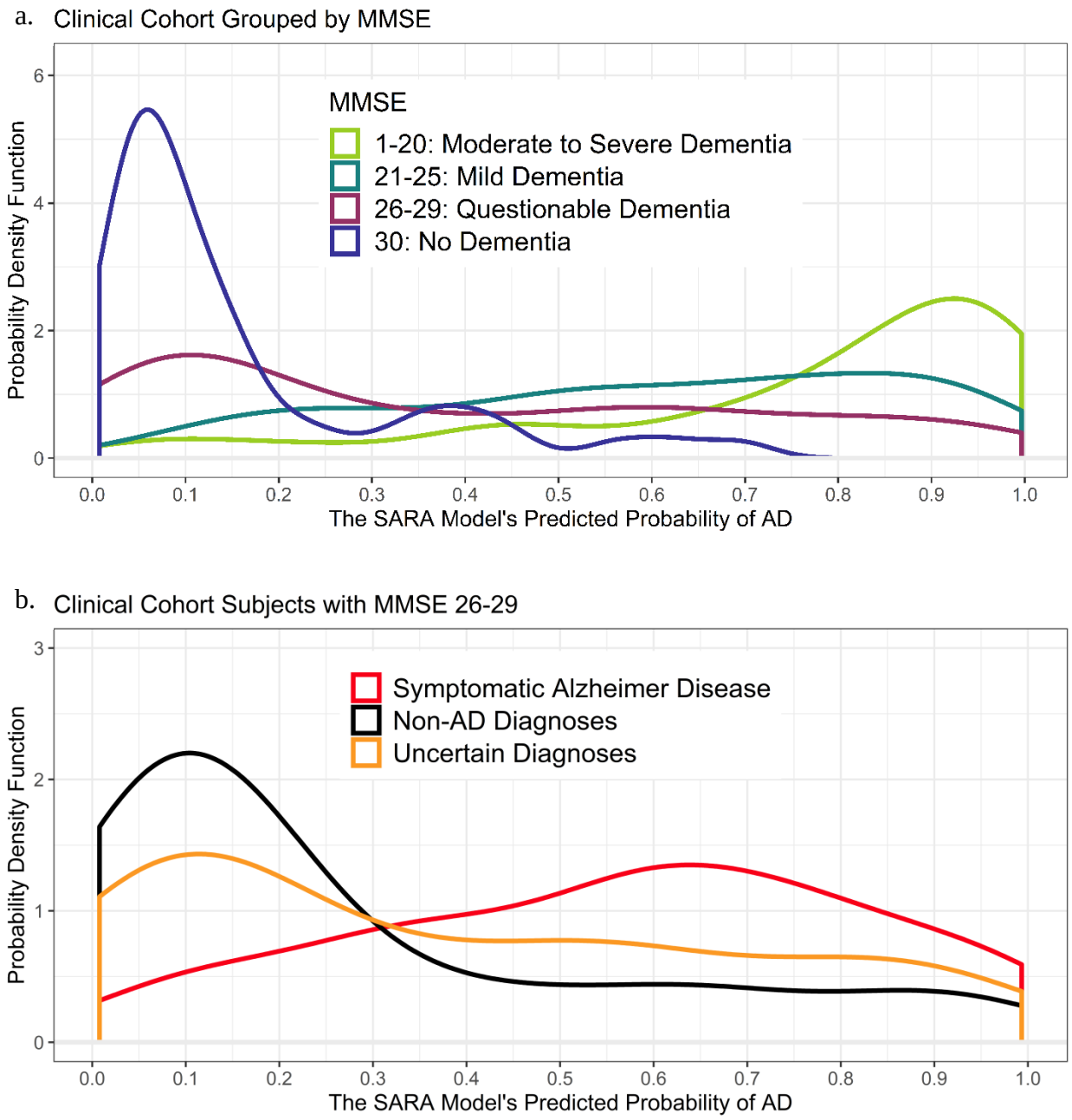

Figure 3.4a displays the distributions of the SARA model's predicted probability of AD for all participants (including Uncertain Diagnoses) in the Clinical cohort, grouped by MMSE score instead of by diagnosis. Note the change in y-axes scale due to the tight distribution of MMSE = 30 participants. 3.4b displays the distribution of SARA model's predicted probability of AD as in Figure 3.2b, but only includes patients with MMSE scores of 26-29 (n = 154).

AD: Alzheimer disease; MMSE: Mini Mental State Exam; SARA: Select Atrophied Regions in Alzheimer disease

3.3.9 SARA as a Possible Clinical Tool

To create an example of how SARA could be used in clinical practice, we developed multiple thresholds reflecting 80% and 90% sensitivities and specificities. Figure 3.5a shows the readout a clinician might be given for an individual patient and Figure 3.5b lists the percent of the Clinical cohort that fell into each category. Over half of the participants who had uncertain diagnoses were given a score within the 90% sensitivity/specificity ranges for AD or non-AD diagnoses, indicating it would be a valuable tool to support clinical decision making.

Figure 3.5: Possible Use of SARA in a Clinical Setting

a.

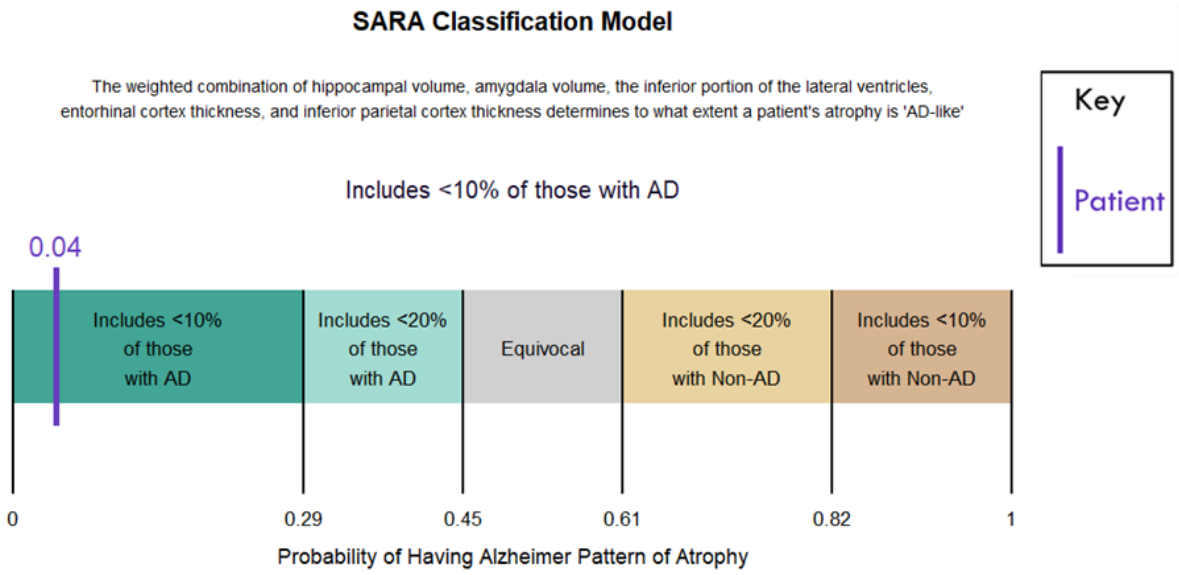

b.

Predicted Probability	Model Output	% Of Clinical Cohort with Known Diagnosis (n = 429)	% Of Clinical Cohort with Uncertain Diagnosis (n = 154)
[0.0-0.29)	< 10% of those with AD	30.8%	37.9%
[0.29-.45)	< 20% of those with AD	8.9%	12.4%
[0.45-0.61]	Equivocal	13.8%	10.4%
(0.61-0.82]	< 20% of those with non-AD	17.4%	21.6%
(0.82-1.0]	< 10% of those with non-AD	29.1%	17.6%

Figure 3.5a displays how the SARA model might be used by a clinician for a single patient, including a description of the model and multiple thresholds. The patient's specific probability of having AD as predicted by SARA is given (4%), as well as a statement reflecting that the sensitivity at that threshold is > 90%, indicating both a measure of atrophy and the reliability of that measure. Figure 3.5b displays the proportion of participants in the Clinical cohort that fell into each bin of ranges of scores output from SARA. The next column shows the Clinical cohort participants with uncertain diagnoses, with the distribution of scores suggesting that SARA would have helped provide a more certain diagnoses for the majority of the participants.

AD: Alzheimer disease; SARA: Select Atrophied Regions in Alzheimer disease

3.4 Discussion

We demonstrated that volumetric models have excellent classification abilities that would aid in diagnosing symptomatic AD in various circumstances. We did observe region-specific atrophy even in our unique cohort of cognitively normal participants known to be without preclinical AD. However, controlling for this age-related atrophy did not improve classification. Doing so actually lowered accuracy within the Clinical cohort if age was not included as an additional predictor. This reinforces the idea that age is a strong predictor of AD dementia and implies that these models require age or age-related atrophy to maintain the highest levels of accuracy. Thus, age-related atrophy may either convey increased risk for development of a neurodegenerative dementing illness, or, more likely, age-related atrophy may act as a proxy for age. Either way, total atrophy appears to be more predictive than atrophy specifically attributable to AD.

Our data-driven region selection approach, optimized to FreeSurfer, saw a specific pattern of atrophy in AD that overlapped with the medial temporal lobe regions reported in many previous papers. We evaluated if using these regions would improve classification of AD. While the single region HCV and multi-region SARA models did not show statistically different AUCs, other evidence suggested SARA was the stronger classifier. First, in both the Test and Clinical cohorts, the value of the AUC was higher in SARA than HCV. Second, in the Clinical cohort, it was only SARA that had an AUC statistically higher than the model using age alone, without any volumetric measures. Third, the pattern of higher AUCs in SARA than in HCV was seen for most specific diagnostic groups within the Clinical cohort.

Our results suggest SARA has the greatest diagnostic specificity when distinguishing AD from frontotemporal dementia or from non-neurodegenerative diagnoses (e.g., mood disorders,

sleep disorders, cognitively normal individuals). The high performance in frontotemporal dementia is especially noteworthy. [18F]-fluorodeoxyglucose (FDG) PET is recommended for patients with AD vs. frontotemporal dementia diagnoses (Silverman et al., 2001), but PET scans are limited in diagnostic sensitivity and by insurance coverage (Medicare will cover it, but often private insurance will not), availability, and cost. This AD vs. frontotemporal dementia differential is often considered, especially in younger patients, and highly available biomarkers would help identify the correct prognosis and treatment for these patients. The Clinical cohort had the lowest diagnostic specificity when distinguishing AD from other neurodegenerative disorders. This was likely due to the disorders impacting overlapping regions and patients having co-incident diagnoses. Comorbidities increase with age and can include multiple neurodegenerative conditions, such as concurrent AD and dementia with Lewy bodies (Irwin and Hurtig, 2018).

Another way SARA reflects clinical reality is the correlation between atrophy and level of impairment measured by MMSE and global CDR. With this in mind, we evaluated the diagnostic utility of SARA beyond predicting impairment and found high classification ability in the Clinical cohort even when limited to early symptomatic participants (CDR = 0.5 or MMSE 26-29). These patients are also the ones for whom additional biomarkers would likely be most useful. These findings indicate SARA is not simply acting as a proxy for MMSE or CDR, but provides additional diagnostic information.

Strengths of this study include the large overall sample size of almost 1300 participants. We benefited from having research cohorts with participants diagnosed with the highest possible accuracy outside of postmortem testing, as well as a heterogeneous group of real-world patients seen at a dementia clinic. By using these cohorts in combination, we were able to demonstrate

that our model approaches the sensitivity and specificity of amyloid PET and CSF biomarkers. Strengths of the SARA algorithm include that it is fairly simple and transparent (unlike machine-learning algorithms), making it easier for doctors and patients to trust, will be freely available, uses MRI scans that are non-invasive and often already collected for dementia patients, and has been shown to work in both research and clinical populations. SARA and the Clinical cohort's data will be made available online at https://github.com/benzinger-icl/SARA and https://www.oasis-brains.org/.

While our results indicate the potential usefulness of quantitative volumetric biomarkers, there are some limitations of this study. Though our cohorts had fairly good representation of African Americans, the general lack racial and socioeconomic diversity may bias our models. Volumetric classification may be further improved if models, including the regions used, are optimized to specific non-AD diagnoses and/or incorporate longitudinal scanning. Our use of a single set of normal aging curves and a binary AD/non-AD prediction model was due to our limited numbers, despite surpassing the sample size of many neuroimaging studies. The threshold used in the reported accuracy statistics was based upon the Training cohort and has not been optimized to a clinical setting. This optimization would need to be validated in a separate cohort, ideally with histopathologically confirmed diagnoses. This confirmation was not available for the Clinical cohort and misdiagnosis may have caused an under-estimation of model accuracy. An important question for future work to address is the overlap of AD and vascular disease, which we were unable to address due to the diagnostic difficulty and limited presence of vascular problems in our research cohorts.

3.5 Acknowledgements

Data collection and sharing for this project was supported by The Dominantly Inherited Alzheimer's Network (DIAN, U19AG032438) funded by the National Institute on Aging (NIA), the German Center for Neurodegenerative Diseases (DZNE), Raul Carrea Institute for Neurological Research (FLENI), Partial support by the Research and Development Grants for Dementia from Japan Agency for Medical Research and Development, AMED, and the Korea Health Technology R&D Project through the Korea Health Industry Development Institute (KHIDI).This manuscript has been reviewed by DIAN Study investigators for scientific content and consistency of data interpretation with previous DIAN Study publications. We acknowledge the altruism of the participants and their families and contributions of the DIAN research and support staff at each of the participating sites for their contributions to this study.

Data collection and sharing for this project was funded by the Alzheimer's Disease Neuroimaging Initiative (ADNI) (National Institutes of Health Grant U01 AG024904) and DOD ADNI (Department of Defense award number W81XWH-12-2-0012). ADNI is funded by the National Institute on Aging, the National Institute of Biomedical Imaging and Bioengineering, and through generous contributions from the following: AbbVie, Alzheimer's Association; Alzheimer's Drug Discovery Foundation; Araclon Biotech; BioClinica, Inc.; Biogen; Bristol-Myers Squibb Company; CereSpir, Inc.; Cogstate; Eisai Inc.; Elan Pharmaceuticals, Inc.; Eli Lilly and Company; EuroImmun; F. Hoffmann-La Roche Ltd and its affiliated company Genentech, Inc.; Fujirebio; GE Healthcare; IXICO Ltd.; Janssen Alzheimer Immunotherapy Research & Development, LLC.; Johnson & Johnson Pharmaceutical Research & Development LLC.; Lumosity; Lundbeck; Merck & Co., Inc.; Meso Scale Diagnostics, LLC.; NeuroRx Research; Neurotrack Technologies; Novartis Pharmaceuticals Corporation; Pfizer Inc.; Piramal

Imaging; Servier; Takeda Pharmaceutical Company; and Transition Therapeutics. The Canadian Institutes of Health Research is providing funds to support ADNI clinical sites in Canada. Private sector contributions are facilitated by the Foundation for the National Institutes of Health (www.fnih.org). The grantee organization is the Northern California Institute for Research and Education, and the study is coordinated by the Alzheimer's Therapeutic Research Institute at the University of Southern California. ADNI data are disseminated by the Laboratory for Neuro Imaging at the University of Southern California.

Data were provided in part by OASIS-3: Principal Investigators: T. Benzinger, D. Marcus, J. Morris; National Institutes of Health (NIH) P50AG00561, P30NS09857781, P01AG026276, P01AG003991, R01AG043434, UL1TR000448, R01EB009352. Florbetapir [^{18}F] ([^{18}F]-AV-45) doses were provided by Avid Radiopharmaceuticals, a wholly owned subsidiary of Eli Lilly.

3.6 Supplemental

Supplemental Table S3.1: Demographics by Data Source and Diagnosis

	Normal Aging Cohort	Training Cohort	Test Cohort	Clinical Cohort – Defined Diagnosis	Clinical Cohort – Uncertain Diagnosis
n	383	216	109	426	153
n by Data Source					
DIAN	134	0	0	0	0
OASIS	249	136	77	0	0
ADNI	0	80	32	0	0
MDC	0	0	0	426	153
Diagnosis (% with symptomatic AD)	0	43.5	43.1	61.5	N/A
By Data Source	OASIS: 0 DIAN: 0	OASIS: 22.1 ADNI: 80.0	OASIS: 24.7 ADNI: 87.5		
Age (median)	18-88 (60)	57-88 (75)	57-86 (74)	46-88 (73)	55-87 (73)
By Data Source	OASIS: 42-88 (68) DIAN: 18-58 (34)	OASIS: 57-88 (72) ADNI: 57-88 (76)	OASIS: 57-86 (73) ADNI: 59-86 (74)		
By Diagnosis		AD: 57-88 (77) Non-AD: 57-87 (71)	AD: 59-86 (76) Non-AD: 57-85 (70)	AD: 50-88 (76) Non-AD: 46-85 (68)	
Sex (% Men)	35.8	49.1	52.3	48.1	49.0
By Data Source	OASIS: 31.7 ADNI: 43.3	OASIS: 46.3 ADNI: 53.8	OASIS: 46.8 ADNI: 65.6		
By Diagnosis		AD: 50.0 Non-AD: 48.4	AD: 68.1 Non-AD: 40.3	AD: 44.7 Non-AD: 53.7	
CDR [0,0.5,1,2,3]	383,0,0,0,0	122,43,44,5,2	62,17,26,4,0	50,235,97,26,0*	8,122,10,3,0*
By Data Source	OASIS: 249,0,0,0,0 ADNI: 134,0,0,0,0	OASIS: 106,24,6,0,0 ADNI: 16,19,38,5,2	OASIS: 58,8,10,1,0 ADNI: 4,9,16,3,0		

	Normal Aging Cohort	Training Cohort	Test Cohort	Clinical Cohort – Defined Diagnosis	Clinical Cohort – Uncertain Diagnosis
By Diagnosis		AD: 0,43,44,5,2 Non-AD:	AD: 0,17,26,4,0 Non-AD: 62,0,0,0,0	AD: 2,155,78,20,0* Non-AD: 48,80,19,6,0*	
MMSE (median)	24-30 (30)*	7-30 (28)	9-30 (28)	1-30 (20)*	1-30 (21)*
By Data Source	OASIS: 26-30 (30) DIAN: 24-30 (30)*	OASIS: 14-30 (29) ADNI: 7-30 (24)	OASIS: 19-30 (29) ADNI: 9-30 (24)		
By Diagnosis		AD: 7-30 (24) Non-AD: 26-30 (30)	AD: 9-29 (24) Non-AD: 25-30 (29)	AD: 1-30 (18) * Non-AD: 3-30 (23)*	
APOE4 (% with an ε4 allele)	27.9	51.6*	39.4	N/A	N/A
By Data Source	OASIS: 51.5 DIAN: 28.4	OASIS: 40.7* ADNI: 70.0	OASIS: 26.8 ADNI: 65.6		
By Diagnosis		AD: 83.0 Non-AD: 27.3*	AD: 74.5 Non-AD: 12.9	N/A	
Amyloid** (median)	-9.34-19.0 (-0.880)*	-8.40-154 (14.0)	-14.0-142 (11.4)	N/A	N/A
By Data Source	OASIS: -9.34-19.0 (-0.880)* DIAN: -5.42-6.84 (-0.246)*	OASIS: -8.40-140 (3.13) ADNI: -6.22-154 (66.0)	OASIS: -14.0-142 (4.21) ADNI: -5.73-113 (61.5)		
By Diagnosis		AD: 21.1-154 (73.7) Non-AD: -8.40-20.4 (2.10)	AD: 43.0-142 (73.1) Non-AD: -14.0-18.3 (0.181)	N/A	
Race (% non-Hispanic White)	91.2*	90.3	79.8	86.9	84.3
By Data Source	OASIS: 88.4 ADNI: 96.9	OASIS: 86.8 ADNI: 96.3	OASIS: 71.4 ADNI: 100		

	Normal Aging Cohort	Training Cohort	Test Cohort	Clinical Cohort – Defined Diagnosis	Clinical Cohort – Uncertain Diagnosis
By Diagnosis		AD: 97.9 Non-AD: 84.4	AD: 93.6 Non-AD: 69.4	AD: 87.8 Non-AD: 85.4	
Education (years) (median)	9-22 (16)*	7-24 (16)	8-22 (16)	Median Completed College*	Median Completed College*
By Data Source	OASIS: 10-20 (16) DIAN: 9-22 (16)	OASIS: 7-24 (16) ADNI: 8-20 (16)	OASIS: 8-22 (16) ADNI: 8-20 (16)		
By Diagnosis		AD: 7-20 (16) Non-AD: 8-24 (16)	AD: 8-20 (16) Non-AD: 10-22 (15)	AD: Median Completed College* Non-AD: Median Completed College*	

Supplemental Table S3.1 presents the demographic information for all cohorts separated by data source and diagnosis. The Clinical cohort has been separated into those given either an AD or non-AD diagnosis vs. those whose diagnosis was uncertain (and thus were not used to measure model accuracy).

A '*' indicates missing data: 2 MMSEs (DIAN), 124 Amyloid (3 OASIS, 121 DIAN – all under age 45), and 6 Races (DIAN) from the Normal Aging cohort; 1 *APOE4* (OASIS, non-AD) from the Training cohort; 4 MMSEs (3 AD, 1 non-AD), 18 CDRs (7 AD, 11 non-AD), and 40 Educations (25 AD, 15 non-AD) from the Clinical cohort – Defined Diagnosis; 1 MMSE, 10 CDRs, and 11 Educations from the Clinical cohort – Uncertain Diagnosis

** Mean Cortical SUVR RSF in Centiloids

AD: Alzheimer disease; ADNI: Alzheimer's Disease Neuroimaging Initiative; *APOE4*: Apolipoprotein E ε4; CDR: Clinical Dementia Rating; DIAN: Dominantly Inherited Alzheimer Network; MDC: Memory Diagnostic Center; MMSE: Mini Mental State Exam; OASIS: Open Access Series of Neuroimaging Studies; SUVR RSF: Standard uptake value ratio (regional spread function applied)

Supplemental Table S3.2: Inclusion Criteria for All Cohorts

	Normal Aging Cohort	Training and Test Cohorts	Clinical Cohort
Sources	-OASIS -DIAN	-OASIS -ADNI	MDC
Inclusion Criteria – AD		-Structural MRI -CDR > 0 within 1 year of MRI -Positive Amyloid PET scan within 1 year of MRI -Clinical evaluation with a diagnosis of 'Alzheimer disease' or 'Dementia of Alzheimer Type'*	-Structural MRI -Clinician visit between January 25, 2015 and June 01, 2018 -Age over 45 -Clinical assessment supports an AD diagnosis*
Inclusion Criteria – Non-AD	-Structural MRI -CDR = 0 within 1 year of MRI If over age 45: -CDR remained 0 at least 3 years after MRI -Negative amyloid PET scan within 1 year of MRI If from DIAN: -non-mutation carrier	-Structural MRI -CDR = 0 within 1 year of MRI -Amyloid negative scan within 1 year of MRI -Clinical evaluation with a diagnosis of 'cognitively normal' or 'not demented' -Age ≥ 56 (age of the youngest AD participant included in the Training and Test cohorts)	-Structural MRI -Clinician visit between January 25, 2015 and June 01, 2018 -Age over 45 -Clinical assessment supports a non-AD diagnosis*

Supplemental Table S3.2 describes the data sources and inclusion criteria that defined the AD and non-AD participants for each cohort.

*Participants in the Clinical cohort not given a diagnosis that clearly supported or rejected AD formed a third 'Uncertain' category.

AD: Alzheimer disease; ADNI: Alzheimer's Disease Neuroimaging Initiative; CDR: Clinical Dementia Rating; DIAN: Dominantly Inherited Alzheimer Network; MDC: Memory Diagnostic Center; MRI: Magnetic resonance imaging; OASIS: Open Access Series of Neuroimaging Studies; PET: Positron emission tomography

Supplemental Table S3.3: Specific Diagnostic Groups in the Clinical Cohort – Definitions and Group Size

	N	Description
AD Diagnoses		
AD Variant	11	Includes Posterior Cortical Atrophy and other less common presentations of AD
AD with Additional Non-Neurodegenerative Condition	10	Patients with AD where other factors such as mood disorders, medications, and sleep disorders were thought to be contributing to symptoms
Early-Onset AD	26	Early onset indicated either in physician notes or by patient age at time of diagnosis being less than 65
Typical AD	215	AD diagnoses given without any other indications and so assumed to be amnestic, late-onset AD. Does not rule out the possibility of atypical presentation or other non-neurodegenerative conditions.
Neurodegenerative Non-AD Diagnoses		
Dementia with Lewy Bodies	10	Dementia with Lewy bodies
Frontotemporal Dementia	20	Includes those with behavioral variant, those that overlap with amyotrophic lateral sclerosis or motor neuron disease, and those with unspecified subtypes. Those with Primary Progressive Aphasia are not included and are instead in the 'Other Neurodegenerative Disorders' group.
Other Neurodegenerative Disorders	15	Less common neurodegenerative disorders (including Primary Progressive Aphasia, Parkinson's, and Corticobasal Degeneration), as well as patients with multiple possible non-AD neurodegenerative disorders listed
Vascular Cognitive Impairment	14	Vascular Cognitive Impairment
Non-Neurodegenerative Non-AD Diagnoses		
Cognitively Normal	45	Includes diagnoses of cognitively normal, subjective impairment only, or age-related cognitive changes
Miscellaneous	15	All other patients that did not fit into any of the other seven non-AD groups but whose diagnoses nonetheless indicate a non-AD etiology
Mood/Pharmacy/Sleep	27	Symptoms were attributed singularly or to a combination of mood disorders, medications (polypharmacy in some cases), and sleep disorders
Neurologic Disease	18	Broad range of (non-neurodegenerative) neurological problems such as traumatic brain injury or seizures

Supplemental Table S3.3 describes the more specific AD and non-AD diagnostic groups the Clinical cohort was split into, and the number of patients in each group.

AD: Alzheimer disease

Supplemental Figure S3.1: Histogram of Ages in the Normal Aging Cohort

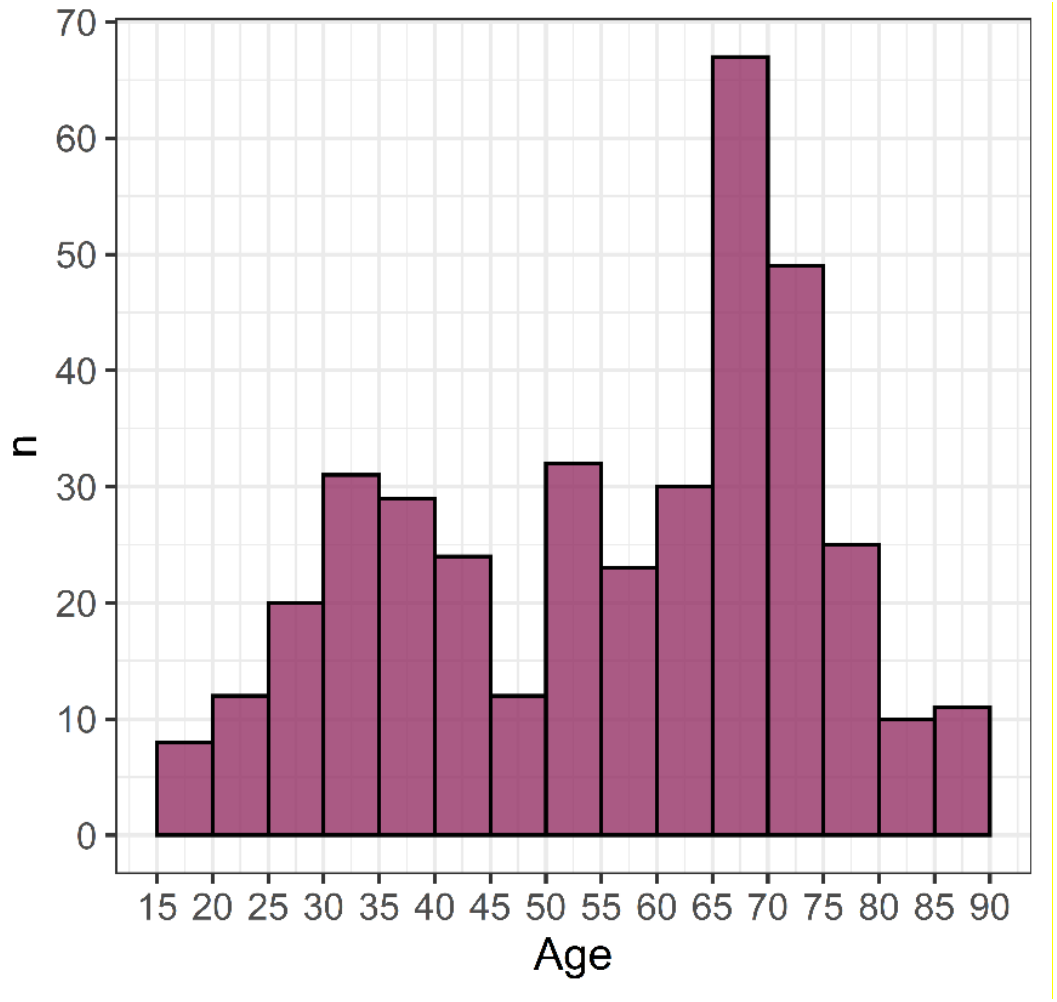

Supplemental Figure S3.1 shows the number of participants present by age in the Normal Aging cohort.

Supplemental Table S3.4: Imaging Acquisition Details

	OASIS	DIAN	ADNI	MDC
MRI				
Scanners	Primarily Siemens Biograph mMR PET/MR and Siemens Trio MR	Siemens BioGraph mMR PET/MR	Mix of Siemens, GE, and Philips MR	Mix of Siemens MR
Scanner Strength (T)	3 (n = 440) 1.5 (n = 22)	3	1.5 (n = 23) 3 (n = 89)	1.5 (n = 30) 3 (n = 549)
Repetition Time (s)	Primarily 2.3 and 2.4	2.3	2.3-10.4	Primarily 2.3 and 2.4
Echo time (ms)	Primarily 2.95 3.16	2.95	2.98-4.1	Primarily 2.95 and 3.05
Flip Angle (degrees)	Primarily 8 and 9	9	8-11	Primarily 8 and 9
Slice Thickness (mm)	1 or 1.2	1.1	1 or 1.2	1 or 1.1
FreeSurfer Version	Primarily 5.3	5.3	5.3	5.3
PET				
Scanners	Mix of Siemens PET/MR and PET/CT	Siemens BioGraph mMR PET/MR	Mix of Siemens, Phillips, and GE PET/CT	
Tracer	PIB (n = 337) and Florbetapir (n = 122)	PIB	Florbetapir	
Tracer Dosage (mCi)	PIB: ~13 Florbetapir: ~10	PIB: ~15	Florbetapir: ~10	
Data collection post-injection (minutes)	PIB: 30-60 Florbetapir: 50-70	PIB: 40-70	Florbetapir: 50-70	

Supplemental Table S3.4 describes the details of the MRI and PET imaging acquisition for each cohort. Numbers are often approximate due to the large number of studies used.

ADNI: Alzheimer's Disease Neuroimaging Initiative; DIAN: Dominantly Inherited Alzheimer Network; MDC: Memory Diagnostic Center; MRI: Magnetic resonance imaging; OASIS: Open Access Series of Neuroimaging Studies; PET: Positron emission tomography; PIB: [^{11}C]-Pittsburgh Compound B

Supplemental Table S3.5: Detailed Description of Centiloid Conversion

a.

PIB Calibration Cohort	Young Controls	Clinically Diagnosed AD
N	34	45
Age (SD) years	31.5 (6.3)	67.5 (10.5)
Male (%)	Unknown	Unknown
APOE4 (% with an ε4 allele)	8 (25)	28 (64)
CDR > 0 (%)	0 (0)	45 (100)

b.

Florbetapir Calibration Cohort	DIAN Non-carrier	DIAN Carrier
N	15	22
Age (SD) years	39.3 (4.6)	54.5 (6.3)
Male (%)	7 (46.7)	14 (63.6)
APOE4 (% with an ε4 allele)	4 (26.7)	9 (40.9)
CDR > 0 (%)	0 (0.0)	16 (72.7)

c.

Florbetapir PET data:

$$\text{Centiloid} = 53.6 \times \text{SUVR\_RSF} - 43.2$$

PIB data from OASIS (processed in the 30-60 minute time window):

$$\text{Centiloid} = 45.0 \times \text{SUVR\_RSF} - 47.5$$

PIB data from DIAN (processed in the 40-70 minute time window):

$$\text{Centiloid} = 40.7 \times \text{SUVR\_RSF} - 42.9$$

Supplemental Table S3.5 describes the Centiloid conversion process in detail. The procedure and requirements to define the Centiloid scale are documented in the initial Centiloid paper (Klunk et al., 2015). The Centiloid scale is defined by two anchor points: the mean amyloid burden measurement of a young control group with no amyloid pathology in their brain, represented as 0 in the Centiloid scale, and the mean amyloid burden of an AD group, represented as 100 in the Centiloid scale (level 1 calibration). Subsequently, a Deming regression and a linear transformation are performed to calibrate the tracer and the local processing methods to the Centiloid scale (i.e., level 2 calibration). The PIB-Centiloid equations were defined using a subset of the Global Alzheimer's Association Information Network dataset (http://www.gaain.org), described in Supplemental Table S5a. The Florbetapir Centiloid conversion equations were obtained using linear regression performed between Florbetapir mean cortical standard uptake value ratios with regional spread function applied (SUVRs) and PIB Centiloid SUVRs for a subset of DIAN-TU (https://www.clinicaltrials.gov/ct2/show/study/NCT01760005), again, using the level-2 (Klunk

et al., 2015), described in Supplemental Table S3.5b. The specific equations used, as listed in Su et al. 2019, are in Supplemental Table S3.5c.

AD: Alzheimer disease; *APOE4*: Apolipoprotein E ε4; CDR: Clinical Dementia Rating; DIAN: Dominantly Inherited Alzheimer Network; OASIS: Open Access Series of Neuroimaging Studies; PET: Positron emission tomography; PIB: [^{11}C]-Pittsburgh Compound B; SD: Standard deviation; SUVR RSF: Standard uptake value ratio (regional spread function applied)

Supplemental Table S3.6: Age-Related Atrophy Adjustment Reduces Volumetric Correlation with Age

	Unadjusted for Age-Related Atrophy		Adjusted for Age-Related Atrophy	
	R	*p*-value	R	*p*-value
Hippocampal Volume	-0.602	< 0.001	-0.177	0.0163
Inferior Lateral Ventricle Volume	0.580	< 0.001	0.186	0.0115
Entorhinal Thickness	-0.428	< 0.001	-0.227	0.00193
Amygdala Volume	-0.505	< 0.001	-0.144	0.0510
Inferior Parietal Thickness	-0.474	< 0.001	-0.150	0.0423

Supplemental Table S3.6 provides the correlation between the regions used in the optimal model and age for the cognitively normal controls in the combined Training and Test cohorts. While correlations are not entirely removed, they are strongly reduced by the z-score procedure we used to adjust for age-related atrophy.

Supplemental Figure S3.2: Frequency of Region Selection for AD Classification

Supplemental Figure S3.2 graphs the frequency each region was selected in the 1000 iterations of random sampling and least absolute shrinkage and selection operator logistic regressions during the region selection process for both the unadjusted and adjusted for age-related atrophy data. The green line indicates the 50% frequency threshold that both datasets needed to meet for a region to be included in the SARA model.

AD: Alzheimer disease; SARA: Select Atrophied Regions in Alzheimer disease

Supplemental Table S3.7: Coefficients for All Classification Models

Model	Intercept	Age	Hippocampal Volume	Inferior Lateral Ventricle Volume	Entorhinal Thickness	Amygdala Volume	Inferior Parietal Thickness
Age	-5.51	0.0714	N/A	N/A	N/A	N/A	N/A
HCV	9.03	N/A	-0.00142	N/A	N/A	N/A	N/A
SARA	14.5	N/A	-0.00067	0.000247	-0.68	-0.00056	-3.28
HCV + Age	11.1	-0.0227	-0.00149	N/A	N/A	N/A	N/A
SARA + Age	19.7	-0.0523	-0.0007	0.000329	-0.628	-0.00072	-3.78
HCV_{adj}	-1.42	N/A	-1.06	N/A	N/A	N/A	N/A
$SARA_{adj}$	-1.7	N/A	-0.411	0.253	-0.296	-0.261	-0.415
HCV_{adj} + Age	-7.3	0.079	-1.08	N/A	N/A	N/A	N/A
$SARA_{adj}$ + Age	-6.65	0.0667	-0.502	0.24	-0.21	-0.203	-0.426

Supplemental Table S3.7 displays the rounded coefficients (unstandardized B values) for each of the classification models. Volumes are input into the models as ml (cm^3), while cortical thicknesses are input in mm. The SARA models include hippocampal volume, inferior lateral ventricle volume, entorhinal thickness, amygdala volume, and inferior parietal thickness. X + Age indicates model X with age added as a covariate; X_{adj} indicates Model X using volumes and cortical thicknesses that have been adjusted for age-related atrophy.

Adj: Adjusted for age-related atrophy; HCV: Hippocampal volume; N/A: Not applicable; SARA: Select Atrophied Regions in Alzheimer disease

Supplemental Table S3.8: Select Models' AUCs for the Specific Diagnoses in the Clinical Cohort

Specific Diagnosis	Age Model's AUCs (95% CI)	HCV Model's AUCs (95% CI)	SARA Model's AUCs (95% CI)
AD Diagnoses			
AD Variant	0.502 *(0.342-0.663)*	0.697 *(0.566-0.829)*	0.795 *(0.689-0.901)*
AD with Additional Non-Neurodegenerative Condition	0.686 *(0.526-0.846)*	0.781 *(0.707-0.855)*	0.852 *(0.786-0.917)*
Early-Onset AD	0.680 *(0.563-0.798)*	0.701 *(0.596-0.806)*	0.767 *(0.668-0.866)*
Typical AD	0.808 *(0.763-0.852)*	0.819 *(0.775-0.863)*	0.827 *(0.783-0.871)*
Non-Neurodegenerative Non-AD Diagnoses			
Cognitively Normal	0.748 *(0.671-0.826)*	0.893 *(0.838-0.948)*	0.914 *(0.856-0.971)*
Miscellaneous	0.755 *(0.631-0.878)*	0.813 *(0.686-0.940)*	0.852 *(0.731-0.973)*
Mood/Pharmacy/Sleep	0.798 *(0.710-0.885)*	0.828 *(0.729-0.926)*	0.862 *(0.772-0.952)*
Neurologic Disease	0.883 *(0.801-0.965)*	0.794 *(0.680-0.910)*	0.830 *(0.717-0.943)*
Neurodegenerative Non-AD Diagnoses			
Dementia with Lewy Bodies	0.537 *(0.366-0.708)*	0.581 *(0.396-0.765)*	0.467 *(0.242-0.692)*
Frontotemporal Dementia	0.780 *(0.690-0.871)*	0.805 *(0.688-0.923)*	0.818 *(0.707-0.929)*
Other Neurodegenerative Disorders	0.712 *(0.595-0.830)*	0.720 *(0.563-0.877)*	0.735 *(0.589-0.882)*
Vascular Cognitive Impairment	0.592 *(0.445-0.738)*	0.686 *(0.532-0.841)*	0.694 *(0.544-0.845)*

Supplemental Table S3.8 displays the AUCs for the Age, HCV, and SARA models when the AD or non-AD Diagnoses are restricted to each of the more specific diagnoses along with the associated 95% CI. For example, the AD Variant AUC is the AUC calculated using participants with AD Variant diagnosis and all non-AD Diagnoses participants, but excludes participants with an AD with Additional Non-Neurodegenerative Condition, Early-Onset AD diagnosis, or Typical AD.

AD: Alzheimer disease; AUC: Receiver operating characteristic's area under the curve; CI: Confidence interval; HCV: Hippocampal volume; SARA: Select Atrophied Regions in Alzheimer disease

Supplemental Figure S3.3: CDR Aligns, but is Not Equivalent, to Predicted Probability in SARA

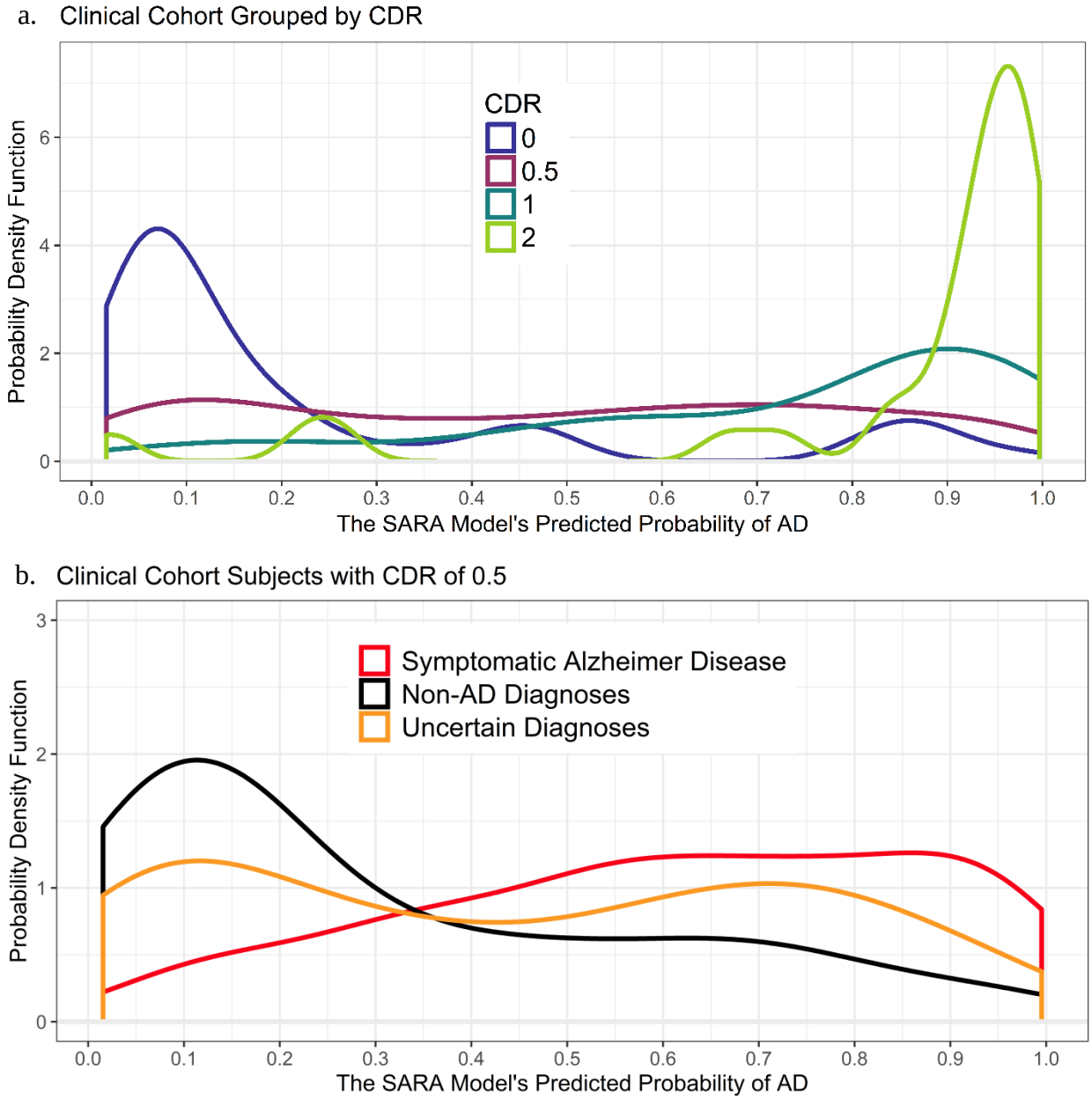

Supplemental Figure S3.3a displays the distributions of the SARA model's predicted probability of AD, grouped by global CDR instead of by diagnosis. This includes the AD, non-AD, and Uncertain diagnoses. Note the change in y-axis scale from previous figures due to the tight distribution of CDR = 2 participants. S3b displays the distribution of SARA model's predicted probability of AD as in Figure 3.2b, but shows only patients with CDR = 0.5 (n = 101).

AD: Alzheimer disease; CDR: Clinical Dementia Rating; SARA: Select Atrophied Regions in Alzheimer disease

Chapter 4: Interaction of Stroke, Race, and Amyloid (Koenig et al., 2021)

Stroke and Alzheimer disease share risk factors and often co-occur, and both have been reported to have a higher prevalence in African Americans as compared to non-Hispanic Whites. However, their interaction has not been established. The objective of this study was to determine if preclinical Alzheimer disease is a risk factor for stroke and post-stroke dementia and whether racial differences moderate this relationship. This case-control study was analyzed in 2019 using retrospective data from 2007-2013. Participants were adults age 65 and older with and without acute ischemic stroke. Recruitment included word of mouth and referrals in Saint Louis, Missouri, with stroke participants recruited from acutely hospitalized patients and non-stroke participants from community living older adults who were research volunteers. Our assessment included radiologic reads of infarcts, microbleeds, and white matter hyperintensities; a [^{11}C]-Pittsburgh Compound B PET measure of cortical β-amyloid binding; quantitative measures of hippocampal and white matter hyperintensities volume; longitudinal Mini Mental State Exam scores; and Clinical Dementia Rating™ 1-year post-stroke. A total of 243 participants were enrolled, 81 of which had a recent ischemic stroke. Participants had a mean age of 75, 57% were women, and 52% were African American. Cortical amyloid did not differ significantly by race, stroke status, or Clinical Dementia Rating post-stroke. There were racial differences in Mini Mental State Exam scores at baseline (mean 26.8 for African Americans, 27.9 for non-Hispanic Whites, $p = 0.03$), but not longitudinally. African Americans were more likely to have microbleeds (32.8% vs. 22.6%, $p = 0.04$), and within the acute stroke group, African Americans were more likely to have small infarcts (75.6% vs. 56.8%, $p = 0.049$). preclinical AD did not show evidence of being a risk factor for stroke nor predictive of post-stroke dementia. We did

not observe racial differences in β-amyloid levels. However, even after controlling for several vascular risk factors, African Americans with clinical stroke presentations had greater levels of vascular pathology on magnetic resonance imaging (MRI).

4.1 Introduction

Medical research on African Americans (AAs) has a fraught history that has resulted in limited knowledge of racial differences in various pathologies, as well as an understandable hesitance for minorities to participate in research (Hooper et al., 2019). Several studies addressing racial disparities in Alzheimer disease (AD) and stroke have found higher incidence rates in the Black population for both diseases as compared with the non-Hispanic White (NHW) population (Benjamin et al., 2017; Manly and Mayeux, 2019). Note that we use both the broader term 'Black' and the more specific term 'African American' depending on the language used in each previously published study. Our use of 'African American' reflects how our participants identify themselves, but this may not be the appropriate term for studies in other regions or outside the United States.

The impact of stroke is severe, with over 140,000 deaths per year caused by stroke in the United States (Yang et al., 2017). Stroke leads to long-term consequences even for those who survive: almost 40% of stroke survivors develop long-term disabilities (Luengo-Fernandez et al., 2013), and stroke is associated with cognitive decline before and after the stroke event (Zheng et al., 2019). Black individuals are twice as likely to have a stroke (Benjamin et al., 2017), and are more likely to die from that stroke (Yang et al., 2017). These racial differences have been attributed to stroke risk factors such as higher rates of hypertension and diabetes, and lower socio-economic status and education (Benjamin et al., 2017).

Similarly, many publications report higher rates of dementia and AD for Black persons compared with NHWs (Neill R Graff-Radford et al., 2016; Green, 2002; Manly and Mayeux, 2019; Mayeda et al., 2016; Tang et al., 2001). While there is little doubt of the racial disparities seen in dementia, most of these studies are based on a clinical diagnosis of AD, which corresponds to neuropathological diagnosis in only 83% of cases at best (Beach et al., 2012) and neuropathological studies are often lacking in racial minorities. Racial differences in AD have been largely attributed to AD risk factors, many of which overlap with stroke risk factors. Higher rates of cardiovascular disease and of apolipoprotein E ε4 (*APOE4*) alleles, and fewer years of education are just a few examples (Neill R Graff-Radford et al., 2016), but the story of *APOE4* is of particular interest. While some papers suggest higher rates of *APOE4* explain the majority of the racial differences in AD, others have found that *APOE4* alleles in AAs have less associated risk for AD compared to *APOE4* in NHW populations (John C Morris et al., 2019). Additionally, some reports show no racial differences in AD (Fillenbaum et al., 1998; Annette L Fitzpatrick et al., 2004; Riudavets et al., 2006b; Xiong et al., 2020), but many of these papers have controlled for baseline racial differences in education, cognitive scores, and *APOE4*.

In addition to racial differences, stroke and AD have a complex and poorly understood relationship with each other. Both diseases are highly prevalent and are strongly associated with age, leading to frequent co-occurrence in older adults. Additionally, one possible direct interaction is post-stroke dementia – wherein older adults develop dementia within a year of having a stroke (Pendlebury and Rothwell, 2009). While post-stroke dementia is correlative based on recent history of stroke, it suggests an interaction of AD and stroke. It is possible that preclinical AD predisposes people to have a stroke, or that stroke accelerates the development of dementia when it occurs in persons with preclinical AD. Previous studies have generally found

greater amyloid pathology in post-stroke dementia (Chi et al., 2019; Gamaldo et al., 2006; Hagberg et al., 2020; Liu Wenyan et al., 2015; Mok et al., 2016; Thiel et al., 2014; Yang et al., 2015). However, these studies measure amyloid pathology months to years after stroke, and do not contrast with the high incidence of Alzheimer pathology in the general population. The only study to examine amyloid within a month of stroke found only a small, highly localized area of higher amyloid deposition in the precuneus (Yasuno et al., 2019). Several recent studies showed that various vascular factors did not directly impact amyloid deposition (Bennett et al., 2020; Bos et al., 2019; Gottesman et al., 2020), suggesting pre-existing preclinical AD may be the important factor in the development of post-stroke dementia.

In this study, we examined AA and NHW older adults who were admitted with acute stroke to the stroke service of a tertiary care facility. For comparison, we used participants without acute or subacute stroke from the Knight Alzheimer Disease Research Center (ADRC) at Washington University in St. Louis. We examined whether pre-existing cortical amyloid positivity is a risk factor for stroke and if it increases the likelihood of dementia at 1-year post-stroke. Additionally, we examined the possibility of racial differences in the frequency of preclinical AD, vascular pathology, and in longitudinal cognitive change.

4.2 Methods

4.2.1 Participants

This study includes acute stroke patients and retrospectively selected non-stroke participants used as a comparison group. All procedures were approved by Washington University's Human Research Protection Office. Written informed consent was obtained from all participants and a stipend was provided.

Acute stroke participants were recruited from the Barnes-Jewish Hospital Stroke Registry and from St. John's Mercy Medical Center between 2009-2012. Persons were eligible to enroll if they were 65 years or older, had a recent ischemic stroke of embolic or occlusive origin, and a National Institutes of Health Stroke Scale (NIHSS) (Ortiz and L. Sacco, 2014) score of 2-18. Participants were excluded if they had moderate-severe aphasia or pre-stroke cognitive decline, as determined by an informant-reported AD8 (Galvin et al., 2005) score > 2 the week prior to the acute stroke.

Non-stroke participants, referred to as the ADRC group, were volunteers in the longitudinal clinical studies at the Knight ADRC from 2007-2013. Details of recruitment at the ADRC have been outlined previously (John C Morris et al., 2019). Due to low enrollment of AAs in the Knight ADRC, the ADRC cohort was not matched 1-to-1 to the stroke cohort. Instead, all AA participants who were 65 years or older, had no known deterministic mutation for AD, and had an MRI were included. The NHW participants from the Knight ADRC who also met these criteria were then matched to the AA ADRC cohort as much as possible on the basis of age and sex.

4.2.2 Demographics

Self-reported race, age at time of MRI, biological sex at birth, years of education, self-reported family history of dementia in first-degree relatives, body mass index (BMI), hemoglobin A1c (HbA1c), *APOE4* allele status, blood pressure, history of stroke, and history of diabetes were assessed. The stroke group was further classified by stroke type using The Trial of Org 10172 in Acute Stroke Treatment (TOAST) and severity using the NIHSS. All of these measures, along with Mini Mental State Exam (MMSE) (Folstein et al., 1975) discussed below, were collected within the stroke group 1-40 (median 10.5) days from stroke occurrence, except

for blood pressure which was collected 1-50 (median 4) days from stroke occurrence. Within the ADRC group, HbA1c was collected 0-3110 (median 365) days from the rest of the clinical assessment. Hypertension was defined as having systolic blood pressure of at least 140 or diastolic blood pressure of at least 90 mm Hg (Whelton et al., 2018).

4.2.3 Imaging Measures

Participants had a structural, T1-weighted magnetization-prepared, rapid gradient-echo (MPRAGE) MRI collected using either a 1.5-T or 3-T Siemens scanner and a resolution of either 1 × 1 × 1.25 mm or 1 × 1 × 1 mm. Most participants additionally had a T2w and T2* scan. MR imaging was acquired 0-385 (median 78) days from clinical assessment for the ADRC group, and 0-592 (median 1) days for the stroke group. Trained radiologists read each set of scans and completed a radiologic report on: A. the number of large infarcts (0, 1, 2, 3+), B. small infarcts (0, 1, 2, 3+), C. microbleeds (0, 1-4, 5-10, 11+), and D. the severity of leukoaraiosis (0 = none, 1 = mild, 2 = moderate, or 3 = severe) according to Fazekas scoring of white matter hyperintensities (WMH) (Fazekas et al., 1987). Scans which passed QC also had hippocampal volumes obtained using FreeSurfer 5.3 (Fischl, 2012) and WMH volumes with the Lesion Segmentation Tool (Schmidt et al., 2012). Hippocampal volumes were adjusted for head size using a regression scaling approach with total intracranial volume (Buckner et al., 2004).

All acute stroke and many ADRC participants underwent [^{11}C]-Pittsburgh compound B (PIB) positron emission tomography (PET) imaging to assess the level of amyloid plaques in their brain. PET imaging was acquired 2-442 (median 112) days from clinical assessment for the ADRC group. For the stroke group, this interval was 0-29 (median 0) days from clinical assessment and 1-50 (median 14.5) days from stroke occurrence. Data from the 30- to 60-minute post-injection window was processed with an in-house pipeline (Su, 2021) using FreeSurfer-

derived regions and a cerebellar cortex reference region. The mean cortical binding potential from the precuneus, prefrontal cortex, gyrus rectus, and lateral temporal regions was used both as a continuous variable and as a marker of amyloid positivity (mean cortical binding potential > 0.18) (Su et al., 2019, 2013).

4.2.4 Clinical and Cognitive Measures

The MMSE was a general measure of cognition collected at the same time as the clinical assessment described in section 3.2.2. Some participants (108 AA and 101 NHW) also had longitudinal MMSE assessed 1-14 (median 4.6) years after the original.

Clinical Dementia Rating™ (CDR™) (Morris, 1993) at 1 year follow-up for a subset of acute stroke participants assessed possible decline in cognitive and functional abilities relative to the participant's previously attained levels. It was determined by experienced clinicians using independent, semi-structured interviews with the participant and a collateral source, and a CDR > 0 was used as an indicator of post-stroke dementia (Jack, 2020; Morris, 2012; Storandt et al., 2006). Baseline CDR was not available for the stroke group.

4.2.5 Statistical Analysis

All analyses were performed on SAS 9.4 or R 4.0.2. Each variable was assessed for cross-sectional racial differences and for differences between the acute stroke and ADRC groups. This was accomplished by modeling race, stroke status, and their interaction with logistic regression for categorical variables (binaries used: presence of large infarcts, presence of small infarcts, moderate-severe WMHs, presence of microbleeds, and 5 or more microbleeds) and general linear models for continuous. The imaging measures and baseline MMSE were additionally analyzed by an adjusted model that included the covariates age (centered), family history, *APOE4*, education, sex, hypertension, and the first order interactions of these variables

with race. The included covariates were selected by first individually testing each of the covariates in Table 4.1 with each of the outcomes. Those shown to be significant with most of the outcomes were included in the full model. If it was significant with only one outcome but then not significant in the full model it was dropped from the list.

Longitudinal MMSE data were examined using linear mixed effects models with random slope and random intercept (Laird and Ware, 1982), and the unstructured correlation matrix between the random intercept and slope. Linear mixed models, an extension of simple linear models, were chosen to allow both fixed and random effects. They are used when there is non-independence in the data, such as arises from a hierarchical structure where there are multiple observations per subject, or participants do not enter the study at the same time point or have different length of follow-up. The longitudinal models were adjusted for baseline age and education.

Due to the infarcts observed in MRIs of the ADRC group, analyses were also repeated with participants re-grouped as stroke and comparison group based upon an infarct definition of stroke. The presence of a small or large infarct on MRI defined the infarct stroke group, while lack of small or large infarct defined the new comparison group. These results are reported separately in section 4.3.8.

To examine the possibility of post-stroke dementia, a logistic regression was used to predict acute stroke participants with CDR = 0 vs. CDR > 0 at the 1-year follow-up using baseline demographics and outcome variables. This was not repeated with the infarct definition of stroke.

4.3 Results

4.3.1 Participants

A total of 243 participants were included: 84 AA ADRC, 78 NHW ADRC, 42 AA stroke, and 39 NHW stroke. At Barnes-Jewish Hospital, 3880 ischemic stroke patients were examined for eligibility, 226 were found eligible, and 72 were enrolled and completed the study. At St. John's Mercy Medical Center, 9 participants were enrolled, but we do not have access to detailed information on their total patient pool. The 162 ADRC participants included were those eligible from the pool of 1368 ADRC participants.

4.3.2 Demographics

Demographic data are summarized in Table 4.1, and boxplots of the continuous demographics are in Supplemental Figure S4.1 in the supplemental material. The stroke participants had fewer years of education and a more frequent history of stroke than the ADRC group, and the NHW ADRC group had a family history of dementia significantly higher than the other three groups.

Overall, there was a high incidence of diabetes and hypertension. HbA1c and hypertension were significantly worse in AA stroke group than in AA ADRC group, with a similar but non-significant pattern seen in NHW group. History of diabetes was more severe only within the AA stroke group as compared to the AA ADRC group. Higher rate of *APOE4* alleles in AAs was observed within the stroke group only (Table 4.1). No differences in *APOE4* were seen by race in the ADRC group, or across stroke status, but *APOE4* frequencies (30-60%) were higher than the ~14% that has previously been reported for the general population (Liu et al., 2013).

All demographic variables in Table 4.1 were used as covariates when modeling our outcome variables, except HbA1c and BMI. Additional demographics specific to the stroke participants indicated that 28.4% had coronary artery disease, 28.4% had prior stroke, and 52.4% were taking statins (missing data n = 4). The TOAST classification (Adams et al., 1993) indicated stroke types were 12.1% large artery atherosclerosis, 27.0% cardioembolism, 36.5% small artery occlusion, and 24.3% undetermined etiology.

Table 4.1: Demographics

	AA	NHW	Race Difference (*p*)	Stroke *p*-value	
				Within AAs	Within NHWs
Participants, n				N/A	N/A
ADRC Group	84	78	0.64		
Stroke Group	42	39	0.74		
Age (y), mean (SD)[a]				> 0.99	**0.008**
ADRC Group	74.7 (7.38)	73.1 (5.96)	0.42		
Stroke Group	75.0 (6.85)	77.4 (6.88)	0.40		
Male, n (%)[a]				0.30	0.12
ADRC Group	30 (35.7)	34 (43.6)	0.31		
Stroke Group	19 (45.2)	23 (59.0)	0.22		
Education (years), mean (SD)[a]				**< 0.001**	**< 0.001**
ADRC Group	14.5 (2.76)	15.3 (2.66)	0.24		
Stroke Group	11.9 (1.66)	12.8 (3.11)	0.43		
Family history of dementia, n (%)[b]				0.15	**< 0.001**
ADRC Group	25 (29.8)	43 (55.1)	**0.001**		
Stroke Group	4 (15.4)	4 (14.8)	0.95		
***APOE4* (n, % with an ε4 allele)[c]**				0.19	0.20
ADRC Group	38 (46.3)	33 (42.3)	0.61		
Stroke Group	22 (59.5)	11 (29.7)	**0.01**		
BMI (kg/m^2), mean (SD)[d]				> 0.99	0.99
ADRC Group	29.2 (5.24)	26.9 (5.55)	**0.03**		
Stroke Group	29.3 (5.20)	27.2 (4.24)	0.27		
Hemoglobin A1c (%), mean (SD)[e]				**< 0.001**	0.06
ADRC Group	5.87 (0.80)	5.68 (0.49)	0.82		
Stroke Group	6.77 (1.67)	6.31 (1.35)	0.30		
Mean Arterial Pressure (mm Hg), mean (SD)[f]				0.09	0.13
ADRC Group	93.9 (11.7)	92.2 (10.2)	0.81		

	AA	NHW	Race Difference (*p*)	Stroke *p*-value	
				Within AAs	Within NHWs
Stroke Group	99.2 (15.8)	93.0 (15.9)	0.93		
Hypertension, n (%)[f]				**< 0.001**	0.09
ADRC Group	24 (28.6)	27 (35.5)	0.35		
Stroke Group	27 (64.3)	19 (52.8)	0.30		
Reported Previous Stroke, n (%)[g]				**0.006**	**< 0.001**
ADRC Group	5 (6.0)	2 (2.6)	0.31		
Stroke Group	10 (24.4)	11 (30.6)	0.55		
History of Diabetes, n (%)[h]				**0.002**	0.15
ADRC Group	14 (16.9)	9 (3.8)	0.35		
Stroke Group	18 (43.9)	8 (3.4)	0.05		

a. Missing data: 0 AA ADRC, 1 AA Stroke, 0 NHW ADRC, 2 NHW Stroke
b. Missing data: 0 AA ADRC, 16 AA Stroke, 0 NHW ADRC, 12 NHW Stroke
c. Missing data: 2 AA ADRC, 5 AA Stroke, 0 NHW ADRC, 2 NHW Stroke
d. Missing data: 1 AA ADRC, 1 AA Stroke, 1 NHW ADRC, 2 NHW Stroke
e. Missing data: 36 AA ADRC, 3 AA Stroke, 22 NHW ADRC, 9 NHW Stroke
f. Missing data: 0 AA ADRC, 0 AA Stroke, 3 NHW ADRC, 3 NHW Stroke
g. Missing data: 1 AA ADRC, 0 AA Stroke, 1 NHW ADRC, 3 NHW Stroke
h. Missing data: 1 AA ADRC, 1 AA Stroke, 1 NHW ADRC, 3 NHW Stroke

AA: African American; ADRC: Alzheimer Disease Research Center comparison cohort; *APOE4*: Apolipoprotein E ε4; BMI: Body mass index; NHW: Non-Hispanic White; SD: Standard deviation

4.3.3 Amyloid PET Outcome Measures

Table 4.2 lists the results from the statistical models and Figure 4.1 displays the amyloid PET results for each group. Amyloid PET, both as a continuous variable and as a binary of amyloid positive and amyloid negative, did not show differences by race or by stroke status. This indicates that preclinical AD was not more common in AAs in our cohort, and that preclinical AD does not appear to be a risk factor for stroke. The overall percentage of amyloid positive participants was high relative to other reports, indicating a high rate of preclinical AD both in the community and in the ADRC research volunteers, who may volunteer because they are at higher risk for AD due to family history.

4.3.4 Quantitative MRI Outcome Measures

Quantitative MRI measures of hippocampal volume and WMH volume (Figure 4.1) did not show an overall effect of race or stroke status (Table 4.2). Quantitative MRI measures were possible only on a subsample of the participants and so may not be representative of our entire cohort. These results did not differ when left and right hippocampal volumes were assessed separately, nor when amyloid positive and negative participants were assessed separately.

4.3.5 Radiologic MRI Outcome Measures

The acute stroke group was more likely to have large infarcts, small infarcts, moderate-severe leukoaraiosis, and microbleeds than the ADRC group (Figure 4.2, Table 4.2). An interaction of race and *APOE4* was observed for large infarcts, such that AA *APOE4* carriers and AA *APOE4* non-carriers were significantly different, but NHWs were not. Within the acute stroke group, AAs were more likely to have small infarcts than NHWs after adjusting for covariates. Before adjusting for covariates, the combined AA group was more likely to have more severe Fazekas stage 3/4 than the NHW group. The presence of microbleeds was more

common in AA in the adjusted model. The cutoff of 5+ microbleeds, used as exclusion criteria in many clinical trials, showed no significant differences.

4.3.6 Cognitive Outcome Measures

AA participants had lower baseline MMSE scores (Figure 4.1) in both unadjusted and adjusted models (Table 4.2). Models of longitudinal MMSE included baseline data for all participants and at least one follow-up exam for 108 AAs and 101 NHWs (average follow-up time 4.1 and 5.2 years, respectively). Estimated change in MMSE per year did not differ significantly by race or stroke status: AA ADRC: -0.68 (standard error (SE) = 0.15), AA Stroke: -1.08 (SE = 0.34), NHW ADRC: -0.58 (SE = 0.15), NHW Stroke: -0.53 (SE = 0.32) (Supplemental Figure S4.1). None of these results differed significantly when controlling for baseline age and education, nor when amyloid positive and negative participants were assessed separately.

Figure 4.1: Continuous Outcome Measures

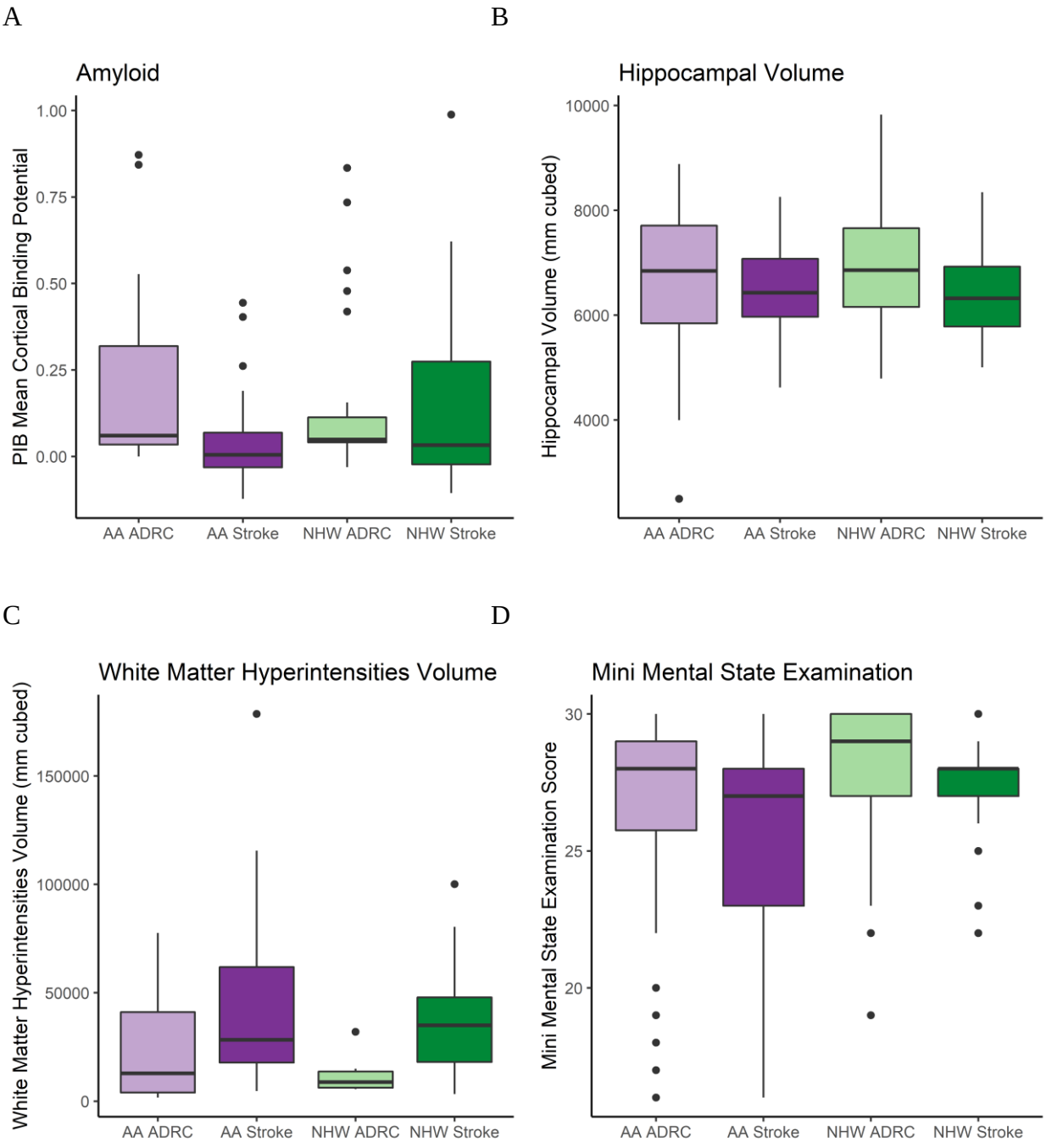

Figure 4.1 displays boxplots of the participants' amyloid PET, hippocampal volume, white matter hyperintensity volume, and Mini Mental State Exam score, with data separated by race (AA or NHW) and cohort (acute stroke or ADRC comparison).

A. Missing data: 52 AA ADRC, 3 AA Stroke, 47 NHW ADRC, 2 NHW Stroke
B. Missing data: 3 AA ADRC, 11 AA Stroke, 0 NHW ADRC, 15 NHW Stroke
C. Missing data: 76 AA ADRC, 6 AA Stroke, 72 NHW ADRC, 11 NHW Stroke

D. Missing data: 0 AA ADRC, 1 AA Stroke, 0 NHW ADRC, 2 NHW Stroke

AA: African American; ADRC: Alzheimer Disease Research Center comparison cohort; NHW: Non-Hispanic White; PIB: [^{11}C]-Pittsburgh Compound B

Figure 4.2: Categorical Outcome Measures

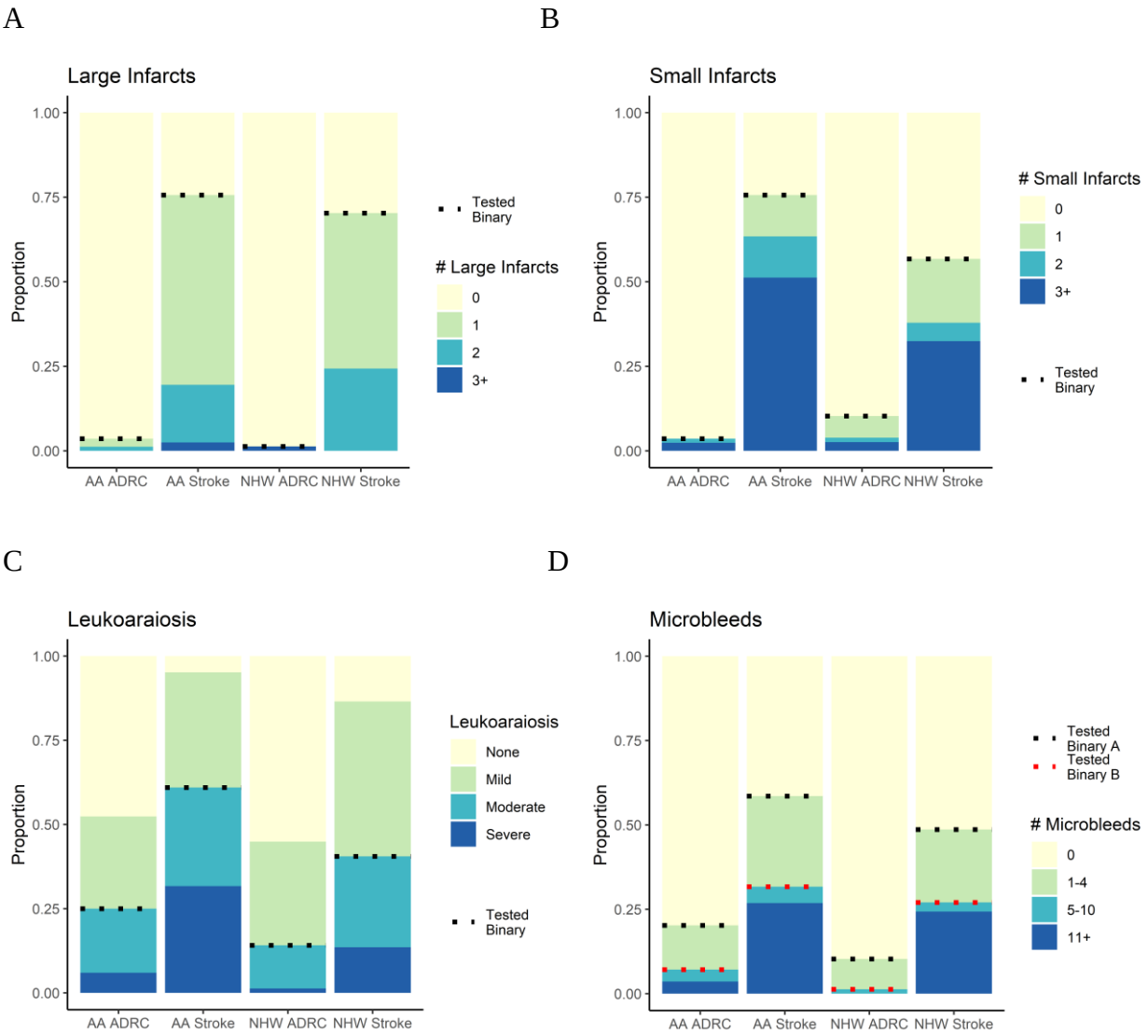

Figure 4.2 displays the participants' radiologic data results for number of large infarcts, small infarcts, leukoaraiosis, and microbleeds, with data separated by race (AA or NHW) and cohort (acute stroke or ADRC comparison).

A-D Missing data: 0 AA ADRC, 1 AA Stroke, 0 NHW ADRC, 2 NHW Stroke

AA: African American; ADRC: Alzheimer Disease Research Center comparison cohort; NHW: Non-Hispanic White

Table 4.2: Group Differences by Race and Stroke Status

		AA	NHW	Race *p*-value	
				Unadjusted Models	Adjusted Models[e]
Amyloid PET	**PIB Mean Cortical Binding Potential, mean (SE)[a]**	0.11 (0.04)	0.11 (0.03)	0.57	0.96
	ADRC Group	0.20 (0.05)	0.13 (0.05)	> 0.99	0.68
	Stroke Group	0.05 (0.06)	0.10 (0.05)	0.98	0.90
	PIB Positive, n (%)[a]	16 (22.5)	17 (25.0)	0.90	0.67
	ADRC Group	10 (31.3)	5 (16.1)	0.92	0.34
	Stroke Group	6 (15.4)	12 (32.4)	0.09	0.94
Quantitative MRI	**Total Hippocampal Volume (normalized), mean (SE)[b]**	6720 (132)	6730 (143)	0.57	0.97
	ADRC Group	6610 (128)	6780 (117)	0.60	0.76
	Stroke Group	6480 (230)	6450 (247)	> 0.99	> 0.99
	WMH Volume, mean (SE)[c]	28400 (10200)	49200 (14500)	0.32	0.25
	ADRC Group	27900 (17600)	55100 (25000)	0.85	0.81
	Stroke Group	31500 (9760)	52100 (12100)	0.91	0.56
Radiologic Read of MRI	**Presence of Large Infarcts, n (%)[d]**	34 (27.2)	27 (23.5)	0.30	0.86
	ADRC Group	3 (3.6)	1 (1.3)	0.37	0.69
	Stroke Group	31 (75.6)	26 (70.3)	0.60	0.91
	Presence of Small Infarcts, n (%)[d]	34 (27.2)	29 (25.2)	0.75	0.48
	ADRC Group	3 (3.6)	8 (10.3)	0.11	0.12
	Stroke Group	31 (75.6)	21 (56.8)	0.08	**0.047**
	Leukoaraiosis Moderate-Severe, n (%)[d]	46 (36.8)	26 (22.6)	**0.01**	0.14
	ADRC Group	21 (25.0)	11 (14.1)	0.09	0.28
	Stroke Group	25 (61.0)	15 (40.5)	0.07	0.24
	Presence of Microbleeds, n (%)[d]	41 (32.8)	26 (22.6)	0.07	**0.04**
	ADRC Group	17 (20.2)	8 (10.3)	0.08	0.07
	Stroke Group	24 (58.5)	18 (48.7)	0.38	0.37
	Microbleeds ≥ 5, n (%)[d]	19 (15.2)	11 (9.6)	0.10	0.93
	ADRC Group	6 (7.1)	1 (1.3)	0.10	0.93

		AA	NHW	Race *p*-value	
				Unadjusted Models	Adjusted Models[e]
	Stroke Group	13 (31.7)	10 (27.0)	0.65	0.54
	MMSE, mean (SE)[d]	26.8 (0.37)	27.9 (0.37)	**< 0.001**	**0.03**
	ADRC Group	26 (0.38)	27.4 (0.35)	**0.03**	0.07
	Stroke Group	26.8 (0.64)	28.1 (0.63)	0.06	0.46

a. Missing data: 52 AA ADRC, 3 AA Stroke, 47 NHW ADRC, 2 NHW Stroke
b. Missing data: 3 AA ADRC, 11 AA Stroke, 0 NHW ADRC, 15 NHW Stroke
c. Missing data: 76 AA ADRC, 6 AA Stroke, 72 NHW ADRC, 11 NHW Stroke
d. Missing data: 0 AA ADRC, 1 AA Stroke, 0 NHW ADRC, 2 NHW Stroke
e. Adjusted models have controlled for baseline age, family history, *APOE4*, education, sex, and hypertension

AA: African American; ADRC: Alzheimer Disease Research Center comparison cohort; *APOE4*: Apolipoprotein E ε4; MMSE: Mini Mental State Exam; MRI: Magnetic resonance imaging; NHW: Non-Hispanic White; PET: Positron emission tomography; PIB: [^{11}C]-Pittsburgh Compound B; SE: Standard error; WMH: White matter hyperintensities

4.3.7 Model Covariates

While many covariates were included in the adjusted models for the outcome variables, the only ones commonly found to be significant were age and *APOE4* status. Both were significant for PIB mean cortical binding potential, PIB positivity, and hippocampal volume; age was additionally significant for Leukoaraiosis and MMSE. No significant interactions of race*age were observed, but WMH volume and large infarcts had a significant race**APOE4* interaction.

4.3.8 Models Using Infarct Definition of Stroke

Demographics when using the infarct definition of stroke are in Supplemental Table S4.1, while Supplemental Table S4.2 lists the results from the statistical models created for each outcome variable. Few differences were observed. The higher rate of *APOE4* alleles in AAs observed within the stroke group lost significance. The adjusted model for continuous amyloid showed significantly lower amyloid in the stroke group (*p*-value changes from 0.10 to 0.02 in the adjusted model; mean cortical binding potential = 0.180 for ADRC group, 0.067 for stroke group). The presence of microbleeds gained significant racial differences in the unadjusted model and within the ADRC group in the adjusted model. The presence of 5 or more microbleeds gained significance such that the combined AA group had higher rates than the combined NHW group.

4.3.9 CDR At One Year Follow-Up

Another measure examined only within the acute stroke participants was CDR at 1-year follow-up (mean 394 days), for which 55 of the 81 stroke participants returned. As shown in Supplemental Table S4.3, those without follow up data were more likely to be male (69.6% vs. 41.8%, $p = 0.03$), have an *APOE4* allele (81.3% vs. 34.6%, $p = 0.003$), and have a higher NIHSS

(7.15 vs. 4.58, $p = 0.01$). Individuals with CDR > 0 at follow-up did not have statistically different levels of baseline amyloid than those with CDR = 0 (mean cortical binding potential of 0.14 vs. 0.05, $p = 0.14$, Supplemental Table S4.4), indicating that preclinical AD did not predict post-stroke dementia. This finding was not impacted by stroke TOAST subtype. CDR at follow-up also did not differ significantly by race (57.7% of AA with stroke vs. 42.3% NHW with stroke had CDR > 0, $p = 0.35$). The only significant predictors of a CDR greater than 0 at the 1-year follow-up were a prior history of stroke (43.2% vs. 7.41%, $p = 0.008$) and having more than 5 microbleeds ($p = 0.046$). When all factors in Supplemental Table S4.4 were assessed in a single model, none significantly predicted CDR > 0. When history of stroke and 5+ microbleeds were combined into a single model, only history of stroke remained significant ($p = 0.01$).

4.4 Discussion

We examined how MRI measures of stroke and AD biomarkers differed by race and presence of acute stroke. We did not see evidence that preclinical AD is a risk factor for stroke or predicts post-stroke dementia, supporting the idea that vascular disease and amyloid pathology are separate disease mechanisms that each may lead to dementia. However, we found that AAs are more likely to have vascular pathology observable on MRI than NHWs. While outside our original aims, our finding that AAs were more likely to have 5 or more microbleeds suggests clinical trials are likely turning away larger numbers of AA volunteers due to this cutoff.

We did not see a higher risk of post-stroke dementia in AAs, in contradistinction to what previous studies have reported (Desmond et al., 2000; Douiri et al., 2013; Levine et al., 2015; Pendlebury and Rothwell, 2009; Stansbury et al., 2005), but this may be due to the sample size and localized recruitment (St. Louis) of this study. Our results also differed from a previous paper (John C Morris et al., 2019) which observed racial differences in hippocampal volume and

used a sample independent from the acute stroke participants in this study. The previously observed lack of racial difference in amyloid PET, however, was replicated in this study (John C Morris et al., 2019). Previous studies have also strongly suggested that AAs are more likely to be *APOE4* carriers (Neill R Graff-Radford et al., 2016; Green, 2002; Manly and Mayeux, 2019; Mayeda et al., 2016; Tang et al., 2001). The ADRC group was not representative of this, and the acute stroke group replicated only the racial difference in *APOE4*. As such, we were unable to test for racial difference mediated by these factors. Similarly, the acute stroke group that had 1-year follow-up had a lower frequency of *APOE4* than the original group, which may have impacted the lack of association we saw between preclinical AD and post-stroke dementia. While we have related *APOE4* and race in this paper, this is not meant to suggest that genetics as opposed to racism is the main driver of racial disparities in health (Boyd et al., 2020). Structural, interpersonal, and internalized racism can be attributed to all of the other risk factors we adjusted for as well as the racial differences that persisted even after this adjustment was made (Williams and Ovbiagele, 2020).

One limitation of this study is the limited statistical power driven by the small number of participants, though our enrollment matched or surpassed similar studies. Another limitation of this study is that we were unable to assess a cardiovascular risk score; all established cardiovascular risk scores require a cholesterol reading, which was not collected at time of the study. We instead examined HbA1c and blood pressure individually. Finally, differences by stroke status, especially in regards to demographic variables, may be due to differences in cohort selection. The acute stroke group came from a community sampling at two local hospitals, while the ADRC group includes volunteers from AD research studies. The low historical inclusion of AAs in research studies means they are particularly pursued as volunteers in the Knight ADRC,

and so may better represent the general community than their NHW counterparts who may be self-selecting from a family history of dementia. This idea is supported by the unusually high rate of family history of dementia seen in the NHW ADRC group but not the AA ADRC group.

While the community sampling of stroke patients makes it more difficult to interpret differences by stroke status, it makes our racial comparisons within the acute stroke group more likely to generalize. This analysis is unique as the intersection of stroke and race in biomarkers of preclinical AD has not been previously explored. Our data supports the idea that preclinical AD does not increase the risk for a stroke nor increase the likelihood developing post-stroke dementia. Future studies should attempt to replicate this in a larger cohort. It would be particularly important to assess regional information of the vascular pathologies, which were not examined in this study but have been shown to impact risk of post-stroke dementia (Zhao et al., 2018). Future work should also examine proteinopathies other than amyloid which may be affecting the development of post-stroke dementia.

4.5 Acknowledgements

This study was supported by grants from the National Institute on Aging awarded to Dr. Morris: P50AG005681, P01AG003991, P01AG026276, U19AG032438. Dr. Benzinger reports grants from the National Institutes of Health (NIH) during the conduct of the study; grants and non-financial support from Eli Lilly / Avid Radiopharmaceuticals outside the submitted work. Dr. Benzinger also reports the following relationships: Speakers' Bureau: Biogen, Eisai; clinical trial investigator: Biogen, Eisai, Roche, Lilly; support for radiopharmaceutical production: Avid Radiopharmaceuticals, Cerveau; unpaid consulting: Siemens, Eisai, Lilly.

4.6 Supplemental

Supplemental Figure S4.1: Continuous Demographic Measures

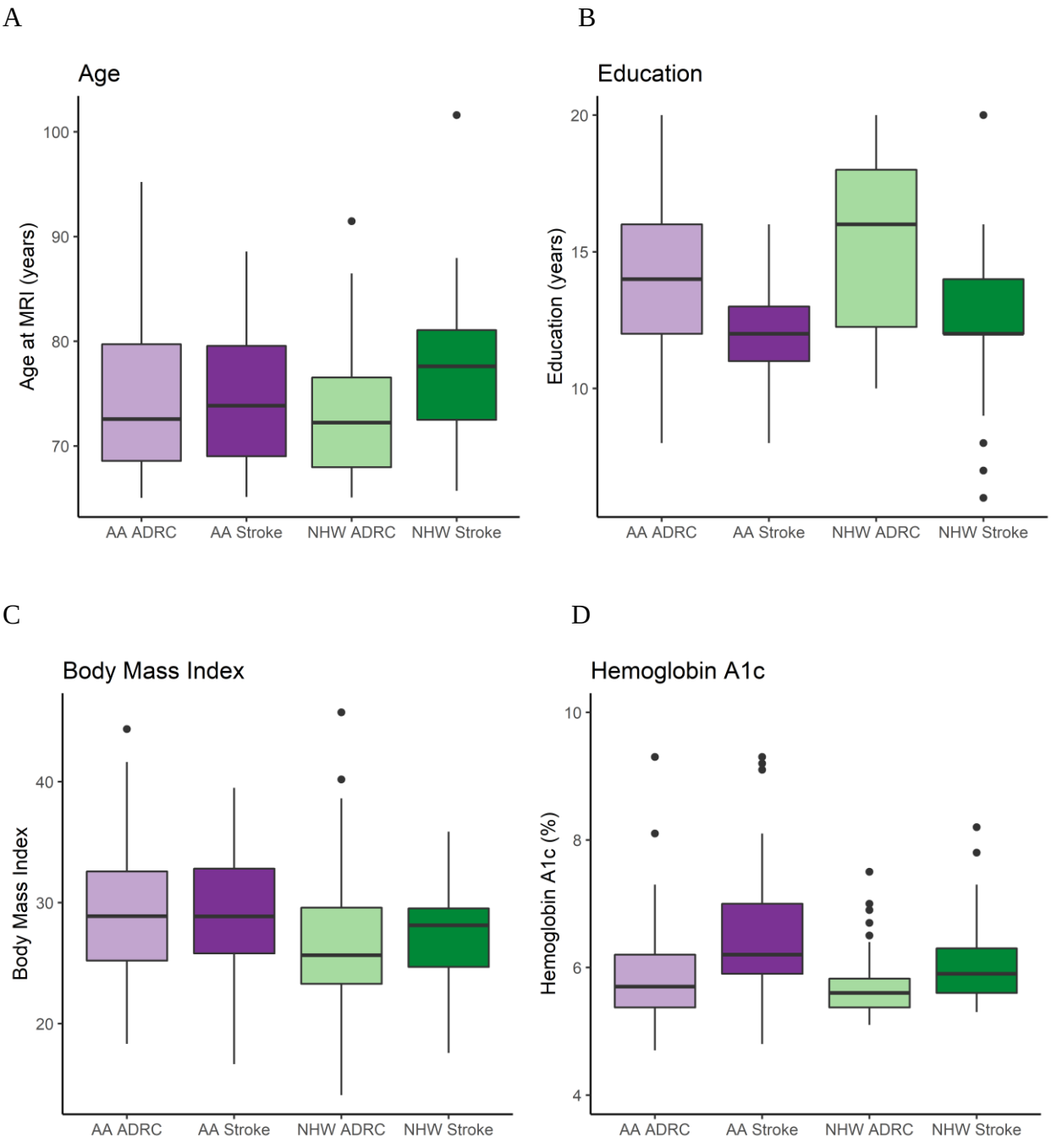

Supplemental Figure S4.1 displays boxplots of the participants' age, years of education, body mass index, and hemoglobin A1c, with data separated by race (AA or NHW) and cohort (acute stroke or ADRC comparison).

A. Missing data: 0 AA ADRC, 1 AA Stroke, 0 NHW ADRC, 2 NHW Stroke

B. Missing data: 0 AA ADRC, 1 AA Stroke, 0 NHW ADRC, 2 NHW Stroke
C. Missing data: 1 AA ADRC, 1 AA Stroke, 1 NHW ADRC, 2 NHW Stroke
D. Missing data: 36 AA ADRC, 3 AA Stroke, 22 NHW ADRC, 9 NHW Stroke

AA: African American; ADRC: Alzheimer Disease Research Center comparison cohort; NHW: Non-Hispanic White

Supplemental Figure S4.2: Longitudinal MMSE Models by Stroke and Race

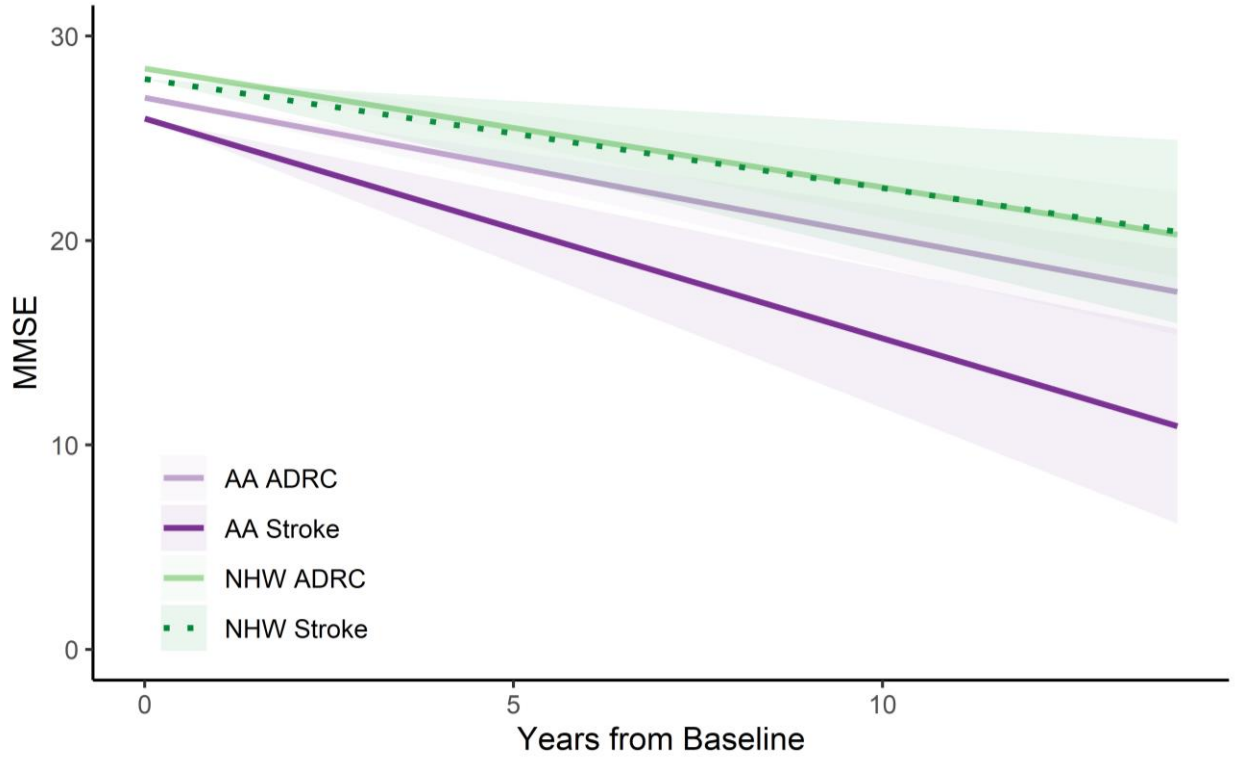

Supplemental Figure S4.2 displays the linear mixed effects models fit to the longitudinal MMSE data, with separate models by race (AA or NHW) and cohort (acute stroke or ADRC comparison). The shading around each line represents the standard error associated with the estimated line from the model.

AA: African American; ADRC: Alzheimer Disease Research Center comparison cohort; MMSE: Mini Mental State Exam; NHW: Non-Hispanic White

Supplemental Table S4.1: Demographics When Stroke is Defined by Radiologic Presence of Infarct

	AA	NHW	Race Difference (*p*)	Stroke *p*-value	
				Within AAs	Within NHWs
Participants, n				N/A	N/A
ADRC Group	80	73	0.57		
Stroke Group	45	42	0.75		
Age (y), mean (SD)				0.99	**0.01**
ADRC Group	74.6 (7.25)	73.0 (5.85)	0.53		
Stroke Group	75.0 (7.14)	77.0 (7.01)	0.43		
Male, n (%)				0.30	0.06
ADRC Group	28 (35.0)	30 (41.1)	0.44		
Stroke Group	20 (44.4)	25 (59.5)	0.16		
Education (years), mean (SD)				**< 0.001**	**< 0.001**
ADRC Group	14.4 (2.75)	15.4 (2.89)	0.14		
Stroke Group	12.2 (2.12)	12.8 (2.64)	0.80		
Family history of dementia, n (%)[a]				0.34	**0.003**
ADRC Group	23 (29.1)	40 (55.6)	**0.001**		
Stroke Group	6 (20.0)	7 (22.6)	0.81		
***APOE4* (n, % with an ε4 allele)[b]**				0.24	0.82
ADRC Group	36 (46.2)	29 (39.7)	0.43		
Stroke Group	23 (57.5)	15 (37.5)	0.08		
BMI (kg/m^2), mean (SD)[c]				> 0.99	0.96
ADRC Group	29.2 (5.13)	26.8 (5.72)	**0.02**		
Stroke Group	29.3 (5.39)	27.3 (4.02)	0.29		
Hemoglobin A1c (%), mean (SD [d]				**0.002**	0.18
ADRC Group	5.87 (0.82)	5.70 (0.51)	0.88		
Stroke Group	6.73 (1.64)	6.20 (1.30)	0.17		
Mean Arterial Pressure (mm Hg), mean (SD)[e]				0.12	0.10
ADRC Group	93.8 (11.5)	91.7 (9.68)	0.73		

	AA	NHW	Race Difference (*p*)	Stroke *p*-value	
				Within AAs	Within NHWs
Stroke Group	98.7 (14.2)	97.3 (14.5)	0.94		
Hypertension, n (%)[e]				**< 0.001**	0.17
ADRC Group	22 (27.5)	25 (35.2)	0.31		
Stroke Group	28 (62.2)	19 (48.7)	0.22		
Reported Previous Stroke, n (%)[f]				**0.04**	0.67
ADRC Group	15 (19.0)	9 (12.5)	0.28		
Stroke Group	16 (36.4)	6 (15.4)	**0.04**		
History of Diabetes, n (%)[g]				**< 0.001**	**0.001**
ADRC Group	3 (3.8)	2 (2.8)	0.74		
Stroke Group	12 (27.3)	11 (28.2)	0.92		

a) Missing data: 0 AA ADRC, 16 AA Stroke, 0 NHW ADRC, 12 NHW Stroke
b) Missing data: 2 AA ADRC, 5 AA Stroke, 0 NHW ADRC, 2 NHW Stroke
c) Missing data: 1 AA ADRC, 1 AA Stroke, 1 NHW ADRC, 2 NHW Stroke
d) Missing data: 36 AA ADRC, 3 AA Stroke, 22 NHW ADRC, 9 NHW Stroke
e) Missing data: 0 AA ADRC, 0 AA Stroke, 3 NHW ADRC, 3 NHW Stroke
f) Missing data: 0 AA ADRC, 1 AA Stroke, 1 NHW ADRC, 3 NHW Stroke
g) Missing data: 1 AA ADRC, 1 AA Stroke, 1 NHW ADRC, 3 NHW Stroke

AA: African American; ADRC: Alzheimer Disease Research Center comparison cohort; *APOE4*: Apolipoprotein E ε4; BMI: Body mass index; NHW: Non-Hispanic White; SD: Standard deviation

Supplemental Table S4.2: Group Differences by Race and Stroke Status When Stroke is Defined by Radiologic Presence of Infarct

		AA	NHW	Race *p*-value	
				Unadjusted Models	Adjusted Models[d]
Amyloid PET	**PIB Mean Cortical Binding Potential, mean (SE)[a]**	0.12 (0.04)	0.11 (0.03)	0.55	0.87
	ADRC Group	0.20 (0.05)	0.16 (0.05)	0.90	0.91
	Stroke Group	0.06 (0.05)	0.07 (0.05)	0.37	> 0.99
	PIB Positive, n (%)[a]	16 (22.5)	17 (25.0)	0.80	0.51
	ADRC Group	10 (31.3)	6 (18.8)	0.25	0.68
	Stroke Group	6 (15.4)	11 (30.6)	0.12	0.57
Quantitative MRI	**Total Hippocampal Volume (normalized), mean (SE)[b]**	6750 (122)	6740 (126)	0.57	0.94
	ADRC Group	6590 (132)	6830 (123)	0.46	0.54
	Stroke Group	6560 (197)	6420 (205)	0.99	0.96
	WMH Volume, mean (SE)[c]	28400 (10100)	51600 (13700)	0.33	0.18
	ADRC Group	27900 (17500)	62200 (23400)	0.80	0.65
	Stroke Group	31500 (9700)	51800 (12100)	0.98	0.56
Radiologic Read of MRI	**Presence of Large Infarcts, n (%)**	34 (14.2)	27 (11.3)	0.51	0.86
	ADRC Group	0 (0.0)	0 (0.0)	[e]	[e]
	Stroke Group	34 (75.6)	27 (64.3)	[e]	[e]
	Presence of Small Infarcts, n (%)	34 (14.2)	29 (12.1)	0.73	0.90
	ADRC Group	0 (0.0)	0 (0.0)	[e]	[e]
	Stroke Group	34 (75.6)	29 (69.1)	[e]	[e]
	Leukoaraiosis Moderate-Severe, n (%)	46 (19.2)	26 (10.8)	**0.01**	0.13
	ADRC Group	19 (23.8)	9 (12.3)	0.07	0.18
	Stroke Group	27 (60.0)	17 (40.5)	0.07	0.33
	Presence of Microbleeds, n (%)	41 (17.1)	26 (10.8)	**0.04**	**0.03**
	ADRC Group	15 (18.8)	6 (8.2)	0.07	**0.047**
	Stroke Group	26 (57.8)	20 (47.6)	0.34	0.40
	Microbleeds ≥ 5, n (%)	19 (7.9)	11 (4.6)	0.09	**0.04**
	ADRC Group	6 (7.5)	1 (1.4)	0.11	0.05

	Stroke Group	13 (28.9)	10 (23.8)	0.59	0.37
	MMSE, mean (SE)	26.6 (0.35)	27.9 (0.34)	**< 0.001**	**0.008**
	ADRC Group	26.3 (0.39)	27.3 (0.37)	0.05	0.23
	Stroke Group	26.4 (0.56)	28.2 (0.55)	**0.03**	0.09

a) Missing data: 48 AA ADRC, 6 AA Stroke, 41 NHW ADRC, 6 NHW Stroke
b) Missing data: 3 AA ADRC, 10 AA Stroke, 0 NHW ADRC, 13 NHW Stroke
c) Missing data: 71 AA ADRC, 10 AA Stroke, 64 NHW ADRC, 17 NHW Stroke
d) Adjusted models have controlled for baseline age, family history of dementia, *APOE4*, education, sex, and hypertension
e) Model does not include stroke status variable because it is defined by the outcome

AA: African American; ADRC: Alzheimer Disease Research Center comparison cohort; *APOE4*: Apolipoprotein E ε4; MMSE: Mini Mental State Exam; MRI: Magnetic resonance imaging; NHW: Non-Hispanic White; PET: Positron emission tomography; PIB: [^{11}C]-Pittsburgh Compound B; SE: Standard error; WMH: White matter hyperintensities

Supplemental Table S4.3: Baseline Data of Acute Stroke Participants with and without Follow-Up

	With Follow-Up	Without Follow-Up	*p*-value
Participants, n (by Race)	55 (27 AA, 28 NHW)	26 (15 AA, 11 NHW)	0.34
Age (y), mean (SD)[a]	75.6 (7.06)	77.4 (6.57)	0.32
Male, n (%)[a]	23 (41.8)	16 (69.6)	**0.03**
Education (years), mean (SD)[a]	12.2 (2.66)	12.2 (1.85)	0.94
Family history of dementia, n (%)[b]	8 (16.7)	0 (0)	1.00
***APOE4* (n, % with an ε4 allele)[c]**	19 (34.6)	13 (81.3)	**0.003**
BMI (kg/m^2), mean (SD) [a]	28.8 (4.86)	27.2 (4.76)	0.18
Hemoglobin A1c (%), mean (SD)[d]	6.67 (1.79)	6.36 (0.82)	0.45
Mean Arterial Pressure (mm Hg), mean (SD)[e]	97.8 (14.4)	98.9 (14.0)	0.75
Hypertension, n (%)[e]	31 (58.49)	12 (54.55)	0.75
PIB Mean Cortical Binding Potential, mean (SE)[f]	0.09 (0.21)	0.07 (0.16)	0.62
PIB Positive, n (%)[f]	13 (23.6)	5 (23.8)	0.99
Total Hippocampal Volume (normalized), mean (SD)[g]	6500 (804)	6210 (914)	0.25
WMH Volume, mean (SD)[h]	37200 (33200)	46000 (28000)	0.31
Presence of Large Infarcts, n (%)[a]	40 (72.7)	17 (73.9)	0.91
Presence of Small Infarcts, n (%)[a]	36 (65.5)	16 (69.6)	0.73
Leukoaraiosis Moderate-Severe, n (%)[a]	29 (52.7)	11 (47.8)	0.69
Presence of Microbleeds, n (%)[a]	30 (54.6)	12 (52.2)	0.85
Microbleeds ≥ 5, n (%)[a]	16 (29.1)	7 (30.4)	0.91
MMSE, mean (SD)[a]	26.9 (2.91)	25.6 (3.27)	0.10
Coronary Artery Disease, n (%)[i]	15 (28.3)	6 (28.6)	0.98
Statin Use, n (%)[i]	28 (52.8)	10 (47.6)	0.68
Reported Previous Stroke, n (%)[i]	13 (24.5)	8 (38.1)	0.25
History of Diabetes, n (%)[i]	14 (26.4)	9 (42.9)	0.17
NIHSS, mean (SD)[j]	4.58 (3.12)	7.15 (4.37)	**0.01**
TOAST Classification, n (%)[i]			

	With Follow-Up	Without Follow-Up	*p*-value
Large artery atherosclerosis	4 (7.55)	5 (23.8)	Ref
Cardioembolism	14 (26.4)	6 (28.6)	0.20
Small artery occlusion	22 (41.5)	5 (23.8)	**0.04**
Undetermined etiology	13 (24.5)	5 (23.8)	0.17

a) Missing data: 0 With Follow-up, 3 Without Follow-up
b) Missing data: 7 With Follow-up, 24 Without Follow-up
c) Missing data: 0 With Follow-up, 10 Without Follow-up
d) Missing data: 8 With Follow-up, 4 Without Follow-up
e) Missing data: 2 With Follow-up, 4 Without Follow-up
f) Missing data: 0 With Follow-up, 5 Without Follow-up
g) Missing data: 16 With Follow-up, 10 Without Follow-up
h) Missing data: 11 With Follow-up, 6 Without Follow-up
i) Missing data: 2 With Follow-up, 5 Without Follow-up
j) Missing data: 3 With Follow-up, 6 Without Follow-up

AA: African American; *APOE4*: Apolipoprotein E ε4; BMI: Body mass index; MMSE: Mini Mental State Exam; NHW: Non-Hispanic White; NIHSS: National Institutes of Health Stroke Scale; PIB: [^{11}C]-Pittsburgh Compound B; SD: Standard deviation; TOAST: Trial of Org 10172 in Acute Stroke Treatment; WMH: White matter hyperintensities

Supplemental Table S4.4: Baseline Data of Acute Stroke Participants By CDR at 1 Year Follow-Up

	CDR = 0	CDR > 0	*p*-value
Participants, n (by Race)	29 (12 AA, 17 NHW)	26 (15 AA, 11 NHW)	0.23
Age (y), mean (SD)	76.6 (8.11)	74.61 (5.66)	0.30
Male, n (%)	12 (41.4)	11 (42.3)	0.94
Education (years), mean (SD)	12.0 (2.74)	12.5 (2.6)	0.46
Family history of dementia, n (%)[a]	2 (8.7)	6 (24.0)	0.17
***APOE4* (n, % with an ε4 allele)**	8 (27.6)	11 (42.3)	0.25
BMI (kg/m^2), mean (SD)	28.8 (4.76)	28.7 (5.07)	0.92
Hemoglobin A1c (%), mean (SD)[b]	6.51 (1.54)	6.83 (2.03)	0.53
Mean Arterial Pressure (mm Hg), mean (SD)[c]	97.9 (15.6)	97.6 (13.2)	0.93
Hypertension, n (%)[c]	16 (57.1)	15 (60)	0.83
PIB Mean Cortical Binding Potential, mean (SE)	0.05 (0.15)	0.14 (0.25)	0.14
PIB Positive, n (%)	5 (17.2)	8 (30.8)	0.24
Total Hippocampal Volume (normalized), mean (SD)[d]	6420 (781)	6580 (842)	0.54
WMH Volume, mean (SD)[e]	34700 (38500)	40000 (26900)	0.60
Large Infarcts Positive, n (%)	21 (72.4)	19 (73.1)	0.96
Small Infarcts Positive, n (%)	17 (58.6)	19 (73.1)	0.26
Leukoaraiosis Positive, n (%)	13 (44.8)	16 (61.5)	0.22
Presence of Microbleeds, n (%)	15 (51.7)	15 (57.7)	0.66
Microbleeds ≥ 5, n (%)	5 (17.2)	11 (42.3)	0.046
MMSE, mean (SD)	26.7 (3.09)	27.1 (2.73)	0.62
Coronary Artery Disease, n (%)[f]	6 (22.2)	9 (34.6)	0.32
Statin Use, n (%)[f]	14 (51.9)	14 (53.9)	0.88
Reported Previous Stroke, n (%)[f]	2 (7.41)	11 (42.3)	0.008
History of Diabetes, n (%)[f]	5 (18.52)	9 (34.62)	0.19
NIHSS, mean (SD)[g]	4.23 (2.72)	4.92 (3.5)	0.42
TOAST Classification, n (%)[f]			

	CDR = 0	CDR > 0	*p*-value
Large artery atherosclerosis	1 (3.7)	3 (11.5)	Ref
Cardioembolism	7 (25.9)	7 (26.9)	0.39
Small artery occlusion	11 (40.7)	11 (42.3)	0.37
Undetermined etiology	8 (29.6)	5 (19.2)	0.22

a) Missing data: 6 CDR = 0, 1 CDR > 0
b) Missing data: 5 CDR = 0, 3 CDR > 0
c) Missing data: 1 CDR = 0, 1 CDR > 0
d) Missing data: 9 CDR = 0, 7 CDR > 0
e) Missing data: 6 CDR = 0, 5 CDR > 0
f) Missing data: 2 CDR = 0, 0 CDR > 0
g) Missing data: 3 CDR = 0, 0 CDR > 0

AA: African American; *APOE4*: Apolipoprotein E ε4; BMI: Body mass index; CDR: Clinical Dementia Rating; MMSE: Mini Mental State Exam; NHW: Non-Hispanic White; NIHSS: National Institutes of Health Stroke Scale; PIB: [^{11}C]-Pittsburgh Compound B; SD: Standard deviation; TOAST: Trial of Org 10172 in Acute Stroke Treatment; WMH: White matter hyperintensities

Chapter 5: White Matter Hyperintensities in Preclinical Alzheimer Disease

Cerebral white matter hyperintensities in older adults are primarily attributed to small vessel ischemic disease. However, white matter hyperintensities are more prevalent in Alzheimer disease dementia and it is unclear if they are from co-morbid cerebrovascular disease or an aspect of Alzheimer disease itself, potentially related to β-amyloid deposition in arterial walls. If white matter hyperintensities are increased in the preclinical AD stage, it would support the hypothesis that they are caused directly by Alzheimer disease. In this study we examine if white matter hyperintensities are different in both the preclinical Alzheimer disease stage and in Alzheimer disease dementia using data from 489 participants in the Knight Alzheimer Disease Research Center. These participants were classified as cognitively normal (amyloid negative and non-demented), preclinical Alzheimer disease (amyloid positive and non-demented), or Alzheimer disease dementia (amyloid positive and demented), with groups matched in age. We use machine learning algorithms to classify participants into their diagnostic categories using only white matter hyperintensity data either from the entire white matter or from predefined regions of the white matter that may be associated with Alzheimer disease. The resulting algorithms were able to separate Alzheimer disease dementia from preclinical Alzheimer disease, even when only voxels from the dorsal parietal or posterior regions were used as input. The algorithms could not separate preclinical Alzheimer disease from the amyloid negative controls, suggesting that white matter hyperintensities are not different in the preclinical stage of Alzheimer disease. These results suggest that white matter hyperintensities may be independent from Alzheimer disease or may not develop until later stages in the disease.

5.1 Introduction

White matter hyperintensities (WMH) of presumed vascular origin are seen as markers of small vessel disease, but the specific pathologies involved are numerous and not well understood (Alber et al., 2019; Hase et al., 2018; Park and Moon, 2016; Wardlaw et al., 2019). Many things influence the volume of WMHs, including modifiable factors such as blood pressure (Alber et al., 2019; Salvadó et al., 2019) as well as non-modifiable factors such as Black race, female sex, and apolipoprotein E ε4 (*APOE4*) allele presence. WMH lesions by themselves can lead to vascular dementia with a slow continuous progression as the lesion count builds (Alber et al., 2019). Additionally, WMHs are also associated with other types of dementia including Alzheimer disease (AD) (Alosco et al., 2018; Bos et al., 2018; Gordon et al., 2015; Joki et al., 2018), as well as normal aging in unimpaired older adults (Alber et al., 2019; Salvadó et al., 2019).

To date, there is little consensus as to whether WMHs are an aspect of AD or if they simply co-occur and have an additive effect on the brain (Koncz and Sachdev, 2018). A prior review of the literature suggests amyloid and WMHs are independent yet additive (Roseborough et al., 2017). WMH's independence from AD would help explain WMH's complex relationship with cognition. More specifically, WMH volume does not impact cognitive progression in AD patients (Eldholm et al., 2018), but it does predict conversion from normal cognition to mild cognitive impairment (MCI) (Bangen et al., 2018b). Furthermore, WMHs have also been linked to perceptual speed in unimpaired older adults (Arvanitakis et al., 2016). In those who are cognitively unimpaired or have MCI, one study reported that amyloid and WMHs have an individual but not an additive effect on cognitive decline (Bos et al., 2017), while another did report an additive effect of amyloid and Framingham risk scores (Rabin et al., 2018).

Conversely, there is some evidence for a direct interaction between WMHs and AD. This is strongest in autosomal dominant AD, which showed that WMHs increase in the preclinical stage of the disease, six years before dementia onset (Lee et al., 2018). This result was shown to be partly due to increased cerebral amyloid angiopathy (CAA) (Lee et al., 2018), which is a specific type of cerebral small vessel disease that involves amyloid build up in the vasculature and is distinct but related to AD (Charidimou et al., 2017). Even in non-demented older adults, amyloid positron emission tomography (PET) correlated with a periventricular pattern of WMHs and was associated with microbleeds in a way that suggests the relationship is due to CAA (Graff-Radford et al., 2019). Other studies have shown an association of amyloid and WMHs, in particular periventricular regions (Marnane et al., 2016), and an association of baseline WMHs and an increase in amyloid load around two years later (Grimmer et al., 2012).

Unlike in autosomal dominant AD, it is not yet clear if WMHs are different in the preclinical stage of sporadic AD. If they are changed in this preclinical stage, it would provide evidence that WMHs are a core aspect of AD. The opposing theory that the WMHs seen in AD are a completely separate pathology that adds to cognitive impairment would not explain a change in the preclinical stage where there is no cognitive impairment.

5.2 Methods

5.2.1 Participants

The 489 participants in this study were collated from Knight Alzheimer Disease Research Center (ADRC) studies (collected 2009-2020) using the 17th Knight ADRC data freeze. Details of recruitment at the ADRC have been outlined previously (John C Morris et al., 2019). All procedures in this study were Health Insurance Portability and Accountability Act (HIPAA) compliant, approved by the Washington University Institutional Review Board, and gained

informed consent for all participants. Participants were included if they had an MR scan with both a T1 and a Fluid Attenuated Inversion Recovery (FLAIR) image (needed for WMH processing), an amyloid PET scan within 1 year of the MR, and a Clinical Dementia Rating™ (CDR™) (Morris, 1993) within 1 year of the MR.

Participants were placed in the AD dementia group if they had an amyloid positive PET scan (see section 5.2.2 below), had a CDR > 0, and were evaluated by a clinician as having dementia. Participants who were amyloid positive, had a CDR = 0, and evaluated clinically as cognitively normal were placed in the preclinical AD group. Finally, participants who were amyloid negative, had a CDR = 0, and evaluated clinically as cognitively normal were placed in the cognitively normal (CN) group. Participants who had a CDR > 0 and amyloid negative (non-AD dementia) were excluded, as were participants with discordant CDR status and clinical evaluation of impairment. While the Knight ADRC data contains longitudinal data, the assembled dataset uses only cross-sectional data, resulting in only one MRI used per participant.

Participants were also split into a ‘Training’ cohort used to train the machine learning algorithms, and a ‘Test’ cohort used to independently evaluate the algorithm’s performance. The AD dementia group was split in half randomly, with one group of 41 assigned to the ‘Training’ cohort and the other group of 40 to the ‘Test’ cohort. The Test cohort was completed by matching the AD dementia Test cohort 1-to-1 by age to participants from the preclinical AD and cognitively normal groups, for a total of 120 participants. The Training cohort was similarly completed, but used 5-to-1 matching for the cognitively normal group and 3-to-1 matching for the preclinical AD group for a total of 369.

5.2.2 Clinical Assessment and Demographics

Experienced clinicians, blinded to amyloid status, evaluated each participant for the possibility of a clinical diagnosis of dementia. Their assessment, outlined previously (Morris et al., 2006), integrated results from a semi-structured interview conducted with the participant and a knowledgeable collateral source, a thorough neurological examination, and bedside measures of cognitive function. Included in this was the CDR (Morris, 1993), which assessed possible decline in cognitive and functional abilities relative to the participant's previously attained levels, and the Mini Mental State Exam (MMSE) (Folstein et al., 1975).

Demographic and clinical data such as age, gender, *APOE4* status (defined as having one or more ε4 alleles), self-reported race, years of education, Hachinski score, blood pressure, body mass index (BMI), smoking status, and self-reported history of diabetes and hypertension were also collected. Hachinski score is a clinical tool used to separate vascular and AD dementia based on a variety of factors such as history of stroke and focal neurologic signs and symptoms, (Hachinski et al., 1975; Moroney et al., 1997). We use the term 'gender' to match the terminology of the questionnaire used in the study, but participants were offered only 'Male' and 'Female' as options and sex was not assessed separately. All the clinical and demographic data listed above were collected within 365 days from the magnetic resonance imaging (MRI) session. Median time difference from MRI was 85 days for most measures, was 82 days for Hachinski, and was 78 days for smoking status, history of hypertension, and history of diabetes. Some of this data was not available for all patients: 9 participants are missing *APOE4* status, 320 are missing Hachinski scores, 1 participant is missing blood pressure, 2 are missing BMI, 130 are missing smoking status, 131 are missing history of diabetes, and 133 are missing history of hypertension.

5.2.3 MR Imaging

The MR imaging occurred on 3T Siemens scanners: n = 318 on Siemens Biograph mMR (PET/MR), n = 99 on Siemens Magnetom Vida, and n = 72 on Siemens 3T Trio Tim. Participants had a structural, T1-weighted magnetization-prepared, rapid gradient-echo (MPRAGE) MRI collected with a resolution of either 1 × 1 × 1.25 mm or 1 × 1 × 1 mm, as well as a FLAIR image. The T1-weighted images underwent regional tissue segmentation with FreeSurfer (version 5.3) (Fischl, 2012). Regional volumes (cortical and subcortical) were adjusted for head size with a regression scaling approach using intracranial volume (Buckner et al., 2004). Left and right hemispheric data were combined by summing volumes and averaging cortical thicknesses.

WMHs were segmented using the Lesion Segmentation Tool (Schmidt et al., 2012) in SPM8. This segmentation tool was selected as it has been previously evaluated in populations of normal aging with the WMHs being of presumed vascular origin (Heinen et al., 2019; Ribaldi et al., 2021; Tubi et al., 2020; Waymont et al., 2020). WMH maps were registered to 2mm Montreal Neurosciences Institute 152 (MNI152) space in FSL. This resulted in each voxel being assigned a probability from 0 to 1 of being a WMH. This probability data, as well as the data binarized at a threshold of 0.5 were used. Whenever counts of WMHs in units of voxels are mentioned, it is using this 0.5 threshold binary. The specific threshold used likely is not important as there were few values in the 0.2-0.8 range. This is evidenced when summing the binarized voxel counts and summing the raw probabilities gave almost the same result within individual participants, with an overall correlation R of 0.99 ($p < 0.001$).

The white matter voxels were then separated into 5 predefined regions (displayed in Figure 5.1) (Phuah et al., 2019). These regions of interest (ROIs) were developed from voxel-

level WMH maps from 1,046 participants in the Alzheimer's Disease Neuroimaging Initiative (ADNI) database with a mix of diagnoses (cognitively normal to AD dementia) through a k-means clustering unsupervised machine learning algorithm. The relative WMH burden in each resulting regions was then linked to Alzheimer-related factors. The Juxtacortical pattern was linked to a diagnosis of probable CAA, while the Dorsal Parietal pattern associated with amyloid PET levels and *APOE4* status. By looking specifically within these regions, we hoped to assess the WMHs at a medium level of detail, between the very rough measure of total WMH volume, and the extremely detailed measure of examining all white matter voxels in the brain.

Figure 5.1: Predefined Regions of White Matter Hyperintensities Clusters (Phuah et al., 2019)

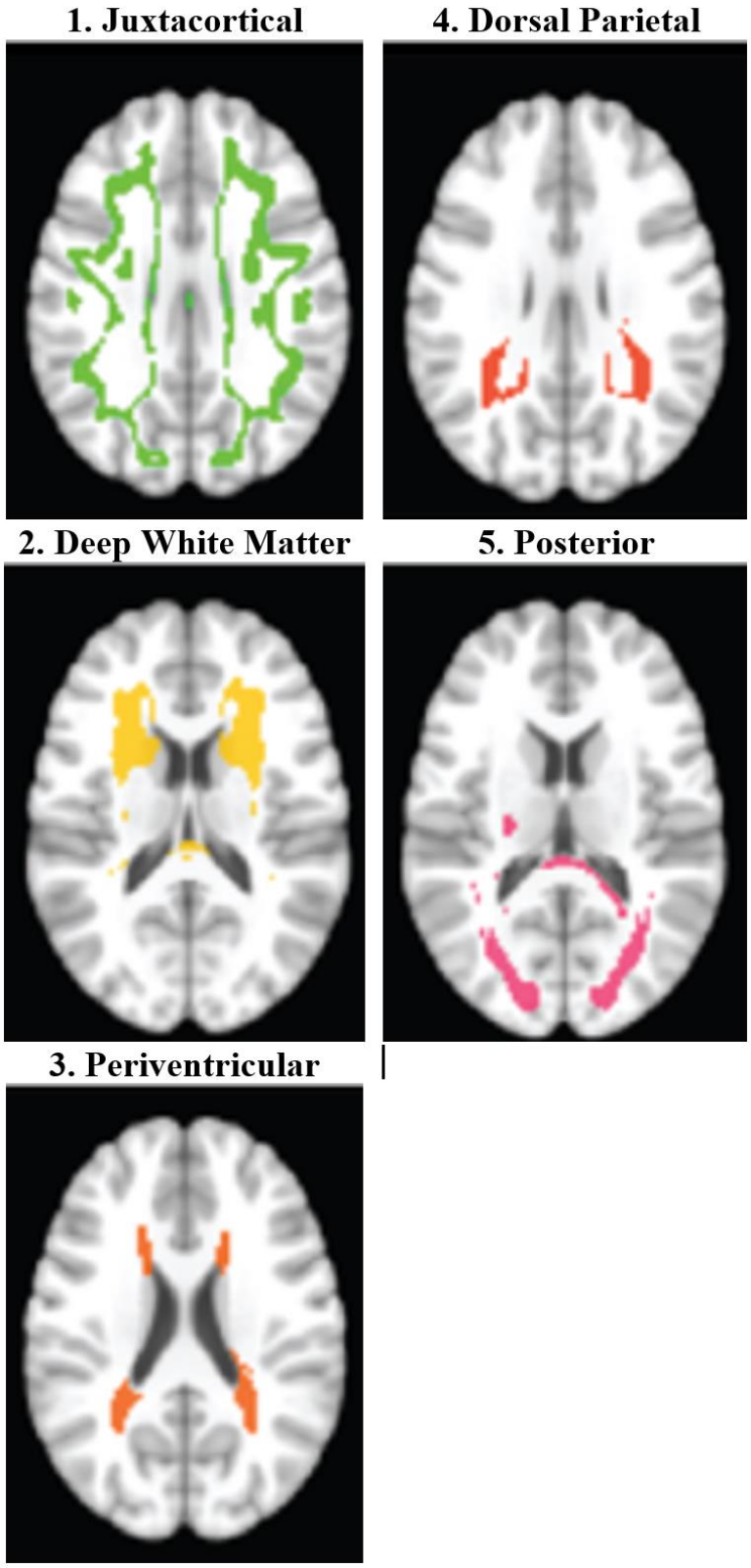

5.2.3 PET Imaging

Amyloid PET imaging on 200 participants was done using [^{11}C]-Pittsburgh compound B (PIB), with a dosage of ~13 mCi and data collected 30-60 minutes post-injection. The remaining 289 participants were imaged using Florbetapir ([^{18}F]-AV45), with a dosage of ~10 mCi and data collected 50-70 minutes post-injection.

PET images were processed with an in-house pipeline (Su, 2021) using FreeSurfer-derived regions and a cerebellar cortex reference region. Signal spillover was addressed with partial volume correction, specifically with a regional spread function (geometric transfer matrix) technique based on the scanner point spread function and the relative distance between regions (Su et al., 2015, 2013). The mean cortical standard uptake value ratio with regional spread function applied (SUVR RSF) was defined as the average SUVR RSF from the precuneus, prefrontal cortex, gyrus rectus, and lateral temporal regions (Su et al., 2019).

A negative amyloid PET scan was defined as having a mean cortical SUVR RSF < 1.42 (Centiloid < 16.4) for PIB PET or SUVR RSF < 1.19 (Centiloid < 20.6) for Florbetapir PET. The Centiloid conversion process, used to more easily compare the two amyloid tracers, is documented in detail in the initial Centiloid paper (Klunk et al., 2015), with specific equations in follow-up papers (Su et al., 2019, 2018). Harmonization procedures such as this are imperfect, and so to remain as accurate as possible we used cutoffs determined individually for each tracer and then converted into Centiloid, as opposed to a unified Centiloid cutoff. PET imaging occurred 0-349 (median 0) days from MRI.

5.2.3 Statistics

All analyses were done in R version 3.5.3. The demographic variables listed in Table 5.1 were compared across diagnostic groups using analyses of variance (ANOVAs). Significant ANOVAs were further examined pairwise using student's t-tests for continuous variables and Chi-square tests for categorical variables. A Bonferroni-Holm corrected p-value of < 0.05 was considered significant. The total number of WMH voxels were similarly evaluated with ANOVAs and follow-up t-tests or chi-squared tests for significant associations, as were the total WMH voxels within each of the five previously defined white matter ROIs.

The primary group differences found – amyloid, *APOE4*, and MMSE, were explored further with linear models in order to assess their ability to predict WMH volumes. Each factor was assessed separately and included age as a covariate. These linear models were first run on all participants, and then explored further by considering them within each diagnostic group separately, and on all participants except the AD dementia group.

5.2.4 Machine Learning

To probe for more complex patterns of WMHs, we used several machine learning classification algorithms within R's 'caret' package (Kuhn et al., 2021). The data was preprocessed by removing the voxels with near zero variance across the Training cohort and z-scoring the remaining voxels. Near zero variance was defined using the default settings in R, such that variables are removed if they have one unique value (zero variance), or the variable has both few unique values as well as a high ratio of the most common value to the second most common value. Specifically, the ratio of the most common variable to the second most common variable is above 95/5, and the number of unique values divided by the total number of participants is below 10. The end result of this process is the removal of voxels for which nearly

every participant had a 0% probability of that voxel being a WMH. All the preprocessing was run on the Training cohort, and then applied identically to the Test cohort to prevent data leakage.

The Training cohort was then used to run 3 different algorithms: Support Vector Machine (method = 'svmLinearWeights'), random forest (method = ranger), and stochastic gradient boosting (method = 'gbm'). Each model used 10-fold cross-validation with five repeats and a tuning grid to optimize parameters. The optimal model (as determined by the receiver operating characteristic's area under the curve (AUC)) from the tuning grid is then automatically selected and applied to the Test cohort.

Additional consideration was given to the problem of class imbalance – the cognitively normal group was much larger than the preclinical AD group, which was much larger than the AD dementia group. As such, we evaluated several methods known to improve machine learning models in the case of class imbalance. In total, we tested whether models could be improved by adding case weights of three different strengths, binning the voxels at a threshold of 0.5, up-sampling the smaller group, or applying principal component analysis (keeping components that in total explained 95% of variance) to the data before training. The lightest, 1x case weights equalized the groups, while the 2x weights doubled the smaller group, and the 3x weights tripled it. As the 2x case weights were found to improve models more than using the 1x, 3x, or no weights, the other methods were done in addition to the 2x case weights (i.e., 2x weights and binning, 2x weights and up-sampling, 2x weights and PCA).

Based on the Test cohort accuracy, we determined the optimal preprocessing steps given the class imbalance and provide detailed metrics from the models run in this optimal manner.

Test cohort accuracy *p*-values are calculated by determining if the accuracy is above the no information rate using a binomial exact test; no information gives a 50% accuracy in our case as the Test cohort has equal group sizes. To ensure the same criteria is applied to all models, we used a Bonferroni correction instead of a Bonferroni-Holm. As we trained three different algorithms and used 6 different sets of white matter voxels (all white matter voxels and ROIs 1-5), our Bonferroni correction was for 18 tests, resulting in a significance level of $p < 0.0028$ for each. Given our sample size, this meant models with a Test cohort accuracy of at least 66% are considered statistically significant.

5.3 Results

5.3.1 Demographic and Clinical Measures

Of the 489 participants in this study, 245 were assigned to the cognitively normal group, 163 were assigned to the preclinical AD group, and 81 were assigned to the AD dementia group. The demographics for these three groups are presented in Table 5.1. Comparing the cognitively normal group to the preclinical AD group showed that the cognitively normal group had lower rates of *APOE4* alleles (22.0% vs. 53.8%, corrected $p < 0.001$), lower amyloid (by definition, 3.36 vs. 52.1 Centiloids, corrected $p < 0.001$), and higher BMI (28.6 vs. 26.4, corrected $p < 0.001$).

All of these differences except for the difference in BMI were also seen when comparing the cognitively normal group to the AD dementia group; the cognitively normal group had lower rates of *APOE4* alleles (22.0% vs. 74.7%, corrected $p < 0.001$) and lower amyloid levels (by definition, 3.36 vs. 85.1 Centiloids, corrected $p < 0.001$). In addition, the cognitively normal group had higher average MMSE than the AD dementia group (29.2 vs. 25.0, corrected $p < 0.001$).

Comparing the preclinical AD group to the AD dementia group showed similar findings; the preclinical AD group had lower rates of *APOE4* alleles (53.8% vs. 74.7%, corrected $p = 0.006$), higher MMSE scores (29.0 vs. 25.0, corrected $p < 0.001$), and lower amyloid levels (52.1 vs. 85.1 Centiloids, corrected $p < 0.001$). In summary, *APOE4* rates and amyloid levels increased stepwise between the three groups, and MMSE was lowered within the AD dementia group.

These same summary measures within just the Training cohort are in Supplemental Table S5.1, while measures within the Test cohort are in Supplemental Table S5.2. No significant differences were found when the cognitively normal, preclinical AD, and AD dementia groups in the Training cohort were compared to their Test cohort counterparts using ANOVAs.

5.3.2 WMH Summary Measures

Within Table 5.1, Supplemental Table S5.1, and Supplemental Table S5.2 are the means and standard deviations for each of the WMH summary measures. This includes the total number of voxels classified as WMHs in the entire brain, as well as the number of voxels within each of the 5 predefined ROIs. The violin plots in Figure 5.2 show WMHs in each region split by diagnosis in order to give a more complete picture of each of these measures. These same plots within the Training and Test cohort can be seen in Supplemental Figure S5.1 and Supplemental Figure S5.2. Comparing the cognitively normal and preclinical AD groups yielded no significant differences. However, several measures indicated that the AD dementia group had higher WMHs than the cognitively normal group and preclinical AD group. The cognitively normal group had lower WMHs than the AD dementia group for total WMH voxels (1760 vs. 2690, corrected $p = 0.001$), voxels in the Periventricular ROI (701 vs. 1050, corrected $p < 0.001$), voxels in the Dorsal Parietal ROI (209 vs. 313, corrected $p = 0.007$), and voxels in the Posterior ROI (193 vs.

320, corrected $p < 0.001$). Similarly, the preclinical AD group had lower WMHs than the AD dementia group for total WMH voxels (1690 vs. 2690, corrected $p = 0.001$), voxels in the Periventricular ROI (687 vs. 1050, corrected $p < 0.001$), voxels in the Dorsal Parietal ROI (195 vs. 313, corrected $p = 0.003$), and voxels in the Posterior ROI (188 vs. 320, corrected $p < 0.001$).

We next used linear models to assess how the main factors differentiating the three diagnostic groups – amyloid, *APOE4*, and MMSE – relate to these group differences in WMHs. As we are now looking within groups our age-matching no longer controls for age, so age was included as a covariate for all models. When modeling WMHs using amyloid within all participants, WMH volumes in the Periventricular ROI (corrected $p = 0.002$) and in the Posterior ROI (corrected $p = 0.002$) were associated with amyloid. WMHs in the Periventricular ROI also significantly associated with *APOE4* (corrected $p = 0.02$), while total WMHs (corrected $p < 0.001$), the Juxtacortical ROI (corrected $p = 0.03$), the Deep White Matter ROI (corrected $p = 0.03$), the Periventricular ROI (corrected $p < 0.001$), the Dorsal Parietal ROI (corrected $p = 0.01$), and the Posterior ROI (corrected $p < 0.001$) all associated with MMSE. None of these relationships persisted in the combined cognitively normal and preclinical AD groups, or in the cognitively normal group, preclinical AD group, or AD dementia group by themselves (see Supplemental Table S5.3. This indicates that the originally observed relationships between WMHs and these factors is driven by group differences in the AD group and not necessarily the factors themselves.

Table 5.1: Demographics and WMH Summary Measures

All	Cognitively Normal	Preclinical AD	AD Dementia
n	245	163	81
CDR [0,0.5,1,2]	245,0,0,0	163,0,0,0	0,57,23,1
Gender (% M)	42.9%	43.6%	51.9%
Age, years (mean)	61.0-92.2 (73.5)	60.7-89.4 (74.2)	61.0-88.4 (74.0)
MMSE (mean)	25-30 (29.2)	23-30 (29.0)	14-30 (25.0)
***APOE4*, % with ε4 allele**	22.0%	53.8%	74.7%
Amyloid* – Centiloid (mean)	-10.2-20.0 (3.36)	16.4-154 (52.1)	21.1-159 (85.1)
Race, % non-Hispanic White	81.6%	90.2%	90.1%
Education, years (mean)	11-20 (16.1)	8-22 (16.2)	6-20 (15.2)
Mean Arterial Pressure (mean)	68-126 (93.4)	70-120 (92.5)	65-125 (94.3)
Hypertensive Blood Pressure, %	62.3%	58.9%	66.7%
History of Hypertension, %	51.4%	41.4%	45.8%
Hachinski Score (mean)	0-4 (0.58)	0-1 (0.45)	0-3 (0.50)
BMI (mean)	13-49 (28.6)	18-45 (26.4)	17-40 (27.4)
History of Diabetes, %	14.4%	4.46%	6.94%
Smoker, %	6.90%	2.65%	1.39%
Total WMH voxels, mean (SD)	1760 (1780)	1690 (1890)	2690 (2140)
Juxtacortical ROI WMH voxels, mean (SD)	187 (296)	188 (373)	302 (532)
Deep White Matter ROI WMH voxels, mean (SD)	347 (543)	322 (615)	505 (640)
Periventricular ROI WMH voxels, mean (SD)	701 (535)	687 (518)	1050 (514)
Dorsal Parietal ROI WMH voxels, mean (SD)	209 (284)	195 (269)	313 (301)
Posterior ROI WMH voxels, mean (SD)	193 (178)	188 (168)	320 (214)

* Mean Cortical SUVR RSF

AD: Alzheimer disease; *APOE4*: Apolipoprotein E ε4; BMI: Body mass index; CDR: Clinical Dementia Rating; MMSE: Mini Mental State Exam; ROI: Region of interest; SD: Standard deviation; SUVR RSF: Standard uptake value ratio (regional spread function applied); WMH: White matter hyperintensities

Figure 5.2: White Matter Hyperintensity Volumes by Diagnosis

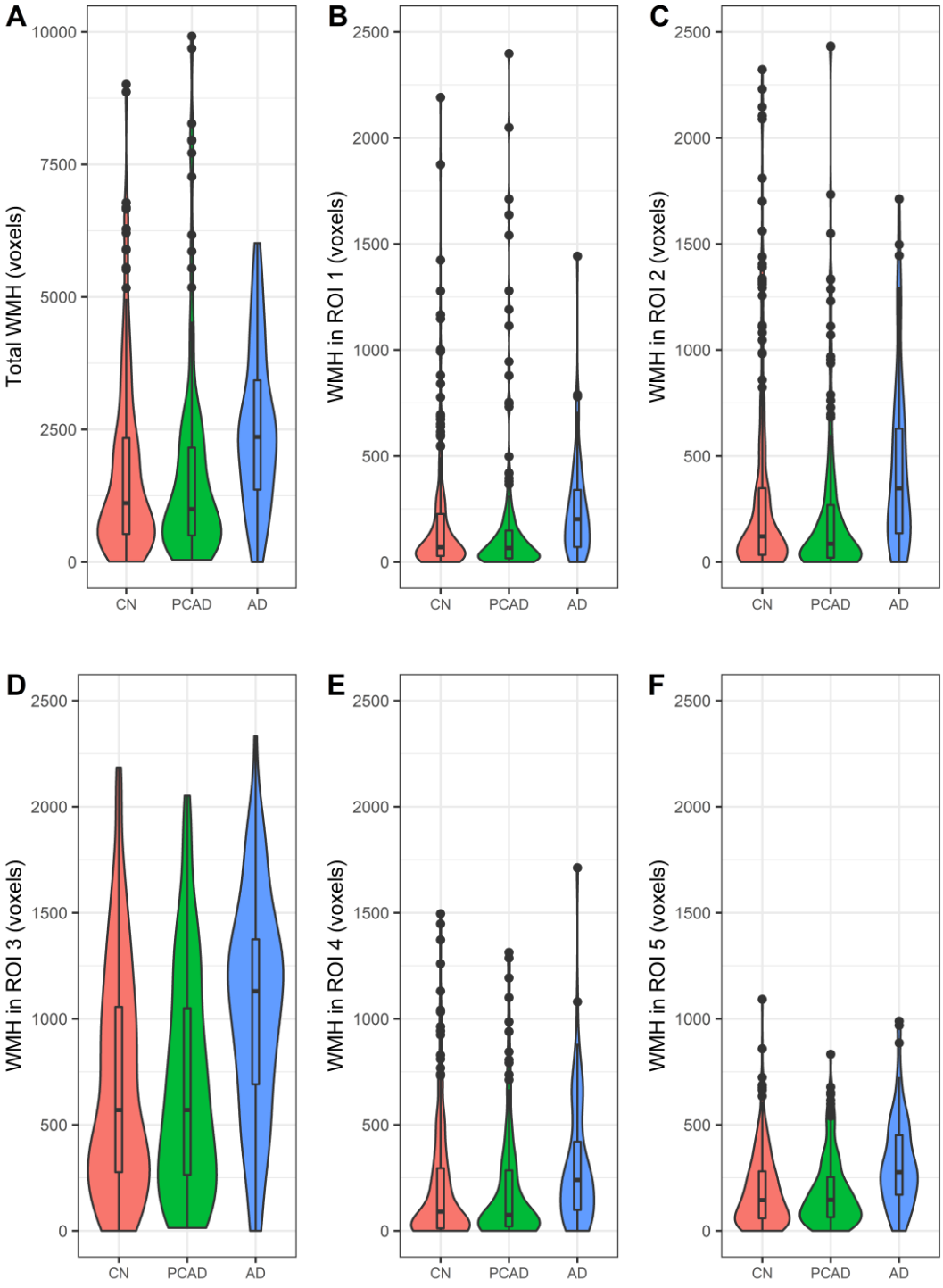

Figure 5.2 shows the distribution of WMHs within the whole brain and within each of the 5 predefined ROIs, shown separately for each diagnostic group. Note the y-axis is different in A, and that voxels are 2mm x 2mm.

ROI 1: Juxtacortical; ROI 2: Deep White Matter; ROI 3: Periventricular; ROI 4: Dorsal Parietal; ROI 5: Posterior

AD: Alzheimer disease; CN: Cognitively normal; PCAD: Preclinical Alzheimer disease; ROI: Region of interest; WMH: White matter hyperintensities

5.3.3 WMH Machine Learning – Optimization

We next used machine learning to assess if subtler patterns existed between diagnostic groups. For this we used the continuous data from the Lesion Segmentation Tool used to segment WMHs, where each voxel is assigned a probability from 0-1 of being a WMH. By using this richer dataset, we may be able to detect group differences that our prior tests could not. Figure 5.3 displays a heat map of the voxel-level WMH data for the cognitively normal, preclinical AD, and AD dementia groups. The color indicates the average probability each voxel is a WMH in that group, with values from 5%-100% displayed.

As part of the preprocessing done before training the machine learning models, voxels with near zero variance were removed. This resulted in the Juxtacortical ROI keeping 799 of 16071 voxels (5%), the Deep White Matter ROI keeping 2614 of 5518 voxels (47%), the Periventricular ROI keeping 2436 of 2623 voxels (93%), the Dorsal Parietal ROI keeping 1402 of 2220 voxels (63%), and the Posterior ROI keeping 1078 of 3135 voxels (34%); overall this was 8329 of 29567 voxels (28%).

The remaining voxels in the Training cohort were then used to train the support vector machine, random forest, and stochastic gradient boosting algorithms, with the resulting algorithms then applied to the Test cohort. The maximum accuracy of the three algorithms in the Training cohort is displayed in Table 5.2. with the statistically significant (above random chance) models in bold. With no additional preprocessing, none of our models were significant (first column in Table 5.2). Adding case weights improved some model's accuracy but not enough to make any models significant. Adding stronger (2x) case weights did make some models significant but increasing the case weights even further to 3x negatively impacted accuracy. As such, the up-sampling of the data, binning the voxels at 0.5, and applying PCA before training

were all tested in tandem with the 2x case weights. Binning the voxel probabilities gave similar results to not binning the data, while up-sampling and applying PCA lowered accuracy such that no models were significant.

5.3.4 WMH Machine Learning – Description of Optimal Models

We next focused more closely on the results from the optimized models (those run with the 2x case weights). The accuracy measures in the Test cohort displayed in Table 5.2 show that we were unable to create a model that used WMHs to separate the cognitively normal group from the preclinical AD group; thus, we do not show evidence to support our original hypothesis. We were able to separate the AD dementia group from the preclinical AD group. This supports our earlier results in section 5.3.2 that WMHs relate to cognitive impairment in our participants, but not to amyloid in the absence of impairment. Even in our models able to significantly separate symptomatic AD WMHs from preclinical AD WMHs, the low model accuracies suggest that the difference in WMHs is small.

To further investigate the models that were successfully able to separate the AD dementia group from the preclinical AD group, we computed a measure of variable importance for each voxel. Specifically, we found the Gini index for the random forest models (the model type that reached significance) that used all white matter voxels to separate the AD dementia group from the preclinical AD group. The results, shown in Figure 5.4, show that no particular region appears to be more important in the separation of the AD dementia group from the preclinical AD group or the cognitively normal group. Instead, it appears to replicate the voxel-level frequency maps in Figure 5.3, indicating the model broadly is looking for greater WMHs in AD dementia and not any particular pattern of WMHs.

Supplemental Table S5.4 describes additional metrics of the models with the 2x case weights: Training and Test cohort sensitivities and specificities, along with Test cohort accuracies and *p*-values are shown for all three model types. While we trained each iteration using support vector machines, Random Forests, and Gradient Boosting, all of our significant models came from the Random Forest algorithm. There was not an appreciable drop in sensitivities and specificities from the Training cohort to the Test cohort, indicating that the models are not overfitting the data. Often models' sensitivities are similar in size to their specificities, indicating that the case weights have appropriately adjusted the model to give similar weight to both diagnostic groups in the model.

Figure 5.3: Voxel-level Frequency Maps of White Matter Hyperintensities

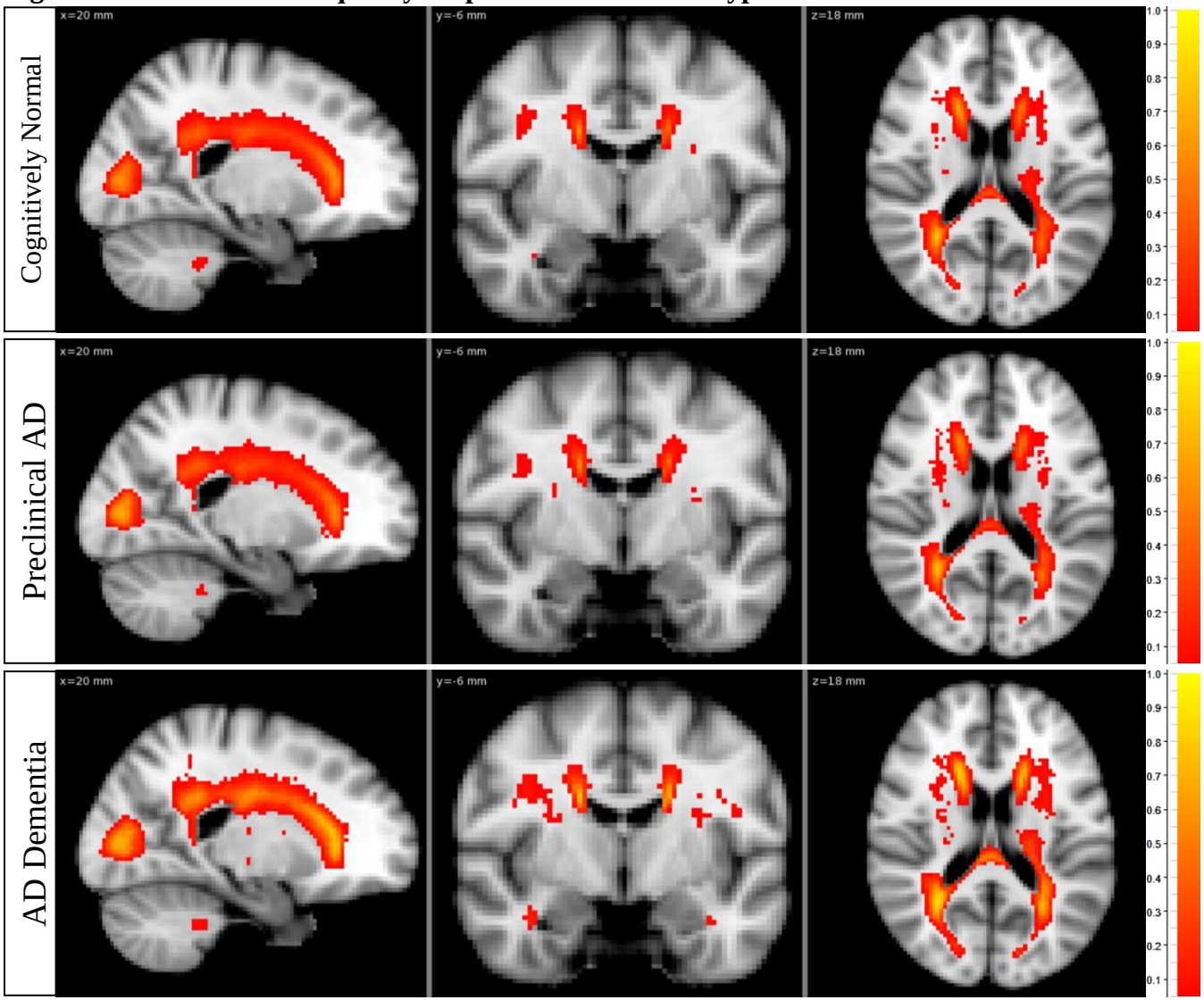

AD: Alzheimer disease

Table 5.2: Model Preprocessing Optimization

Groups	Data	Original	Case Weights	Case Weights 2x	Case Weights 3x	Case Weights 2x and binned at 0.5	Case Weights 2x and up-sampling	Case Weights 2x and principal component analysis
CN vs. PCAD	ROI 1	46	44	44	46	46	40	51
	ROI 2	50	46	51	46	51	45	55
	ROI 3	51	50	48	48	48	46	51
	ROI 4	50	55	51	51	51	42	51
	ROI 5	59	60	55	55	55	54	59
	All white matter voxels	50	50	50	50	50	51	44
CN vs. AD	ROI 1	52	54	61	64	62	50	56
	ROI 2	52	59	56	62	57	51	54
	ROI 3	52	55	56	60	57	52	55
	ROI 4	52	52	57	57	57	50	54
	ROI 5	56	56	61	59	61	51	56
	All white matter voxels	52	54	60	62	60	52	52
PCAD vs. AD	ROI 1	60	56	59	54	57	52	64
	ROI 2	60	59	60	59	59	56	64
	ROI 3	56	59	65	**66**	65	55	62
	ROI 4	57	57	**68**	56	**68**	56	65
	ROI 5	60	65	**68**	65	**68**	62	56
	All white matter voxels	56	64	**69**	62	**68**	57	55

Significant models are in bold. ROI 1: Juxtacortical; ROI 2: Deep White Matter; ROI 3: Periventricular; ROI 4: Dorsal Parietal; ROI 5: Posterior

AD: Alzheimer disease dementia; CN: Cognitively normal; PCAD: Preclinical Alzheimer disease; ROI: Region of interest

Figure 5.4: Voxel-level Variable Importance in the Random Forest Model with All Voxels

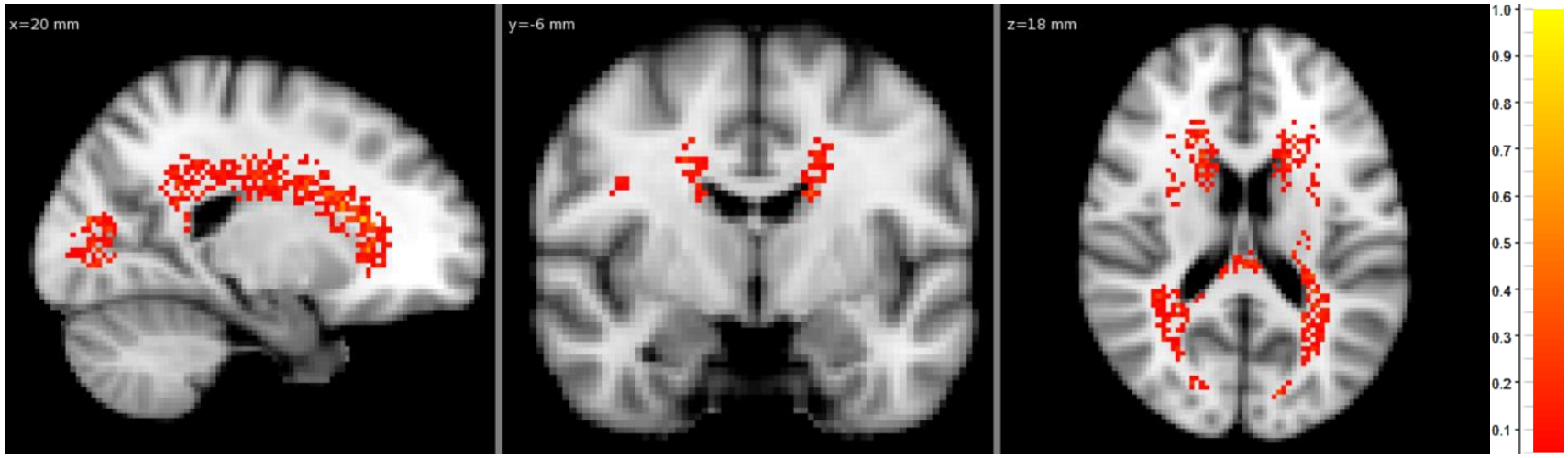

Figure 5.4 shows the variable importance of individual voxels in the Random Forest model that used all white matter voxels to separate preclinical AD from AD dementia. No obvious pattern is observed, with voxels evenly distributed in areas that are likely to have WMHs (see Figure 5.3).

AD: Alzheimer disease; WMH: White matter hyperintensities

5.4 Discussion

In this study we have shown that WMH volumes are larger in AD dementia than in amyloid negative controls or in the preclinical stage of sporadic AD. We did not see evidence of group difference in WMHs between unimpaired participants who were amyloid positive vs. amyloid negative. We further saw relationships between WMH volumes and amyloid levels, *APOE4* status, and MMSE scores, but only at the level of group differences between our unimpaired and impaired participants. These relationships were not seen within the unimpaired or within the impaired groups by themselves, making causality less clear. Our machine learning algorithms were unable to pick out patterns of WMHs that differed between our preclinical AD group and our cognitively normal group. However, they were able to separate preclinical AD from AD dementia, even when only using WMH data from within the Dorsal Parietal or the Posterior ROIs. As this was not possible using data from the Juxtacortical, Deep White Matter, or Periventricular ROIs, the greater WMH volume in AD dementia appears to have specific regional patterns.

Our results match prior literature, which reported WMHs associated with AD (Alosco et al., 2018; Bos et al., 2018; Gordon et al., 2015; Joki et al., 2018) as well as normal aging in unimpaired older adults (Alber et al., 2019; Salvadó et al., 2019). We also saw the previously reported correlation between *APOE4* and WMH volume (Alber et al., 2019; Salvadó et al., 2019). Our results in sporadic AD did differ from studies in dominantly inherited AD, where WMHs increases six years before dementia onset (Lee et al., 2018). However, this study was longitudinal in design and so had more power to detect a preclinical increase in WMHs.

With no differences detected in the WMHs of preclinical AD, there is no evidence that WMHs are a part of the sporadic AD pathologic process. The higher volumes of WMHs seen in

AD dementia either are separate from the AD process, and/or do not develop until after symptom onset. To detect this second scenario, we would need longitudinal data of participants with AD dementia to measure if they develop WMHs at an increased rate. In either case, the low accuracies shown in our results suggests that WMHs as measured in this study would not be particularly useful for clinical diagnosis of AD. WMHs may still be of use in determining balance of comorbid AD and vascular dementia clinically, but this was not directly explored.

One limitation of this study was our ability to assess vascular factors. We measured blood pressure only at one time-point, which is imperfect for diagnosing hypertension. We also did not have the requisite blood tests to measure cholesterol and determine participants' Framingham Risk Scores. While we had participants' history of diabetes and hypertension, we do not know the full scope of how these comorbidities affected participants. There likely is variability in how long participants have had these diseases, the severity/stage, and how well controlled they are. Future directions should assess WMHs along with other vascular pathologies such as microbleeds and lacunes in a cohort with better characterized vascular factors.

Another major limitation is that this study was not able to address CAA, which is amyloid in the vasculature. Amyloid in AD is primarily parenchymal, but most AD patients also have some degree of CAA. The amyloid we are detecting in amyloid PET is the combination of these two and is unable to be separated. This separation gains additional importance as anti-amyloid therapies for AD are finally realized. Amyloid-related imaging abnormalities (ARIA) are a common complication from anti-amyloid medications. One type is caused when a patient also has CAA and the drug targets the amyloid built up in blood vessels. This leads to leaky blood vessels that also appear as WMHs on MRI. Studies like this one are important because they help pick apart these various etiologies that can look similar on MRI. This concept can also

be applied more broadly as there are many different ways for a person to develop dementia that are pathologically distinct but present the same way clinically. Cerebrovascular disease can impact the brain through an intense acute lesion such as what occurs in stroke, or can be chronic and slowly build up over time as is seen in cerebral small vessel disease. Being able to determine the specific etiology helps us realize therapies to treat these different diseases.

5.5 Supplemental

Supplemental Table S5.1: Demographics and WMH Summary Measures in the Training Cohort

All	Cognitively Normal	Preclinical AD	AD Dementia
n	205	123	41
CDR [0,0.5,1,2]	205,0,0,0	123,0,0,0	0,28,12,1
Gender (% M)	42.4%	44.7%	51.2%
Age, years (mean)	61.7-92.2 (73.3)	61.7-89.4 (74.2)	61.8-88.4 (73.7)
MMSE (mean)	25-30 (29.2)	25-30 (29.1)	14-30 (24.5)
***APOE4*, % with ε4 allele**	22.3%	54.1%	77.5%
Amyloid* – Centiloid (mean)	-10.2-20.0 (3.52)	16.4-139 (51.6)	21.1-154 (81.4)
Race, % non-Hispanic White	81.0%	90.2%	85.4%
Education, years (mean)	11-20 (16.2)	8-22 (16.2)	6-20 (14.9)
Mean Arterial Pressure (mean)	68-126 (93.3)	70-120 (92.7)	65-112 (92.5)
Hypertensive Blood Pressure, %	62.3%	59.3%	63.4%
History of Hypertension, %	51.4%	40.4%	45.7%
Hachinski Score (mean)	0-4 (0.536)	0-1 (0.451)	0-1 (0.231)
BMI (mean)	13-49 (28.3)	18-45 (26.4)	20-39 (27.5)
History of Diabetes, %	15.9%	4.49%	2.86%
Smoker, %	6.90%	3.33%	2.86%
WMH voxels, mean (SD)	1780 (1800)	1790 (2090)	2810 (2580)
Juxtacortical ROI WMH voxels, mean (SD)	183 (292)	215 (423)	344 (716)
Deep White Matter ROI WMH voxels, mean (SD)	349 (553)	371 (695)	558 (787)
Periventricular ROI WMH voxels, mean (SD)	711 (542)	693 (535)	1050 (508)
Dorsal Parietal ROI WMH voxels, mean (SD)	212 (289)	198 (280)	311 (330)
Posterior ROI WMH voxels, mean (SD)	197 (179)	192 (177)	337 (234)

* Mean Cortical SUVR RSF

AD: Alzheimer disease; *APOE4*: Apolipoprotein E ε4; BMI: Body mass index; CDR: Clinical Dementia Rating; MMSE: Mini Mental State Exam; ROI: Region of interest; SD: Standard deviation; SUVR RSF: Standard uptake value ratio (regional spread function applied); WMH: White matter hyperintensities

Supplemental Table S5.2: Demographics and WMH Summary Measures in the Test Cohort

All	Cognitively Normal	Preclinical AD	AD Dementia
n	40	40	40
CDR [0,0.5,1,2]	40,0,0,0	40,0,0,0	0,29,11,0
Gender (% M)	45.0%	40.0%	52.5%
Age, years (mean)	61.0-88.4 (74.2)	60.7-88.0 (74.1)	61.0-88.0 (74.2)
MMSE (mean)	28-30 (29.4)	23-30 (28.7)	17-30 (25.6)
***APOE4*, % with ε4 allele**	20.5%	52.6%	71.8%
Amyloid* – Centiloid (mean)	-6.91-19.5 (2.56)	18.7-154 (53.6)	30.1-159 (88.8)
Race, % non-Hispanic White	85.0%	90.0%	95.0%
Education, years (mean)	12-20 (15.9)	12-20 (16.4)	12-19 (15.6)
Mean Arterial Pressure (mean)	68-117 (94.1)	76-113 (91.9)	72-125 (96.2)
Hypertensive Blood Pressure, %	62.5%	57.5%	70.0%
History of Hypertension, %	51.7%	45.5%	45.9%
Hachinski Score (mean)	0-3 (0.833)	0-1 (0.455)	0-3 (0.769)
BMI (mean)	21-41 (30.0)	18-37 (26.4)	17-40 (27.2)
History of Diabetes, %	6.90%	4.35%	10.80%
Smoker, %	6.90%	0%	0%
WMH voxels, mean (SD)	1690 (1730)	1390 (994)	2570 (1590)
Juxtacortical ROI WMH voxels, mean (SD)	204 (316)	103 (90.1)	259 (225)
Deep White Matter ROI WMH voxels, mean (SD)	338 (498)	173 (177)	451 (446)
Periventricular ROI WMH voxels, mean (SD)	653 (504)	670 (468)	1050 (526)
Dorsal Parietal ROI WMH voxels, mean (SD)	196 (263)	186 (233)	314 (272)
Posterior ROI WMH voxels, mean (SD)	176 (171)	175 (138)	304 (194)

* Mean Cortical SUVR RSF

AD: Alzheimer disease; *APOE4*: Apolipoprotein E ε4; BMI: Body mass index; CDR: Clinical Dementia Rating; MMSE: Mini Mental State Exam; ROI: Region of interest; SD: Standard deviation; SUVR RSF: Standard uptake value ratio (regional spread function applied); WMH: White matter hyperintensities

Supplemental Figure S5.1: WMH by Diagnosis in the Training Cohort

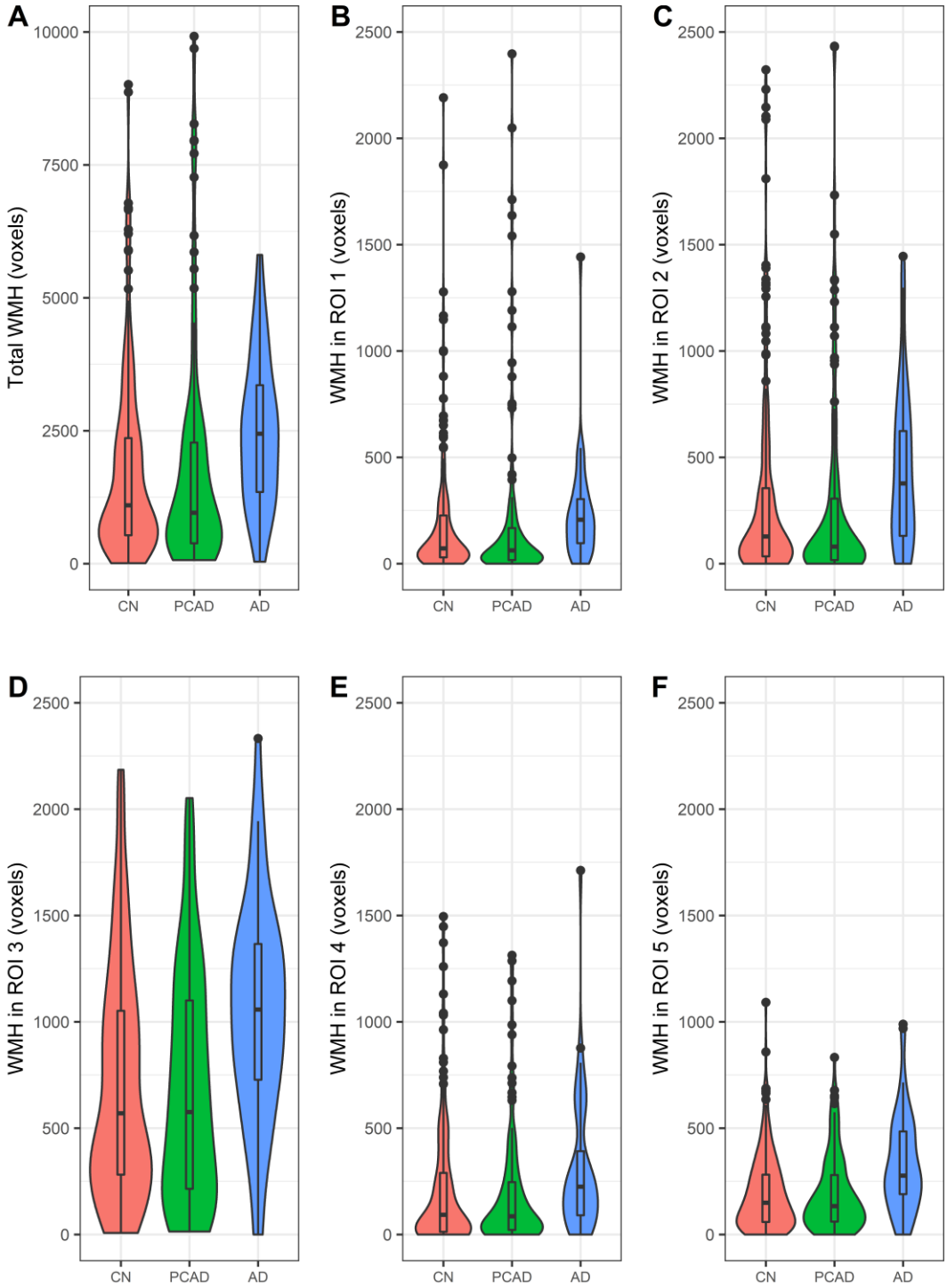

Supplemental Figure S5.1 shows the distribution of WMHs within the whole brain and within each of the 5 predefined ROIs within the Training cohort, with measures shown separately for each diagnostic group. ROI 1: Juxtacortical; ROI 2: Deep White Matter; ROI 3: Periventricular; ROI 4: Dorsal Parietal; ROI 5: Posterior

AD: Alzheimer disease; CN: Cognitively normal; PCAD: Preclinical Alzheimer disease; ROI: Region of interest; WMH: White matter hyperintensities

Supplemental Figure S5.2: WMH by Diagnosis in the Test Cohort

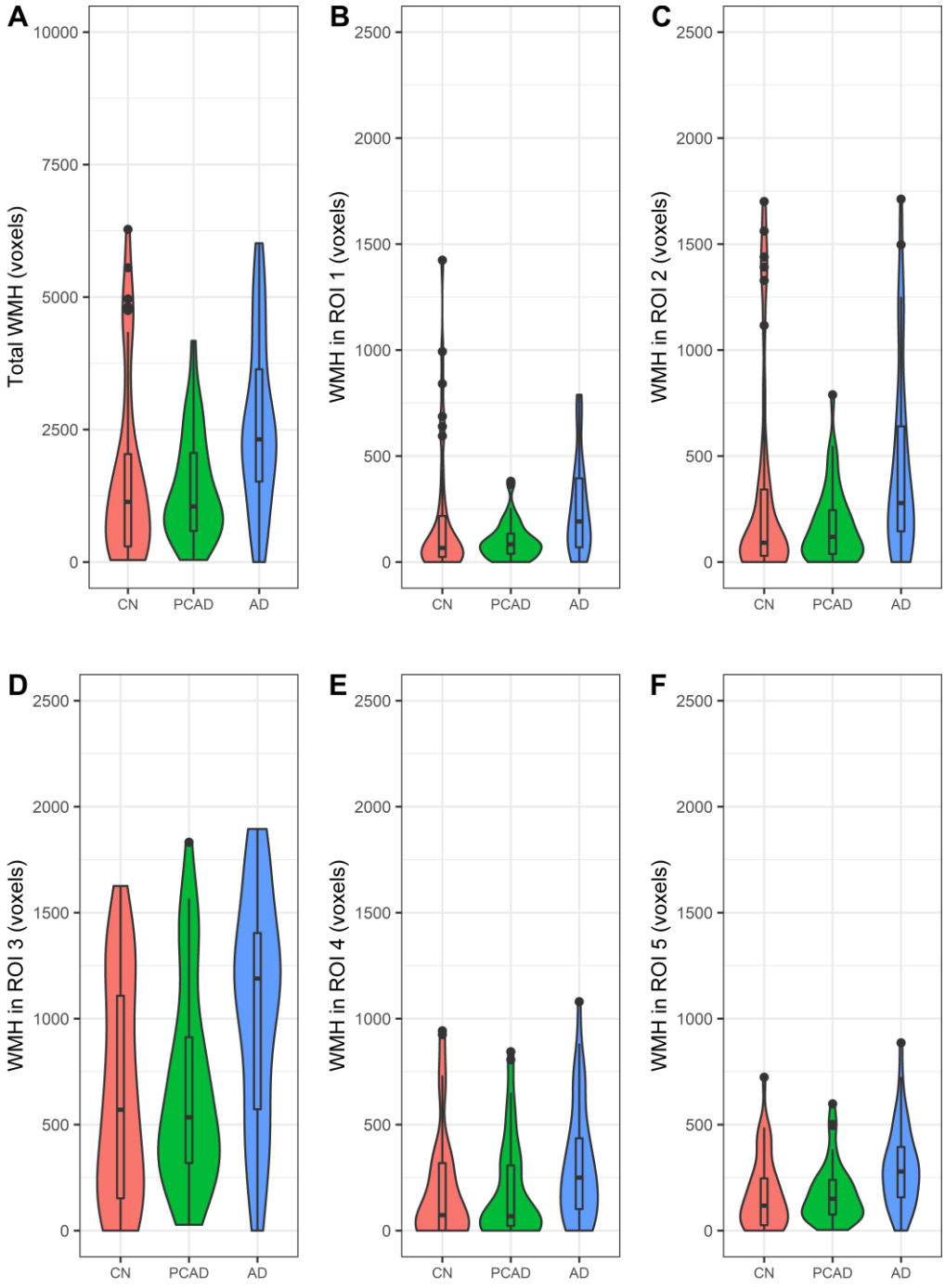

Supplemental Figure S5.2 shows the distribution of WMHs within the whole brain and within each of the 5 predefined ROIs within the Test cohort, with measures shown separately for each diagnostic group. ROI 1: Juxtacortical; ROI 2: Deep White Matter; ROI 3: Periventricular; ROI 4: Dorsal Parietal; ROI 5: Posterior

AD: Alzheimer disease; CN: Cognitively normal; PCAD: Preclinical Alzheimer disease; ROI: Region of interest; WMH: White matter hyperintensities

Supplemental Table S5.3: WMH Linear Models with Amyloid, *APOE4*, and MMSE

Amyloid												
	Corrected *p*-values						B-values					
	Total	ROI 1	ROI 2	ROI 3	ROI 4	ROI 5	Total	ROI 1	ROI 2	ROI 3	ROI 4	ROI 5
All	0.07	0.21	0.43	**0.002**	0.21	**0.002**	4.77	0.66	0.50	2.04	0.57	0.71
CN and PCAD	1	1	1	1	1	1	-2.10	-0.17	-0.96	-0.16	-0.25	-0.23
CN only	1	1	1	1	0.66	1	9.19	0.65	0.07	5.55	4.05	0.54
PCAD only	1	1	1	1	1	1	-0.19	-0.05	-0.78	0.78	-0.09	-0.10
AD only	1	1	1	1	1	1	3.05	1.12	0.62	0.02	0.63	0.54
APOE4												
	Corrected *p*-values						B-values					
	Total	ROI 1	ROI 2	ROI 3	ROI 4	ROI 5	Total	ROI 1	ROI 2	ROI 3	ROI 4	ROI 5
All	0.62	1	1	**0.02**	0.90	0.16	220.87	3.68	23.18	132.05	25.39	33.72
CN and PCAD	1	1	1	0.66	1	1	91.90	-0.03	5.40	75.47	10.70	13.58
CN only	0.98	0.98	0.98	0.46	0.98	0.98	311.63	41.99	73.17	127.91	46.29	28.60
PCAD only	1	1	1	1	1	1	29.33	-33.73	-21.28	81.17	-1.51	13.24
AD only	1	1	1	1	1	1	-567.93	-166.02	-136.23	-97.07	-67.88	-67.31
MMSE												
	Corrected *p*-values						B-values					
	Total	ROI 1	ROI 2	ROI 3	ROI 4	ROI 5	Total	ROI 1	ROI 2	ROI 3	ROI 4	ROI 5
All	**< 0.001**	**0.03**	**0.03**	**< 0.001**	**0.01**	**< 0.001**	-129.34	-16.13	-21.27	-45.46	-14.46	-19.63
CN and PCAD	0.49	0.69	0.69	0.48	0.57	0.40	-105.50	-9.45	-21.04	-32.35	-14.54	-12.06
CN only	0.39	0.62	0.39	0.62	0.62	0.22	-169.80	-18.80	-50.57	-35.52	-20.94	-20.26
PCAD only	1	1	1	1	1	1	-58.30	-1.33	3.11	-32.74	-10.10	-6.09
AD only	1	1	1	1	1	0.64	-31.02	-7.50	-1.33	-7.12	-1.42	-10.64

ROI 1: Juxtacortical; ROI 2: Deep White Matter; ROI 3: Periventricular; ROI 4: Dorsal Parietal; ROI 5: Posterior

AD: Alzheimer disease; *APOE4*: Apolipoprotein E ε4; CN: Cognitively normal; MMSE: Mini Mental State Exam; PCAD: Preclinical Alzheimer disease; ROI: Region of interest; WMH: White matter hyperintensities

Supplemental Table S5.4: Accuracy Metrics for All Models with the 2x Case Weights

Data	Groups	Classification Algorithm	Training Sensitivity	Training Specificity	Test Sensitivity	Test Specificity	Test Accuracy	Test Accuracy *p*-value
Juxtacortical ROI	CN vs. PCAD	Support Vector Machine	55	50	52	35	44	0.89
		Random Forest	56	55	45	40	42	0.93
		Gradient Boosting	62	47	57	30	44	0.89
	CN vs. AD	Support Vector Machine	21	89	5	95	50	0.54
		Random Forest	52	74	50	72	61	0.03
		Gradient Boosting	40	75	38	78	57	0.11
	PCAD vs. AD	Support Vector Machine	34	83	12	95	54	0.29
		Random Forest	72	60	75	42	59	0.07
		Gradient Boosting	52	70	55	42	49	0.63
Deep White Matter ROI	CN vs. PCAD	Support Vector Machine	41	65	32	57	45	0.84
		Random Forest	60	52	42	40	41	0.95
		Gradient Boosting	84	16	90	12	51	0.46
	CN vs. AD	Support Vector Machine	16	87	10	90	50	0.54
		Random Forest	61	65	48	65	56	0.16
		Gradient Boosting	53	67	32	70	51	0.46
	PCAD vs. AD	Support Vector Machine	32	83	25	92	59	0.07
		Random Forest	79	56	72	42	57	0.11
		Gradient Boosting	57	75	40	80	60	0.05

Data	Groups	Classification Algorithm	Training Sensitivity	Training Specificity	Test Sensitivity	Test Specificity	Test Accuracy	Test Accuracy *p*-value
Periventricular ROI	CN vs. PCAD	Support Vector Machine	43	66	22	72	48	0.71
		Random Forest	65	44	40	25	32	1.00
		Gradient Boosting	55	55	35	32	34	1.00
	CN vs. AD	Support Vector Machine	26	83	12	90	51	0.46
		Random Forest	47	81	30	82	56	0.16
		Gradient Boosting	33	89	22	82	52	0.37
	PCAD vs. AD	Support Vector Machine	41	78	25	82	54	0.29
		Random Forest	71	62	57	72	65	0.005
		Gradient Boosting	48	80	25	78	51	0.46
Dorsal Parietal ROI	CN vs. PCAD	Support Vector Machine	57	47	50	42	46	0.78
		Random Forest	93	9	82	5	44	0.89
		Gradient Boosting	86	14	85	18	51	0.46
	CN vs. AD	Support Vector Machine	21	90	12	90	51	0.46
		Random Forest	40	77	28	68	48	0.71
		Gradient Boosting	49	81	35	80	57	0.11
	PCAD vs. AD	Support Vector Machine	33	85	20	92	56	0.16
		Random Forest	81	50	85	50	**68**	**0.001**
		Gradient Boosting	46	77	35	88	61	0.03

Data	Groups	Classification Algorithm	Training Sensitivity	Training Specificity	Test Sensitivity	Test Specificity	Test Accuracy	Test Accuracy *p*-value
Posterior ROI	CN vs. PCAD	Support Vector Machine	42	68	42	68	55	0.22
		Random Forest	59	44	65	45	55	0.22
		Gradient Boosting	51	55	50	52	51	0.46
	CN vs. AD	Support Vector Machine	29	90	18	95	56	0.16
		Random Forest	36	82	35	88	61	0.03
		Gradient Boosting	39	78	30	72	51	0.46
	PCAD vs. AD	Support Vector Machine	36	81	30	90	60	0.05
		Random Forest	66	64	65	70	**68**	**0.001**
		Gradient Boosting	32	78	25	95	60	0.05
All White Matter Voxels	CN vs. PCAD	Support Vector Machine	43	70	32	68	50	0.54
		Random Forest	66	45	40	32	36	1.00
		Gradient Boosting	47	61	38	48	42	0.93
	CN vs. AD	Support Vector Machine	18	83	20	82	51	0.46
		Random Forest	47	81	38	82	60	0.05
		Gradient Boosting	33	88	22	82	52	0.37
	PCAD vs. AD	Support Vector Machine	38	78	22	85	54	0.29
		Random Forest	77	56	75	62	**69**	**0.0005**
		Gradient Boosting	48	80	30	75	52	0.37

AD: Alzheimer disease; CN: Cognitively normal; PCAD: Preclinical Alzheimer disease; ROI: Region of interest

Chapter 6: Conclusions

6.1 Overall Summary

As stated at the beginning of this dissertation, the overall goal of these studies was to gain a better understanding of how Alzheimer disease (AD) interacts with normal aging and cerebrovascular disease, and how this interaction impacts neuroimaging measures in a clinically meaningful way. In Chapter 2, we found that the amount of atrophy that occurs with age and the pattern of that atrophy across the lifespan exhibit two unique spatial patterns. This first spatial pattern broadly indicated greatest atrophy in the temporal lobe and subcortical regions. The second pattern, which associated with regional myelination, indicated a linear pattern of decline in temporal lobe regions, accelerating declines in subcortical regions, and decelerating declines in frontal regions. Despite screening our Normal Aging cohort with measures of amyloid positron emission tomography (PET) and longitudinal measures of Clinical Dementia Rating™ (CDR™), we did not show measurable differences in atrophy between our Normal Aging cohort and a cohort of preclinical AD.

In Chapter 3, we showed that Select Atrophied Regions in Alzheimer disease (SARA), our magnetic resonance imaging (MRI)-based volumetric classification model, can be used to separate AD from cognitively normal controls and other dementia types. Our results indicate SARA may be useful as a first step for selecting symptomatic AD participants for entrance into clinical trials or as an adjunct to the diagnostic algorithm when a clinical differential diagnosis includes AD vs. frontotemporal dementia or AD vs. non-neurodegenerative conditions. However, our method for controlling for age-related atrophy did not improve model performance, and lowered performance if age was not also included as a predictor. As such,

SARA, our final model, looks at total atrophy instead of separating out AD-related and age-related atrophy.

In Chapter 4 we were unable to show evidence that preclinical AD is a risk factor for stroke or predicts post-stroke dementia. This supports the concept that stroke and amyloid pathology are separate disease mechanisms that independently can lead to dementia. We also found that African Americans (AAs) are more likely to have vascular pathology observable on MRI than non-Hispanic Whites (NHWs), indicating racial disparities at the neuropathological level within stroke. As part of this finding, we noted that AAs were more likely to have 5 or more microbleeds. This is a common exclusion criterion in AD clinical trials, and so suggests that this racial difference is leading to clinical trials turning away a larger proportion of AA volunteers.

Finally, in Chapter 5 we did not find evidence that white matter hyperintensities (WMH) are different in the preclinical stages of AD, even when looking for more detailed patterns than the traditional total WMH volume measurements. However, we did see a higher volume of WMHs in symptomatic AD, and that there were certain regions in the white matter where this difference allowed separation of AD dementia from healthy controls.

6.2 Comments on Chapter 2: Regional Age-Related Atrophy After Screening for Preclinical Alzheimer Disease

In Chapter 2 we report one spatial pattern describing the amount of age-related atrophy occurring in regions in the brain, and a second spatial pattern describing how the rate of that atrophy changes across the lifespan. The greatest amount of atrophy was seen in temporal regions, which declined in an accelerated pattern such that more atrophy was seen in late life relative to mid-life. This same acceleration of atrophy with age was seen in subcortical regions. In contrast, frontal and cingulate areas showed higher atrophy in mid-life than late-life (a

deceleration of atrophy with age). These non-linear patterns spatially correlated with the T1w/T2w intensity ratio, which is used as a rough correlate of myelin levels. This demonstrates that the spatial pattern we observed for strength of age-related atrophy and the spatial pattern we observed for pattern across the lifespan are two distinct spatial patterns. By correlating with a biologically-based measure, it also suggests that the patterns of atrophy seen in different regions across the lifespan reflects a fundamental property of how the brain is organized. This interpretation is further strengthened because the measure of myelin used in the spatial correlation is not from the same individuals whose atrophy we measured, but from a separate cohort of healthy adults. That these patterns from separate cohorts relate to each other indicates they reflect fundamental organizational properties of the brain. The direction of the correlation suggests that regions that characteristically have higher myelin content are more vulnerable to accelerated atrophy in late life. This could be a direct vulnerability of myelinating cells, or due to other tissue properties of brain regions that tend to have higher levels of myelin. It is possible that this pattern directly links to myelin as myelinating cells have been reported to have a greater vulnerability to oxidative stress, which could then lead to accelerated atrophy in later years as oxidative stress builds up (Nasrabady et al., 2018).

One of the more surprising findings in this study was the lack of difference we saw in atrophy between our Normal Aging cohort and our Preclinical AD cohort. AD is a neurodegenerative disorder, and as such atrophy is a key biomarker of the disease. At first glance, our results appear to disagree with the general consensus that even the earliest stages of AD include atrophy. One explanation for our results is that prior studies that reported atrophy have focused on groups with mild impairment, while our participants can confidently be considered unimpaired. Atrophy ties closely with impairment, both in AD and outside of it, so it

may be that any distinguishable atrophy in AD would lead to enough impairment that a participant would be excluded from our study. The second possibility is that there truly is atrophy in unimpaired preclinical AD and we, for several possible reasons, were unable to detect it. If there is only a small amount of atrophy, detecting it may require more statistical power. We could increase our power by using an even larger sample size than what was used in this study or a more sensitive measure of atrophy. The scans used in this study were primarily 3T with some 1.5T, and the FreeSurfer regions we used to divide the brain into different regions were quite large and heterogeneous. These regions are based on gyral and sulcal landmarks, not necessarily differences in the underlying tissue. Differences in the preclinical AD stage may be revealed if we use a higher magnetic field scanner to give more accurate and precise volumetric measures, and/or if we use smaller regions or voxel-level data in our analysis.

Our definition of preclinical AD in this study was imperfect. At the cross-sectional stage we are only able to define preclinical AD as those with amyloid deposits in their brain but no cognitive impairment. The assumption (which in itself is contested) is that all of these people will eventually develop AD dementia, but we do not know if that will be in the near future or in 20 years. Those with highly resilient brains may never convert to AD dementia before they die. Regardless of these possibilities, our results indicate that studies of older adults done in a similar context to ours do not need to worry overly much about preclinical AD confounding their measures of atrophy, so long as they do careful cognitive screening.

One aspect of this study that was not addressed directly was the inter-individual variability within regions. When individual regions are examined, the majority of them appear to have variability that is relatively stable across the lifespan. The most obvious exception to this pattern is FreeSurfer's measure of WMHs. While in general this measure has low accuracy, it

does demonstrate a nice contrast to the majority of regions in that it shows an increasing variability with age. At older ages the mean volume of WMHs increases, but also the standard deviations for those means increases rapidly. While the journal articles on these studies do not address this directly, our creation of an R Shiny app (an interactive web app built in R) (https://lnkoenig.shinyapps.io/NormalAgingVolumetrics_ShinyApp/) that shows all data for all regions allows us to share this insight. By adding the R Shiny app to this study, we were able to share a more information and data with researchers in an easily digestible format. Scientists will be able to go and look at whichever regions and the specific demographics they are interested in, possibly to compare with their own results or to notice interesting patterns that were not part of the original study.

Even researchers not directly interested in our results on aging may be impacted by our results. Many neuroimaging studies are occurring in older adults for a variety of pathologies other than AD, or occur across a large age range. When these studies look at measures of atrophy, or even other measures that are impacted by atrophy such as PET imaging or resting-state functional connectivity, they often need to control for age. This study shows that controlling for age-related atrophy using age by itself does not account for the diverse and complex impact that age has on the brain. Studies that have inadequately controlled for the non-linear and region-specific impact of age-related atrophy may misinterpret their results.

Future studies looking to build upon our understanding of atrophy in normal aging and in preclinical AD should ideally use longitudinal data in a diverse cohort. This would enable tracking of specific trajectories in individuals as opposed to our study which assumes atrophy based on group averages at each age. Tracking volumetric measures longitudinally within individuals would also give a more specific measure of atrophy and may be enough to allow us

to detect differences in normal aging and preclinical AD if they exist. Longitudinal studies would also allow us to refine our definition of preclinical AD to those who do eventually convert to AD dementia. Additionally, longitudinal data would be safe from survivorship bias in a way our study is not. Regions that show less (decelerating) atrophy at older ages in our study may actually be a reflection of low resiliency and not true differences in atrophy. Atrophy in these regions may be more likely to lead to cognitive impairment, which would cause someone to be excluded from this study.

By using a diverse, longitudinal cohort we would also be able to examine more fully the factors that impact inter-individual variability in the trajectories of age-related atrophy. In our study, we are using the term 'normal aging' to look at atrophy that occurs in synchrony with increasing age in people who are generally healthy. But that does not mean that the atrophy itself is healthy or that it cannot be prevented. By examining these factors, which likely include things such as demographic, socioeconomic, and genetic components, we will get a better sense of what leads to the atrophy seen in normal aging. For this type of study, it is even more important to have a cohort diverse in all ways; without variability in the factors you are assessing, the impact they have on atrophy cannot be measured.

6.3 Comments on Chapter 3: Improving Volumetric Models for Symptomatic Alzheimer Disease

In Chapter 3, we found that models using volumetric measures of atrophy can be used to diagnose symptomatic AD in a variety of circumstances. Our final model, SARA, had good diagnostic accuracy in research cohorts of AD and healthy controls, and in a more realistic clinical setting with a variety of diagnoses. We saw the greatest diagnostic specificity when differentiating AD from frontotemporal dementia or from non-neurodegenerative diagnoses (e.g.,

mood disorders, sleep disorders, cognitively normal individuals). We also found that that our model related to measures of impairment such as CDR, but was still useful in distinguishing diagnoses in those with similar levels of impairment.

While our final model had these strengths, our hypothesis that classification would be improved by controlling for the age-related atrophy described in Chapter 2 was not supported by our data. Instead, the opposite was the case; controlling for the age-related atrophy lowered the accuracy in our Clinical cohort for the models that did not include age. As age and age-related atrophy are linked in this paradigm, this indicates that either age or age-related atrophy are an integral factor in determining which clinical patients received a diagnosis of AD. This could be because age-related atrophy increases cognitive impairment, and greater impairment increases the likelihood of someone being seen by a clinician and getting diagnosed with AD. Age is well known as a strong risk factor for AD, and so it is also possible that age is contributing to the model even without direct influence of age-related atrophy. No matter the specific interpretation, our study indicates that total atrophy (the combination of age-related and AD-related atrophy) is more predictive of a clinical diagnosis of AD than atrophy specifically attributable to AD.

One of the first steps in this study was to select which FreeSurfer regions to include in our models. While we also tested the more traditional route of using Hippocampal volume alone, we also wanted to include a multi-region model that is expected to be more robust to different presentations of AD and to measurement error. This did appear to be the case in our study; while our multi-region model was not an improvement in the research cohort, it outperformed the model using hippocampal volume alone when looking at AD variants in the Clinical cohort. We alternatively could have included every brain region in our algorithm, but this overlooks the time and effort it takes to obtain these volumetric measures. Even FreeSurfer's automated volumetric

processing requires quality checking to ensure regions are segmented properly. This is less of a concern in healthy young adults where FreeSurfer tends to be most accurate, but older adults and especially those with neurodegenerative disorders have more variable brain structures that can be more challenging to automatically segment. As the models we trained in this study were intended for use in dementia clinics or for clinical trials, it is important to reduce the amount of time and manpower they require. By using only a few brain regions in our model, quality checking of the FreeSurfer segmentation in a clinical setting can focus on the specific regions needed instead of the entire brain.

This intention for our algorithm to be used as a clinical tool also led us to use simple logistic regressions, when many similar studies using MRI to classify AD skip straight to using complex machine learning algorithms. While effective, machine learning algorithms are not always necessary – in AD classification they have often achieved the same accuracy as a simpler regression models (Mateos-Pérez et al., 2018b). The disadvantage to using more complex algorithms is that they are much more difficult to train and interpret, resulting in a 'black box' that is more difficult for a clinician to trust. We chose to keep our model simple, easy to implement, and transparent in the hope that others will be encouraged to try it. This was also why we focused on measures taken from structural MRI, as this scan is already obtained as part of the standard of care for those presenting with dementia symptoms. As such, our algorithm places no additional burden on the patient; it extracts additional information from a test that is already occurring.

One concern from this study is the lower classification ability of our model in the Clinical cohort relative to the Test cohort. This is likely due to several reasons. One reason is that the Test cohort compares AD dementia to healthy controls, while the Clinical cohort compares AD to a

variety of disorders. It is to be expected that the non-AD patients in the Clinical cohort have more atrophy overall in their brain than healthy controls. A second reason is that the criteria for who is considered to have AD dementia is very different between the two cohorts. In the research cohort, we get as close to the gold-standard, neuropathological diagnosis as is possible in living participants by using amyloid PET, CDR, and a clinical evaluation of AD dementia. In the Clinical cohort, the standards are much more variable. These are real patients in a clinical setting. Their diagnosis is restricted much more by which tests the patients are willing to undergo (which often does not include lumbar puncture), and which tests their health insurance is willing to cover (which does not include amyloid PET). With limited treatments for AD, patients also have limited incentive to undergo additional testing to make their diagnosis more definitive. A final reason is that research studies are more likely to select the 'purest' AD patients, excluding those with other neurodegenerative conditions or major health problems in a way that does not occur in a clinical setting. The self-selection of those who participate in research studies also skews research cohorts towards those with high socioeconomic status – those who have the time and ability to participate in studies – which also likely correlates with fewer comorbidities associated with atrophy. These factors all likely lead to the labels of AD and non-AD in the Clinical cohort being less accurate than in the Test cohort, which would explain the lowered model performance that we observed.

A major strength of this study is that we made use of these different types of cohorts – both research and clinical. The research cohorts are better characterized but less diverse, while the Clinical cohort may be less diagnostically accurate but gives us important insights on how the algorithm would perform in a realistic clinical setting. By using them in combination we get a more comprehensive understanding of our model. An additional strength of research cohorts is

that they are possible to harmonize. The research participants in this study came from multiple different research studies that made their data open to other researchers and used similar protocols to allow harmonization. Because of this, we were able to combine the datasets to form a cohort with a large enough group of participants with AD dementia to train our models. It is following this example of open science that we have made both our algorithm and the data from the Clinical cohort available online at https://github.com/benzinger-icl/SARA and https://www.oasis-brains.org/.

6.4 Comments on Chapter 4: Interaction of Stroke, Race, and Amyloid

In Chapter 4 we examined how race and amyloid burden impact several MRI measures in an acute stroke population. We had hypothesized that post-stroke dementia could be explained by people in the preclinical stages of AD having a stroke which then accelerated the development of AD. However, in our study the amyloid levels at the time of stroke did not predict who in the study went on to develop post-stroke dementia one year later. We also did not see a difference when comparing amyloid levels in the stroke cohort to healthy controls. This means that amyloid accumulation also did not predispose the brain to having a stroke. If post-stroke dementia is related to AD at all, the remaining possibility is that the stroke event itself leads to rapid amyloid accumulation and dementia onset. We were unable to collect amyloid in our follow-up and so we could not address this possibility. Other studies have shown amyloid deposition in the brains of those with post-stroke dementia (Mok et al., 2016; Yang et al., 2015), but these have been at rates similar to what is seen in otherwise healthy older adults. Thus, it is not evident that AD is contributing to the dementia of the amyloid positive participants with post-stroke dementia. They may have developed dementia completely independently from AD

and amyloid, but concurrently happened to be one of the many older adults in the preclinical stage of AD.

While not designed originally to examine racial disparities, the unique recruitment of our participants from two local hospitals' stroke services in St. Louis resulted in a cohort diverse enough that we had enough statistical power to compare NHWs to AAs. Research cohorts are often self-selected in a way that biases the populations heavily towards NHWs, making it difficult for studies to examine race even when it is known to be relevant. This is the case in both AD and in stroke, where there are known racial disparities that would benefit from more research to uncover the underlying causes (Benjamin et al., 2017; Neill R Graff-Radford et al., 2016; Green, 2002; Manly and Mayeux, 2019; Mayeda et al., 2016; John C Morris et al., 2019; Tang et al., 2001; Yang et al., 2017).

With both the motive and the ability to examine racial differences in this study, we were thus convinced it needed to be added as a component. As expected, we did uncover some differences, with NHWs less likely to have vascular pathology than AAs. What we could not measure was the cause of these differences. While we discuss racial differences in this study, race itself is a social construct that we are using as a proxy for a variety of other factors including differences in socioeconomic status, quality of education, comorbid health issues, and racial discrimination (Williams and Ovbiagele, 2020). There may be some impact of genetics, such as the finding that AAs have higher rates of apolipoprotein E ε4 (*APOE4*) alleles, but historically genetic factors have been overestimated – assumed to be the cause of racial disparities without evidence (Boyd et al., 2020). While some of these assumptions are driven by racial biases among researchers, any study that reports racial differences can be misused for racist agendas. Because

of this, it is essential that studies that involve race such as this one are not just unbiased, but explicitly anti-racist.

This study allowed us to assess racial differences and the impact of baseline amyloid in a unique cohort of patients. The benefit of these sorts of specialized cohorts is that they allow us to ask important questions that most studies cannot address. However, their uniqueness can also be a limitation. In this case, it made it difficult to compare our stroke patients to our non-stroke participants; many differences we found could be interpreted as due to differences in recruitment. The more unique a cohort is, the more difficult it is to compare to other studies' cohorts. Additionally, our stroke patients had to have the unique requirements of a recent stroke and a willingness to immediately undergo amyloid PET imaging; this resulting in our cohort being quite small. This makes our negative results more difficult to trust as we did not have the power to detect smaller effects.

6.5 Comments on Chapter 5: White Matter Hyperintensities in Alzheimer Disease

In Chapter 5 we examined WMHs in both preclinical and symptomatic AD. We replicated prior findings that WMH volumes are higher in AD dementia. However, we did not find evidence for our hypothesis that WMHs are different in the preclinical stage of AD. If we had seen differences in the preclinical stage of AD, it would have been evidence that WMHs develop as part of the AD process and would explain the higher volume of WMHs seen in symptomatic AD. However, WMHs that develop separate from AD could also lead to these results; WMHs may impact cognition such that a person having both WMHs and AD is more likely to exhibit symptoms and to be diagnosed than someone without the additional WMHs.

However, the lack of differences we saw in the preclinical stage does not disprove the direct linkage of WMHs and AD; WMHs could still develop as part of AD in later disease stages. Our results mean that longitudinal studies will be necessary to determine if WMHs are directly part of AD. Whether or not this is found to be the case, it does not preclude WMHs from also developing separately from AD and contributing to cognition.

In Chapter 3, we argued against using machine learning because of its black box approach. Our use of it in Chapter 5 may sound like a contradiction, but this choice is explained by the differences in motivation and design of the two studies. Our goal in Chapter 5 was to answer a simple yes/no question: are WMHs in cognitively normal, amyloid negative participants different from WMHs in cognitively normal, amyloid positive participants. Our primary aim was not to interpret how the model separated the groups, but to determine with as much certainty as possible if the groups could be separated in the first place. As such, we leaned towards the more powerful and less interpretable machine learning models. In Chapter 3 we were creating a model intended to be used in a clinical setting, so we made the opposite choice and used simpler but more interpretable models.

It is this lack of interpretability, along with the more complex implementation, that make machine learning models more common in industry than in science. Traditional machine learning was used for tasks like automatically detecting numbers on an image or determining if an email was spam or not. It did not matter how it was accomplished, it just needed to work. While this is understandable, it can lead to biased models if biased data is used to train the model (Obermeyer et al., 2019). Since all data is biased in some way, it's important to understand how and why your model is working even in these circumstances where the 'why' does not explicitly matter – in case your model does something unexpected.

Our interpretations from this study came from the yes/no answer we got from the machine learning models, along with the specifics of what data and whose data we gave the algorithms. For instance, we restricted the models to only using WMH data and had carefully matched cohorts that allowed us to control for age and other factors. By restricting which areas of the brain were included in the model, we were able to find that WMH data from within our Dorsal Parietal region of interest (ROI) or our Posterior ROI are sufficient to separate out symptomatic AD from controls. Conversely, the other ROIs – Juxtacortical, Deep White Matter, and Periventricular – were unable to separate symptomatic AD from controls. This indicates a regional specificity in the higher volume of WMHs seen in symptomatic AD. Those ROIs may be where AD-specific WMHs develop, or they may be regions that are more likely to lead to cognitive decline. With this sort of careful planning, and in combination with more traditional statistical analysis, we showed that machine learning can be used for hypothesis testing.

6.6 Overall Conclusions

Taken together, these studies have shown patterns of grey matter atrophy and of white matter hyperintensities that are seen in symptomatic AD and distinguishable from normal aging. With our cross-sectional definition of preclinical AD, we were not able to distinguish atrophy and WMHs in preclinical AD from normal aging. In other words, we did not see AD-associated atrophy and WMHs in the absence of impairment. While our WMH study saw overlap between AD and vascular dementia, our study of post-stroke dementia did not see a relationship with AD. This shows the complexity of cerebrovascular disease, which comprises multiple subtypes with various etiologies. In these studies, we also discuss the various algorithms that can be used for group classification. There is invariably a trade-off between a model's complexity and transparency. For models that plan to be implemented clinically, transparency is key. In more

restricted experiments where there are limited possible interpretations, more complex models may be able to detect group differences that otherwise would be overlooked. With these studies, we have contributed to the understanding of how aging and cerebrovascular disease are interacting with neuroimaging measures of AD. We show that pathologies can be separated out by their etiology through the spatial patterns in which those pathologies occur.

Separating these etiologies is important clinically – they may all result in dementia, but the specific medications and treatments depend on the etiology. Historically, this has been about determining when a patient has something other than AD, as there was little treatment available for AD. With the recent approval of Aducanumab by the United States Food and Drug Administration (Dunn et al., 2021), there is renewed hope for amyloid-targeting therapies to improve treatment options for AD. However, the amyloid-targeting therapies being developed will be helpful only for AD so accurate diagnosis is essential. Similarly, these treatments themselves can cause non-specific imaging findings, such as amyloid-related imaging abnormalities (ARIA). As such, it is important to know when and to what extent pathologies such as atrophy and WMHs are caused by AD, normal aging, and cerebrovascular disease so that we can attribute these findings in patients to their correct causes.

Conversely, when evaluating a person as a whole it is not always appropriate to separate these pathologies by etiology. In Chapter 3 we found that separating out age-related atrophy made it more difficult to classify AD dementia instead of less. While not all atrophy measured was caused by AD, this reflects the fact that the brain is still a single organ. All of these pathologies are affecting the brain in parallel, and so their impact on individuals must also be evaluated together. While we may focus on studying a single disease at a time, we can never forget the broader context of what else is happening in the brain.

References

Adams, H.P., Bendixen, B.H., Kappelle, L.J., Biller, J., Love, B.B., Gordon, D.L., Marsh, E.E., 1993. Classification of subtype of acute ischemic stroke. Definitions for use in a multicenter clinical trial. TOAST. Trial of Org 10172 in Acute Stroke Treatment. Stroke 24, 35–41. https://doi.org/10.1161/01.STR.24.1.35

Alber, J., Alladi, S., Bae, H., Barton, D.A., Beckett, L.A., Bell, J.M., Berman, S.E., Biessels, G.J., Black, S.E., Bos, I., Bowman, G.L., Brai, E., Brickman, A.M., Callahan, B.L., Corriveau, R.A., Fossati, S., Gottesman, R.F., Gustafson, D.R., Hachinski, V., Hayden, K.M., Helman, A.M., Hughes, T.M., Isaacs, J.D., Jefferson, A.L., Johnson, S.C., Kapasi, A., Kern, S., Kwon, J.C., Kukolja, J., Lee, A., Lockhart, S.N., Murray, A., Osborn, K.E., Power, M.C., Price, B.R., Rhodius-Meester, H.F.M., Rondeau, J.A., Rosen, A.C., Rosene, D.L., Schneider, J.A., Scholtzova, H., Shaaban, C.E., Silva, N.C.B.S., Snyder, H.M., Swardfager, W., Troen, A.M., Veluw, S.J., Vemuri, P., Wallin, A., Wellington, C., Wilcock, D.M., Xie, S.X., Hainsworth, A.H., 2019. White matter hyperintensities in vascular contributions to cognitive impairment and dementia (VCID): Knowledge gaps and opportunities. Alzheimers Dement. Transl. Res. Clin. Interv. 5, 107–117. https://doi.org/10.1016/j.trci.2019.02.001

Alosco, M.L., Sugarman, M.A., Besser, L.M., Tripodis, Y., Martin, B., Palmisano, J.N., Kowall, N.W., Au, R., Mez, J., DeCarli, C., Stein, T.D., McKee, A.C., Killiany, R.J., Stern, R.A., 2018. A Clinicopathological Investigation of White Matter Hyperintensities and Alzheimer's Disease Neuropathology. J. Alzheimers Dis. JAD 63, 1347–1360. https://doi.org/10.3233/JAD-180017

Arbabshirani, M.R., Plis, S., Sui, J., Calhoun, V.D., 2017. Single subject prediction of brain disorders in neuroimaging: Promises and pitfalls. NeuroImage 145, 137–165. https://doi.org/10.1016/j.neuroimage.2016.02.079

Armstrong, N.M., An, Y., Beason-Held, L., Doshi, J., Erus, G., Ferrucci, L., Davatzikos, C., Resnick, S.M., 2019a. Predictors of neurodegeneration differ between cognitively normal and subsequently impaired older adults. Neurobiol. Aging 75, 178–186. https://doi.org/10.1016/j.neurobiolaging.2018.10.024

Armstrong, N.M., An, Y., Shin, J.J., Williams, O.A., Doshi, J., Erus, G., Davatzikos, C., Ferrucci, L., Beason-Held, L.L., Resnick, S.M., 2020. Associations between cognitive and brain volume changes in cognitively normal older adults. NeuroImage 223, 117289. https://doi.org/10.1016/j.neuroimage.2020.117289

Armstrong, N.M., Huang, C.-W., Williams, O.A., Bilgel, M., An, Y., Doshi, J., Erus, G., Davatzikos, C., Wong, D.F., Ferrucci, L., Resnick, S.M., 2019b. Sex differences in the association between amyloid and longitudinal brain volume change in cognitively normal older adults. NeuroImage Clin. 22, 101769. https://doi.org/10.1016/j.nicl.2019.101769

Armstrong, R.A., 2019. Risk factors for Alzheimer's disease. Folia Neuropathol. 57, 87–105. https://doi.org/10.5114/fn.2019.85929

Arvanitakis, Z., Fleischman, D.A., Arfanakis, K., Leurgans, S.E., Barnes, L.L., Bennett, D.A., 2016. Association of white matter hyperintensities and gray matter volume with cognition in older individuals without cognitive impairment. Brain Struct. Funct. 221, 2135–2146. https://doi.org/10.1007/s00429-015-1034-7

Bangen, K.J., Preis, S.R., Delano-Wood, L., Wolf, P.A., Libon, D.J., Bondi, M.W., Au, R., DeCarli, C., Brickman, A.M., 2018a. Baseline White Matter Hyperintensities and Hippocampal Volume are Associated with Conversion from Normal Cognition to Mild Cognitive Impairment in the Framingham Offspring Study. Alzheimer Dis. Assoc. Disord. 32, 50–56. https://doi.org/10.1097/WAD.0000000000000215

Bangen, K.J., Preis, S.R., Delano-Wood, L., Wolf, P.A., Libon, D.J., Bondi, M.W., Au, R., DeCarli, C., Brickman, A.M., 2018b. Baseline White Matter Hyperintensities and Hippocampal Volume are Associated With Conversion From Normal Cognition to Mild Cognitive Impairment in the Framingham Offspring Study: Alzheimer Dis. Assoc. Disord. 32, 50–56. https://doi.org/10.1097/WAD.0000000000000215

Bateman, R.J., Xiong, C., Benzinger, T.L.S., Fagan, A.M., Goate, A., Fox, N.C., Marcus, D.S., Cairns, N.J., Xie, X., Blazey, T.M., Holtzman, D.M., Santacruz, A., Buckles, V., Oliver, A., Moulder, K., Aisen, P.S., Ghetti, B., Klunk, W.E., McDade, E., Martins, R.N., Masters, C.L., Mayeux, R., Ringman, J.M., Rossor, M.N., Schofield, P.R., Sperling, R.A., Salloway, S., Morris, J.C., 2012. Clinical and Biomarker Changes in Dominantly Inherited Alzheimer's Disease. N. Engl. J. Med. 367, 795–804. https://doi.org/10.1056/NEJMoa1202753

Beach, T.G., Monsell, S.E., Phillips, L.E., Kukull, W., 2012. Accuracy of the Clinical Diagnosis of Alzheimer Disease at National Institute on Aging Alzheimer Disease Centers, 2005–2010. J. Neuropathol. Exp. Neurol. 71, 266–273. https://doi.org/10.1097/NEN.0b013e31824b211b

Becker, J.A., Hedden, T., Carmasin, J., Maye, J., Rentz, D.M., Putcha, D., Fischl, B., Greve, D.N., Marshall, G.A., Salloway, S., Marks, D., Buckner, R.L., Sperling, R.A., Johnson, K.A., 2011. Amyloid-β Associated Cortical Thinning in Clinically Normal Elderly. Ann. Neurol. 69, 1032–1042. https://doi.org/10.1002/ana.22333

Benjamin, E.J., Blaha, M.J., Chiuve, S.E., Cushman, M., Das, S.R., Deo, R., de Ferranti, S.D., Floyd, J., Fornage, M., Gillespie, C., Isasi, C.R., Jiménez, M.C., Jordan, L.C., Judd, S.E., Lackland, D., Lichtman, J.H., Lisabeth, L., Liu, S., Longenecker, C.T., Mackey, R.H., Matsushita, K., Mozaffarian, D., Mussolino, M.E., Nasir, K., Neumar, R.W., Palaniappan, L., Pandey, D.K., Thiagarajan, R.R., Reeves, M.J., Ritchey, M., Rodriguez, C.J., Roth, G.A., Rosamond, W.D., Sasson, C., Towfighi, A., Tsao, C.W., Turner, M.B., Virani, S.S., Voeks, J.H., Willey, J.Z., Wilkins, J.T., Wu, J.H., Alger, H.M., Wong, S.S., Muntner, P., American Heart Association Statistics Committee and Stroke Statistics Subcommittee, 2017. Heart Disease and Stroke Statistics-2017 Update: A Report From the American Heart Association. Circulation 135, e146–e603. https://doi.org/10.1161/CIR.0000000000000485

Bennett, E.E., Gianattasio, K.Z., Hughes, T.M., Mosley, T.H., Wong, D.F., Gottesman, R.F., Power, M.C., 2020. The association between midlife lipid levels and late-life brain amyloid deposition. Neurobiol. Aging 92, 73–74. https://doi.org/10.1016/j.neurobiolaging.2020.03.015

Bolar, K., 2019. STAT: Interactive Document for Working with Basic Statistical Analysis.

Bondi, M.W., Edmonds, E.C., Salmon, D.P., 2017. Alzheimer's Disease: Past, Present, and Future. J. Int. Neuropsychol. Soc. JINS 23, 818–831. https://doi.org/10.1017/S135561771700100X

Bondi, M.W., Salmon, D.P., Galasko, D., Thomas, R.G., Thal, L.J., 1999. Neuropsychological function and apolipoprotein E genotype in the preclinical detection of Alzheimer's disease. Psychol. Aging 14, 295–303. https://doi.org/10.1037//0882-7974.14.2.295

Bondi, M.W., Salmon, D.P., Monsch, A.U., Galasko, D., Butters, N., Klauber, M.R., Thal, L.J., Saitoh, T., 1995. Episodic memory changes are associated with the APOE-epsilon 4 allele in nondemented older adults. Neurology 45, 2203–2206. https://doi.org/10.1212/wnl.45.12.2203

Bos, D., Wolters, F.J., Darweesh, S.K.L., Vernooij, M.W., de Wolf, F., Ikram, M.A., Hofman, A., 2018. Cerebral small vessel disease and the risk of dementia: A systematic review and meta-analysis of population-based evidence. Alzheimers Dement. 14, 1482–1492. https://doi.org/10.1016/j.jalz.2018.04.007

Bos, I., Verhey, F.R., Ramakers, I.H.G.B., Jacobs, H.I.L., Soininen, H., Freund-Levi, Y., Hampel, H., Tsolaki, M., Wallin, Å.K., van Buchem, M.A., Oleksik, A., Verbeek, M.M., Olde Rikkert, M., van der Flier, W.M., Scheltens, P., Aalten, P., Visser, P.J., Vos, S.J.B., 2017. Cerebrovascular and amyloid pathology in predementia stages: the relationship with neurodegeneration and cognitive decline. Alzheimers Res. Ther. 9, 101. https://doi.org/10.1186/s13195-017-0328-9

Bos, I., Vos, S.J.B., Schindler, S.E., Hassenstab, J., Xiong, C., Grant, E., Verhey, F., Morris, J.C., Visser, P.J., Fagan, A.M., 2019. Vascular risk factors are associated with longitudinal changes in cerebrospinal fluid tau markers and cognition in preclinical Alzheimer's disease. Alzheimers Dement. 15, 1149–1159. https://doi.org/10.1016/j.jalz.2019.04.015

Boyd, R.W., Lindo, E.G., Weeks, L.D., McLemore, M.R., 2020. On Racism: A New Standard For Publishing On Racial Health Inequities | Health Affairs. https://doi.org/10.1377/hblog20200630.939347

Brickman, A.M., Schupf, N., Manly, J.J., Luchsinger, J.A., Andrews, H., Tang, M.X., Reitz, C., Small, S.A., Mayeux, R., DeCarli, C., Brown, T.R., 2008. Brain Morphology in Older African Americans, Caribbean Hispanics, and Whites From Northern Manhattan. Arch. Neurol. 65. https://doi.org/10.1001/archneur.65.8.1053

Brier, M.R., Thomas, J.B., Fagan, A.M., Hassenstab, J., Holtzman, D.M., Benzinger, T.L., Morris, J.C., Ances, B.M., 2014a. Functional connectivity and graph theory in preclinical

Alzheimer's disease. Neurobiol. Aging 35, 757–768. https://doi.org/10.1016/j.neurobiolaging.2013.10.081

Brier, M.R., Thomas, J.B., Snyder, A.Z., Wang, L., Fagan, A.M., Benzinger, T.L., Morris, J.C., Ances, B.M., 2014b. Unrecognized preclinical Alzheimer disease confounds rs-fcMRI studies of normal aging. Neurology 83, 1613–1619. https://doi.org/10.1212/WNL.0000000000000939

Buckner, R.L., Head, D., Parker, J., Fotenos, A.F., Marcus, D., Morris, J.C., Snyder, A.Z., 2004. A unified approach for morphometric and functional data analysis in young, old, and demented adults using automated atlas-based head size normalization: reliability and validation against manual measurement of total intracranial volume. NeuroImage 23, 724–738. https://doi.org/10.1016/j.neuroimage.2004.06.018

Charidimou, A., Boulouis, G., Gurol, M.E., Ayata, C., Bacskai, B.J., Frosch, M.P., Viswanathan, A., Greenberg, S.M., 2017. Emerging concepts in sporadic cerebral amyloid angiopathy. Brain 140, 1829–1850. https://doi.org/10.1093/brain/awx047

Chételat, G., Villemagne, V.L., Pike, K.E., Baron, J.-C., Bourgeat, P., Jones, G., Faux, N.G., Ellis, K.A., Salvado, O., Szoeke, C., Martins, R.N., Ames, D., Masters, C.L., Rowe, C.C., 2010. Larger temporal volume in elderly with high versus low beta-amyloid deposition. Brain 133, 3349–3358. https://doi.org/10.1093/brain/awq187

Chételat, G., Villemagne, V.L., Villain, N., Jones, G., Ellis, K.A., Ames, D., Martins, R.N., Masters, C.L., Rowe, C.C., 2012. Accelerated cortical atrophy in cognitively normal elderly with high β-amyloid deposition. Neurology 78, 477–484. https://doi.org/10.1212/WNL.0b013e318246d67a

Chi, N.-F., Chao, S.-P., Huang, L.-K., Chan, L., Chen, Y.-R., Chiou, H.-Y., Hu, C.-J., 2019. Plasma Amyloid Beta and Tau Levels Are Predictors of Post-stroke Cognitive Impairment: A Longitudinal Study. Front. Neurol. 10. https://doi.org/10.3389/fneur.2019.00715

Coutu, J.-P., Lindemer, E.R., Konukoglu, E., Salat, D.H., 2017. Two distinct classes of degenerative change are independently linked to clinical progression in Mild Cognitive Impairment. Neurobiol. Aging 54, 1–9. https://doi.org/10.1016/j.neurobiolaging.2017.02.005

Day, G.S., Lim, T.S., Hassenstab, J., Goate, A.M., Grant, E.A., Roe, C.M., Cairns, N.J., Morris, J.C., 2017. Differentiating cognitive impairment due to corticobasal degeneration and Alzheimer disease. Neurology 88, 1273–1281. https://doi.org/10.1212/WNL.0000000000003770

DeLong, E.R., DeLong, D.M., Clarke-Pearson, D.L., 1988. Comparing the areas under two or more correlated receiver operating characteristic curves: a nonparametric approach. Biometrics 44, 837–45.

Desikan, R.S., Ségonne, F., Fischl, B., Quinn, B.T., Dickerson, B.C., Blacker, D., Buckner, R.L., Dale, A.M., Maguire, R.P., Hyman, B.T., Albert, M.S., Killiany, R.J., 2006. An

automated labeling system for subdividing the human cerebral cortex on MRI scans into gyral based regions of interest. NeuroImage 31, 968–980. https://doi.org/10.1016/j.neuroimage.2006.01.021

Desmond, D.W., Moroney, J.T., Paik, M.C., Sano, M., Mohr, J.P., Aboumatar, S., Tseng, C.L., Chan, S., Williams, J.B., Remien, R.H., Hauser, W.A., Stern, Y., 2000. Frequency and clinical determinants of dementia after ischemic stroke. Neurology 54, 1124–1131. https://doi.org/10.1212/wnl.54.5.1124

Dickerson, B.C., Bakkour, A., Salat, D.H., Feczko, E., Pacheco, J., Greve, D.N., Grodstein, F., Wright, C.I., Blacker, D., Rosas, H.D., Sperling, R.A., Atri, A., Growdon, J.H., Hyman, B.T., Morris, J.C., Fischl, B., Buckner, R.L., 2009. The Cortical Signature of Alzheimer's Disease: Regionally Specific Cortical Thinning Relates to Symptom Severity in Very Mild to Mild AD Dementia and is Detectable in Asymptomatic Amyloid-Positive Individuals. Cereb. Cortex 19, 497–510. https://doi.org/10.1093/cercor/bhn113

Douiri, A., Rudd, A.G., Wolfe, C.D.A., 2013. Prevalence of poststroke cognitive impairment: South London Stroke Register 1995-2010. Stroke 44, 138–145. https://doi.org/10.1161/STROKEAHA.112.670844

Dubois, B., Feldman, H.H., Jacova, C., Dekosky, S.T., Barberger-Gateau, P., Cummings, J., Delacourte, A., Galasko, D., Gauthier, S., Jicha, G., Meguro, K., O'brien, J., Pasquier, F., Robert, P., Rossor, M., Salloway, S., Stern, Y., Visser, P.J., Scheltens, P., 2007. Research criteria for the diagnosis of Alzheimer's disease: revising the NINCDS-ADRDA criteria. Lancet Neurol. 6, 734–746. https://doi.org/10.1016/S1474-4422(07)70178-3

Duits, F.H., Martinez-Lage, P., Paquet, C., Engelborghs, S., Lleó, A., Hausner, L., Molinuevo, J.L., Stomrud, E., Farotti, L., Ramakers, I.H., Tsolaki, M., Skarsgård, C., Åstrand, R., Wallin, A., Vyhnalek, M., Holmber-Clausen, M., Forlenza, O. V, Ghezzi, L., Ingelsson, M., Hoff, E.I., Roks, G., de Mendonça, A., Papma, J.M., Izagirre, A., Taga, M., Struyfs, H., Alcolea, D.A., Frölich, L., Balasa, M., Minthon, L., Twisk, J.W., Persson, S., Zetterberg, H., van der Flier, W.M., Teunissen, C.E., Scheltens, P., Blennow, K., 2016. Performance and complications of lumbar puncture in memory clinics: Results of the multicenter lumbar puncture feasibility study. Alzheimers Dement. 12, 154–163. https://doi.org/10.1016/j.jalz.2015.08.003

Dunn, B., Stein, P., Cavazzoni, P., 2021. Approval of Aducanumab for Alzheimer Disease—the FDA's Perspective. JAMA Intern. Med. https://doi.org/10.1001/jamainternmed.2021.4607

Eldholm, R.S., Persson, K., Barca, M.L., Knapskog, A.-B., Cavallin, L., Engedal, K., Selbaek, G., Skovlund, E., Saltvedt, I., 2018. Association between vascular comorbidity and progression of Alzheimer's disease: a two-year observational study in Norwegian memory clinics. BMC Geriatr. 18, 120. https://doi.org/10.1186/s12877-018-0813-4

Erten-Lyons, D., Dodge, H.H., Woltjer, R., Silbert, L.C., Howieson, D.B., Kramer, P., Kaye, J.A., 2013. Neuropathologic Basis of Age-Associated Brain Atrophy. JAMA Neurol. 70, 616. https://doi.org/10.1001/jamaneurol.2013.1957

Fagan, A.M., Head, D., Shah, A.R., Marcus, D., Mintun, M., Morris, J.C., Holtzman, D.M., 2009. Decreased cerebrospinal fluid Aβ42 correlates with brain atrophy in cognitively normal elderly. Ann. Neurol. 65, 176–183. https://doi.org/10.1002/ana.21559

Fazekas, F., Chawluk, J.B., Alavi, A., 1987. MR signal abnormalities at 1.5 T in Alzheimer's dementia and normal aging. Am. J. Neuroradiol. 8, 421–426.

Fillenbaum, G.G., Heyman, A., Huber, M.S., Woodbury, M.A., Leiss, J., Schmader, K.E., Bohannon, A., Trapp-Moen, B., 1998. The Prevalence and 3-Year Incidence of Dementia in Older Black and White Community Residents. J. Clin. Epidemiol. 51, 587–595. https://doi.org/10.1016/S0895-4356(98)00024-9

Fischl, B., 2012. FreeSurfer. NeuroImage 62, 774–781. https://doi.org/10.1016/j.neuroimage.2012.01.021

Fitzpatrick, Annette L., Kuller, L.H., Ives, D.G., Lopez, O.L., Jagust, W., Breitner, J.C.S., Jones, B., Lyketsos, C., Dulberg, C., 2004. Incidence and Prevalence of Dementia in the Cardiovascular Health Study: INCIDENCE OF DEMENTIA IN CHS. J. Am. Geriatr. Soc. 52, 195–204. https://doi.org/10.1111/j.1532-5415.2004.52058.x

Fitzpatrick, Annette L, Kuller, L.H., Ives, D.G., Lopez, O.L., Jagust, W., Breitner, J.C.S., Jones, B., Lyketsos, C., Dulberg, C., 2004. Incidence and Prevalence of Dementia in the Cardiovascular Health Study. J. Am. Geriatr. Soc. 52, 195–204. https://doi.org/10.1111/j.1532-5415.2004.52058.x

Fjell, A.M., McEvoy, L., Holland, D., Dale, A.M., Walhovd, K.B., 2014a. What is normal in normal aging? Effects of aging, amyloid and Alzheimer's disease on the cerebral cortex and the hippocampus. Prog. Neurobiol. 117, 20–40. https://doi.org/10.1016/j.pneurobio.2014.02.004

Fjell, A.M., McEvoy, L., Holland, D., Dale, A.M., Walhovd, K.B., for the Alzheimer's Disease Neuroimaging Initiative, 2013a. Brain Changes in Older Adults at Very Low Risk for Alzheimer's Disease. J. Neurosci. 33, 8237–8242. https://doi.org/10.1523/JNEUROSCI.5506-12.2013

Fjell, A.M., Walhovd, K.B., Fennema-Notestine, C., McEvoy, L.K., Hagler, D.J., Holland, D., Blennow, K., Brewer, J.B., Dale, A.M., 2010. Brain Atrophy in Healthy Aging Is Related to CSF Levels of Aβ1-42. Cereb. Cortex N. Y. NY 20, 2069–2079. https://doi.org/10.1093/cercor/bhp279

Fjell, A.M., Westlye, L.T., Grydeland, H., Amlien, I., Espeseth, T., Reinvang, I., Raz, N., Dale, A.M., Walhovd, K.B., 2014b. Accelerating Cortical Thinning: Unique to Dementia or Universal in Aging? Cereb. Cortex 24, 919–934. https://doi.org/10.1093/cercor/bhs379

Fjell, A.M., Westlye, L.T., Grydeland, H., Amlien, I., Espeseth, T., Reinvang, I., Raz, N., Holland, D., Dale, A.M., Walhovd, K.B., 2013b. Critical ages in the life course of the adult brain: nonlinear subcortical aging. Neurobiol. Aging 34, 2239–2247. https://doi.org/10.1016/j.neurobiolaging.2013.04.006

Fletcher, E., Filshtein, T.J., Harvey, D., Renaud, A., Mungas, D., DeCarli, C., 2018a. Staging of amyloid β, t-tau, regional atrophy rates, and cognitive change in a nondemented cohort: Results of serial mediation analyses. Alzheimers Dement. Diagn. Assess. Dis. Monit. 10, 382–393. https://doi.org/10.1016/j.dadm.2018.04.001

Fletcher, E., Gavett, B., Harvey, D., Farias, S.T., Olichney, J., Beckett, L., DeCarli, C., Mungas, D., 2018b. Brain volume change and cognitive trajectories in aging. Neuropsychology 32, 436–449. https://doi.org/10.1037/neu0000447

Fletcher, E., Villeneuve, S., Maillard, P., Harvey, D., Reed, B., Jagust, W., DeCarli, C., 2016. β-amyloid, hippocampal atrophy and their relation to longitudinal brain change in cognitively normal individuals. Neurobiol. Aging 40, 173–180. https://doi.org/10.1016/j.neurobiolaging.2016.01.133

Folstein, M.F., Folstein, S.E., McHugh, P.R., 1975. "Mini-mental state": A practical method for grading the cognitive state of patients for the clinician. J. Psychiatr. Res. 12, 189–198. https://doi.org/10.1016/0022-3956(75)90026-6

Fotenos, A.F., Snyder, A.Z., Girton, L.E., Morris, J.C., Buckner, R.L., 2005. Normative estimates of cross-sectional and longitudinal brain volume decline in aging and AD. Neurology 64, 1032–1039. https://doi.org/10.1212/01.WNL.0000154530.72969.11

Frisoni, G.B., Fox, N.C., Jack, C.R., Scheltens, P., Thompson, P.M., 2010. The clinical use of structural MRI in Alzheimer disease. Nat. Rev. Neurol. 6, 67–77. https://doi.org/10.1038/nrneurol.2009.215

Galvin, J.E., Roe, C.M., Powlishta, K.K., Coats, M.A., Muich, S.J., Grant, E., Miller, J.P., Storandt, M., Morris, J.C., 2005. The AD8: A brief informant interview to detect dementia. Neurology 65, 559–564. https://doi.org/10.1212/01.wnl.0000172958.95282.2a

Gamaldo, A., Moghekar, A., Kilada, S., Resnick, S.M., Zonderman, A.B., O'Brien, R., 2006. Effect of a clinical stroke on the risk of dementia in a prospective cohort. Neurology 67, 1363–1369. https://doi.org/10.1212/01.wnl.0000240285.89067.3f

Glasser, M.F., Coalson, T.S., Robinson, E.C., Hacker, C.D., Harwell, J., Yacoub, E., Ugurbil, K., Andersson, J., Beckmann, C.F., Jenkinson, M., Smith, S.M., Van Essen, D.C., 2016a. A multi-modal parcellation of human cerebral cortex. Nature 536, 171–178. https://doi.org/10.1038/nature18933

Glasser, M.F., Goyal, M.S., Preuss, T.M., Raichle, M.E., Van Essen, D.C., 2014. Trends and properties of human cerebral cortex: correlations with cortical myelin content. NeuroImage 93 Pt 2, 165–175. https://doi.org/10.1016/j.neuroimage.2013.03.060

Glasser, M.F., Smith, S.M., Marcus, D.S., Andersson, J.L.R., Auerbach, E.J., Behrens, T.E.J., Coalson, T.S., Harms, M.P., Jenkinson, M., Moeller, S., Robinson, E.C., Sotiropoulos, S.N., Xu, J., Yacoub, E., Ugurbil, K., Van Essen, D.C., 2016b. The Human Connectome Project's neuroimaging approach. Nat. Neurosci. https://doi.org/10.1038/nn.4361

Glasser, M.F., Van Essen, D.C., 2011. Mapping human cortical areas in vivo based on myelin content as revealed by T1- and T2-weighted MRI. J. Neurosci. Off. J. Soc. Neurosci. 31, 11597–11616. https://doi.org/10.1523/JNEUROSCI.2180-11.2011

Gordon, B.A., Najmi, S., Hsu, P., Roe, C.M., Morris, J.C., Benzinger, T.L.S., 2015. The effects of white matter hyperintensities and amyloid deposition on Alzheimer dementia. NeuroImage Clin. 8, 246–252. https://doi.org/10.1016/j.nicl.2015.04.017

Gordon, E.M., Laumann, T.O., Adeyemo, B., Huckins, J.F., Kelley, W.M., Petersen, S.E., 2016. Generation and Evaluation of a Cortical Area Parcellation from Resting-State Correlations. Cereb. Cortex 26, 288–303. https://doi.org/10.1093/cercor/bhu239

Gottesman, R.F., Mosley, T.H., Knopman, D.S., Hao, Q., Wong, D., Wagenknecht, L.E., Hughes, T.M., Qiao, Y., Dearborn, J., Wasserman, B.A., 2020. Association of Intracranial Atherosclerotic Disease With Brain β-Amyloid Deposition: Secondary Analysis of the ARIC Study. JAMA Neurol. 77, 350–357. https://doi.org/10.1001/jamaneurol.2019.4339

Graff-Radford, J., Arenaza-Urquijo, E.M., Knopman, D.S., Schwarz, C.G., Brown, R.D., Rabinstein, A.A., Gunter, J.L., Senjem, M.L., Przybelski, S.A., Lesnick, T., Ward, C., Mielke, M.M., Lowe, V.J., Petersen, R.C., Kremers, W.K., Kantarci, K., Jack, C.R., Vemuri, P., 2019. White matter hyperintensities: relationship to amyloid and tau burden. Brain J. Neurol. 142, 2483–2491. https://doi.org/10.1093/brain/awz162

Graff-Radford, Neill R, Besser, L.M., Crook, J.E., Kukull, W., Dickson, D.W., 2016. Neuropathologic differences by race from the National Alzheimer's Coordinating Center. Alzheimers Dement. 12, 669–677. https://doi.org/10.1016/j.jalz.2016.03.004

Graff-Radford, Neill R., Besser, L.M., Crook, J.E., Kukull, W.A., Dickson, D.W., 2016. Neuropathologic differences by race from the National Alzheimer's Coordinating Center. Alzheimers Dement. 12, 669–677. https://doi.org/10.1016/j.jalz.2016.03.004

Green, R.C., 2002. Risk of Dementia Among White and African American Relatives of Patients With Alzheimer Disease. JAMA 287, 329. https://doi.org/10.1001/jama.287.3.329

Grimmer, T., Faust, M., Auer, F., Alexopoulos, P., Förstl, H., Henriksen, G., Perneczky, R., Sorg, C., Yousefi, B.H., Drzezga, A., Kurz, A., 2012. White matter hyperintensities predict amyloid increase in Alzheimer's disease. Neurobiol. Aging 33, 2766–2773. https://doi.org/10.1016/j.neurobiolaging.2012.01.016

Habes, M., Pomponio, R., Shou, H., Doshi, J., Mamourian, E., Erus, G., Nasrallah, I., Launer, L.J., Rashid, T., Bilgel, M., Fan, Y., Toledo, J.B., Yaffe, K., Sotiras, A., Srinivasan, D., Espeland, M., Masters, C., Maruff, P., Fripp, J., Völzk, H., Johnson, S.C., Morris, J.C., Albert, M.S., Miller, M.I., Bryan, R.N., Grabe, H.J., Resnick, S.M., Wolk, D.A., Davatzikos, C., 2021. The Brain Chart of Aging: Machine-learning analytics reveals links between brain aging, white matter disease, amyloid burden, and cognition in the iSTAGING consortium of 10,216 harmonized MR scans. Alzheimers Dement. 17, 89–102. https://doi.org/10.1002/alz.12178

Hachinski, V.C., Iliff, L.D., Zilhka, E., Du Boulay, G.H., McAllister, V.L., Marshall, J., Russell, R.W., Symon, L., 1975. Cerebral blood flow in dementia. Arch. Neurol. 32, 632–637. https://doi.org/10.1001/archneur.1975.00490510088009

Hagberg, G., Ihle-Hansen, Hege, Fure, B., Thommessen, B., Ihle-Hansen, Håkon, Øksengård, A.R., Beyer, M.K., Wyller, T.B., Müller, E.G., Pendlebury, S.T., Selnes, P., 2020. No evidence for amyloid pathology as a key mediator of neurodegeneration post-stroke - a seven-year follow-up study. BMC Neurol. 20, 174. https://doi.org/10.1186/s12883-020-01753-w

Hamed, S.A., 2017. Brain injury with diabetes mellitus: evidence, mechanisms and treatment implications. Expert Rev. Clin. Pharmacol. 10, 409–428. https://doi.org/10.1080/17512433.2017.1293521

Hardy, J.A., Higgins, G.A., 1992. Alzheimer's disease: the amyloid cascade hypothesis. Science 256, 184–185. https://doi.org/10.1126/science.1566067

Hase, Y., Horsburgh, K., Ihara, M., Kalaria, R.N., 2018. White matter degeneration in vascular and other ageing-related dementias. J. Neurochem. 144, 617–633. https://doi.org/10.1111/jnc.14271

Hassenstab, J., Chasse, R., Grabow, P., Benzinger, T.L., Fagan, A.M., Xiong, C., Jasielec, M.S., Grant, E.A., Morris, J.C., 2016. Certified normal: Alzheimer's disease biomarkers and normative estimates of cognitive functioning. Neurobiol. Aging 43, 23–33. https://doi.org/10.1016/j.neurobiolaging.2016.03.014

Heinen, R., Steenwijk, M.D., Barkhof, F., Biesbroek, J.M., van der Flier, W.M., Kuijf, H.J., Prins, N.D., Vrenken, H., Biessels, G.J., de Bresser, J., 2019. Performance of five automated white matter hyperintensity segmentation methods in a multicenter dataset. Sci. Rep. 9. https://doi.org/10.1038/s41598-019-52966-0

Heiss, W.-D., Rosenberg, G.A., Thiel, A., Berlot, R., de Reuck, J., 2016. Neuroimaging in vascular cognitive impairment: a state-of-the-art review. BMC Med. 14, 174. https://doi.org/10.1186/s12916-016-0725-0

Hooper, M.W., Mitchell, C., Marshall, V.J., Cheatham, C., Austin, K., Sanders, K., Krishnamurthi, S., Grafton, L.L., 2019. Understanding multilevel factors related to urban community trust in healthcare and research. Int. J. Environ. Res. Public. Health 16. https://doi.org/10.3390/ijerph16183280

Irwin, D.J., Hurtig, H.I., 2018. The Contribution of Tau, Amyloid-Beta and Alpha-Synuclein Pathology to Dementia in Lewy Body Disorders. J. Alzheimer's Dis. Park. 08, 139–148. https://doi.org/10.4172/2161-0460.1000444

Irwin, K., Sexton, C., Daniel, T., Lawlor, B., Naci, L., 2018. Healthy Aging and Dementia: Two Roads Diverging in Midlife? Front. Aging Neurosci. 10. https://doi.org/10.3389/fnagi.2018.00275

Jack, C.R., 2020. Preclinical Alzheimer's disease: a valid concept. Lancet Neurol. 19, 31. https://doi.org/10.1016/S1474-4422(19)30440-5

Jack, C.R., Bennett, D.A., Blennow, K., Carrillo, M.C., Dunn, B., Haeberlein, S.B., Holtzman, D.M., Jagust, W., Jessen, F., Karlawish, J.H., Liu, E., Molinuevo, J.L., Montine, T.J., Phelps, C.H., Rankin, K.P., Rowe, C.C., Scheltens, P., Siemers, E., Snyder, H.M., Sperling, R.A., Elliott, C., Masliah, E., Ryan, L., Silverberg, N., 2018. NIA-AA Research Framework: Toward a biological definition of Alzheimer's disease. Alzheimers Dement. 14, 535–562. https://doi.org/10.1016/j.jalz.2018.02.018

Jack, C.R., Knopman, D.S., Jagust, W.J., Petersen, R.C., Weiner, M.W., Aisen, P.S., Shaw, L.M., Vemuri, P., Wiste, H.J., Weigand, S.D., Lesnick, T.G., Pankratz, V.S., Donohue, M.C., Trojanowski, J.Q., 2013. Update on hypothetical model of Alzheimer's disease biomarkers. Lancet Neurol. 12, 207–216. https://doi.org/10.1016/S1474-4422(12)70291-0

Jack, C.R., Knopman, D.S., Jagust, W.J., Shaw, L.M., Aisen, P.S., Weiner, M.W., Petersen, R.C., Trojanowski, J.Q., 2010. Hypothetical model of dynamic biomarkers of the Alzheimer's pathological cascade. Lancet Neurol. 9, 119–128. https://doi.org/10.1016/S1474-4422(09)70299-6

Jack, C.R., Wiste, H.J., Weigand, S.D., Knopman, D.S., Vemuri, P., Mielke, M.M., Lowe, V., Senjem, M.L., Gunter, J.L., Machulda, M.M., Gregg, B.E., Pankratz, V.S., Rocca, W.A., Petersen, R.C., 2015. Age, Sex, and APOE ε4 Effects on Memory, Brain Structure, and β-Amyloid Across the Adult Life Span. JAMA Neurol. 72, 511–519. https://doi.org/10.1001/jamaneurol.2014.4821

Jack, C.R., Wiste, H.J., Weigand, S.D., Rocca, W.A., Knopman, D.S., Mielke, M.M., Lowe, V.J., Senjem, M.L., Gunter, J.L., Preboske, G.M., Pankratz, V.S., Vemuri, P., Petersen, R.C., 2014. Age-specific population frequencies of cerebral β-amyloidosis and neurodegeneration among people with normal cognitive function aged 50–89 years: a cross-sectional study. Lancet Neurol. 13, 997–1005. https://doi.org/10.1016/S1474-4422(14)70194-2

Johnson, K.A., Minoshima, S., Bohnen, N.I., Donohoe, K.J., Foster, N.L., Herscovitch, P., Karlawish, J.H., Rowe, C.C., Carrillo, M.C., Hartley, D.M., Hedrick, S., Pappas, V., Thies, W.H., 2013. Appropriate use criteria for amyloid PET: A report of the Amyloid Imaging Task Force, the Society of Nuclear Medicine and Molecular Imaging, and the Alzheimer's Association. Alzheimers Dement. 9, E1–E16. https://doi.org/10.1016/j.jalz.2013.01.002

Joki, H., Higashiyama, Y., Nakae, Y., Kugimoto, C., Doi, H., Kimura, K., Kishida, H., Ueda, N., Nakano, T., Takahashi, T., Koyano, S., Takeuchi, H., Tanaka, F., 2018. White matter hyperintensities on MRI in dementia with Lewy bodies, Parkinson's disease with dementia, and Alzheimer's disease. J. Neurol. Sci. 385, 99–104. https://doi.org/10.1016/j.jns.2017.12.018

Joseph-Mathurin, N., Wang, G., Kantarci, K., Jack, C.R., McDade, E., Hassenstab, J., Blazey, T.M., Gordon, B.A., Su, Y., Chen, G., Massoumzadeh, P., Hornbeck, R.C., Allegri, R.F.,

Ances, B.M., Berman, S.B., Brickman, A.M., Brooks, W.S., Cash, D.M., Chhatwal, J.P., Chui, H.C., Correia, S., Cruchaga, C., Farlow, M.R., Fox, N.C., Fulham, M., Ghetti, B., Graff-Radford, N.R., Johnson, K.A., Karch, C.M., Laske, C., Lee, A.K.W., Levin, J., Masters, C.L., Noble, J.M., O'Connor, A., Perrin, R.J., Preboske, G.M., Ringman, J.M., Rowe, C.C., Salloway, S., Saykin, A.J., Schofield, P.R., Shimada, H., Shoji, M., Suzuki, K., Villemagne, V.L., Xiong, C., Yakushev, I., Morris, J.C., Bateman, R.J., Benzinger, T.L.S., Network, on behalf of the D.I.A., 2021. Longitudinal Accumulation of Cerebral Microhemorrhages in Dominantly Inherited Alzheimer Disease. Neurology 96, e1632–e1645. https://doi.org/10.1212/WNL.0000000000011542

Katzman, R., Kawas, C., 1994. The epidemiology of dementia and Alzheimer disease, in: Alzheimer Disease. Raven Press, New York, NY, US, pp. 105–122.

Kelly, D.A., Seidenberg, M., Reiter, K., Nielson, K.A., Woodard, J.L., Smith, J.C., Durgerian, S., Rao, S.M., 2018. Differential 5-year brain atrophy rates in cognitively declining and stable APOE-ε4 elders. Neuropsychology 32, 647–653. https://doi.org/10.1037/neu0000444

Klunk, W.E., Koeppe, R.A., Price, J.C., Benzinger, T.L., Devous, M.D., Jagust, W.J., Johnson, K.A., Mathis, C.A., Minhas, D., Pontecorvo, M.J., Rowe, C.C., Skovronsky, D.M., Mintun, M.A., 2015. The Centiloid Project: Standardizing quantitative amyloid plaque estimation by PET. Alzheimers Dement. 11, 1-15.e4. https://doi.org/10.1016/j.jalz.2014.07.003

Knopman, D.S., DeKosky, S.T., Cummings, J.L., Chui, H., Corey-Bloom, J., Relkin, N., Small, G.W., Miller, B., Stevens, J.C., 2001. Practice parameter: Diagnosis of dementia (an evidence-based review): Report of the Quality Standards Subcommittee of the American Academy of Neurology. Neurology 56, 1143–1153. https://doi.org/10.1212/WNL.56.9.1143

Knopman, D.S., Jack, C.R., Wiste, H.J., Weigand, S.D., Vemuri, P., Lowe, V.J., Kantarci, K., Gunter, J.L., Senjem, M.L., Mielke, M.M., Roberts, R.O., Boeve, B.F., Petersen, R.C., 2013. Selective Worsening of Brain Injury Biomarker Abnormalities in Cognitively Normal Elderly Persons With β-Amyloidosis. JAMA Neurol. 70, 1030. https://doi.org/10.1001/jamaneurol.2013.182

Koenig, L.N., Day, G.S., Salter, A., Keefe, S., Marple, L.M., Long, J., LaMontagne, P., Massoumazada, P., Snider, B.J., Kanthamneni, M., Raji, C.A., Ghoshal, N., Gordon, B.A., Miller-Thomas, M., Morris, J.C., Shimony, J.S., Benzinger, T.L.S., 2020. Select Atrophied Regions in Alzheimer disease (SARA): An improved volumetric model for identifying Alzheimer disease dementia. NeuroImage Clin. 26, 102248. https://doi.org/10.1016/j.nicl.2020.102248

Koenig, L.N., LaMontagne, P., Glasser, M.F., Bateman, R., Holtzman, D., Yakushev, I., Chhatwal, J., Day, G.S., Jack, C., Mummery, C., Perrin, R.J., Gordon, B.A., Morris, J.C., Shimony, J.S., Benzinger, T.L.S., 2022. Regional age-related atrophy after screening for preclinical alzheimer disease. Neurobiol. Aging 109, 43–51. https://doi.org/10.1016/j.neurobiolaging.2021.09.010

Koenig, L.N., McCue, L.M., Grant, E., Massoumzadeh, P., Roe, C.M., Xiong, C., Moulder, K.L., Wang, L., Zazulia, A.R., Kelly, P., Dincer, A., Zaza, A., Shimony, J.S., Benzinger, T.L.S., Morris, J.C., 2021. Lack of Association Between Acute Stroke, Post-Stroke Dementia, Race, and B-amyloid Status. NeuroImage Clin. 102553. https://doi.org/10.1016/j.nicl.2020.102553

Koncz, R., Sachdev, P.S., 2018. Are the brain's vascular and Alzheimer pathologies additive or interactive? Curr. Opin. Psychiatry 31, 147–152. https://doi.org/10.1097/YCO.0000000000000395

Kuhn, M., Wing, J., Weston, S., Williams, A., Keefer, C., Engelhardt, A., Cooper, T., Mayer, Z., Kenkel, B., R Core Team, Benesty, M., Lescarbeau, R., Ziem, A., Scrucca, L., Tang, Y., Candan, C., Hunt, T., 2021. caret: Classification and Regression Training.

Laird, N.M., Ware, J.H., 1982. Random-effects models for longitudinal data. Biometrics 38, 963–974.

LaMontagne, P.J., Benzinger, T.L., Morris, J.C., Keefe, S., Hornbeck, R., Xiong, C., Grant, E., Hassenstab, J., Moulder, K., Vlassenko, A.G., Raichle, M.E., Cruchaga, C., Marcus, D., 2019. OASIS-3: Longitudinal Neuroimaging, Clinical, and Cognitive Dataset for Normal Aging and Alzheimer Disease. medRxiv 2019.12.13.19014902. https://doi.org/10.1101/2019.12.13.19014902

Lee, S., Viqar, F., Zimmerman, M.E., Narkhede, A., Tosto, G., Benzinger, T.L.S., Marcus, D.S., Fagan, A.M., Goate, A., Fox, N.C., Cairns, N.J., Holtzman, D.M., Buckles, V., Ghetti, B., McDade, E., Martins, R.N., Saykin, A.J., Masters, C.L., Ringman, J.M., Ryan, N.S., Förster, S., Laske, C., Schofield, P.R., Sperling, R.A., Salloway, S., Correia, S., Jack, C., Weiner, M., Bateman, R.J., Morris, J.C., Mayeux, R., Brickman, A.M., 2016. White matter hyperintensities are a core feature of Alzheimer's disease: Evidence from the dominantly inherited Alzheimer network. Ann. Neurol. 79, 929–939. https://doi.org/10.1002/ana.24647

Lee, S., Zimmerman, M.E., Narkhede, A., Nasrabady, S.E., Tosto, G., Meier, I.B., Benzinger, T.L.S., Marcus, D.S., Fagan, A.M., Fox, N.C., Cairns, N.J., Holtzman, D.M., Buckles, V., Ghetti, B., McDade, E., Martins, R.N., Saykin, A.J., Masters, C.L., Ringman, J.M., Förster, S., Schofield, P.R., Sperling, R.A., Johnson, K.A., Chhatwal, J.P., Salloway, S., Correia, S., Jack, C.R., Weiner, M., Bateman, R.J., Morris, J.C., Mayeux, R., Brickman, A.M., Dominantly Inherited Alzheimer Network, 2018. White matter hyperintensities and the mediating role of cerebral amyloid angiopathy in dominantly-inherited Alzheimer's disease. PloS One 13, e0195838. https://doi.org/10.1371/journal.pone.0195838

Levine, D.A., Kabeto, M., Langa, K.M., Lisabeth, L.D., Rogers, M.A.M., Galecki, A.T., 2015. Does Stroke Contribute to Racial Differences in Cognitive Decline? Stroke J. Cereb. Circ. 46, 1897–1902. https://doi.org/10.1161/STROKEAHA.114.008156

Liu, C.C., Kanekiyo, T., Xu, H., Bu, G., 2013. Apolipoprotein e and Alzheimer disease: Risk, mechanisms and therapy. Nat. Rev. Neurol. https://doi.org/10.1038/nrneurol.2012.263

Liu, J., Hlavka, J., Hillestad, R., Mattke, S., 2017. Assessing the Preparedness of the U.S. Health Care System Infrastructure for an Alzheimer's Treatment, Assessing the Preparedness of the U.S. Health Care System Infrastructure for an Alzheimer's Treatment. RAND Corporation. https://doi.org/10.7249/RR2272

Liu Wenyan, Wong Adrian, Au Lisa, Yang Jie, Wang Zhaolu, Leung Eric Y.L., Chen Sirong, Ho Chi L., Mok Vincent C.T., 2015. Influence of Amyloid-β on Cognitive Decline After Stroke/Transient Ischemic Attack. Stroke 46, 3074–3080. https://doi.org/10.1161/STROKEAHA.115.010449

Lockhart, S.N., DeCarli, C., 2014. Structural Imaging Measures of Brain Aging. Neuropsychol. Rev. 24, 271–289. https://doi.org/10.1007/s11065-014-9268-3

Luengo-Fernandez, R., Paul, N.L.M., Gray, A.M., Pendlebury, S.T., Bull, L.M., Welch, S.J.V., Cuthbertson, F.C., Rothwell, P.M., 2013. Population-Based Study of Disability and Institutionalization After Transient Ischemic Attack and Stroke. Stroke 44, 2854–2861. https://doi.org/10.1161/STROKEAHA.113.001584

Manly, J.J., Mayeux, R., 2019. Ethnic Differences in Dementia and Alzheimer ' s Disease, in: Critical Perspectives on Racial and Ethnic Differences in Health in Late Life. National Academies Press (US), Washington (DC), pp. 1–32.

Marnane, M., Al-Jawadi, O.O., Mortazavi, S., Pogorzelec, K.J., Wang, B.W., Feldman, H.H., Hsiung, G.-Y.R., For the Alzheimer's Disease Neuroimaging Initiative, 2016. Periventricular hyperintensities are associated with elevated cerebral amyloid. Neurology 86, 535–543. https://doi.org/10.1212/WNL.0000000000002352

Mateos-Pérez, J.M., Dadar, M., Lacalle-Aurioles, M., Iturria-Medina, Y., Zeighami, Y., Evans, A.C., 2018a. Structural neuroimaging as clinical predictor: A review of machine learning applications. NeuroImage Clin. 20, 506–522. https://doi.org/10.1016/j.nicl.2018.08.019

Mateos-Pérez, J.M., Dadar, M., Lacalle-Aurioles, M., Iturria-Medina, Y., Zeighami, Y., Evans, A.C., 2018b. Structural neuroimaging as clinical predictor: A review of machine learning applications. NeuroImage Clin. 20, 506–522. https://doi.org/10.1016/j.nicl.2018.08.019

Mayeda, E.R., Glymour, M.M., Quesenberry, C.P., Whitmer, R.A., 2016. Inequalities in dementia incidence between six racial and ethnic groups over 14 years. Alzheimers Dement. 12, 216–224. https://doi.org/10.1016/j.jalz.2015.12.007

McDade, E., Wang, G., Gordon, B.A., Hassenstab, J., Benzinger, T.L.S., Buckles, V., Fagan, A.M., Holtzman, D.M., Cairns, N.J., Goate, A.M., Marcus, D.S., Morris, J.C., Paumier, K., Xiong, C., Allegri, R., Berman, S.B., Klunk, W., Noble, J., Ringman, J., Ghetti, B., Farlow, M., Sperling, R.A., Chhatwal, J., Salloway, S., Graff-Radford, N.R., Schofield, P.R., Masters, C., Rossor, M.N., Fox, N.C., Levin, J., Jucker, M., Bateman, R.J., Dominantly Inherited Alzheimer Network, 2018. Longitudinal cognitive and biomarker changes in dominantly inherited Alzheimer disease. Neurology 91, e1295–e1306. https://doi.org/10.1212/WNL.0000000000006277

McKeith, I.G., Boeve, B.F., Dickson, D.W., Halliday, G., Taylor, J.-P., Weintraub, D., Aarsland, D., Galvin, J., Attems, J., Ballard, C.G., Bayston, A., Beach, T.G., Blanc, F., Bohnen, N.I., Bonanni, L., Bras, J., Brundin, P., Burn, D., Chen-Plotkin, A., Duda, J.E., El-Agnaf, O., Feldman, H., Ferman, T.J., Ffytche, D., Fujishiro, H., Galasko, D., Goldman, J.G., Gomperts, S.N., Graff-Radford, N.R., Honig, L.S., Iranzo, A., Kantarci, K., Kaufer, D., Kukull, W., Lee, V.M., Leverenz, J.B., Lewis, S., Lippa, C., Lunde, A., Masellis, M., Masliah, E., McLean, P., Mollenhauer, B., Montine, T.J., Moreno, E., Mori, E., Murray, M., O'Brien, J.T., Orimo, S., Postuma, R.B., Ramaswamy, S., Ross, O.A., Salmon, D.P., Singleton, A., Taylor, A., Thomas, A., Tiraboschi, P., Toledo, J.B., Trojanowski, J.Q., Tsuang, D., Walker, Z., Yamada, M., Kosaka, K., 2017. Diagnosis and management of dementia with Lewy bodies. Neurology 89, 88–100. https://doi.org/10.1212/WNL.0000000000004058

McKhann, G.M., Knopman, D.S., Chertkow, H., Hyman, B.T., Jack, C.R., Kawas, C.H., Klunk, W.E., Koroshetz, W.J., Manly, J.J., Mayeux, R., Mohs, R.C., Morris, J.C., Rossor, M.N., Scheltens, P., Carrillo, M.C., Thies, B., Weintraub, S., Phelps, C.H., 2011. The diagnosis of dementia due to Alzheimer's disease: Recommendations from the National Institute on Aging-Alzheimer's Association workgroups on diagnostic guidelines for Alzheimer's disease. Alzheimers Dement. 7, 263–269. https://doi.org/10.1016/j.jalz.2011.03.005

Mishra, S., Blazey, T.M., Holtzman, D.M., Cruchaga, C., Su, Y., Morris, J.C., Benzinger, T.L.S., Gordon, B.A., 2018. Longitudinal brain imaging in preclinical Alzheimer disease: impact of APOE ε4 genotype. Brain 141, 1828–1839. https://doi.org/10.1093/brain/awy103

Mok, V., Liu, W., Wong, A., 2016. Detection of amyloid plaques in patients with post-stroke dementia. HKMJ.

Moroney, J.T., Bagiella, E., Desmond, D.W., Hachinski, V.C., Mölsä, P.K., Gustafson, L., Brun, A., Fischer, P., Erkinjuntti, T., Rosen, W., Paik, M.C., Tatemichi, T.K., 1997. Meta-analysis of the Hachinski Ischemic Score in pathologically verified dementias. Neurology 49, 1096–1105. https://doi.org/10.1212/wnl.49.4.1096

Morris, E., Chalkidou, A., Hammers, A., Peacock, J., Summers, J., Keevil, S., 2016. Diagnostic accuracy of 18 F amyloid PET tracers for the diagnosis of Alzheimer's disease : a systematic review and meta-analysis 374–385. https://doi.org/10.1007/s00259-015-3228-x

Morris, J.C., 2012. Revised Criteria for Mild Cognitive Impairment May Compromise the Diagnosis of Alzheimer Disease Dementia. Arch. Neurol. 69, 700–708. https://doi.org/10.1001/archneurol.2011.3152

Morris, J.C., 1993. The Clinical Dementia Rating (CDR): current version and scoring rules. Neurology 43, 2412–2414. https://doi.org/10.1212/wnl.43.11.2412-a

Morris, John C, Schindler, S.E., McCue, L.M., Moulder, K.L., Benzinger, T.L., Cruchaga, C., Fagan, A.M., Grant, E.A., Gordon, B.A., Holtzman, D.M., Xiong, C., 2019. Assessment of Racial Disparities in Biomarkers for Alzheimer Disease. JAMA Neurol. 76, 264. https://doi.org/10.1001/jamaneurol.2018.4249

Morris, John C., Schindler, S.E., McCue, L.M., Moulder, K.L., Benzinger, T.L.S., Cruchaga, C., Fagan, A.M., Grant, E., Gordon, B.A., Holtzman, D.M., Xiong, C., 2019. Assessment of Racial Disparities in Biomarkers for Alzheimer Disease. JAMA Neurol. 76, 264. https://doi.org/10.1001/jamaneurol.2018.4249

Morris, J.C., Storandt, M., McKeel, D.W., Rubin, E.H., Price, J.L., Grant, E.A., Berg, L., 1996. Cerebral amyloid deposition and diffuse plaques in "normal" aging: Evidence for presymptomatic and very mild Alzheimer's disease. Neurology 46, 707–719. https://doi.org/10.1212/wnl.46.3.707

Morris, J.C., Weintraub, S., Chui, H.C., Cummings, J., Decarli, C., Ferris, S., Foster, N.L., Galasko, D., Graff-Radford, N., Peskind, E.R., Beekly, D., Ramos, E.M., Kukull, W.A., 2006. The Uniform Data Set (UDS): clinical and cognitive variables and descriptive data from Alzheimer Disease Centers. Alzheimer Dis. Assoc. Disord. 20, 210–216. https://doi.org/10.1097/01.wad.0000213865.09806.92

Nasrabady, S.E., Rizvi, B., Goldman, J.E., Brickman, A.M., 2018. White matter changes in Alzheimer's disease: a focus on myelin and oligodendrocytes. Acta Neuropathol. Commun. 6, 22. https://doi.org/10.1186/s40478-018-0515-3

Nelson, A.R., Sweeney, M.D., Sagare, A.P., Zlokovic, B.V., 2016. Neurovascular Dysfunction and Neurodegeneration in Dementia and Alzheimer's disease. Biochim. Biophys. Acta 1862, 887–900. https://doi.org/10.1016/j.bbadis.2015.12.016

Obermeyer, Z., Powers, B., Vogeli, C., Mullainathan, S., 2019. Dissecting racial bias in an algorithm used to manage the health of populations. Science 366, 447–453. https://doi.org/10.1126/science.aax2342

Oh, H., Madison, C., Villeneuve, S., Markley, C., Jagust, W.J., 2014. Association of Gray Matter Atrophy with Age, β-Amyloid, and Cognition in Aging. Cereb. Cortex N. Y. NY 24, 1609–1618. https://doi.org/10.1093/cercor/bht017

Ortiz, G.A., L. Sacco, R., 2014. National Institutes of Health Stroke Scale (NIHSS), in: Wiley StatsRef: Statistics Reference Online. John Wiley & Sons, Ltd, Chichester, UK. https://doi.org/10.1002/9781118445112.stat06823

Ossenkoppele, R., Rabinovici, G.D., Smith, R., Cho, H., Schöll, M., Strandberg, O., Palmqvist, S., Mattsson, N., Janelidze, S., Santillo, A., Ohlsson, T., Jögi, J., Tsai, R., La Joie, R., Kramer, J., Boxer, A.L., Gorno-Tempini, M.L., Miller, B.L., Choi, J.Y., Ryu, Y.H., Lyoo, C.H., Hansson, O., 2018a. Discriminative Accuracy of [^{18} F]flortaucipir Positron Emission Tomography for Alzheimer Disease vs Other Neurodegenerative Disorders. JAMA 320, 1151. https://doi.org/10.1001/jama.2018.12917

Ossenkoppele, R., Rabinovici, G.D., Smith, R., Cho, H., Schöll, M., Strandberg, O., Palmqvist, S., Mattsson, N., Janelidze, S., Santillo, A., Ohlsson, T., Jögi, J., Tsai, R., La Joie, R., Kramer, J.H., Boxer, A.L., Gorno-Tempini, M.-L., Miller, B.L., Choi, J.Y., Ryu, Y.H., Lyoo, C.H., Hansson, O., 2018b. Discriminative Accuracy of [18 F]flortaucipir Positron Emission Tomography for Alzheimer Disease vs Other Neurodegenerative Disorders. JAMA 320, 1151. https://doi.org/10.1001/jama.2018.12917

Park, M., Moon, W.-J., 2016. Structural MR Imaging in the Diagnosis of Alzheimer's Disease and Other Neurodegenerative Dementia: Current Imaging Approach and Future Perspectives. Korean J. Radiol. 17, 827. https://doi.org/10.3348/kjr.2016.17.6.827

Pendlebury, S.T., Rothwell, P.M., 2009. Prevalence, incidence, and factors associated with pre-stroke and post-stroke dementia: a systematic review and meta-analysis. Lancet Neurol. 8, 1006–1018. https://doi.org/10.1016/S1474-4422(09)70236-4

Petersen, R.C., Morris, J.C., 2005. Mild Cognitive Impairment as a Clinical Entity and Treatment Target. Arch. Neurol. 62, 1160–1163. https://doi.org/10.1001/archneur.62.7.1160

Pettigrew, C., Soldan, A., Sloane, K., Cai, Q., Wang, J., Wang, M.-C., Moghekar, A., Miller, M.I., Albert, M., BIOCARD Research Team, 2017. Progressive medial temporal lobe atrophy during preclinical Alzheimer's disease. NeuroImage Clin. 16, 439–446. https://doi.org/10.1016/j.nicl.2017.08.022

Phuah, C.-L., Chen, Y., Liu, Z., Yechoor, N., Hwang, H., Laurido-Soto, O., Marcus, D.S., Lee, J.-M., 2019. White Matter Hyperintensity Spatial Pattern Variations reflect distinct Cerebral Small Vessel Disease Pathologies.

Rabin, J.S., Schultz, A.P., Hedden, T., Viswanathan, A., Marshall, G.A., Kilpatrick, E., Klein, H., Buckley, R.F., Yang, H.-S., Properzi, M., Rao, V., Kirn, D.R., Papp, K.V., Rentz, D.M., Johnson, K.A., Sperling, R.A., Chhatwal, J.P., 2018. Interactive Associations of Vascular Risk and β-Amyloid Burden With Cognitive Decline in Clinically Normal Elderly Individuals: Findings From the Harvard Aging Brain Study. JAMA Neurol. 75, 1124–1131. https://doi.org/10.1001/jamaneurol.2018.1123

Rabinovici, G.D., Gatsonis, C., Apgar, C., Chaudhary, K., Gareen, I., Hanna, L., Hendrix, J.A., Hillner, B.E., Olson, C., Lesman-Segev, O.H., Romanoff, J., Siegel, B.A., Whitmer, R.A., Carrillo, M.C., 2019. Association of Amyloid Positron Emission Tomography With Subsequent Change in Clinical Management Among Medicare Beneficiaries With Mild Cognitive Impairment or Dementia. JAMA 321, 1286. https://doi.org/10.1001/jama.2019.2000

Rascovsky, K., Hodges, J.R., Knopman, D.S., Mendez, M.F., Kramer, J.H., Neuhaus, J., van Swieten, J.C., Seelaar, H., Dopper, E.G., Onyike, C.U., Hillis, A.E., Josephs, K.A., Boeve, B.F., Kertesz, A., Seeley, W.W., Rankin, K.P., Johnson, J.K., Gorno-Tempini, M.-L., Rosen, H., Prioleau-Latham, C.E., Lee, A., Kipps, C.M., Lillo, P., Piguet, O., Rohrer, J.D., Rossor, M.N., Warren, J.D., Fox, N.C., Galasko, D., Salmon, D.P., Black, S.E., Mesulam, M., Weintraub, S., Dickerson, B.C., Diehl-Schmid, J., Pasquier, F., Deramecourt, V., Lebert, F., Pijnenburg, Y.A.L., Chow, T.W., Manes, F., Grafman, J., Cappa, S.F., Freedman, M., Grossman, M., Miller, B.L., 2011. Sensitivity of revised diagnostic criteria for the behavioural variant of frontotemporal dementia. Brain 134, 2456–2477. https://doi.org/10.1093/brain/awr179

Raz, N., Ghisletta, P., Rodrigue, K.M., Kennedy, K.M., Lindenberger, U., 2010. Trajectories of brain aging in middle-aged and older adults: Regional and individual differences. NeuroImage 51, 501–511. https://doi.org/10.1016/j.neuroimage.2010.03.020

Raz, N., Lindenberger, U., Rodrigue, K.M., Kennedy, K.M., Head, D., Williamson, A., Dahle, C., Gerstorf, D., Acker, J.D., 2005. Regional Brain Changes in Aging Healthy Adults: General Trends, Individual Differences and Modifiers. Cereb. Cortex 15, 1676–1689. https://doi.org/10.1093/cercor/bhi044

Reed, T., Carmelli, D., Swan, G.E., Breitner, J.C.S., Welsh, K.A., Jarvik, G.P., Deeb, S., Auwerx, J., 1994. Lower cognitive performance in normal older adult male twins carrying the apolipoprotein E !e4 allele. Arch. Neurol. 51, 1189–1192. https://doi.org/10.1001/archneur.1994.00540240033012

Ribaldi, F., Altomare, D., Jovicich, J., Ferrari, C., Picco, A., Pizzini, F.B., Soricelli, A., Mega, A., Ferretti, A., Drevelegas, A., Bosch, B., Müller, B.W., Marra, C., Cavaliere, C., Bartrés-Faz, D., Nobili, F., Alessandrini, F., Barkhof, F., Gros-Dagnac, H., Ranjeva, J.-P., Wiltfang, J., Kuijer, J., Sein, J., Hoffmann, K.-T., Roccatagliata, L., Parnetti, L., Tsolaki, M., Constantinidis, M., Aiello, M., Salvatore, M., Montalti, M., Caulo, M., Didic, M., Bargallo, N., Blin, O., Rossini, P.M., Schonknecht, P., Floridi, P., Payoux, P., Visser, P.J., Bordet, R., Lopes, R., Tarducci, R., Bombois, S., Hensch, T., Fiedler, U., Richardson, J.C., Frisoni, G.B., Marizzoni, M., 2021. Accuracy and reproducibility of automated white matter hyperintensities segmentation with lesion segmentation tool: A European multi-site 3T study. Magn. Reson. Imaging 76, 108–115. https://doi.org/10.1016/j.mri.2020.11.008

Riudavets, M.A., Rubio, A., Cox, C., Rudow, G., Fowler, D., Troncoso, J.C., 2006a. The Prevalence of Alzheimer Neuropathologic Lesions Is Similar in Blacks and Whites: J. Neuropathol. Exp. Neurol. 65, 1143–1148. https://doi.org/10.1097/01.jnen.0000248548.20799.a3

Riudavets, M.A., Rubio, A., Cox, C., Rudow, G., Fowler, D., Troncoso, J.C., 2006b. The Prevalence of Alzheimer Neuropathologic Lesions Is Similar in Blacks and Whites. J. Neuropathol. Exp. Neurol. 65, 1143–1148. https://doi.org/10.1097/01.jnen.0000248548.20799.a3

Roseborough, A., Ramirez, J., Black, S.E., Edwards, J.D., 2017. Associations between amyloid β and white matter hyperintensities: A systematic review. Alzheimers Dement. 13, 1154–1167. https://doi.org/10.1016/j.jalz.2017.01.026

Salvadó, G., Brugulat-Serrat, A., Sudre, C.H., Grau-Rivera, O., Suárez-Calvet, M., Falcon, C., Fauria, K., Cardoso, M.J., Barkhof, F., Molinuevo, J.L., Gispert, J.D., ALFA Study, 2019. Spatial patterns of white matter hyperintensities associated with Alzheimer's disease risk factors in a cognitively healthy middle-aged cohort. Alzheimers Res. Ther. 11, 12. https://doi.org/10.1186/s13195-018-0460-1

Schmidt, P., Gaser, C., Arsic, M., Buck, D., Förschler, A., Berthele, A., Hoshi, M., Ilg, R., Schmid, V.J., Zimmer, C., Hemmer, B., Mühlau, M., 2012. An automated tool for detection of FLAIR-hyperintense white-matter lesions in Multiple Sclerosis. NeuroImage 59, 3774–3783. https://doi.org/10.1016/j.neuroimage.2011.11.032

Schott, J.M., Bartlett, J.W., Fox, N.C., Barnes, J., 2010. Increased brain atrophy rates in cognitively normal older adults with low cerebrospinal fluid Aβ1-42. Ann. Neurol. 68, 825–834. https://doi.org/10.1002/ana.22315

Sevigny, J., Chiao, P., Bussière, T., Weinreb, P.H., Williams, L., Maier, M., Dunstan, R., Salloway, S., Chen, T., Ling, Y., O'Gorman, J., Qian, F., Arastu, M., Li, M., Chollate, S., Brennan, M.S., Quintero-Monzon, O., Scannevin, R.H., Arnold, H.M., Engber, T., Rhodes, K., Ferrero, J., Hang, Y., Mikulskis, A., Grimm, J., Hock, C., Nitsch, R.M., Sandrock, A., 2016. The antibody aducanumab reduces Aβ plaques in Alzheimer's disease. Nature 537, 50–56. https://doi.org/10.1038/nature19323

Shaw, L.M., Arias, J., Blennow, K., Galasko, D., Molinuevo, J.L., Salloway, S., Schindler, S.E., Carrillo, M.C., Hendrix, J.A., Ross, A., Illes, J., Ramus, C., Fifer, S., 2018. Appropriate use criteria for lumbar puncture and cerebrospinal fluid testing in the diagnosis of Alzheimer's disease. Alzheimers Dement. 14, 1505–1521. https://doi.org/10.1016/j.jalz.2018.07.220

Silverman, D.H.S., Small, G.W., Chang, C.Y., Lu, C.S., de Aburto, M.A.K., Chen, W., Czernin, J., Rapoport, S.I., Pietrini, P., Alexander, G.E., Schapiro, M.B., Jagust, W., Hoffman, J.M., Welsh-Bohmer, K.A., Alavi, A., Clark, C.M., Salmon, E., de Leon, M.J., Mielke, R., Cummings, J.L., Kowell, A.P., Gambhir, S.S., Hoh, C.K., Phelps, M.E., 2001. Positron Emission Tomography in Evaluation of Dementia. JAMA 286, 2120. https://doi.org/10.1001/jama.286.17.2120

Skrobot, O.A., Black, S.E., Chen, C., DeCarli, C., Erkinjuntti, T., Ford, G.A., Kalaria, R.N., O'Brien, J., Pantoni, L., Pasquier, F., Roman, G.C., Wallin, A., Sachdev, P., Skoog, I., Ben-Shlomo, Y., Passmore, A.P., Love, S., Kehoe, P.G., Taragano, F.E., Kril, J., Cavalieri, M., Jellinger, K.A., Kovacs, G.G., Engelborghs, S., Lafosse, C., Bertolucci, P.H., Brucki, S., Caramelli, P., de Toledo Ferraz Alves, T.C., Bocti, C., Fulop, T., Hogan, D.B., Hsiung, G.R., Kirk, A., Leach, L., Robillard, A., Sahlas, D.J., Guo, Q., Tian, J., Hokkanen, L., Jokinen, H., Benisty, S., Deramecourt, V., Hauw, J., Lenoir, H., Tsatali, M., Tsolaki, M., Sundar, U., Coen, R.F., Korczyn, A.D., Altieri, M., Baldereschi, M., Caltagirone, C., Caravaglios, G., Di Carlo, A., Di Piero, V., Gainotti, G., Galluzzi, S., Logroscino, G., Mecocci, P., Moretti, D.V., Padovani, A., Fukui, T., Ihara, M., Mizuno, T., Kim, S.Y., Akinyemi, R., Baiyewu, O., Ogunniyi, A., Szczudlik, A., Bastos-Leite, A.J., Firmino, H., Massano, J., Verdelho, A., Kruglov, L.S., Ikram, M.K., Kandiah, N., Arana, E., Barroso-Ribal, J., Calatayud, T., Cruz-Jentoft, A.J., López-Pousa, S., Martinez-Lage, P., Mataro, M., Börjesson-Hanson, A., Englund, E., Laukka, E.J., Qiu, C., Viitanen, M., Biessels, G.J., de Leeuw, F.-E., den Heijer, T., Exalto, L.G., Kappelle, L.J., Prins, N.D., Richard, E., Schmand, B., van den Berg, E., van der Flier, W.M., Bilgic, B., Allan, L.M., Archer, J., Attems, J., Bayer, A., Blackburn, D., Brayne, C., Bullock, R., Connelly, P.J., Farrant, A., Fish, M., Harkness, K., Ince, P.G., Langhorne, P., Mann, J., Matthews, F.E., Mayer, P., Pendlebury, S.T., Perneczky, R., Peters, R., Smithard, D., Stephan, B.C., Swartz, J.E., Todd, S., Werring, D.J., Wijayasiri, S.N., Wilcock, G., Zamboni, G., Au, R., Borson, S., Bozoki, A., Browndyke, J.N., Corrada, M.M., Crane, P.K., Diniz, B.S., Etcher, L., Fillit, H., Greenberg, S.M., Grinberg, L.T., Hurt, S.W., Lamar, M., Mielke, M., Ott, B.R., Perry, G., Powers, W.J., Ramos-Estebanez, C., Reed, B., Roberts, R.O., Romero, J.R., Saykin, A.J., Seshadri, S., Silbert, L., Stern, Y., Zarow,

C., 2018. Progress toward standardized diagnosis of vascular cognitive impairment: Guidelines from the Vascular Impairment of Cognition Classification Consensus Study. Alzheimers Dement. 14, 280–292. https://doi.org/10.1016/j.jalz.2017.09.007

Smith, C.D., Andersen, A.H., Gold, B.T., Neuroimaging Initiative, 2012. Structural Brain Alterations before Mild Cognitive Impairment in ADNI: Validation of Volume Loss in a Predefined Antero-Temporal Region. J. Alzheimers Dis. 31, S49–S58. https://doi.org/10.3233/JAD-2012-120157

Sperling, R.A., Rentz, D.M., Johnson, K.A., Karlawish, J.H., Donohue, M., Salmon, D.P., Aisen, P.S., 2014. The A4 Study: Stopping AD Before Symptoms Begin? Sci. Transl. Med. 6, 228fs13-228fs13. https://doi.org/10.1126/scitranslmed.3007941

Stansbury, J.P., Jia, H., Williams, L.S., Vogel, W.B., Duncan, P.W., 2005. Ethnic Disparities in Stroke. Stroke 36, 374–386. https://doi.org/10.1161/01.STR.0000153065.39325.fd

Storandt, M., Grant, E.A., Miller, J.P., Morris, J.C., 2006. Longitudinal course and neuropathologic outcomes in original vs revised MCI and in pre-MCI. Neurology 67, 467–473. https://doi.org/10.1212/01.wnl.0000228231.26111.6e

Storandt, M., Mintun, M.A., Head, D., Morris, J.C., 2009. Cognitive Decline and Brain Volume Loss as Signatures of Cerebral Amyloid-β Peptide Deposition Identified With Pittsburgh Compound B: Cognitive Decline Associated With Aβ Deposition. Arch. Neurol. 66, 1476–1481. https://doi.org/10.1001/archneurol.2009.272

Strittmatter, W.J., Saunders, A.M., Schmechel, D., Pericak-Vance, M., Enghild, J., Salvesen, G.S., Roses, A.D., 1993. Apolipoprotein E: high-avidity binding to beta-amyloid and increased frequency of type 4 allele in late-onset familial Alzheimer disease. Proc. Natl. Acad. Sci. U. S. A. 90, 1977–1981. https://doi.org/10.1073/pnas.90.5.1977

Su, Y., 2021. ysu001/PUP.

Su, Y., Blazey, T.M., Snyder, A.Z., Raichle, M.E., Marcus, D.S., Ances, B.M., Bateman, R.J., Cairns, N.J., Aldea, P., Cash, L., Christensen, J.J., Friedrichsen, K.A., Hornbeck, R.C., Farrar, A.M., Owen, C.J., Mayeux, R., Brickman, A.M., Klunk, W.E., Price, J.C., Thompson, P.M., Ghetti, B., Saykin, A.J., Sperling, R.A., Johnson, K.A., Schofield, P.R., Buckles, V., Morris, J.C., Benzinger, T.L., 2015. Partial volume correction in quantitative amyloid imaging. NeuroImage 107, 55–64. https://doi.org/10.1016/j.neuroimage.2014.11.058

Su, Y., D'Angelo, G.M., Vlassenko, A.G., Zhou, G., Snyder, A.Z., Marcus, D.S., Blazey, T.M., Christensen, J.J., Vora, S., Morris, J.C., Mintun, M.A., Benzinger, T.L., 2013. Quantitative Analysis of PiB-PET with FreeSurfer ROIs. PLoS ONE 8, e73377. https://doi.org/10.1371/journal.pone.0073377

Su, Y., Flores, S., Hornbeck, R.C., Speidel, B., Vlassenko, A.G., Gordon, B.A., Koeppe, R.A., Klunk, W.E., Xiong, C., Morris, J.C., Benzinger, T.L.S., 2018. Utilizing the Centiloid scale in cross-sectional and longitudinal PiB PET studies. NeuroImage Clin. 19, 406–416. https://doi.org/10.1016/j.nicl.2018.04.022

Su, Y., Flores, S., Wang, G., Hornbeck, R.C., Speidel, B., Joseph-Mathurin, N., Vlassenko, A.G., Gordon, B.A., Koeppe, R.A., Klunk, W.E., Jack, C.R., Farlow, M.R., Salloway, S., Snider, B.J., Berman, S.B., Roberson, E.D., Brosch, J., Jimenez-Velazques, I., van Dyck, C.H., Galasko, D., Yuan, S.H., Jayadev, S., Honig, L.S., Gauthier, S., Hsiung, G.-Y.R., Masellis, M., Brooks, W.S., Fulham, M., Clarnette, R., Masters, C.L., Wallon, D., Hannequin, D., Dubois, B., Pariente, J., Sanchez-Valle, R., Mummery, C., Ringman, J.M., Bottlaender, M., Klein, G., Milosavljevic-Ristic, S., McDade, E., Xiong, C., Morris, J.C., Bateman, R.J., Benzinger, T.L., 2019. Comparison of Pittsburgh compound B and florbetapir in cross-sectional and longitudinal studies. Alzheimers Dement. Diagn. Assess. Dis. Monit. 11, 180–190. https://doi.org/10.1016/j.dadm.2018.12.008

Suzuki, H., Venkataraman, A.V., Bai, W., Guitton, F., Guo, Y., Dehghan, A., Matthews, P.M., Alzheimer's Disease Neuroimaging Initiative, 2019. Associations of Regional Brain Structural Differences With Aging, Modifiable Risk Factors for Dementia, and Cognitive Performance. JAMA Netw. Open 2, e1917257. https://doi.org/10.1001/jamanetworkopen.2019.17257

Sweeney, M.D., Sagare, A.P., Zlokovic, B.V., 2015. Cerebrospinal fluid biomarkers of neurovascular dysfunction in mild dementia and Alzheimer's disease. J. Cereb. Blood Flow Metab. 35, 1055–1068. https://doi.org/10.1038/jcbfm.2015.76

Tang, M.X., Cross, P., Andrews, H., Jacobs, D.M., Small, S.A., Bell, K., Merchant, C., Lantigua, R., Costa, R., Stern, Y., Mayeux, R., 2001. Incidence of AD in African-Americans, Caribbean Hispanics, and Caucasians in northern Manhattan. Neurology 56, 49–56. https://doi.org/10.1212/WNL.56.1.49

Thiel, A., Cechetto, D.F., Heiss, W.-D., Hachinski, V., Whitehead, S.N., 2014. Amyloid Burden, Neuroinflammation, and Links to Cognitive Decline After Ischemic Stroke. Stroke 45, 2825–2829. https://doi.org/10.1161/STROKEAHA.114.004285

Tubi, M.A., Feingold, F.W., Kothapalli, D., Hare, E.T., King, K.S., Thompson, P.M., Braskie, M.N., 2020. White matter hyperintensities and their relationship to cognition: effects of segmentation algorithm. NeuroImage 206, 116327. https://doi.org/10.1016/j.neuroimage.2019.116327

van den Berg, E., Geerlings, M.I., Biessels, G.J., Nederkoorn, P.J., Kloppenborg, R.P., 2018. White Matter Hyperintensities and Cognition in Mild Cognitive Impairment and Alzheimer's Disease: A Domain-Specific Meta-Analysis. J. Alzheimers Dis. 63, 515–527. https://doi.org/10.3233/JAD-170573

Vargas-González, J.-C., Hachinski, V., 2019. Insidious Cerebrovascular Disease—the Uncool Iceberg. JAMA Neurol. 70, S11–S14. https://doi.org/10.1001/jamaneurol.2019.3933

Wang, Y., Xu, Q., Luo, J., Hu, M., Zuo, C., 2019. Effects of Age and Sex on Subcortical Volumes. Front. Aging Neurosci. 11, 259. https://doi.org/10.3389/fnagi.2019.00259

Wardlaw, J.M., Smith, C., Dichgans, M., 2019. Small vessel disease: mechanisms and clinical implications. Lancet Neurol. 18, 684–696. https://doi.org/10.1016/S1474-4422(19)30079-1

Waymont, J.M.J., Petsa, C., McNeil, C.J., Murray, A.D., Waiter, G.D., 2020. Validation and comparison of two automated methods for quantifying brain white matter hyperintensities of presumed vascular origin. J. Int. Med. Res. 48, 300060519880053. https://doi.org/10.1177/0300060519880053

Whelton, P.K., Carey, R.M., Aronow, W.S., Casey, D.E., Collins, K.J., Dennison Himmelfarb, C., DePalma, S.M., Gidding, S., Jamerson, K.A., Jones, D.W., MacLaughlin, E.J., Muntner, P., Ovbiagele, B., Smith, S.C., Spencer, C.C., Stafford, R.S., Taler, S.J., Thomas, R.J., Williams, K.A., Williamson, J.D., Wright, J.T., 2018. 2017 ACC/AHA/AAPA/ABC/ACPM/AGS/APhA/ASH/ASPC/NMA/PCNA Guideline for the Prevention, Detection, Evaluation, and Management of High Blood Pressure in Adults: Executive Summary: A Report of the American College of Cardiology/American Heart Association Task Force on Clinical Practice Guidelines. Circulation 138, e426–e483. https://doi.org/10.1161/CIR.0000000000000597

Williams, O., Ovbiagele, B., 2020. Stroking Out While Black—The Complex Role of Racism. JAMA Neurol. https://doi.org/10.1001/jamaneurol.2020.3510

Wollman, D.E., Prohovnik, I., 2003. Sensitivity and specificity of neuroimaging for the diagnosis of Alzheimer's disease. Dialogues Clin. Neurosci. 5, 89–99.

Xie, L., Wisse, L.E.M., Das, S.R., Vergnet, N., Dong, M., Ittyerah, R., Flores, R. de, Yushkevich, P.A., Wolk, D.A., 2020. Longitudinal atrophy in early Braak regions in preclinical Alzheimer's disease. Hum. Brain Mapp. 41, 4704–4717. https://doi.org/10.1002/hbm.25151

Xiong, C., Luo, J., Coble, D., Agboola, F., Kukull, W., Morris, J.C., 2020. Complex interactions underlie racial disparity in the risk of developing Alzheimer's disease dementia. Alzheimers Dement. alz.12060. https://doi.org/10.1002/alz.12060

Yang, J., Wong, A., Wang, Z., Liu, W., Au, L., Xiong, Y., Chu, W.W.C., Leung, E.Y.L., Chen, S., Lau, C., Chan, A.Y.Y., Lau, A.Y.L., Fan, F., Ip, V., Soo, Y., Leung, T., Ho, C.L., Wong, L.K.S., Mok, V.C.T., 2015. Risk factors for incident dementia after stroke and transient ischemic attack. Alzheimers Dement. 11, 16–23. https://doi.org/10.1016/j.jalz.2014.01.003

Yang, Q., Tong, X., Schieb, L., Vaughan, A., Gillespie, C., Wiltz, J.L., King, S.C., Odom, E., Merritt, R., Hong, Y., George, M.G., 2017. Vital Signs: Recent Trends in Stroke Death Rates — United States, 2000–2015. MMWR Morb. Mortal. Wkly. Rep. 66, 933–939. https://doi.org/10.15585/mmwr.mm6635e1

Yasuno, F., Kajimoto, K., Ihara, M., Taguchi, A., Yamamoto, A., Fukuda, T., Kazui, H., Iida, H., Nagatsuka, K., 2019. Amyloid β deposition in subcortical stroke patients and effects of educational achievement: A pilot study. Int. J. Geriatr. Psychiatry 34, 1651–1657. https://doi.org/10.1002/gps.5178

Youden, W.J., 1950. Index for rating diagnostic tests. Cancer 3, 32–35. https://doi.org/10.1002/1097-0142(1950)3:1<32::AID-CNCR2820030106>3.0.CO;2-3

Zhao, L., Biesbroek, J.M., Shi, L., Liu, W., Kuijf, H.J., Chu, W.W., Abrigo, J.M., Lee, R.K., Leung, T.W., Lau, A.Y., Biessels, G.J., Mok, V., Wong, A., 2018. Strategic infarct location for post-stroke cognitive impairment: A multivariate lesion-symptom mapping study. J. Cereb. Blood Flow Metab. Off. J. Int. Soc. Cereb. Blood Flow Metab. 38, 1299–1311. https://doi.org/10.1177/0271678X17728162

Zheng, F., Yan, L., Zhong, B., Yang, Z., Xie, W., 2019. Progression of cognitive decline before and after incident stroke. Neurology 93, e20–e28. https://doi.org/10.1212/WNL.0000000000007716

Zlokovic, B.V., 2011. Neurovascular pathways to neurodegeneration in Alzheimer's disease and other disorders. Nat. Rev. Neurosci. 12, 723–738. https://doi.org/10.1038/nrn3114